On Carbon Dot Based Drug Delivery Systems: Mechanochemical Formation of Surface Imine Bonds

Gianluca Fuoco

A Thesis

In

The Department

of

Chemistry and Biochemistry

Presented in Partial Fulfillment of the Requirements

For the Degree of Master of Science in Chemistry at

Concordia University

Montréal, Québec, Canada

Month 2025

© Gianluca Fuoco, 2025

CONCORDIA UNIVERSITY

SCHOOL OF GRADUATE STUDIES

Inis is to certify that	t the thesis prepared	
By:	Gianluca Fuoco	
Entitled:	Mechanochemically-N	Mediated Imine Bond Conjugation for Drug Delivery
	Using Carbon Dots	
and submitted in par	tial fulfillment of the red	quirements for the degree of
	Master of S	Science (Chemistry)
Complies with the re	egulations of the Univer	sity and meets the accepted standards with respect to
originality and quali-	ty.	
Signed by the final F	Examining Committee:	Chair
Dr. Rafik Naccache		Examiner
Dr. Pat Forgione		Examiner
Dr. Alisa Piekny		Supervisor
Dr. Rafik Naccache		
	ouis Cuccia, Graduate I	Program Director
July 28, 2025	Du Dagagla (Sinotta Dagu of Eggultu of Auta and Science
	Dr. Pascale S	Sicotte, Dean of Faculty of Arts and Science

ABSTRACT

On Carbon Dot Based Drug Delivery Systems: Mechanochemical Formation of Surface

Imine Bonds

Gianluca Fuoco

Efficient delivery of hydrophobic drugs remains a significant challenge, often hindered by poor distribution within aqueous bloodstreams. Current medical literature shows that over 40% of all drugs in clinical use are hydrophobic, and 90% or more of newly developed drugs are described as Class II (high permeability, low solubility), or Class IV (low permeability, low solubility). Carbon dots (CDs) offer a promising solution as drug delivery vehicles due to their aqueous dispersibility, generally low cytotoxicity and ease of surface functionalization. Traditional conjugation methods widely rely on covalent bonds such as amide bonds, which are robust but difficult to cleave, hindering drug release. Furthermore, their formation often requires expensive and hazardous coupling agents such as 1-Ethyl-3-(3-dimethylaminoporpyl)carbodiimide. Herein and to the best of our knowledge, we report for the first time, the solid-state mechanochemical formation of imine bonds to conjugate a hydrophobic model drug to the surfaces of CDs. Initial efforts focused on solution-based conjugation before transitioning to mechanochemistry, which was ultimately successful. ¹H-NMR analysis confirmed successful formation of imine bond linkages through the conversion of an aldehyde into an imine functional group without the need for a solvent, or any additional reagents. Additionally, release of the model drug was achieved reaching a plateau after 24 hours. A preliminary resazurin cytotoxicity assay demonstrated the low cytotoxicity of the CDs before and after altering the surfaces with imine bonds. Our findings highlight a straightforward and sustainable method for CD functionalization, paving the way for alternative covalent linkages and greener conjugation strategies.

Acknowledgements

First and foremost, I cannot thank Dr. Rafik Naccache enough for his guidance and support throughout this project. I first started academic research in Dr. Naccache's laboratory during my CHEM 450 undergraduate thesis, and I now find myself completing a master's degree within the same laboratory. Throughout the years, he has shown me how to have confidence in one's own work and how to remain positive when obstacles are inevitably encountered. I've always appreciated the fact that he would allow me the freedom to explore whichever research route I wanted and when things wouldn't work out (which happened a lot), then he would always be there to calm my worries. "That's research" he would say, and these few words carried great merit. They reminded me that at the end of the day, the essence of true research lies upon not being scared of failure in the pursuit of knowledge. So, thank you again Dr. Naccache, oh and "LC, BRNE".

I am also grateful to Dr. Alisa Piekny and Dr. Pat Forgione who have been on my committee since my undergraduate thesis. Throughout the years you have provided me with valuable guidance, whether it be through our committee meetings or simply talking in your offices about my research. Your doors were always open, and you were always available to speak, so for this I am very grateful.

To my lab colleagues, I cannot thank you enough for making the laboratory a safe and friendly environment. You have been a big part of my success whether it be through your help with my experiments or by simply talking and providing guidance and feedback. To Michelle Pains Duarte who has been a huge pillar of support and has always been there to talk to me when I was worried about the next steps, I cannot thank you enough. To Luis Alfonso Páramo Serrano who has always been there to provide a helping hand in and out of the lab, thank you, you are truly amazing. To Dr. Adeola Adedapo who has been a huge part of my success, thank you. You have

provided me with invaluable guidance and support which has shaped me into the scientist that I am today. To Adryanne Clermont-Paquette, thank you for being you and always being a source of light, you've taught me how to keep a smile and positive attitude throughout all the ups and downs. To Dr. Gabrielle A. Mandl who has helped me immensely by conducting the cell viability assay found in this thesis, thank you, you never said no to anything I would ask and have always been there to offer assistance. To Dr. Pedro Mena-Giraldo, thank you for always being available to talk, whether it be about life or sports, our conversations are always something I will value and remember. To Camilo Garcia, thank you for always being there to support me throughout many of our presentation practices. I will always cherish the time we spent piecing together the 26th CBGRC book of abstracts. To the amazing students who I've had the pleasure of mentoring, Carissa de Mesa and Noah Carisse, thank you for being so passionate about science and offering to help in any which way possible. You have made me a better mentor and teacher, and I am grateful for the dedication, joy and curiosity you have brought to our work together.

To my wonderful family who I most certainly cannot leave out, starting with my parents. I am extremely grateful for my parents Luigi Fuoco and Mina Ianniello who have been another huge pillar of support and a large reason that I am completing this thesis today. They have always been there to talk to me and pull me up when things got tough. You've believed in my abilities since day 1 and you've never doubted me. Your unwavering support and love means the world to me, and I truly couldn't have asked for better people to call my parents. This degree is as much yours as it is mine.

To my loving girlfriend Emily Degni, who has been by my side since we were 16 years old in high-school. I've had the pleasure of calling you my first lab partner and words cannot describe how much your unconditional love and support means to me. You and your family have always

welcomed me with open arms and for this I am thankful. Thank you for always being there for me and sticking by me for all this time. I wouldn't be completing this degree if it weren't for you.

To my amazing uncles, aunts and cousins, you mean the world to me. I want to thank you for always being so proud of me. All of your love and support throughout my degree has been nothing short of exceptional.

To my brother Alessandro Fuoco, you have always been a huge source of love and motivation. You never failed to let everyone know how proud you are of your little brother and for this I am grateful. I am equally proud of all your achievements including the latest and biggest, becoming a father. Together with my amazing sister-in-law Tara Barone, you have brought our family one of the greatest joys in the world, my beautiful niece Oliva Rosa Fuoco.

I am also thankful for my grandparents Rosa Petruccelli, Antonio Ianniello, Gilda Gallo and Sabatino Fuoco. Being first generation immigrants, they taught me the meaning of hard work and sacrifice to succeed. They also taught me that family is everything and without them I wouldn't be the man I am today. For this, I dedicate this thesis to my late grandfather Antonio Ianniello who has been present in nearly every aspect of my life from driving me to school every day as a child, to watching every single one of my soccer and hockey games. Unfortunately, he is no longer here to see out this milestone, but I know that he is proud and smiling down at me.

Dedicated to the memory of my grandfather, Ant	onio Ianniello
	(1938- 2024)

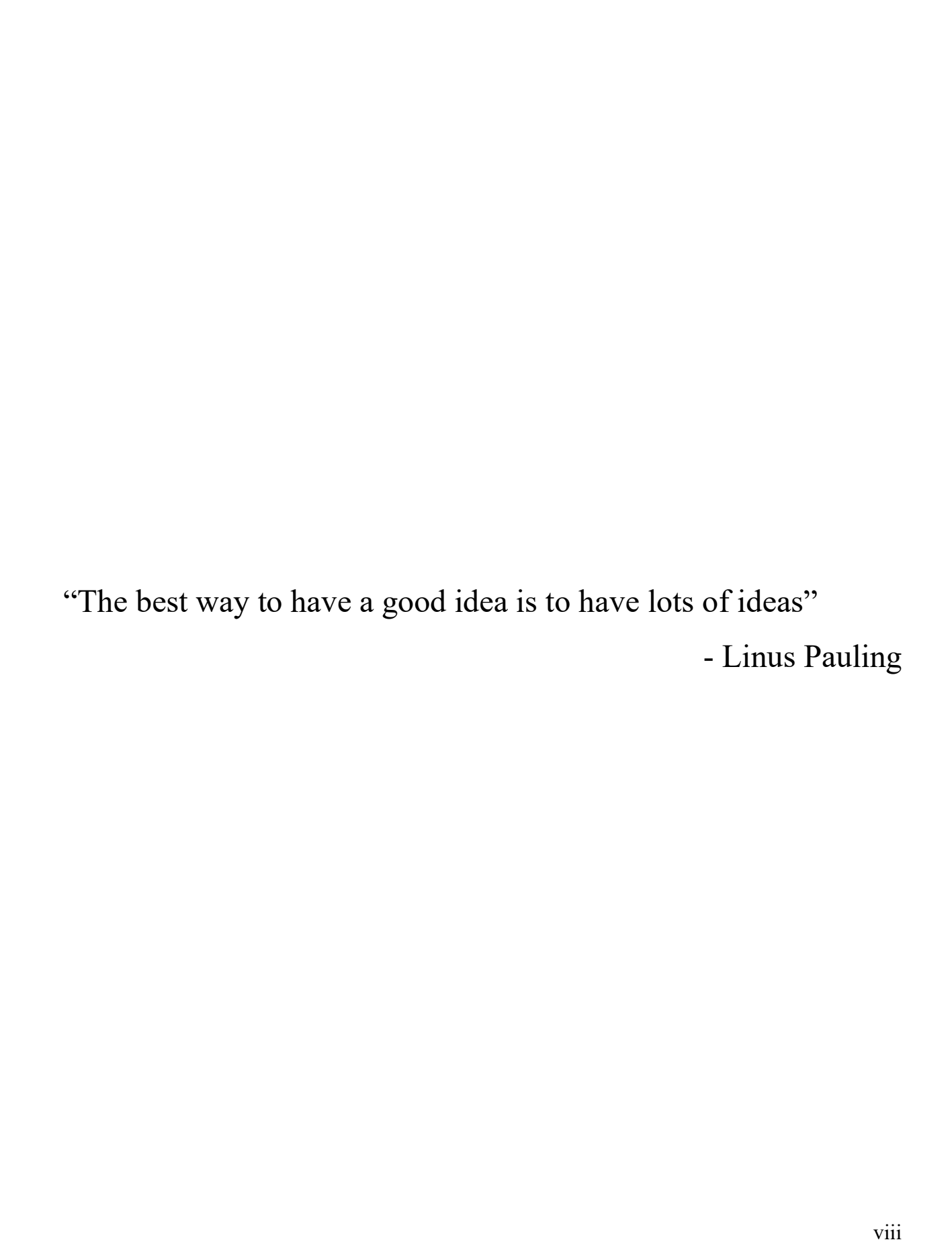


TABLE OF CONTENTS

List of Figures	Xiii
List of Tables	xvii
List of Abbreviations	xviii
Chapter 1. Introduction	1
1.1 Nanomaterials, Their Definition and Applications	1
1.1.1 What Are Nanomaterials?	1
1.1.2 Catalysis	2
1.1.2 Sensing.	4
1.1.3 Bioimaging	5
1.1.4 Drug Delivery	6
1.1.5 Limitations	7
1.2 Introduction to Carbon Dots	8
1.2.1 Their accidental discovery	8
1.2.2 Physical Properties	8
1.2.3 Chemical Properties	9
1.2.4 Optical Properties	11
1.2.5 Toxicity of CDs	12
1.2.6 Synthesis of CDs	14
1.2.7 Microwave Assisted Synthesis	15
1.3 CDs as Drug Delivery Tools	17
1.3.1 Current Systems	17
1.3.2 Functionalization Strategies	19

1.4 What is an Imine Bond?	21
1.4.1 Equilibrium Reaction	21
1.4.2 Ketones	23
1.4.3 Aldehydes	24
1.5 Mechanochemistry	26
1.5.1 Solid State Chemistry	26
1.5.2 Grinding and Milling	27
1.5.3 Covalent Bond Formation	28
1.6 Statement of the Problem	29
Chapter 2. Materials and Methods	32
2.1 Chemicals & Reagents	32
2.2 Synthesis of PH6-CDs	32
2.2.1 Microwave Assisted Synthesis	32
2.2.2 Purification of CDs	33
2.3 Model Drug Conjugation	33
2.3.1 Solution Based: Molecular Sieves	33
2.3.2 Solution Based: Dean-Stark	33
2.3.3 Solution Based: Unassisted Condensation	34
2.3.4 Solid State Reaction: Planetary Ball Miller	34
2.4 Characterization of Native and Conjugated CDs	34
2.4.1 Transmission Electron Microscopy (TEM)	34
2.4.2 Powder X-Ray Diffraction (PXRD)	34
2.4.3 X-Ray Photoelectron Spectroscopy (XPS)	35

2.4.4 Fourier Transform Infrared Spectroscopy Attenuated Total Reflects	ance (FTIR-
ATR)	35
2.4.5 Proton Nuclear Magnetic Resonance (¹ H-NMR) Spectroscopy	35
2.4.6 Ultraviolet-Visible (UV-Vis) Spectroscopy	35
2.4.7 Fluorescence (FL) Spectroscopy	36
2.4.8 Thermogravimetric Analysis (TGA)	36
2.4.9 Cytotoxicity Assay	36
2.5 Drug Release	37
Chapter 3. Results and Discussion	38
3.1 Characterization of PH6-CDs	38
3.1.1 Assessing Physical Properties	38
3.1.2 Assessing Chemical Properties	40
3.1.3 Assessing Optical Properties	43
3.2 Solution based conjugation of CDs	45
3.2.1 Molecular Sieves	45
3.2.2 Dean-Stark Trap	48
3.2.3 Unassisted Condensation	51
3.3 Mechanochemistry Based Conjugation	53
3.3.1 Imine Bond Formation	53
3.3.2 Drug Loading	64
3.3.3 Drug Release	66
3.3.4 Cytotoxicity	68
Chanter 4 Conclusions and Future Works	70

4.1 Concluding Remarks	70
4.2 Future Works	71
Chapter 5. References	72
Chapter 6. Appendix	83

List of Figures

Figure 1. Changes in surface area of a cube highlighting the effect of smaller particle sizes1
Figure 2. Suzuki-Miyaura cross coupling reaction scheme.
Figure 3. Schematic of the typical structure of CDs showing a two-part system consisting of a core
and surfaces decorated in many different functional groups. Adapted with permission from M
Jorns and D. Pappas, A Review of Fluorescent Carbon Dots, Their Synthesis, Physical and
Chemical Characteristics, and Applications, Nanomaterials, 2021, 11, 1448. Copyright 2021 M.
Jorns and D. Pappas, license: https://creativecommons.org/licenses/by/4.0/. ³⁰ 9
Figure 4. Image depicting the tunable fluorescence of CDs. Adapted with permission from C.
Kang et al., A Review of Carbon Dots Produced from Biomass Wastes, Nanomaterials, 2020, 10,
2316. Copyright 2020 C. Kang et al., license: https://creativecommons.org/licenses/by/4.0/. ³⁹ 11
Figure 5. Histopathological analyses of mice liver, spleen and kidneys showing no steatosis
necrosis or degeneration and easily distinguishable structures after intravenous exposure of CDs
(40mg/kg) for 4 weeks. Adapted with permission from ST. Yang et al., Carbon Dots as Nontoxic
and High-Performance Fluorescence Imaging Agents, The Journal of Physical Chemistry C, 2009
113, 18110–18114. Copyright 2009 American Chemical Society. ⁴³
Figure 6. Temperature gradients of microwave (left) versus oil bath (right) heating, clearly
depicting the homogeneous heat distribution of microwave irradiation whereas oil bath heating is
much more heterogeneous with the walls being heated first. Reproduced with permission
Copyright 2004 Wiley Online Library. ⁵⁰ 16
Figure 7. Peptide coupling reaction scheme involving EDC/NHS activation
Figure 8. Imine bond formation mechanism between an aldehyde/ketone and an amine group21
Figure 9 . Schematic representation of a Dean-Stark apparatus.

Figure 10 . Structural differences between a ketone molecule and an aldehyde molecule24
Figure 11. Images of common grinding and milling tools and machines. (A) Mortar and pestle.
(B) Planetary ball miller
Figure 12. Schematic representation of imine bond conjugation to the surfaces of CDs31
Figure 13 . TEM image of 500 μg/mL dispersion of PH6-CDs
Figure 14. PXRD of the solid crystalline citric acid precursor and the synthesized amorphous PH6-
CDs39
Figure 15. FTIR showing comparison of PH6-CDs relative to the starting materials41
Figure 16. ¹ H-NMR (300MHz, MeOH-D4) showing comparison of PH6-CDs relative to the
starting materials
Figure 17. UV-Vis spectra of PH6-CDs and synthetic precursors pentaethylenehexamine and citric
acid43
Figure 18. FL spectra of PH6-CDs and synthetic precursors pentaethylenehexamine and citric
acid44
Figure 19. FTIR carried out to study imine bond formation on the surfaces of PH6-CDs using 4
${ m A}^{\circ}$ molecular sieves (10 mg PH6-CDs, 5 mL acetone, 5 mL MeOH and 5 drops of 1M HCl, stirred
overnight at 50 °C under reflux)
Figure 20. 4 A° molecular sieve contamination. (A) image of the murky solution after an overnight
reaction containing shed sieve powder. (B) FTIR of the sieve powder47
Figure 21. FTIR carried out to study imine bond formation on the surfaces of PH6-CDs using a
Dean-Stark trap (40 mg PH6-CDS, 40 mg NAB, 50 mL toluene and 500 μ L 1M HCl, 110 $^{\circ}$ C
overnight, three 25mL acetone washes)
Figure 22. Chemical structure of NAB

Figure 23. H-NMR (300MHz, MeOH-D4) carried out to study imine bond formation on the
surfaces of PH6-CDs using a Dean-Stark trap (40 mg PH6-CDS, 40 mg NAB, 50 mL toluene and
500 μL 1M HCl, 110 °C overnight, three 25mL acetone washes)
Figure 24. FTIR carried out to study the unassisted formation of imine bonds on the surfaces of
PH6-CDs (20 mg PH6-CDs, 2mL MeOH, 500 μL 0.04M NAB solution (dissolved in MeOH) and
2 drops of 0.1 M HCl, 50 °C overnight, three 25mL acetone washes)
Figure 25. ¹ H-NMR (300 MHz, MeOH-D4) carried out to study the unassisted formation of imine
bonds on the surfaces of PH6-CDs (20 mg PH6-CDs, 2mL MeOH, 500 µL 0.04M NAB solution
(dissolved in MeOH) and 2 drops of 0.1 M HCl, 50 °C overnight, three 25mL acetone washes).
Figure 26. FTIR carried out to study the mechanochemical formation of imine bonds on the
surfaces of PH6-CDs (20 mg PH6-CDs, 40 mg NAB, three stainless steel 10 mm diameter beads,
30 minutes, 60 Hz, three 10 mL acetone washes)54
Figure 27. ¹ H-NMR (300MHz, MeOH-D4) carried out to study the unassisted formation of imine
bonds on the surfaces of PH6-CDs (20 mg PH6-CDs, 40 mg NAB, three stainless steel 10 mm
diameter beads, 30 minutes, 60 Hz, three 10 mL acetone washes)55
Figure 28. Chemical structure of VAN
Figure 29. FTIR carried out to study the conjugation of VAN to the surfaces of PH6-CDs (60 mg
PH6-CDs, 90 mg VAN, three stainless steel 10 mm diameter beads, 30 minutes, 60 Hz, three 25
mL acetone washes)
Figure 30. ¹ H-NMR (300MHz, MeOH-D4) depicting the formation of imine bonds when
mechanochemically conjugating VAN to the surfaces of PH6-CDs (20 mg PH6-CDs, 40 mg NAB,
three stainless steel 10 mm diameter beads, 30 minutes, 60 Hz, three 10 mL acetone washes)58

Figure 31. ¹ H-NMR (300MHz, MeOH-D4) highlighting the downfield region of the imine bonded
VAN model (20 mg PH6-CDs, 40 mg NAB, three stainless steel 10 mm diameter beads, 30
minutes, 60 Hz, three 10 mL acetone washes).
Figure 32. Schematic representation of imine bonded VAN to CDs
Figure 33 . ¹ H-NMR of ball milled PH6-CDs and ball milled VAN controls
Figure 34. PXRD carried out to assess the crystallinity of PH6-CDs after drug conjugation (20
mg PH6-CDs, 40 mg NAB, three stainless steel 10 mm diameter beads, 30 minutes, 60 Hz, three
10 mL acetone washes)
Figure 35. XPS Surface Elemental Composition Analysis of PH6-CDs before and after van
conjugation. (A) Survey scan for PH6-CDs. (B) Survey scan of VAN-CDS. (C) Deconvoluted high
resolution C1S spectrum of PH6-CDs. (D) Deconvoluted high resolution N1S spectrum of PH6-
CDs. (E) Deconvoluted high resolution O1S spectrum of PH6-CDs. (F) Deconvoluted high
resolution C1S spectrum of VAN-CDs. (G) Deconvoluted high resolution N1S spectrum of VAN-
CDs. (H) Deconvoluted high resolution O1S spectrum of VAN-CDs
Figure 36. TGA carried out to investigate drug loading. (A) TGA of native VAN-CDs before drug
conjugation. (B) TGA of VAN conjugated CDs. (C) TGA of VAN64
Figure 37. qNMR for the determination of a DLC. 27 mg VAN-CDs and 16.8 mg VAN-CDs
dispersed in 0.75mL MeOH-D4 containing 0.03% v/v TMS and 0.75 mL D ₂ O containing 0.05
wt.% TSP-D4 respectively65
Figure 38. Standard curve and release profiles. (A) calibration curve of VAN. (B) % cumulative
release of VAN from conjugated CDs at pH 7.4, 6.0 and 5.0
Figure 39. Resazurin cell viability assay of A549 lung cancer cells treated with PBS (control),
PH6-CDs. VAN-CDs and VAN.

List of Tables

Table 1. Non-exhaustive list of CDs synthesized through a bottom-up approach using common
carbon-based precursors. Adapted with permission from M. Jorns and D. Pappas, A Review of
Fluorescent Carbon Dots, Their Synthesis, Physical and Chemical Characteristics, and
Applications, Nanomaterials, 2021, 11, 1448. Copyright 2021 M. Jorns and D. Pappas, license:
https://creativecommons.org/licenses/by/4.0/. ³⁰
Table 2. Non-exhaustive list of CDs rapidly synthesized through a microwave assisted route.
Adapted from Microchemical Journal, 165, H. K. Melvin Ng, G. K. Lim, C. P. Leo. Comparison
between hydrothermal and microwave-assisted synthesis of carbon dots from biowaste and
chemical for heavy metal detection: A review, 106116, Copyright 2021, with permission from
Elsevier, DOI: https://doi.org/10.1016/j.microc.2021.106116. 52

List of Abbreviations

NM Nanomaterial

LSPR Localized Surface Plasmon Resonance

QD Quantum Dot CD Carbon Dot

MRI Magnetic Resonance Imaging

DOX Doxorubicin

TEM Transmission Electron Microscopy

AFM Atomic Force Microscopy

NAB Nabumetone

VAN Vanillin

EDC 1-ethyl-3-(3-dimethylaminopropyl) carbodiimide

NHS N-Hydroxysuccinimide

MeOH Methanol

CHCl₃ Chloroform

HCl Hydrochloric acid

DMEM Dulbecco Modified Eagle Medium

PBS Phosphate Buffered Saline

TEM Transmission Electron Microscopy

PXRD Powder X-Ray Diffraction

XPS X-Ray Photoelectron Spectroscopy

FTIR-ATR Fourier Transform Infrared Spectroscopy Attenuated Total Reflectance

¹H-NMR Proton Nuclear Magnetic Resonance Spectroscopy

UV-VIS Ultraviolet-Visible Spectroscopy

FL Fluorescence Spectroscopy

TGA Thermogravimetric Analysis

DLC Drug Loading Capacity

NSAID Non-Steroidal Anti-Inflammatory Drug

qNMR quantitative Nuclear Magnetic Resonance

TMS Tetramethylsilane

TSP-D4 3-(trimethylsilyl) propionic-2,2,3,3-D4 acid, sodium salt

MeOH-D4 Deuterated Methanol

D₂O Deuterium Oxide

Chapter 1. Introduction

1.1 Nanomaterials, Their Definition and Applications

1.1.1 What Are Nanomaterials?

A nanomaterial (NM) is described as a material, which is 1-100 nm in size in a single dimension.¹ To put this into perspective, the length of a nanometer is the equivalent of 10 hydrogen atoms lined up.² These small sizes typically lead to properties that are much different than their bulk form. Gold in the bulk form appears yellow whereas in the nanoscale it is actually purple or red. The magnetic behavior of materials may change as well. Bulk gold which is usually a noble metal is non-magnetic whereas gold nanoparticles exhibit considerable magnetism.³ Lastly, surface area to volume ratios of NMs tend to significantly increase relative to their bulk counterparts and can be explained by the rather simple analogy found in **Figure 1**.

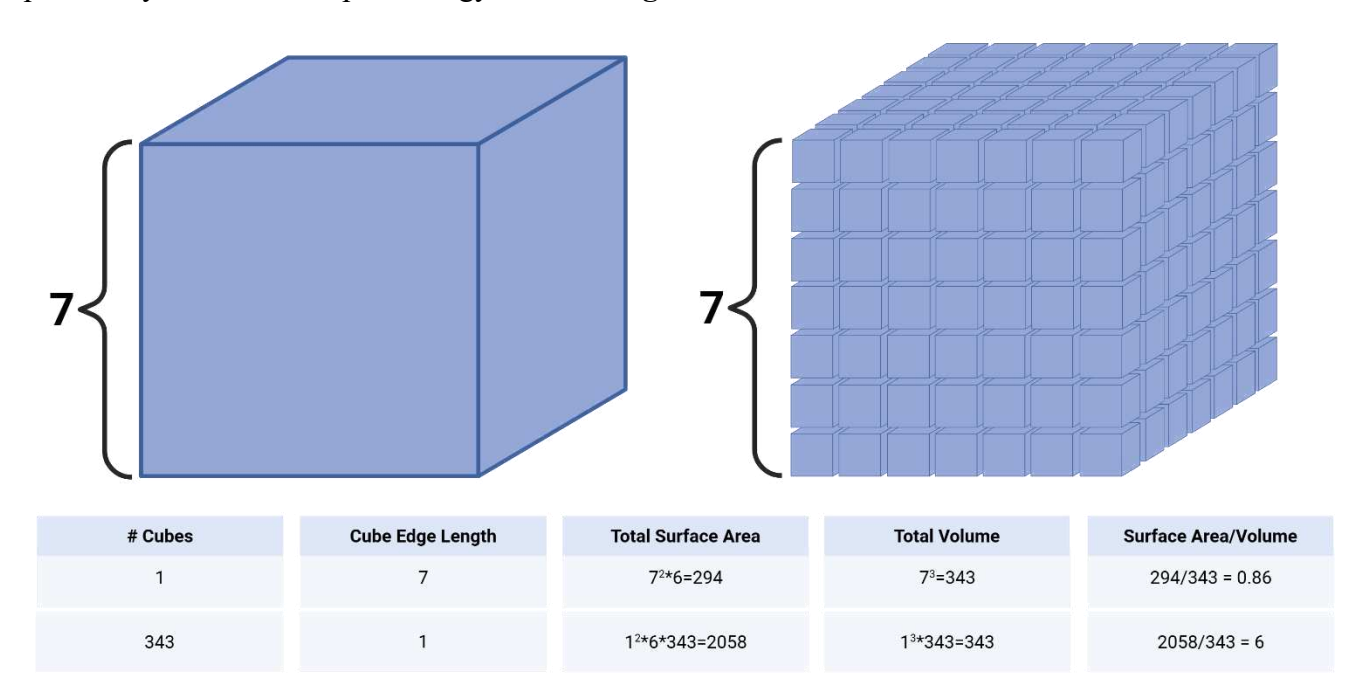


Figure 1. Changes in surface area of a cube highlighting the effect of smaller particle sizes.

As the bulk cube is divided into smaller parts the total volume remains unchanged whereas the surface area increases drastically. This same principle can be applied to NMs versus their bulk structures. The large surface area to volume increase is typically seen as a huge advantage in the nano world and is often the reason why they are applied to many fields such as catalysis, drug delivery and sensing.^{4,5}

NMs, which contain chemical functionalities that can catalyze chemical reactions, are often highly desired due to their increased surface areas and thus larger area of contact with reactant molecules leading to a greater number of possible interactions. This same logic can be applied to drug delivery, offering larger contact surfaces for drug loading, and to sensing offering the potential to sense more analytes due to increased interactions. NMs come in different sizes and shapes; many are spherical whereas some may be rod, or cube-shaped. They can also differ in chemical composition being either inorganic, or organic and may possess different surface charges. These different and unique properties can be fine-tuned, or completely altered depending on their desired application and is another reason why NMs have been at the forefront of modern research.

1.1.2 Catalysis

A catalyst can be either homogenous or heterogeneous existing in the same phase as the reagents, or in a separate phase, respectively. NMs often exist as heterogeneous materials due to the nature of their physical makeup. They are not small enough to be dissolved as is the case with small molecules, however, they are large enough to exist as solid dispersions which may appear as "dissolved" in a clear solution to the naked eye. Often these dispersions are quite stable and are given the name "colloidal suspensions". Colloidal suspensions are often described as a mixture containing two phases. One insoluble phase residing within a second continuous phase (usually the suspension medium). In all cases, NMs are typically not dissolved (taken apart from the bulk)

but are rather dispersed. Owing to their large surface area to volume ratios, NMs are highly researched for catalysis applications. Moreover, they can be easily recovered through filtration and can often be reused for multiple catalytic cycles. This is usually challenging when dealing with soluble homogeneous catalysts typically residing in the same phase as the reactants.⁶

Reactions that produce new carbon-carbon bonds can benefit largely from the presence of a NM heterogeneous catalyst. These reactions are widely regarded as crucial in terms of the production of fine chemicals. Traditionally these reactions are carried out using homogeneous palladium-based organometallic catalysts. A reaction schematic of the popular Suzuki-Miyaura coupling reaction can be found in **Figure 2**, widely known for its ability to couple an organoborane and an aryl halide typically proceeding via palladium-based catalysis.⁷

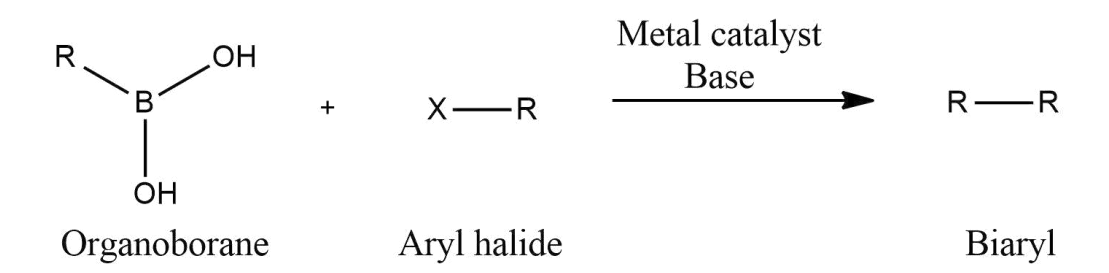


Figure 2. Suzuki-Miyaura cross coupling reaction scheme.

Palladium catalysis is extremely effective for Suzuki-Miyaura coupling reactions, allowing for many to proceed with yields greater than 90 % and catalyst loadings as small as 0.01 %. At the industrial scale, reactions employing these catalysts (often Pd) can bring about economic concerns. For this reason, research into recyclable nano-sized heterogenous catalysts has become quite popular in the past decade. It has been recently reported that formation of a hybrid NM with immobilized Pd on the surfaces of a carbon nanosphere can also allow for yields greater than 90 % while simultaneously allowing for the recovery of the catalyst. Recovery was possible through

centrifugation without any noticeable decrease in catalytic activity over the course of 5 reaction cycles.¹⁰

1.1.2 Sensing

NMs are also applied in the field of sensing due to their unique optical properties, which often display changes upon interactions with analytes. Noble metal NMs containing metals such as gold, or silver may exhibit a localized surface plasmon resonance (LSPR) effect. This causes conduction electrons near the surfaces of noble metal containing NMs to oscillate when excited by photons. 11 LSPR frequency is largely dictated by changes in the local dielectric environment, which can change in the presence of an analyte. These changes can either lead to a shift In LSPR peak wavelengths, or intensities, which can ultimately be related to the sensing of an analyte. 12 Depending on their structure and makeup, some NMs can also fluoresce. For instance, quantum dots (QDs), which are NMs typically less than 10 nm in size, can exhibit fluorescence which can be fine tuned by simply altering their sizes. This inherent fluorescence property can allow for their development as sensors by simply measuring changes to their fluorescence band in the presence of an analyte. Analytes can either quench or enhance the intensity of fluorescence, which can be directly related to their detection.

In addition to their unique optical properties, some NMs including carbon nanotubes and graphene can also conduct electricity. Changes in their electrical conductivities upon interaction with analytes can thus be measured and related to analyte concentration and detection. Some NMs can even catalyze electrochemical reactions involving analytes of interest to help in their detection. As an example, an electrochemical sensor formed using nanostructured platinum-palladium alloy can be used to catalyze the oxidation of formaldehyde. This oxidation reaction leads to changes in

electrochemical responses, such as potential changes, and can be used for detection of the original analyte.¹³

1.1.3 Bioimaging

Apart from chemical catalysis and sensing, NMs have also found their way into the realm of biological applications such as bioimaging. Bioimaging simply refers to viewing biological substances that have been fixed for the purposes of monitoring. ¹⁴ There are many ways in which bioimaging can be carried out including the use of optical and magnetic resonance imaging (MRI).

Optical imaging, a class of bioimaging makes use of photons to view different anatomical structures. As previously mentioned, several classes of NMs have different and unique optical properties such as the ability to fluoresce. This property means that we can allows researchers to use them in imaging living organisms, or cells. To achieve this, the NMs must be excited at a certain wavelength to observe their corresponding fluorescence. Often these excitation wavelengths should be approaching the near infrared region (NIR) to allow for good signal detection with minimal toxicity arising from the incident excitation source. While many small molecules can fluoresce and may be used for imaging (e.g. dyes), many offer numerous shortcomings such as photobleaching and the requirement for excitation wavelength ranges that are far from optimal. For this reason, fluorescent NMs are employed as they can be fine-tuned to address all these drawbacks. For instance, biocompatible erbium-based rare earth NMs have been functionalized with hydrophilic polymers bearing anti-bodies and used to clearly image crucial proteins in a mouse model of colon cancer at 1600 nm with a long luminescence lifetime of ~ 4.6 ms. 16

1.1.4 Drug Delivery

While some medication may be administered in their molecular forms, most medication is typically administered as formulations in combination with drug delivery vehicles to enhance their bioavailabilities. NMs are currently highly researched as drug delivery vehicles as they can provide many benefits such as longer circulation times within aqueous blood streams, better penetration across biological membranes and controlled release of medication. ¹⁷ A significant amount of NMs have either received approval by the Food & Drug Administration (FDA) or have progressed through various stages of clinical study. ¹⁸

As previously mentioned, many different types of NMs are employed for drug delivery. Dendrimers are described as nano sized materials with a core with a series of protruding symmetric branches. These branched sites act as bridges for drug conjugation and the large cavity found in the core can be tuned to control the release of encapsulated/conjugated cargo. They typically offer many advantages over non-nanosized delivery vehicles such as ease of surface modification and reproductive pharmacokinetic parameters. 19,20

Metal NMs can also be used in drug delivery. As an example, iron based NMs are often used for a targeted therapy approach as conjugated cargo can be released through the use of an external magnetic field due to the inherent magnetic properties of iron (II). FePt NMs residing inside polymer-based hydrogels can be triggered to release medication by a magnetic thermal heating event.¹⁷

Liposomes are another class of important NMs used for drug delivery. They are formed by using phospholipids to generate spherical particles whose membranes are formed by either a single layer or multiple bilayers. Doxil is reported as one of the first commercialized formulations of NMs and it takes advantage of a liposome to encapsulate Doxorubicin (Dox), a widely used

chemotherapeutic drug with many adverse side effects. Doxil allowed for the reduction of cardiotoxicity by limiting contact with cardiac tissue. Furthermore, Doxil was found to be superior in the treatment of ovarian cancer compared to other types of formulations highlighting the potential of NMs to change the course of modern medicine.²¹

1.1.5 Limitations

NMs are revolutionizing many aspects of modern science and are without a doubt a remarkable feet in scientific evolution, however, there do exist some challenges including complex syntheses involving multiple steps, metal precursors which can sometimes be toxic or expensive and the lack of surface functionalities, to name a few. It is in this regard that new NMs are constantly being researched and engineered in the hopes of addressing some of these limitations.

Of the many types of NMs currently being developed and researched, carbon dots (CDs) have emerged as a promising alternative, which can address many of the aforementioned drawbacks. Their synthesis is relatively straightforward and is carried out in a single pot without the need for multiple steps. Additionally, the precursors used during synthesis are carbon based without the introduction of any metals and are often derived from natural sources. Lastly, their surfaces are rich in many functional groups enhancing their surface reactivity which can be beneficial for many fields such a sensing and drug delivery. As such, researchers have realized the vast potential of CDs to improve upon current nanotechnologies and their use in various fields are currently being investigated.²²

1.2 Introduction to Carbon Dots

1.2.1 Their accidental discovery

CDs have garnered significant attention since their accidental discovery in 2004 by the Scrivens groups. ²³ Scrivens was interested in the arc-discharge synthesis of carbon nanotubes, a method by which carbon atoms are evaporated using hot plasma arc and high currents produced by opposing electrodes. ^{24,25} It was only after electrophoretic purification that his group discovered a fast-moving band containing a fluorescent impurity that separated into different colors under UV light. Due to their unique properties, these fluorescent carbon materials attracted the attention of many researchers and are now known as CDs after their definition was brought forward in 2006. ²⁶

1.2.2 Physical Properties

Various techniques have been used to probe the physical characteristics of CDs such as their sizes, their shapes, their surface charges and their atomic arrangements. Instruments such as transmission electron microscopy (TEM) have allowed researchers to visualize CDs at the nanoscale. The most common reporting is the fact that they are quasi spherical particles with diameters usually less than 10 nm. High quality TEM images of CDs are often difficult to obtain due to the fact that they are amorphous. The amorphous nature of CDs means that no lattice fringes can be observed by TEM, rendering them unable to diffract electrons translating to a more difficult task of visualization. Moreover, CDs are mostly composed of carbon and have poor electron density, ascribed to a lower atomic number Z, compared to inorganic NMs leading to images that are lacking in contrast.²⁷

Powder X-ray diffraction (PXRD), a common technique used to analyze the crystallinity of materials, is also often used in combination with TEM to assess the structure of CDs. The PXRD of CDs is most often consistent with that of an amorphous material. PXRDs of CDs typically lack

any Bragg's diffraction peaks and most often show an amorphous halo throughout, indicating that the materials lack any sort of long-range repeating order.²⁸ It is however common to observe a broad reflection at ~25 °2θ associated with the graphitic structure of CDs.^{28,29} CDs are said to be comprised of two important regions namely a core and a surface. The cores of CDs are thought to be mostly comprised of graphitic structures with a dominance of sp² hybridized carbon atoms and would explain the broad reflection that is often seen at 25 °2θ. The surfaces of CDs are said to be composed of many organic functional groups usually dependent on the precursors used for synthesis which is substantially different than the makeup of their graphitic cores.

1.2.3 Chemical Properties

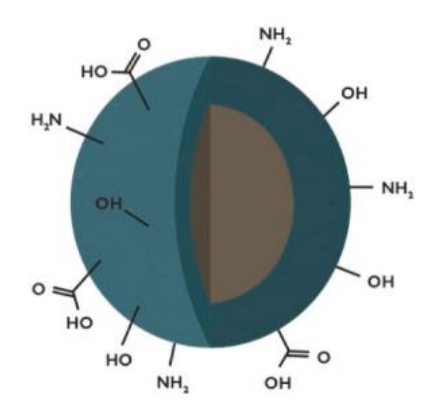


Figure 3. Schematic of the typical structure of CDs showing a two-part system consisting of a core and surfaces decorated in many different functional groups. Adapted with permission from M. Jorns and D. Pappas, A Review of Fluorescent Carbon Dots, Their Synthesis, Physical and Chemical Characteristics, and Applications, Nanomaterials, 2021, 11, 1448. Copyright 2021 M. Jorns and D. Pappas, license: https://creativecommons.org/licenses/by/4.0/. 30

The surfaces of CDs are composed of many different types of organic functional groups which include carboxylic acids, amines, amides, ketones and alcohols, among many others.³¹ A schematic representation of quasi spherical CDs with surface functional groups can be found in **Figure 3**. These surface functional groups are at the core of many unique properties that CDs can offer. For

instance, many of these functional groups are either electrophilic, or nucleophilic in nature, which can allow for facile conjugation with molecules such as drugs, targeting ligands, anti-bodies, polymers, among many others.^{32–34}

The chemical functional groups of CDs are often charcaterized through a variety of different techniques such as Fourier-transform infrared attenuated total reflectance (FTIR-ATR) spectroscopy, proton nuclear magnetic resonance spectroscopy (¹H-NMR) and x-ray photoelectron spectroscopy (XPS). FTIR provides information based on molecular vibrational frequences such as stretches and bends to relay information on the types of functional groups present. While usually a first line technique due to ease of use and quick analysis times, FTIR is usually limited to providing qualitative results. Nonetheless, FTIR has been used to confirm the presence of a wide range of surface functional groups for CDs.³⁵

¹H-NMR is often used to further describe the chemical environment and make up of the dots. This technique focuses on the proton nucleus due to its resonance when exposed to a magnetic field. ¹H-NMR will often confirm the presence of protons attached to aldehydes when chemical shifts are found between 9-10 ppm. Imine functional groups can also be observed when singlets are observed between 7.5-8.5 ppm. Aromatic systems or conjugated alkene containing systems are often present when multiplets are found between 6.5 – 8 ppm and 4.5 – 6.5 ppm respectively. Furthermore, up field chemical shifts usually confirm the presence of alkane protons or protons that are neighboring other functional groups such as ketones, alcohols and amines.³⁶

Lastly XPS, can be used to confirm the presence of certain functional groups based on their respective binding energies, as well as describe the nature of the chemical environment. Briefly, XPS measures the binding energy of electrons ejected after the surface is irradiated with a monochromatic X-ray beam and thus is a surface sensitive technique widely applied to studying

chemical functionalities in NMs including CDs. The binding energy measured can be directly correlated to which atom it originated from, as well as its mode of chemical bonding (functional group). A combination of two or more of these mentioned techniques are often used to ensure a thorough understanding of the chemical makeup of the surfaces of CDs.

1.2.4 Optical Properties

CDs have many interesting physical and chemical properties but amongst them also exists unique optical properties such as fluorescence. Most functional groups on the surfaces of CDs may exist in many different oxidation states and many have π -bonded electronegative atoms allowing for n to π^* transitions. Many researchers attribute this as the main reason behind CDs fluorescence. Surface oxidation can also create many surface defects and lead to various emission sites.^{37,38} The more surface defects that exist, the more excitons (electrons or holes) can be trapped and radiation from the recombination of these trapped excitons can lead to fluorescence.³⁷ Interestingly, by tuning the surface functional groups and/or their degree of surface oxidation, this can lead to shifted emissions and thus the color of fluorescence can also be tuned (**Figure 4**).

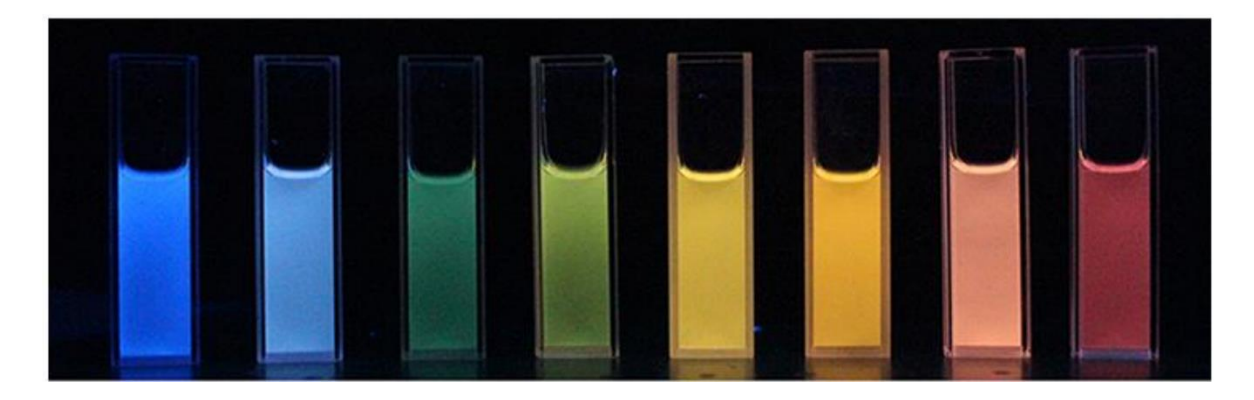


Figure 4. Image depicting the tunable fluorescence of CDs. Adapted with permission from C. Kang et al., A Review of Carbon Dots Produced from Biomass Wastes, Nanomaterials, 2020, 10, 2316. Copyright 2020 C. Kang et al., license: https://creativecommons.org/licenses/by/4.0/. 39

The cores of CDs are just as important in dictating the observed fluorescence. The extended π conjugation of the cores allows for electron delocalization over a larger region and a smaller band gap between the conduction and valence bands, all facilitating fluorescence. By altering their sizes, then the region of π conjugation originating from the core will also change and thus fluorescence may also be tuned in this manner (**Figure 4**). Furthermore, while the surfaces and cores of CDs are mostly viewed as two separate entities, many researchers believe a synergistic effect may also be at play between both states. Briefly, the π electron domain may couple with electronic surface states further altering the overall electronic structure and further decreasing the band gap.⁴⁰

1.2.5 Toxicity of CDs

CDs have been generally found to exhibit low toxicities in biological model systems. Researchers have attributed this to the nature of their non-toxic precursors. For the most part, CDs are synthesized using non-toxic materials often derived from natural sources, which many believe to be a reason for their inherently low cytotoxicities. All Recently it's been shown that amine passivated citric acid-derived CDs exhibit low cytotoxicity in both HeLa (human cervical carcinoma) and HFF-1 (human foreskin fibroblast) cells. In the work by Clermont-Paquette et al., each cell line was treated with increasing concentrations of CDs up to 10,000 µg/mL. It was found that some of the CDs reach an IC₅₀ (concentration at which half the cell population die) in both cell lines after 7,500 µg/mL while most never reach this threshold even when treated with 10,000 µg/mL.

Although rare, some biocompatibility studies were also performed to assess the toxicity of CDs in living organisms. Research studies focused on the bioimaging capabilities of CDs have been conducted *in vivo* using mice models to ensure no toxic effects are observed at the concentrations needed for bioimaging. Yang et al. have injected mice intravenously at doses of 40

mg/kg and found that there were no noticeable toxic effects on the mice. They noted that the CDs accumulated in some essential organs including the liver, spleen and kidneys, however, the levels of accumulation were noted to be low, and the CDs were cleared through the renal pathway after 24 hours. The researchers noted no clinical symptoms even after 4 weeks post-administration. Furthermore, the structure of organs of the treated mice were no different than those from a control group treated with a saline solution (**Figure 5**).⁴³

While these results suggest that CDs exhibit high biocompatibility and low cytotoxicity, more studies need to be conducted to ensure that this applies to more complex biological systems and ultimately to humans as well. Most of these studies are performed using animal models such as mice or nematodes, however, their behavior inside of the human body remains widely unknown. Many studies do however show that these NMs are widely accepted by many human cell lines and thus show great promise as being biocompatible within our bodies.

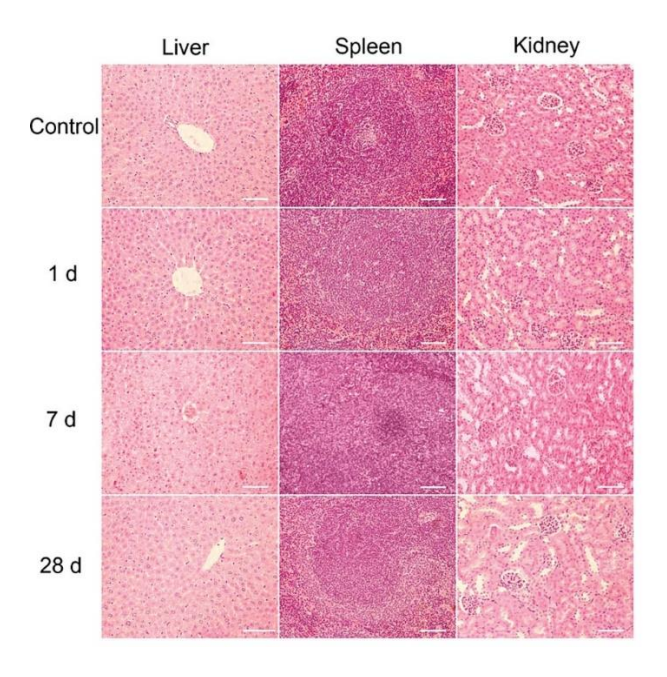


Figure 5. Histopathological analyses of mice liver, spleen and kidneys showing no steatosis necrosis or degeneration and easily distinguishable structures after intravenous exposure of CDs (40mg/kg) for 4 weeks. Adapted with permission from S.-T. Yang et al., Carbon Dots as Nontoxic and High-Performance Fluorescence Imaging Agents, The Journal of Physical Chemistry C, 2009, 113, 18110–18114. Copyright 2009 American Chemical Society.⁴³

1.2.6 Synthesis of CDs

Table 1. Non-exhaustive list of CDs synthesized through a bottom-up approach using common carbon-based precursors. Adapted with permission from M. Jorns and D. Pappas, A Review of Fluorescent Carbon Dots, Their Synthesis, Physical and Chemical Characteristics, and Applications, Nanomaterials, 2021, 11, 1448. Copyright 2021 M. Jorns and D. Pappas, license: https://creativecommons.org/licenses/by/4.0/. 30

Carbon Precursor	Solvent	Synthesis Technique
Citric acid	Formamide	Solvothermal
Malic acid	Water	Microwave
Citric acid	Dimethylformamide	Solvothermal
Citric acid	Water	Microwave
Sucrose	Nitroso or nitrobenzene	Solvothermal
p-Phenylenediamine	Water	Hydrothermal
Folic acid	Water	Hydrothermal
Milk	Water	Hydrothermal

Synthesis of CDs has been reported using two main routes, which can be categorized as either a bottom-up, or top-down. A bottom-up approach relies on the preparation of CDs starting from much smaller molecular precursors such as citric acid, malic acid, urea and many others. Alternatively, a top-down approach makes use of breaking down larger carbon materials such as carbon nanotubes, graphene and graphite into smaller structures. While both routes can generate CDs, the bottom-up approach is often preferred due to it being more environmentally friendly, less time consuming, while offering more control over the surface composition of the synthesized CDs.

Each route can be further divided into different techniques. For example, the more preferred bottom-up approach can be carried out using hydrothermal, solvothermal, or microwave syntheses.³⁰ **Table 1** summarizes several types of CDs, which have been synthesized through a bottom-up approach using common carbon-based precursors.

The hydrothermal synthesis technique is widely used to achieve a bottom-up synthesis and is simply classified as a synthesis performed in an aqueous solution at high temperatures and pressures, often requiring a high-pressure reactor. A solvothermal approach is similar to that of its hydrothermal counterpart in the sense that reactions are also often carried out at high temperatures and pressures with the assistance of a pressure reactor, however, the solvent used is not aqueous, but rather an organic solvent such as nitrobenzene, formamide and dimethylformamide as seen in **Table 1**. While hydrothermal and solvothermal pathways have all been shown to be useful techniques to synthesize CDs, they often suffer from long reaction times often on the time scale of many hours to days. This makes these synthetic routes less eco-friendly due to the need for high energy consumption, however, microwave assisted pathways come to light as a more interesting alternative.

1.2.7 Microwave Assisted Synthesis

Microwave synthesis dates to 1986 where organic chemists at Laurentian University discovered that many organic reactions are significantly faster when irradiated with microwaves. ⁴⁹ They found that the esterification of methanol with benzoic acid would typically occur over 8 hours, however, when the samples were irradiated with microwaves, the reaction only required 5 minutes, a drastic 96-fold increase in reaction rate. Additionally, they discovered that an S_N2 reaction involving 4-cyanoperoxide ion and benzyl chloride could be completed in 4 minutes under microwave irradiation compared to 16 hours when synthesized classically. ⁴⁹

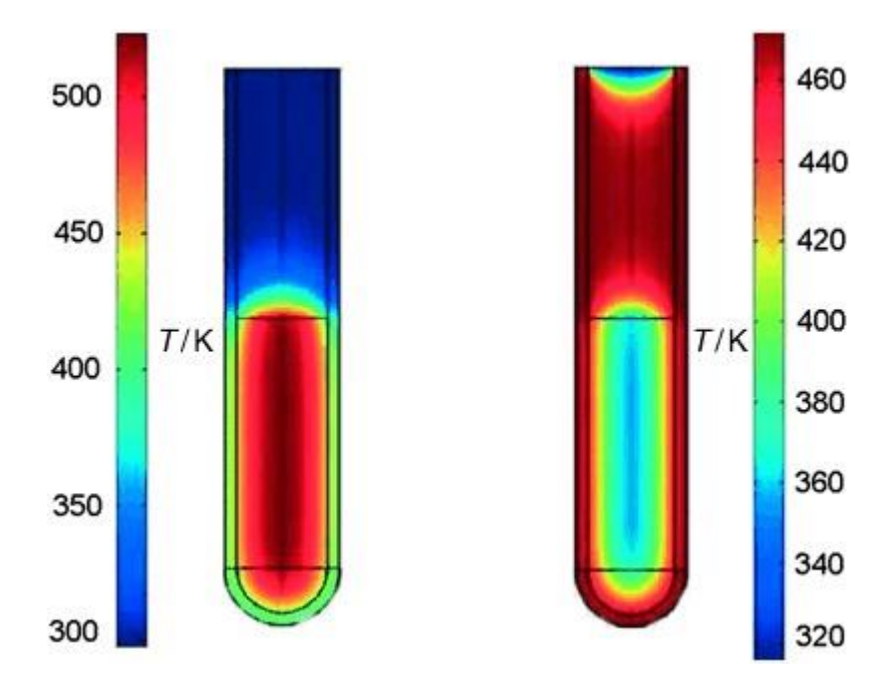


Figure 6. Temperature gradients of microwave (left) versus oil bath (right) heating, clearly depicting the homogeneous heat distribution of microwave irradiation whereas oil bath heating is much more heterogeneous with the walls being heated first. Reproduced with permission, Copyright 2004 Wiley Online Library.⁵⁰

The success of microwave irradiation compared to conventional methods stems from its ability to heat a given medium from the inside out rather than outside in (Figure 6). This simply means that conventional methods often use a heat source such as a hotplate to provide heat to a given vessel. In doing so, heat is transferred through conduction resulting in heterogenous energy distribution. Often the peripheries of the vessel are much hotter than the center due to thermodynamics and the laws of heat transfer. This may often lead to incomplete reactions or the formation of unwanted species due to side reactions which might be competing. Microwave irradiation allows for a more homogenous distribution of heat as the walls of reaction vessels are not at play. Energy from the microwaves is directly absorbed by the solvent and reactants in the solution mixture. Molecules, which have an electric dipole moment, will rotate in the alternating electric field as they continuously attempt to realign themselves, generating heat. As such the

molecules themselves are the sources of heat rather than relying on heat transfer from the walls into the center of the vessel translating to a much more efficient synthesis (**Figure 6**).⁵¹ While organic chemists were one of the first to pioneer microwave assisted chemical synthesis, materials researchers were quick to adapt microwave irradiation for the synthesis of many materials including CDs. A non-exhaustive list of CDs synthesized through microwave assistance can be found in **Table 2**, and highlights the short timescales required for such syntheses.

Table 2. Non-exhaustive list of CDs rapidly synthesized through a microwave assisted route. Adapted from Microchemical Journal, 165, H. K. Melvin Ng, G. K. Lim, C. P. Leo. Comparison between hydrothermal and microwave-assisted synthesis of carbon dots from biowaste and chemical for heavy metal detection: A review, 106116, Copyright 2021, with permission from Elsevier, DOI: https://doi.org/10.1016/j.microc.2021.106116. So

Carbon Precursor (s)	Time (min)	Power (W)
Citric acid	5	450
Citric acid	5	550
Citric acid	5	550
Thiomalic acid	7	700
Phthalic acid	3	700
Levodopa	1	700
Glucose	1	100

1.3 CDs as Drug Delivery Tools

1.3.1 Current Systems

Drug delivery has become a widely researched field due to the ability of vehicles such as NMs to improve upon the efficacy of an administered therapeutic by improving their solubilities, circulation times, controlling their release and enhancing their bio availabilities. 53–55 CDs are no exception and have been researched extensively since their discovery as potential drug delivery vehicles. In one instance, CDs have been investigated for anti-microbial drug delivery where researchers conjugated the dots with metronidazole, an FDA approved therapeutic used to treat *Trichomonas* infection, *P*orphyromonas *gingivalis* and amebiasis (an infection in the gastrointestinal system). 56,57 Wang et al. recognized the potential for CDs to improve upon penetration into the host cells of pathogens, a limitation that most antibiotics suffer from, especially with eukaryotic cells. 58 The drug conjugated CD complex revealed high cellular internalization and enhanced antibacterial activity against *P*orphyromonas *gingivalis* using oral epithelial cells (H413 cells). Furthermore, at the lowest concentration tested (0.26 µM metronidazole), the conjugated CDs inhibited bacterial growth by 72 % more than metronidazole alone, depicting how CDs can be used to improve upon the efficiency of anti-biotic drug delivery. 59

CDs have also shown potential as drug delivery tools to improve upon cancer treatments. Paclitaxel (PTX), is widely regarded as one of the most effective chemotherapeutics for solid tumors due to its ability to cause mitotic arrest and cell death. While extremely effective, this chemotherapy suffers from many drawbacks such as poor water solubility and severe toxicity. To address these challenges, Gomez et al. have conjugated PTX to CDs synthesized from a microwave assisted approach utilizing arginine as a carbon based precursor. Their main finding highlighted that the drug conjugated CDs were much more effective in treating cervix carcinoma cells (C33-A) than PTX alone. They observed an IC50 when the cells were treated with 930 ng/mL of conjugated CDs compared to 2820 ng/mL for PTX alone. While the concentrations used are rather large for drug delivery applications, these findings can potentially extend to lower concentrations applicable for drug delivery and improve upon the required dose of PTX. Moreover,

since CDs are also highly aqueous dispersible, they offered a means to improve upon the solubility issues of PTX.⁶²

1.3.2 Functionalization Strategies

Association of therapeutics to NMs including CDs is typically achieved via two primary pathways namely covalent and non-covalent modification. Briefly, covalent modification involves a newly formed chemical linkage between the therapeutic agent and the CD, while a non-covalent association relies on physical interactions such as hydrogen bonding and/or electrostatic means.³¹ Both methods are highly dependent on the chemical properties of the CDs. Depending on the reactivity of the surface functional groups, different covalent linkages/physical interactions can be achieved.

Non-covalent interactions such as electrostatic interactions, or hydrogen bonding can be used to load organic molecules on the surface of CDs. Zeng et al. have recently developed green emitting CDs via a one-step microwave assisted synthesis to load DOX on their surfaces via electrostatic interactions/hydrogen bonds.⁶³ The authors claimed that this is achieved via the carboxylic acid functionalities on the CD surface, which interact with the terminal amine groups of DOX. Furthermore, their delivery system was tested *in vivo* in HepG2 tumor-bearing mice. The mice were treated intravenously with the drug-loaded CDs and the highest concentration of CDs were localized in the tumor when compared to other essential organs such as the liver, spleen, kidneys, heat and lungs. This was attributed to the enhanced permeability and retention effect of the dots.⁶³ This is plausible as solid tumors present larger fenestrations between endothelial cells allowing for NMs to easily pass through compared to healthy cells.⁶⁴ Zeng et al. also found that the tumour volume shrunk by 50 % after 72 hours when treated with the drug-loaded CDs in

comparison to a reduction of 30 % when treated with only DOX, highlighting the benefits of employing a NM for drug delivery.

While non-covalent interactions can be used, the most common linkage between a drug and a CD is through a covalent amide bond. Peptide coupling or amide coupling involves a carboxylic acid and an amine group. Depending on the chemical nature of the precursors used, CDs typically will have abundant carboxylic acid, or amine functional groups on their surfaces making this method of conjugation facile and efficient. A typical amide coupling reaction is carried out using EDC and N-Hydroxysuccinimide (NHS). These reagents lead to the activation of carboxylic acids which can then react with amine groups to ultimately form amide bonds (**Figure** 7).⁶⁵

Figure 7. Peptide coupling reaction scheme involving EDC/NHS activation.

An example of this bond being utilized in the conjugation of therapeutic agents to CDs can be depicted in the work of Hettiarachchi et al.⁶⁶ The researchers conjugated three molecules to the CD surface via amide bonds using EDC/NHS coupling to improve the treatment of brain tumors. While most vehicles suffer from increased sizes post drug loading, the researchers found that CDs are sufficiently small that the size barely increased from ~1.5 nm to ~3.5 nm post conjugation. Transferrin, a targeting ligand along with epirubicin and temozolomide, both anti-cancer agents, were covalently attached through peptide coupling reactions via carboxylic acids on the surfaces of CDs. They found that their triple conjugated system was much more cytotoxic to SJGBM2

glioblastoma brain tumor cells than the free drug. Cell viability decreased from >80% at a concentration of 0.01 μ M epirubicin and 1 μ M temzolomide to <20% after treatment with 0.1 μ M of the triple conjugated CDs, a drastic change in cytotoxicity. While these findings suggest great potential in the use of amide coupled drugs, it should be noted that none of the therapeutic molecules were released from the delivery vehicle, which could potentially affect therapeutic activity if the active site of the drug is altered during conjugation. Furthermore, the amide linkage is typically non-reversible and difficult to cleave, which can also hinder the release of medication in cases where release from the vehicle is needed. It is in this regard that imine bonds offer a promising alternative as cleavable covalent bonds.

1.4 What is an Imine Bond?

1.4.1 Equilibrium Reaction

$$R_{2}/H$$
 R_{2}/H
 R_{3}
 R_{1}/H
 R_{2}/H
 R_{3}/H
 R_{3}/H
 R_{4}/H
 R_{5}/H
 R_{1}/H
 R_{2}/H
 R_{3}/H
 R_{4}/H
 R_{5}/H
 R_{1}/H
 R_{2}/H
 R_{3}/H
 R_{4}/H
 R_{5}/H

Figure 8. Imine bond formation mechanism between an aldehyde/ketone and an amine group.

An imine bond is a covalent bond which can be formed through a reaction involving a carbonyl group and a primary amine often in the presence of an acid catalyst. The carbonyl group originates

from either a ketone, or aldehyde functional group and acts as the electrophilic site for a nucleophilic attack by a primary amine. Imine bond formation is known as a condensation reaction with water produced as a by product. Additionally, it is an equilibrium reaction and water is often removed during imine bond formation to drive the equilibrium in the forward direction.⁶⁷

The reaction begins with a nucleophilic attack onto the electrophilic carbon atom of the carbonyl originating from the lone pair on the amine group. This results in the formation of a zwitterion which can then undergo a proton transfer directly from the positively charged nitrogen atom onto the negatively charged oxygen atom. The next step occurs at the same time forming a new C-N bond in a concerted fashion because of bond rearrangement. Water is generated as a by product and the C=N imine is formed (**Figure 8**).⁶⁷ As previously mentioned water is typically removed during such reactions due to Le Chatelier's principle, which states that when a dynamic equilibrium is disturbed then the equilibrium will shift to counteract that change.⁶⁸ Water being a formed by product will lie on the right hand side (product side) of the equilibrium and if actively removed; the equilibrium will shift to try and regenerate the missing water, at the same time generating more imine product. Many procedures can be employed to actively remove water during synthesis with two of the most commonly used techniques involving the use of molecular sieves which have a high affinity for water, or azeotropic distillation using a dean-stark trap.⁶⁹

The use of molecular sieves is quite straight forward requiring simple activation of the material by heating under vacuum to remove any guests in the pores followed by addition to the reaction flask to actively adsorb and remove produced water. The use of azeotropic distillation is a more complex process and involves the use of a dean-stark trap. An azeotrope is described as a combination of chemicals whose ratio of constituents in the vapor phase is the same as in the liquid phase. ⁷⁰ In other words, both chemicals can be distilled together and there is no temperature, which

preferentially distills one chemical over the other. This concept is key to understanding how the dean stark trap works. The solvent chosen must form an azeotrope with water and must be immiscible with water. The azeotrope is then distilled meaning that both water and the second solvent will condense simultaneously onto a reflux condenser and collect into the dean stark trap. The chosen solvent is usually toluene as it is less dense than water and will accumulate on the top layer causing water to be forced into the bottom of the trap. The toluene will then spill back over and re-enter the reaction flask essentially leaving behind water at the bottom of the trap effectively removing it from the ongoing synthesis (**Figure 9**).⁷¹

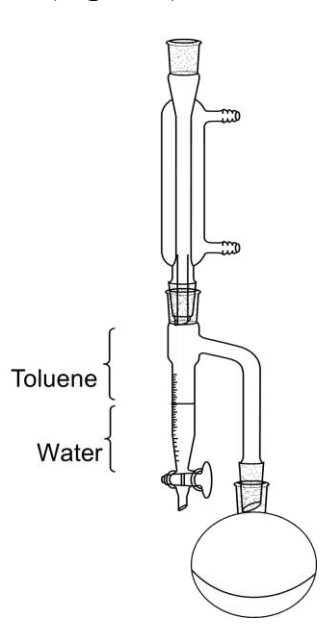


Figure 9. Schematic representation of a Dean-Stark apparatus.

1.4.2 Ketones

Carbonyl groups are a requirement for imine bond formation and ketones are a class of carbonyl containing functional groups. Ketones are generally less reactive than aldehyde molecules due their inherent larger steric hindrance and lower polarizability. Ketones have two substituents on the carbonyl carbon compared to one for aldehydes (**Figure 10**), rendering an approach from a nucleophile difficult due to greater steric hindrance⁷². Electronically, the carbonyl carbon atom of

a ketone has a partial positive charge which is more stable due to two adjacent carbon containing electron donating groups whereas the aldehyde's partial positive charge is less stable and therefore more reactive due to the presence of only one adjacent group.⁷² Seeing as they are often described as being much less reactive than aldehyde groups, ketones are used less frequently for the formation of imine bonds.⁷³

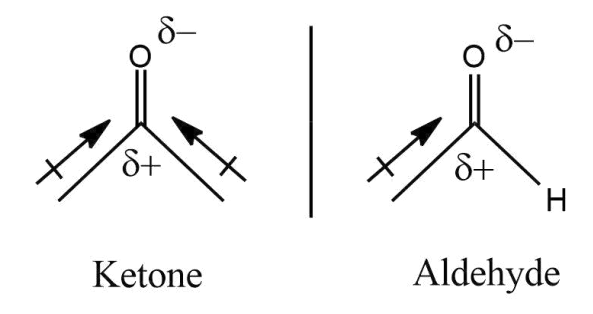


Figure 10. Structural differences between a ketone molecule and an aldehyde molecule.

Nonetheless, the use of ketones to form imine bonds is still possible and often requires the use of a catalyst. Yadav et al. have recently shown that novel quinoline-based derivatives can be synthesized via an imine intermediate synthesized from a ketone precursor. Further functionalization of the quinoline scaffold is of particular importance due to the formation of numerous derivatives which are pharmacologically active.⁷⁴ The authors described the use of HCl as a catalyst to react the ketone of the starting quinoline with the primary amine compound, p-toluidine with yields of 70-80 %.⁷⁵

1.4.3 Aldehydes

Aldehyde functional groups are often more reactive and used more frequently in the synthesis of imine bonds. Since the carbonyl group is more accessible, aldehydes tend to be more susceptible to nucleophilic addition reactions. One of the best examples of this would be a Grignard reaction allowing chemists to form new carbon-carbon bonds.⁷⁶ A typical Grignard reaction involves the

nucleophilic addition of an organomagnesium compound (Grignard reagent) to carbonyl groups such as aldehydes.⁷⁷ Oxidation of aldehydes into their corresponding alcohols also includes a nucleophilic addition step and is another important reaction allowing chemists to utilize the generated alcohols as building blocks for further reactions such as esterification reactions. All in all, nucleophilic addition reactions are important for generating novel compounds and aldehydes are generally considered to be good starting materials.

In what concerns imine synthesis, a nucleophilic addition of an amine to the carbonyl group is essential as shown in Figure 8. An example of an aldehyde being used as a starting material for imine synthesis can be shown in a study conducted by Heigl et al. 78 The researchers employed imine donors chelated through alkylidene groups to synthesize a series of ruthenium-based metathesis catalysts. The syntheses of such catalysts are important as they are employed in the use of olefin metathesis and allow for the generation of new carbon-carbon bonds.⁷⁸ In order to synthesize the imine ligands, simple condensation reactions involving aldehydes and primary amines were carried out. One particular synthesis discussed in this work proceeds via the use of activated molecular sieves to drive the equilibrium towards the generation of product (imine) in dichloromethane for 12 hours resulting in a yield of 57 %. ⁷⁸ While no acid catalyst was used in the transformation, sieves were employed as the generation of imine bonds can be difficult without the use of a dehydrating agent even with aldehyde starting materials. Dehydration using sieves or a Dean-Stark trap does however come with some challenges. Molecular sieves shed zeolite powder into solution, which is difficult to remove, and the Dean-Stark trap is limited by a certain number of solvents that can be used and thus solubility challenges arise. For this reason, solvent free approaches such as mechanochemistry are being investigated as interesting alternatives for carrying out condensation reactions.

1.5 Mechanochemistry

1.5.1 Solid State Chemistry

Synthetic chemistry is often thought about in terms of solid reactants, which are dissolved, or dispersed in a given solvent to drive their chemical transformation. Solvation allows for reagents to be taken apart from their bulk structures and to react more efficiently. An input of energy is often required in addition to a solvent in order to cross the activation energy barrier of a given chemical reaction. This energy is typically administered by heating the reaction mixture, however, heat is not the only form of energy that exists. It has been found that mechanical energy can also be used to provide sufficient energy to drive chemical reactions in the solid state.

Mechanical energy refers to physical forces exerted on materials to induce chemical transformation. The remarkable aspect of such energy is that solvation is not required. This is generally considered to be advantageous as the avoidance of organic solvents can render the chemistry greener. Furthermore, choosing an appropriate solvent can also be a daunting task as reagents will have different solubilities depending on their chemical makeup. Some solvents may be more polar than others and some may be capable of hydrogen bonding while others are not. All of these properties will dictate whether a solvent can solvate a given molecule. In the solid state, such complexities do not exist as mechanical energy from friction and shearing forces can be exerted without a solvent. ⁷⁹ In 1891, the term mechanochemistry was first introduced by a Latvian chemist, Wilhelm Ostwald in his "Textbook of General Chemistry" and later a mechano-chemical reaction was defined by IUPAC as a "chemical reaction that is induced by the direct absorption of mechanical energy". ^{80,81} Mechanical energy can be generated manually with tools such as a mortar and pestle, or with the aid of a planetary ball miller.

1.5.2 Grinding and Milling

Grinding and milling of reagents in the solid state allows for the generation of mechanical energy. The most accessible tools to grind solid reactants are a mortar and pestle (**Figure 11A**). Briefly, the mortar is defined as a solid bowl typically made of agate, granite or porcelain and will house the reagents, while the pestle is the grinding apparatus often made from similar materials. ⁸² The strength and speed of the pestle grinding the reagents together will ultimately dictate reaction kinetics and thus the success of these tools to achieve a chemical transformation. As a result, grinding of reagents using the mortar and pestle is heavily reliant on the operator and thus can lead to reproducibility issues among users. Furthermore, the manual grinding process can be quite labour intensive for reactions which require extensive reaction times.

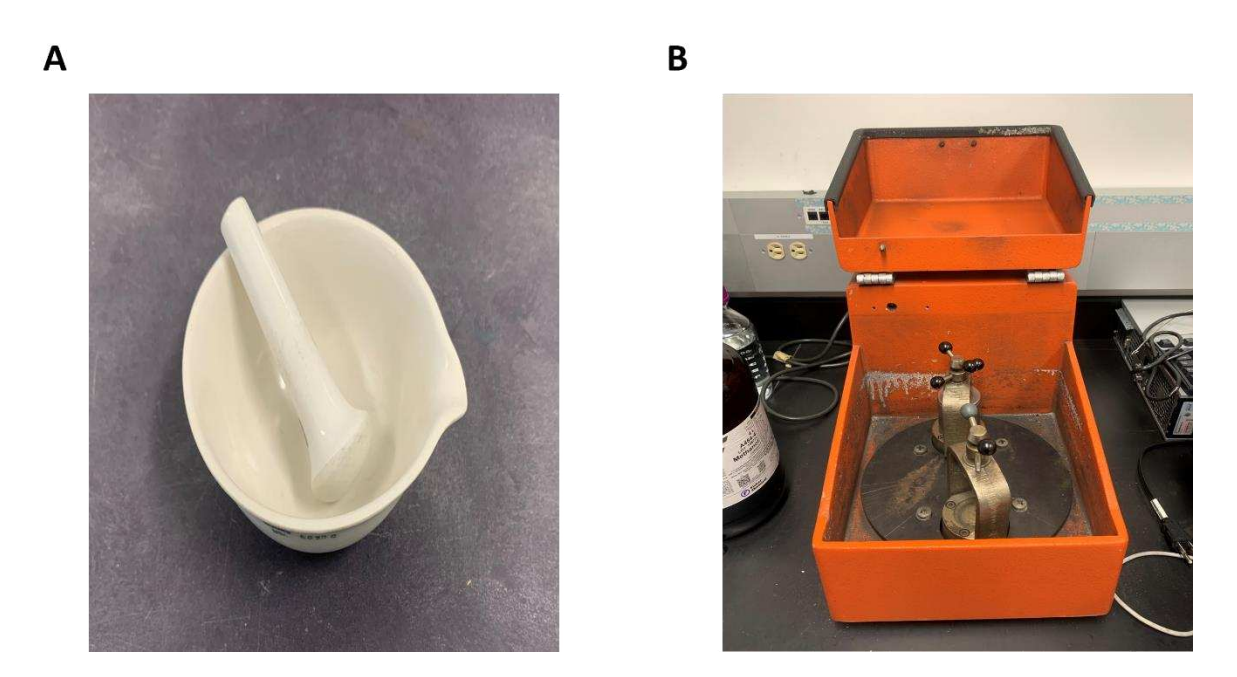


Figure 11. Images of common grinding and milling tools and machines. (A) Mortar and pestle. (B) Planetary ball miller.

To address this challenge, automated machines such as the planetary ball mill (**Figure 11B**) have been developed. Planetary ball mills have 2 or 4 pots which can hold milling jars containing starting materials and milling media. These pots are directly mounted on a rotating disk while the pots themselves can rotate around their own axis. The machine can generate high rotational speeds for both the rotating disk and pots allowing the milling media to collide with starting materials and generate mechanical energy.⁸³ The mechanical energy generated can be ascribed to many forces that are experienced during the milling process with the most common being impact, shear and centrifugal forces.⁸³ The summation of such forces directly results in the total energy provided to drive chemical reactions in the forward direction. Moreover, this approach addresses reproducibility issues that manual grinding may introduce and is thus more often used in modern synthesis.

1.5.3 Covalent Bond Formation

The remarkable aspect of mechanochemistry is its ability to efficiently form covalent bonds. It has been recently shown by Espro et al. that the previously discussed Suzuki-Miyaura cross coupling reaction can be improved with the use of mechanochemistry. 1,2-dibromobenzene was coupled to 4-(dimethylamino)-phenylboronic acid and many other arylboronic acids to selectively form monoarylated products in high yields whereas traditional solution-based syntheses resulted in diarylated products. The authors attributed this mechanochemically induced selectivity to a low diffusion efficiency of the crystalline monoarylated product in the reaction mixture formed with the liquid brominated starting material. It should be noted that while solids mostly dominate in the field of mechanochemistry, starting materials may also be milled in the liquid form. These findings highlighted mechanochemistry as a force of synthesis able to efficiently couple common

molecular building blocks in a selective manner that has otherwise not been reported using traditional methodologies.

Mechanochemistry can also be used to generate amide bonds, a very important covalent bond naturally occurring in the backbones of polypeptides and proteins. ⁸⁶ The amide bond is also found extensively in the skeleton of many artificial compounds such as paracetamol and thus improving its formation may be of particular interest. ⁸⁷ It has been shown that mechanochemistry can efficiently couple a morpholine amine with the carboxylic acid of nicotinic acid to form an amide bond with increased reaction times and yields. ⁸⁸ Zhu et al. showed that the coupling reaction required 16 hours in solution with yields ranging from 65-79% depending on the coupling agent used. In contrast, the use of mechanochemistry significantly cut down reaction times to a range of 5-10 minutes with yields ranging from 78-94% underscoring the efficiency of mechanochemistry. ⁸⁸ Covalent bonds are not only utilized in organic synthesis but the are also used in the chemistry of materials. Many materials employ covalent bonds inherently in their structure or post synthetically in their modification. For example, Han et al. have shown that a polymer with terminal amine groups can be mechanochemically conjugated to the aldehyde group of cinnamaldehyde to afford an acid labile imine bonded drug for the purposes of drug delivery. ⁸⁹

1.6 Statement of the Problem

Recently, NMs have gained significant attention due to their immense potential impact in the fields of chemistry, biology and physics. ^{90–92} A wide range of different NMs have been studied in drug delivery applications including those previously discussed, as well as inorganic (e.g. quantum dots and lanthanide-doped nanoparticles), polymeric (e.g. polyethylene glycol and polyethyleneimine nanoparticles), nanogels (e.g. chitosan and alginate nanogels) and lipid-based (e.g. liposomes and solid lipid nanoparticles) NMs. ^{93–100} NM-based drug delivery is currently being used to enhance

the targeted and controlled release of therapeutic molecules, improve drug circulation time and enhance permeability of molecules across bioavailability, well as biological as membranes. 31,58,63,101-109 Many NMs used for drug delivery show remarkable properties, however, they suffer from limitations such as high cytotoxicity, lack of intrinsic traceable markers, and low aqueous dispersibility. It is in this regard that CDs offer a promising alternative, as they possess low cytotoxicity, exhibit intrinsic fluorescence with high fluorescence quantum yields and are aqueously dispersible. 42,109-114 Current medical literature shows that over 40% of all drugs in clinical use are hydrophobic, and 90% or more of newly developed drugs are described as Class II (high permeability, low solubility), or Class IV (low permeability, low solubility). 115 Hydrophilic drug delivery vehicles can help address the poor aqueous dissolution of such medication and thus CDs show promise as ideal candidates. Currently, drug conjugation to CDs typically relies on robust covalent amide bonds to conjugate molecules to their surfaces. These bonds, which are highly stable, are typically non-reversible and difficult to cleave under physiological conditions, limiting release of the surface functionalized molecule. 116 Furthermore the formation of such bonds often requires the need for expensive and hazardous coupling agents such as EDC listed at 116 \$ CAD/ 100 mg (Thermo Fisher Scientific) and classified as toxic in contact with skin and very toxic to aquatic life with long lasting effects according to its safety data sheet. 117,118

Imine bonds have been shown to be great alternatives, as they are described as covalent linkages, which can cleave in response to acidic evironments. 119–121 Bonds which are acid labile are often desirable as nanocarriers often encounter changes in pH ranging from a pH of 7.4 (blood stream) to a pH of 6.0 (early endosome) and finally a pH of 5.0 (late endosome/lysosome), when uptaken into cells through endocytosis. 122 Imine bonds are further interesting as they can be formed using mechanochemical approaches 89 removing he requirement for solvents and transforming the

reaction to a greener process. Furthermore, a solvent-free approach can also allow for the conjugation of hydrophobic molecules to hydrophilic CDs, overcoming any solubility barriers and rendering syntheses more sustainable. Despite its great potential, the use of mechanochemistry to form imine bonds on the surfaces of CDs remains unexplored.

Herein, the solid-state mechanochemical formation of imine bonds to conjugate vanillin (VAN), a hydrophobic model aldehyde molecule, to the surface of CDs was achieved in comparison to nabumetone (NAB), a ketone model molecule (**Figure 12**). Initial efforts focused on solution-based conjugation before ultimately transitioning to mechanochemistry. Ketone model molecules were first explored before transitioning to the more reactive aldehyde, VAN, as a model drug achieving the desired imine linkage by leveraging mechanochemistry. Furthermore, the mechanochemical functionalization process, kinetics of drug release, and the potential *in vitro* effects of this novel functionalization strategy were also explored.

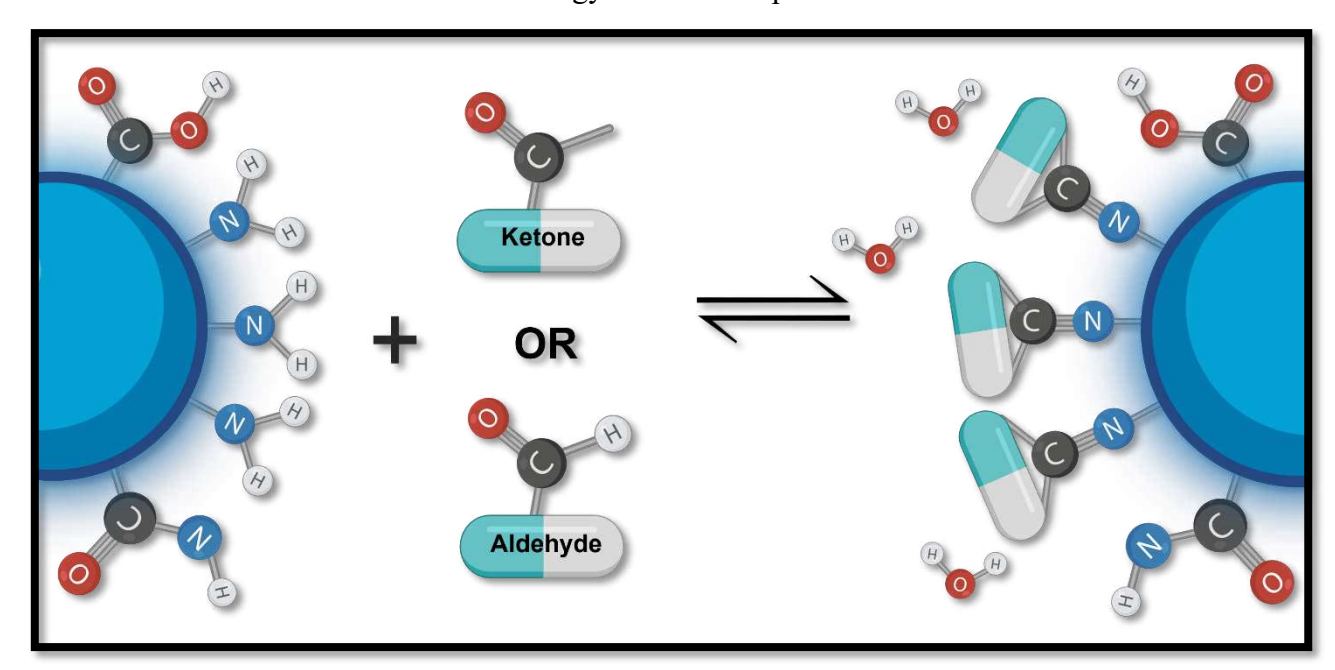


Figure 12. Schematic representation of imine bond conjugation to the surfaces of CDs

Chapter 2. Materials and Methods

2.1 Chemicals & Reagents

Methanol (MeOH), chloroform (CHCl₃), toluene, citric acid, pentaethylenehexamine (PH6), methanol-d4, methanol-d4 (0.03 % v/v TMS), D₂O (0.05 wt.%) and vanillin were all purchased from Sigma Aldrich. Nabumetone (NAB) and 4 A° molecular sieves (3-5mm, 0.12-0.20 beads) were purchased from Thermo Fisher Scientific. Sodium phosphate monobasic monohydrate, sodium phosphate dibasic heptahydrate, hydrochloric acid (HCl) and uranyl acetate were purchased from fisher scientific. Acetone was purchased from Caledon Laboratories Ltd. 3.5-5kDa regenerated cellulose membranes were purchased from Cole-Parmer Canada. Milli-Q water was produced in-house, Dulbecco's modified eagle medium (DMEM, 319-065 CL) and Fetal bovine serum (Heat Inactivated, US origin, cat no 080-150) and Phosphate Buffered Saline 10X (311-410-CL) were purchased from Wisent Bioproducts. Resazurin ready-to-use solution for cell proliferation assays was purchased from TCI America (R0195). Sterile 96 well culture plates were obtained from Sarstedt (cat no. 83.3924.005).

2.2 Synthesis of PH6-CDs

2.2.1 Microwave Assisted Synthesis

375 mM of pentaethylenehexamine (PH6) and 500mM of citric acid were added to an Erlenmeyer flask containing Milli-Q water. A magnetic stir bar was introduced, and the solution was stirred and occasionally sonicated to ensure a homogeneous mixture. The homogeneous solution was placed into a CEM Discover SP microwave for smaller scale synthesis, or a MARS 6 microwave reactor for scaled up syntheses and reacted at 210 °C for 10 minutes.

2.2.2 Purification of CDs

The contents of the microwave reactor tubes were dialyzed in Milli-Q water using 3.5-5 kDa regenerated cellulose membranes for 5 days. After dialysis, each CD solution was concentrated using lyophilization and further purified using acetone organic washes. The purified material was then lyophilized for a day and crushed into a fine powder using a mortar and pestle resulting in purified PH6-CDs.

2.3 Model Drug Conjugation

2.3.1 Solution Based: Molecular Sieves

4 A° molecular sieves were vacuum dried at 300°C overnight in order to reach complete activation.

10 mg PH6-CDs, 5 mL acetone (ketone model reagent), 5 mL MeOH and 250μL 1 M HCl were all added to a round bottom flask and stirred overnight at 50°C under reflux. Once complete the solution was filtered and concentrated by rotary evaporation to remove solvent and unreacted acetone.

2.3.2 Solution Based: Dean-Stark

40 mg PH6-CDS, 40 mg NAB, 50 mL toluene and 500 μL 1M HCl were all added to a round bottom flask. The flask was attached to a Dean-Stark trap and the reaction was carried out under vigorous stirring at 110 °C overnight. The solution was then concentrated by rotary evaporation and washed with 25 mL acetone three times to remove unreacted NAB.

2.3.3 Solution Based: Unassisted Condensation

20 mg PH6-CDs, 2mL MeOH, 500 μ L 0.04M NAB solution (dissolved in MeOH) and 100 μ L of 0.1 M HCl were all added to a sealed round bottom flask equipped with a reflux condenser at 50 °C overnight. Three 25 mL acetone washes were carried out to remove all unbound NAB.

2.3.4 Solid State Reaction: Planetary Ball Miller

Nabumetone conjugation: 20 mg PH6-CDs, 40 mg NAB and milling media (3 stainless steel beads, 10 mm in diameter) were added to a milling jar and milled for 30 minutes at 60 Hz using a Fritsch Planetary Micro Mill model "pulverisette 7". A secondary empty jar was also placed in the planetary ball mill as a counterweight. Three 10 mL acetone washes were carried out and the oily/wet product was lyophilized overnight to obtain the conjugated NAB-CDs. Vanillin conjugation was performed in a similar manner using 60 mg PH6-CDs and 90 mg VAN.

2.4 Characterization of Native and Conjugated CDs

2.4.1 Transmission Electron Microscopy (TEM)

A Thermo Fisher Scientific Talos transmission electron microscope operating at 120 kV with LaB₆ as the electron source was utilized to obtain images of PH6-CDs. TEM grids were prepped by drop casting 2 drops of a 500 μg/mL CD dispersion (prepared in MeOH) onto the grid (formvar/carbon 300 mesh copper) followed by evaporation of the solvent. Once dry, another 2 drops of uranyl acetate negative stain solution were drop casted and left to evaporate.

2.4.2 Powder X-Ray Diffraction (PXRD)

A Rigaku MiniFlex 6G diffractometer (Cu K α source; λ = 1.54 Å) was used to obtain all XRD spectra with a scan rate set to of 10 °C/min.

2.4.3 X-Ray Photoelectron Spectroscopy (XPS)

A Thermo Scientific Nexsa G2 XPS was used to obtain all XPS spectra. The instrument was equipped with an Aluminum-k α X-ray source and a spot size of Φ 400 μ m. High resolution scans of C1s, O1s and N1s were carried out in triplicate with pass energies of 50 eV and step sizes of 0.1 eV with 10 runs for each scan. Additionally, survey scans were carried out in triplicate with a pass energy of 200 eV and a step size of 1 eV with 10 runs for each scan.

2.4.4 Fourier Transform Infrared Spectroscopy Attenuated Total Reflectance (FTIR-ATR)

A Thermo Scientific Nicolet iS5, equipped with an ID5 attenuated total reflectance (ATR) accessory, was used to collect all FTIR data. Every acquisition was carried out using 64 scans at a resolution of 0.4 cm⁻¹ and performed on a laminate-diamond crystal window.

2.4.5 Proton Nuclear Magnetic Resonance (¹H-NMR) Spectroscopy

A Bruker Fourier UltrashieldTM (Bruker, Germany) operating at 300 MHz was used to obtain all spectra. All samples were prepared and analyzed in MeOH-D4 (deuterated methanol) due to its superior ability to dissolve/disperse model molecules and CDs.

2.4.6 Ultraviolet-Visible (UV-Vis) Spectroscopy

Characterization absorbance spectra were acquired using a Cary 5000 series UV-Vis-NIR Spectrophotometer (Agilent Technologies). A 1 cm path length quartz cuvette was used to collect absorption spectra over a range of 200-800 nm. Quantification of VAN during release kinetics studies was carried out using a Cary 60 UV-Vis spectrophotometer (Agilent Technologies). A 1 cm path length quartz cuvette was also used to collect absorption spectra over a range of 200-800 nm.

2.4.7 Fluorescence (FL) Spectroscopy

A Cary Eclipse fluorescence spectrophotometer (Agilent Technologies) was used to acquire fluorescence spectra of CDs. Analyses were carried out over a spectral range of 360-800 nm using a quartz cuvette with a 1 cm path length.

2.4.8 Thermogravimetric Analysis (TGA)

A TGA Q500 analyzer was used to obtain the quantitative composition and thermal properties of all samples. The sample temperature was raised from 25 to 900 °C at a rate of 10 °C/min under an inert argon atmosphere with a flow of 50 mL/min for all samples.

2.4.9 Cytotoxicity Assay

A549 cells were cultured in DMEM supplemented with 10% fetal bovine serum and incubated under standard culture conditions. Cells were routinely passaged after reaching 80-90% confluency prior to plating. The assay was performed in flat-bottom 96 well plates treated for adherent tissue culture. Cells were seeded at 3000 cells/well and incubated for 24 hours prior to treatment. VAN, CDs and VAN-CDs were suspended directly in DMEM. Cells were incubated with 100 μL solutions of 500 μg/mL CDs or 70.5 μM VAN for 72 hours, equivalent to three cell division cycles. 72 hours post-treatment, cells were rinsed with 1X PBS and incubated with 10% resazurin solution (TCI Chemicals) in DMEM and metabolic activity was evaluated using an Agilent Synergy H1M microplate reader operating in absorbance mode with an endpoint at 600 nm, 4 hours post-incubation with resazurin. All treatment conditions (vehicle, CDs, VAN, VAN-CDs) were studied with a sample size of n=8, and all assays were independently repeated in triplicate.

2.5 Drug Release

5 mg VAN-CDs was added to a 20 mL scintillation vial along with 10 mL McIlvaine buffer (0.1M citric acid, 0.2M sodium phosphate dibasic heptahydrate) at pH 5.0, 6.0, or 7.4 and 10 mL CHCl₃. Release was carried out a 37 °C at different time points and 1 mL of chloroform was extracted and replaced with 1 mL of fresh solvent to maintain sink conditions. The extracted samples were analyzed using a Cary 60 UV-Vis spectrophotometer (Agilent Technologies) to obtain absorbance spectra from 200-800 nm. VAN λ_{max} at 275 nm was used for quantification and compared to a standard curve generated with known concentrations of VAN to determine % cumulative release.

Chapter 3. Results and Discussion

3.1 Characterization of PH6-CDs

3.1.1 Assessing Physical Properties

The first characterization techniques carried out involved investigating the physical properties of the synthesized PH6-CDs. A TEM image of a 500 µg/mL dispersion of the CDs was obtained and shows sub 50 nm quasi spherical particles. It is worth noting that obtaining TEM images of CDs remains a significant challenge as image quality is largely dictated by the crystallinity and Z number (atomic number) of the material in question. Crystalline materials will show visible lattice fringes on a TEM image due to their ability to diffract electrons making them more visible. ¹²⁵ Elements with high atomic Z numbers are also able to scatter electrons more intensely leading to higher contrast images. ¹²⁶ As previously mentioned, CDs are amorphous materials hindering diffraction of electrons and mostly made up of carbon atoms which have low Z numbers limiting their contrast; nonetheless a TEM image was obtained and shown in **Figure 13**.

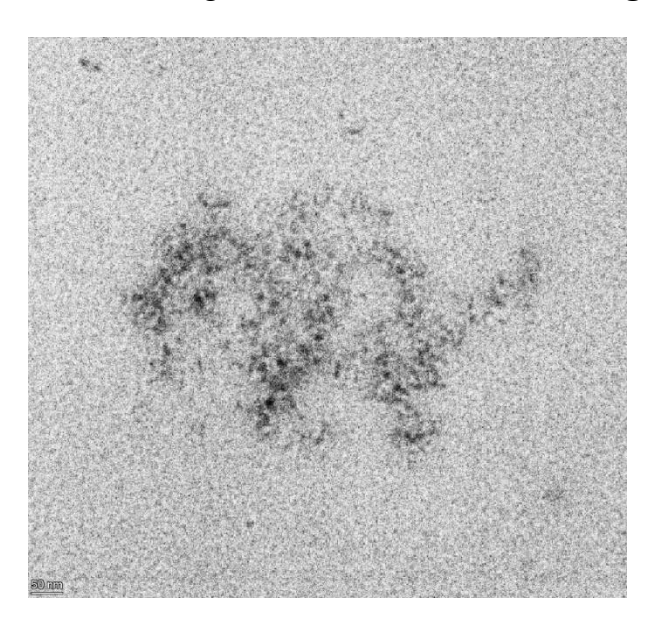


Figure 13. TEM image of 500 μg/mL dispersion of PH6-CDs.

To further highlight the amorphous nature of the synthesized PH6-CDs, PXRD analyses of the material and of the solid citric acid precursor was carried out (**Figure 14**). The PXRD of citric acid shows clear Bragg's diffractions spanning 10-70 °20, depicting a clear crystalline precursor. The PXRD of PH6-CDs clearly shows the absence of any sharp and intense Bragg's diffractions ranging from 10-70 °20, however, a broad reflection spanning the range of 10-30 °20 was noted and likely stemming from the graphitic core of the CDs. ²⁸ As previously mentioned, their amorphous nature can hinder imaging processes relying on electron scattering such as TEM, however, other methods of characterization can also be utilized to investigate the formation of CDs and involve assessing other unique properties such as chemical and optical properties.

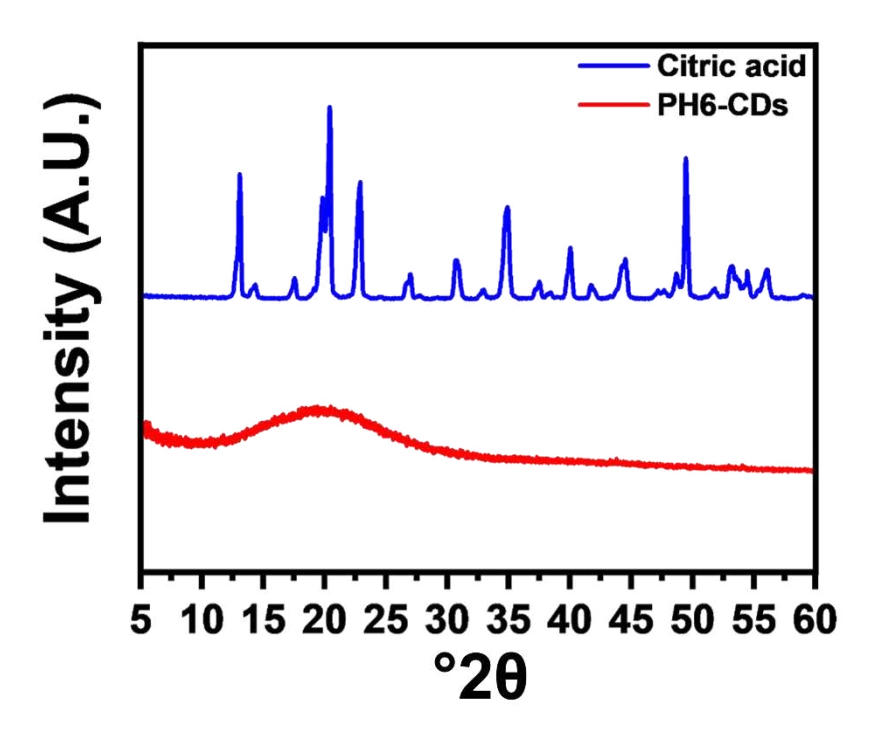


Figure 14. PXRD of the solid crystalline citric acid precursor and the synthesized amorphous PH6-CDs.

3.1.2 Assessing Chemical Properties

Following physical characterization of the PH6-CDs, chemical characterization was carried out to obtain a better understanding of their chemical makeup. FTIR was used as a first-line technique due to ease of use, quick analysis time and its non-destructive sample analysis nature. The obtained FTIR spectra of the precursors and of PH6-CDs can be found in (**Figure 15**). The FTIR of citric acid shows a clear O-H stretching vibration at 3276 cm⁻¹ and an intense stretching vibration at 1691 cm⁻¹ due to the hydroxyl and carbonyl groups of the associated carboxylic acid functionalities, respectively. The FTIR of pentaethylenehexamine shows amine (N-H) stretches and bends at 3273 cm⁻¹ and 1601 cm⁻¹, respectively. The FTIR of the obtained CDs shows overlapping signals ascribed to the O-H and N-H stretches at 3339 cm⁻¹ and associated carboxylic acid carbonyl stretch at 1695 cm⁻¹, as well as its own distinct signals such as the newly formed amide bonds clearly evidenced by the nitrogen bonded carbonyl (N-C=O) stretch at 1645 cm⁻¹, as well as a new alkene (C=C) stretch at 1540 cm⁻¹.

The vibrations listed confirm the successful incorporation of the citric acid and pentaethylenehexamine precursors into the final purified CD structure. New vibrations such as the amide stretch at 1645 cm⁻¹ confirm the formation of new bonds as would be expected from the synthesis of a material from its precursors. Other stretches shift to higher wavenumbers such as the C-H sp3 stretching vibrations and the C=O stretch indicating that the local environment around certain bonds is also changing evidencing the formation of CDs. Overall FTIR remains a quick and efficient first line technique to monitor changes to chemical groups and confirm functional group modifications consistent with the formation of CDs.

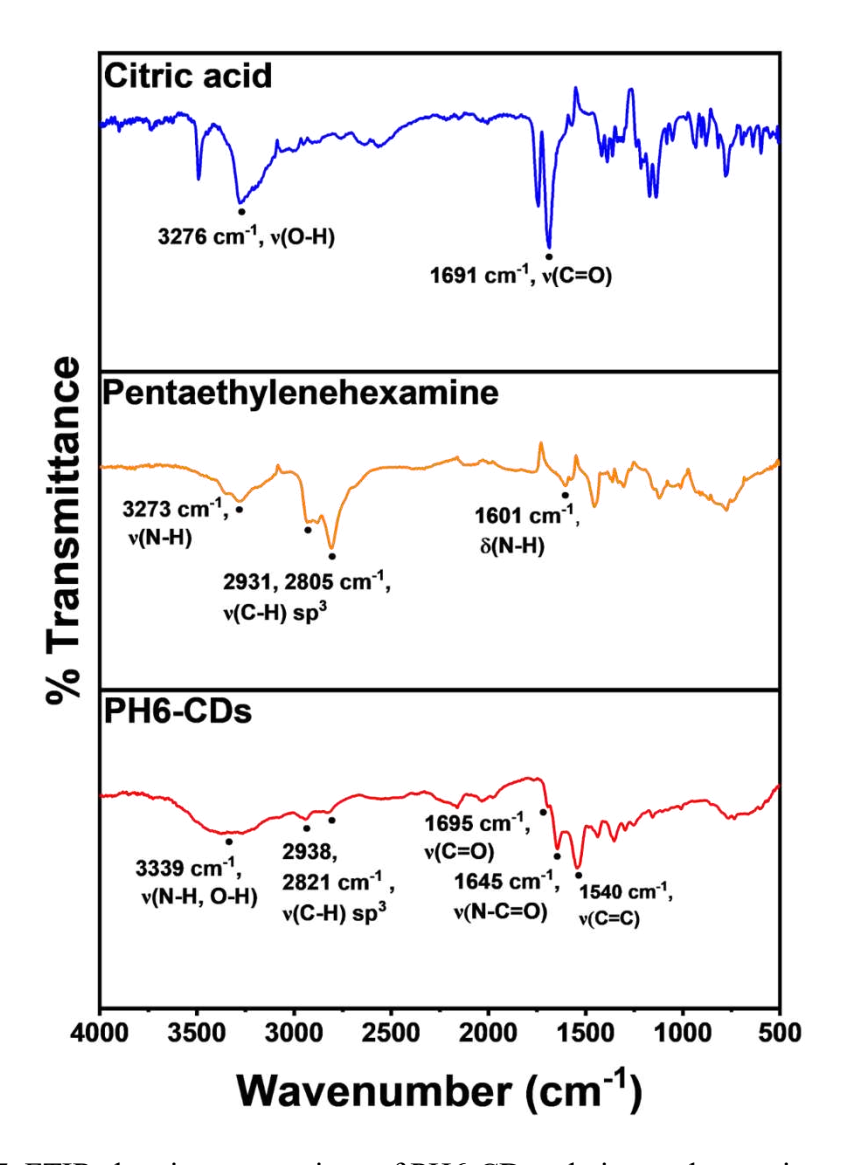


Figure 15. FTIR showing comparison of PH6-CDs relative to the starting materials.

¹H-NMR spectroscopy was also used in combination with FTIR to further assess the chemical makeup of PH6-CDs as shown in **Figure 16**. The deuterated solvent chosen was deuterated methanol (MeOH-D4) due to its superior ability to dissolve/disperse both the starting materials and the CDs.

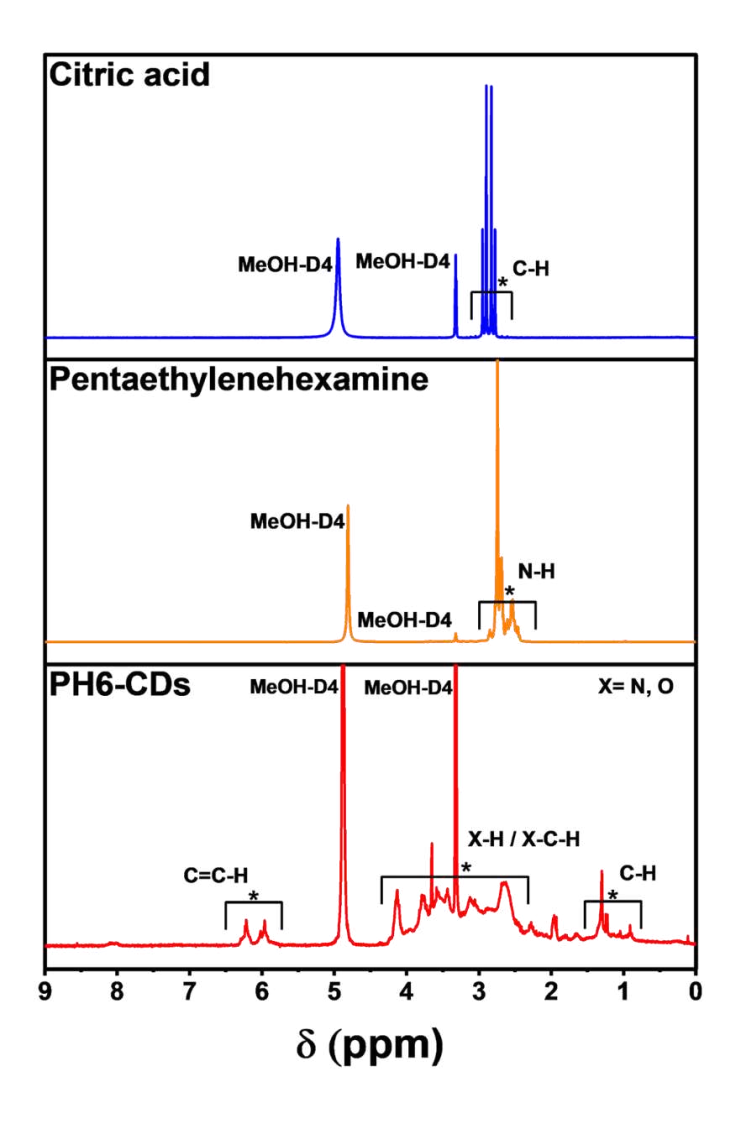


Figure 16. ¹H-NMR (300MHz, MeOH-D4) showing comparison of PH6-CDs relative to the starting materials.

The ¹H-NMR of citric acid shows a clear quartet at 3 ppm due to the proton attached to the alpha carbon. Pentaethylenehexamine shows a multiplet at 3 ppm associated with protons attached to the bridging ethyl chains. The ¹H-NMR of PH6-CDs shows a clear multiplet spanning 5.5 – 6.5 ppm ascribed to the alkene groups, or sp² domains of the CDs. Signals further up field at 2.5-4.25 ppm are noted as rather broad, a common occurrence for higher molecular weight species such as CDs. Nonetheless, these broad signals stem from the presence of protons directly bonded to

oxygen, or nitrogen, or protons bound to carbon atoms which are attached to oxygen or nitrogen atoms. Many multiplets can also be seen even further downfield spanning 0-2 ppm associated with protons attached to carbon atoms not neighboring any electronegative atoms.

3.1.3 Assessing Optical Properties

The optical properties of PH6-CDs were first assessed using UV-Vis analysis. Molecules/materials which absorb in the UV/Visible range of the electromagnetic spectrum and will often show absorbance peaks. The UV-Vis spectrum of the precursors and PH6-CDs is shown in **Figure 17**.

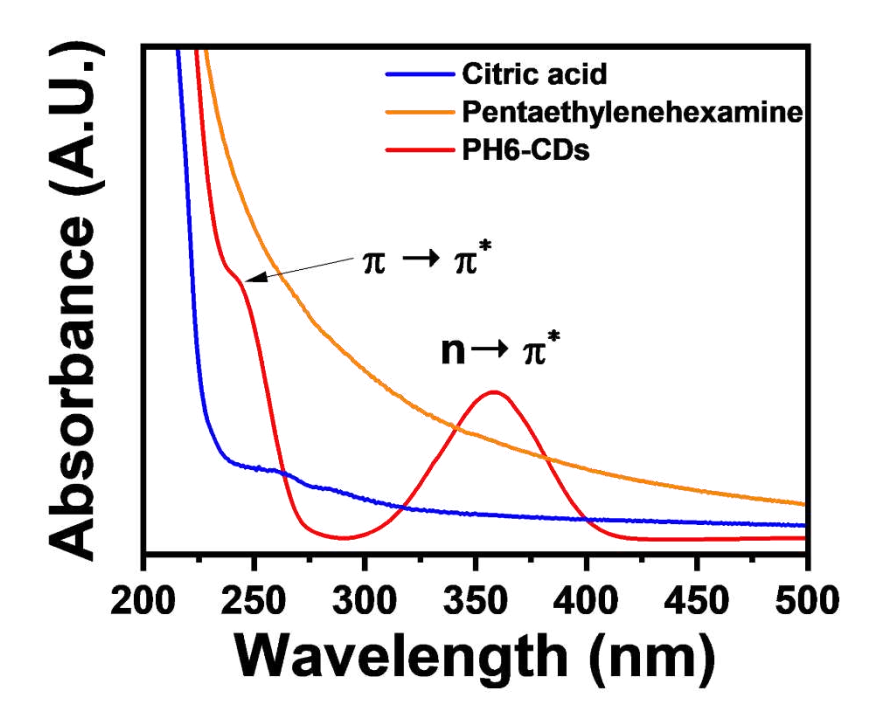


Figure 17. UV-Vis spectra of PH6-CDs and synthetic precursors pentaethylenehexamine and citric acid.

The UV-Vis profile of PH6-CDs shows two absorption signals. The first peak with a λ_{max} of ~240 nm is associated with a $\pi \to \pi^*$ transition originating from the sp² domains (conjugated alkenes/aromatic motifs) found within the structure of the CDs. The second absorption signal at 350 nm is associated with an $n \to \pi^*$ transition attributed to double bonded electronegative atoms

typically decorating the surfaces (e.g. carbonyl (C=O) functional groups originating from carboxylic acids and amides). These results are corroborated by numerous findings in the literature concerning the optical characterization of CDs and provide additional evidence pointing to their formation. It should also be noted that the UV-Vis profile of the CDs significantly differs relative to that of the starting materials providing more evidence pointing towards the formation of CDs from the starting materials. Both citric acid and pentaethylenehexamine lack any observable absorption bands due to their unique molecular structures. The lack of any π conjugation is the main reason why both of these molecules to do not absorb any UV-Vis light, however, their combination as precursors during CD synthesis will produce a material containing conjugated π systems and thus lead to the absorption of UV-Vis radiation as shown by the clear absorption bands at ~240 and 350 nm.

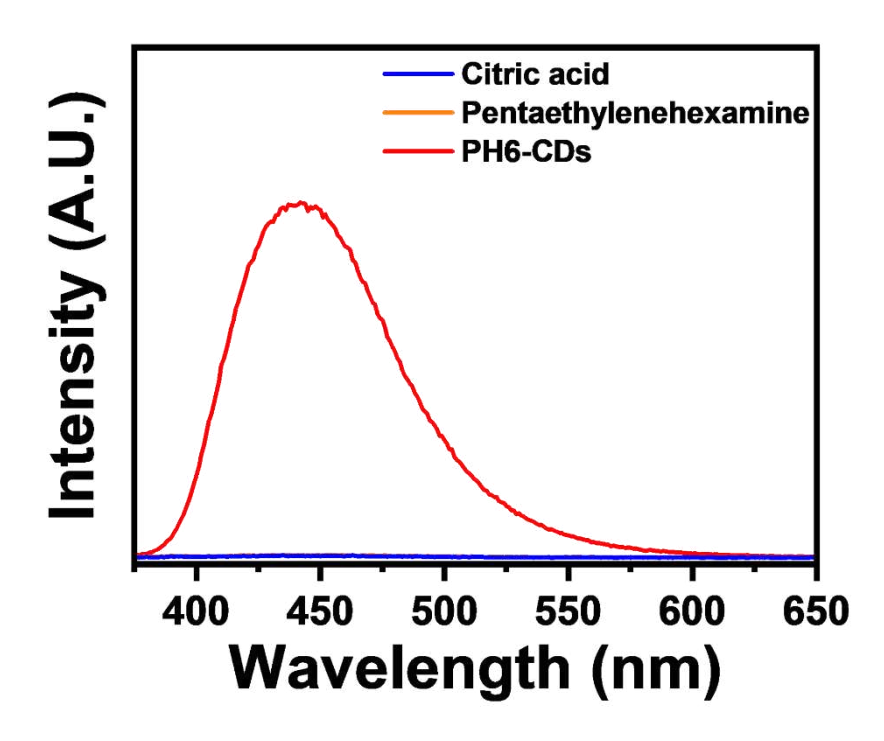


Figure 18. FL spectra of PH6-CDs and synthetic precursors pentaethylenehexamine and citric acid.

According to the FL profile (**Figure 18**), the CDs show a characteristic blue fluorescence with an emission maximum centered at ~450 nm, when the material is excited at 350 nm. ⁴² Once again, this emission is substantially different than those from the precursors. Citric acid and pentaethylenehexamine are non-fluorescent molecules with no observable emission when using the same excitation wavelength.

3.2 Solution based conjugation of CDs

3.2.1 Molecular Sieves

As previously mentioned, imine bond formation is an equilibrium reaction, which generates water. Due to Le Chatelier's principle, that water is often removed in order to shift the equilibrium to the product side and favor the formation of imine bonds. Initial attempts at removing water during the synthesis process were carried out using 4 A° molecular sieves. Molecular sieves are described as dehydrating agents which are often used in condensation reactions such as imine bond formation to selectively adsorb generated water during the synthetic process. ¹²⁸

The starting materials chosen were PH6-CDs due to their high amine content necessary for imine bond formation and acetone as a highly accessible laboratory solvent and a model ketone reagent. Furthermore, the removal of free acetone after the reaction was carried out was rather simple to achieve. The flask housing the reaction was concentrated using a rotary evaporator and any free acetone was removed via it's conversion into a gas and collected into the appropriate collection vessel. FTIR was initially used to glean the surface of the CDs and assess changes to chemical functionalities during the conjugation process (**Figure 19**).

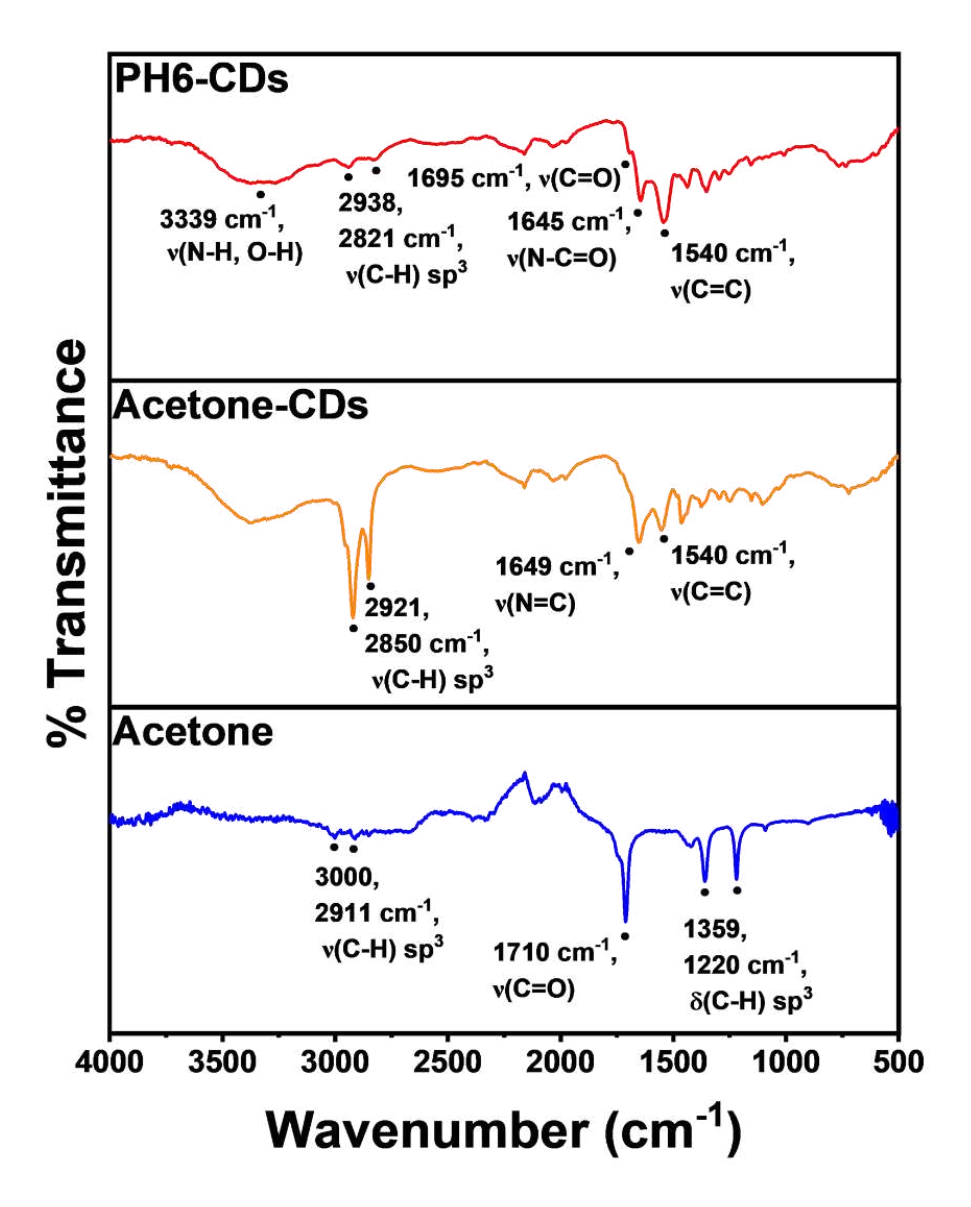


Figure 19. FTIR carried out to study imine bond formation on the surfaces of PH6-CDs using 4 A° molecular sieves (10 mg PH6-CDs, 5 mL acetone, 5 mL MeOH and 5 drops of 1M HCl, stirred overnight at 50 °C under reflux).

New alkane (C-H) stretching vibrations were observed at 2921 and 2850 cm⁻¹ likely indicating an association of acetone with the CDs after conjugation. A slightly stronger stretching vibration at 1649 cm⁻¹ was also observed and was initially associated with newly formed imine bonds, however, it was later discovered that these signals arise from sieve powder which was shed into solution during synthesis.

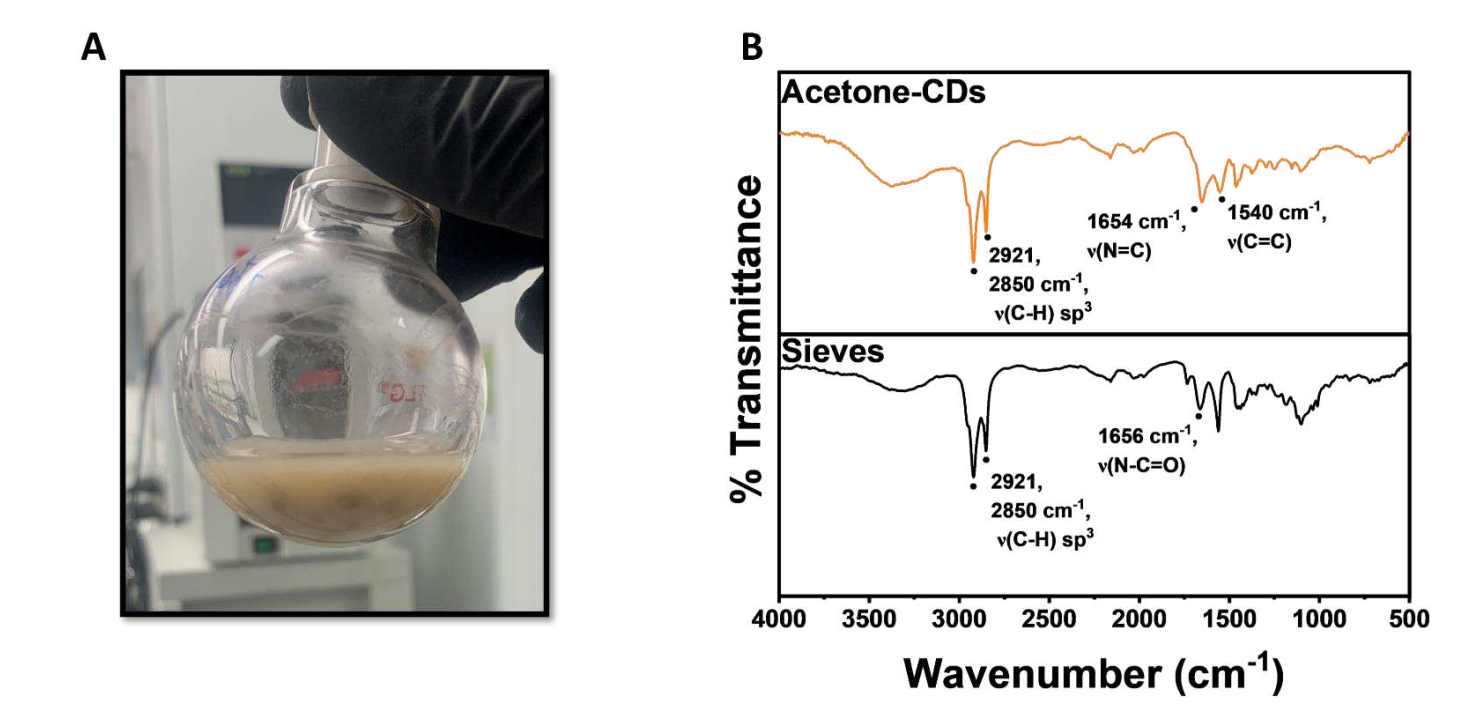


Figure 20. 4 A° molecular sieve contamination. (A) image of the murky solution after an overnight reaction containing shed sieve powder. (B) FTIR of the sieve powder.

Figure 20A shows an image taken of the solution following an overnight reaction. The solution begins as transparent and overnight, it becomes a murky, cloudy solution. This was ascribed to the powder, which was shed from the molecular sieves over the course of the reaction. Every effort to filter off the powder (filter paper, 0.22 μm filter, celite) was unsuccessful. The powder was characterized by FTIR and clearly shows the same alkane stretches at 2921 and 2850 cm⁻¹ and a stretch at 1656 cm⁻¹ originating from the carbonyl of the amide groups in the structure of the sieves (**Figure 20B**). This of course meant that studying imine bond formation using sieves would be quite challenging and having leftover powder would simply not be desirable for further use in biological cells and thus an alternative route incorporating a dean-stark trap was explored.

3.2.2 Dean-Stark Trap

The dean-stark trap is a clever piece of glassware used to remove water from an azeotropic distillation due to a built-in trap design as previously mentioned and shown in **Figure 9**. Following its incorporation into the experimental setup, FTIR analyses of the purified material were first carried out to determine conjugation of the model ketone NAB to CDs as shown in **Figure 21**.

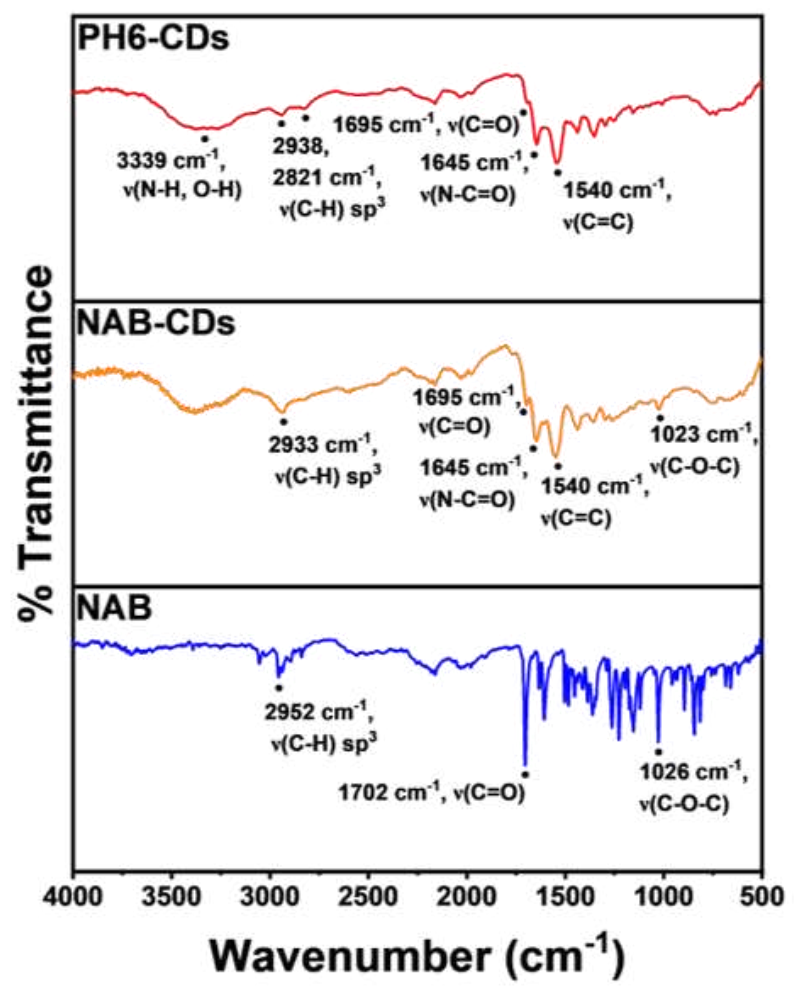


Figure 21. FTIR carried out to study imine bond formation on the surfaces of PH6-CDs using a Dean-Stark trap (40 mg PH6-CDS, 40 mg NAB, 50 mL toluene and 500 μ L 1M HCl, 110 °C overnight, three 25mL acetone washes).

It should be mentioned that the model ketone reagent used was changed to NAB due to a slightly more complex chemical structure allowing for easier monitoring of drug conjugation.

NAB offers additional stretches and bends by FTIR, relative to acetone, along with the presence

of additional signals for other analyses that would be carried out (e.g. ¹H NMR). Furthermore, NAB is a non-steroidal anti-inflammatory drug (NSAID) with a relatively inert chemical structure apart from the isolated ketone (**Figure 22**) allowing it to act as a model molecule for imine formation while retaining some therapeutic effects applicability to the field of drug delivery. ¹²⁹ Moreover, since the aqueous solubility of NAB is extremely poor (~0.09 mg/mL in 1:10 DMSO:PBS solution), its functionalization to CDs can potentially improve its dissolution profile and allow for its transport in aqueous systems. ¹³⁰

Figure 22. Chemical structure of NAB

Association of NAB with PH6-CDs was successfully confirmed by FTIR (**Figure 21**). A new C-H alkane stretching vibration was observed at 2933 cm⁻¹ along with a corresponding ether (C-O-C) stretch at 1023 cm⁻¹. While the association of NAB to the CDs was successful, FTIR seemed to suggest that an imine bond was not formed. The carbonyl stretch at 1695 cm⁻¹ appeared to increase in intensity relative to other stretches and bends following conjugation. This indicated that conversion of the ketone into an imine bond likely did not occur.

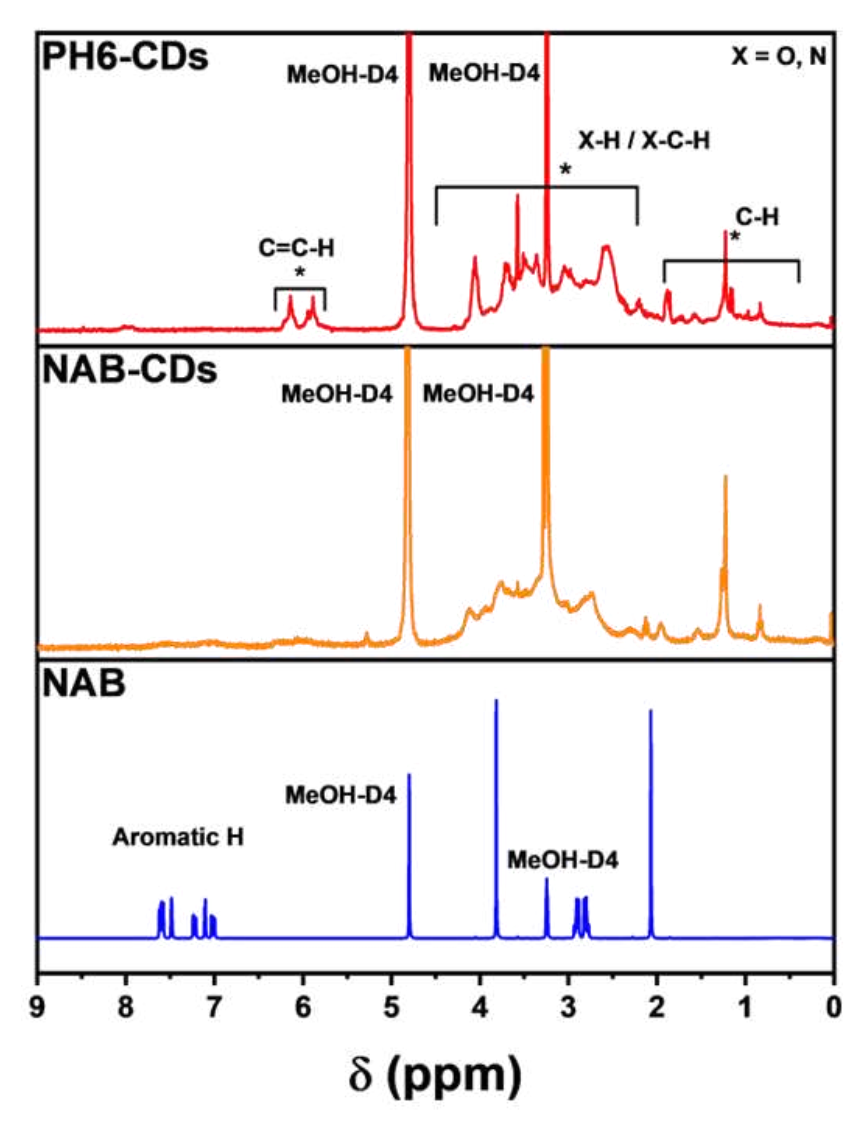


Figure 23. ¹H-NMR (300MHz, MeOH-D4) carried out to study imine bond formation on the surfaces of PH6-CDs using a Dean-Stark trap (40 mg PH6-CDS, 40 mg NAB, 50 mL toluene and 500 μ L 1M HCl, 110 °C overnight, three 25mL acetone washes).

¹H-NMR spectroscopy analysis was also carried out to study conjugation of NAB. Interestingly enough, observing protons from the conjugation of NAB was quite challenging. Signals were however present in the aromatic region albeit very weak. Nonetheless, these signals were at the same exact chemical shift before and after conjugation indicating that had conjugation occurred, it was likely not through a covalent bond. Furthermore, the alkene protons of the CDs, before and after conjugation, seem to be diminished indicating that the methodology being used is

likely having an effect on the π -bonded framework of the CDs. We hypothesize that the need for toluene using the dean stark trap was quite problematic in this scenario as the CDs are not soluble in this organic solvent and only become slightly more soluble upon heating.

3.2.3 Unassisted Condensation

A third route employing no dehydrating agents, or the use of a water trap such as a Dean-Stark trap was attempted since the current literature suggested it may be posssible.¹³¹ FTIR was again used as a first line technique to assess the formation of imine bonds (**Figure 24**).

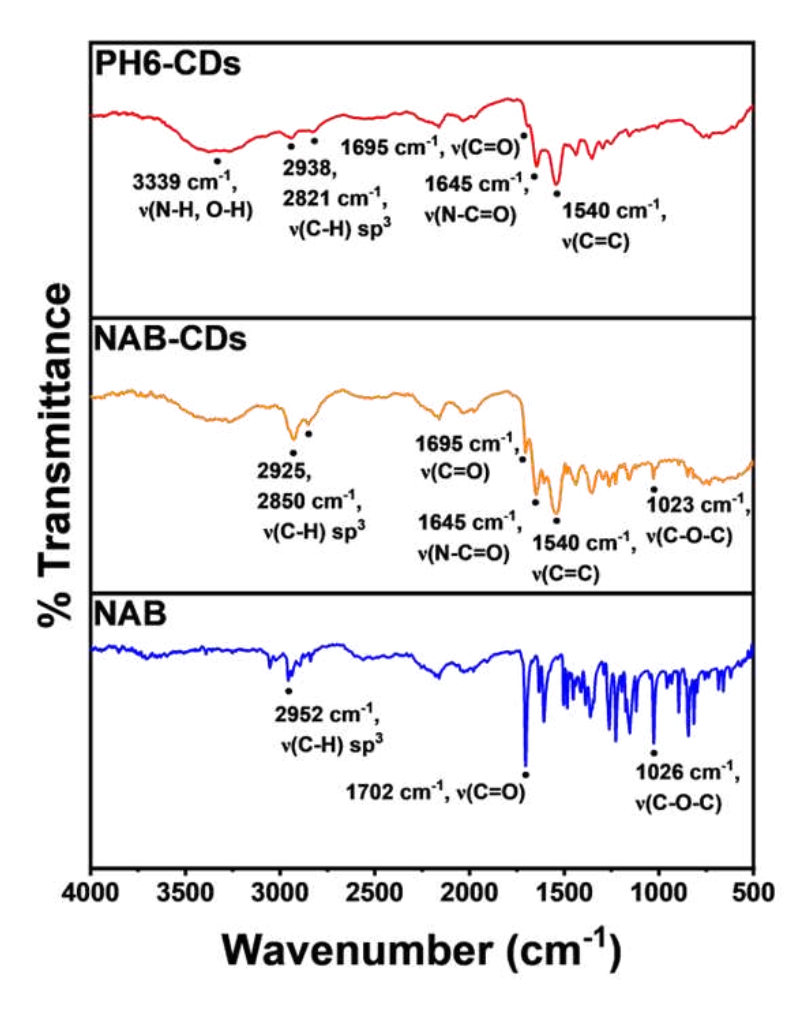


Figure 24. FTIR carried out to study the unassisted formation of imine bonds on the surfaces of PH6-CDs (20 mg PH6-CDs, 2mL MeOH, 500 μL 0.04M NAB solution (dissolved in MeOH) and 2 drops of 0.1 M HCl, 50 °C overnight, three 25mL acetone washes).

It is quite clear that NAB was successfully conjugated to the CDs evidenced by the new alkane (C-H) stretching vibrations at 2925 and 2850 cm⁻¹. We also noted a visible ether stretch at 1023 cm⁻¹ arising from the ether bond of NAB which is now present on the surface of the dots. However, imine formation likely did not occur due to the presence of the carbonyl stretch at 1695 cm⁻¹ which seems to increase in intensity relative to other stretches and bends. This indicates that the carbonyl group of NAB is not being used in the formation of imine bonds but is rather being used to form non-covalent interactions with PH6-CDs. In order to gain additional insights into the state of functionalization, ¹H-NMR analysis was used to further identify the manner of conjugation.

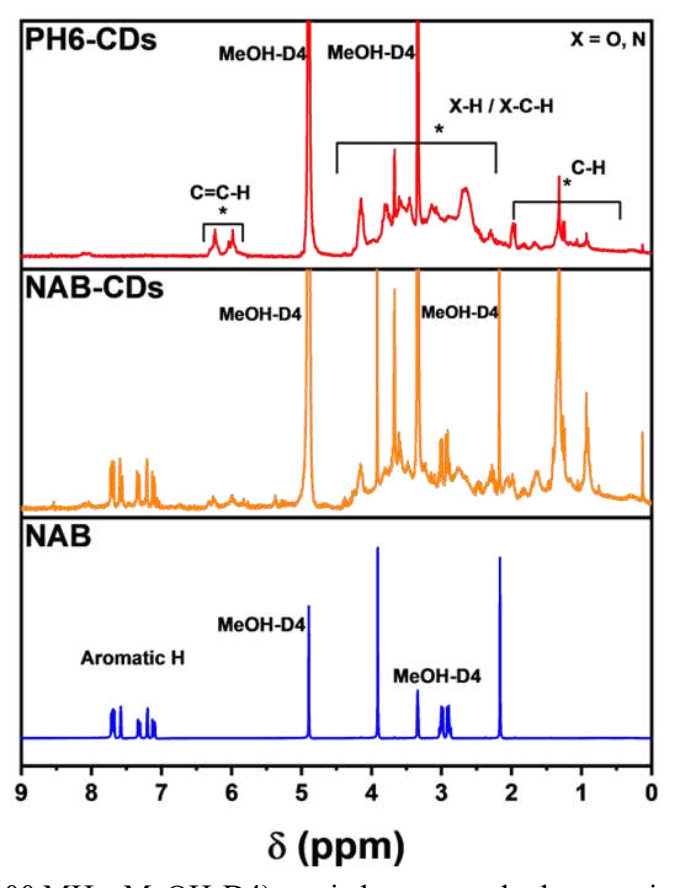


Figure 25. ¹H-NMR (300 MHz, MeOH-D4) carried out to study the unassisted formation of imine bonds on the surfaces of PH6-CDs (20 mg PH6-CDs, 2mL MeOH, 500 μL 0.04M NAB solution (dissolved in MeOH) and 2 drops of 0.1 M HCl, 50 °C overnight, three 25mL acetone washes).

Aromatic protons can be seen spanning the downfield region from 7-8 ppm due to the two aromatic rings of NAB both bearing protons. A singlet at ~4 ppm can also be seen arising from the protons of the ether carbon. A multiplet at 3 ppm is also present stemming from the alkane group connecting the carbonyl group to the aromatic rings, which also bears protons. Finally, a singlet at ~2.15 ppm was observed and associated with the terminal carbon of the ketone group bearing protons. All these signals were present in both the ¹H-NMR spectrum of NAB and that of NAB-CDs at identical chemical shifts. It would be expected that the singlet at 2.15 ppm would be most affected if the carbonyl group was converted to an imine bond, however, this was not observed and thus conjugation was likely stemming from a non-covalent interaction.

3.3 Mechanochemistry Based Conjugation

3.3.1 Imine Bond Formation

While many attempts at forming imine bonds on the surface of PH6-CDs proved to challenging, mechanochemistry remained an unexplored route with promising potential. As previously mentioned, Han et al. have shown that mechanochemistry can also be leveraged to form imine bonds. Additionally their research involved forming these bonds for the purposes of drug delivery, which aligns quite well with the research conducted in this thesis. Initial attempts at using mechanochemistry for imine bond formation were firstly carried out with NAB as a model drug in order to remain consistent with previous attempts. While the first attempts were unsuccessful this experiment was pivotal in kickstarting subsequent mechanochemistry based trials which eventually lead to the successful formation of imine bonds. Once again, FTIR was used as a first line technique to study drug conjugation (Figure 26).

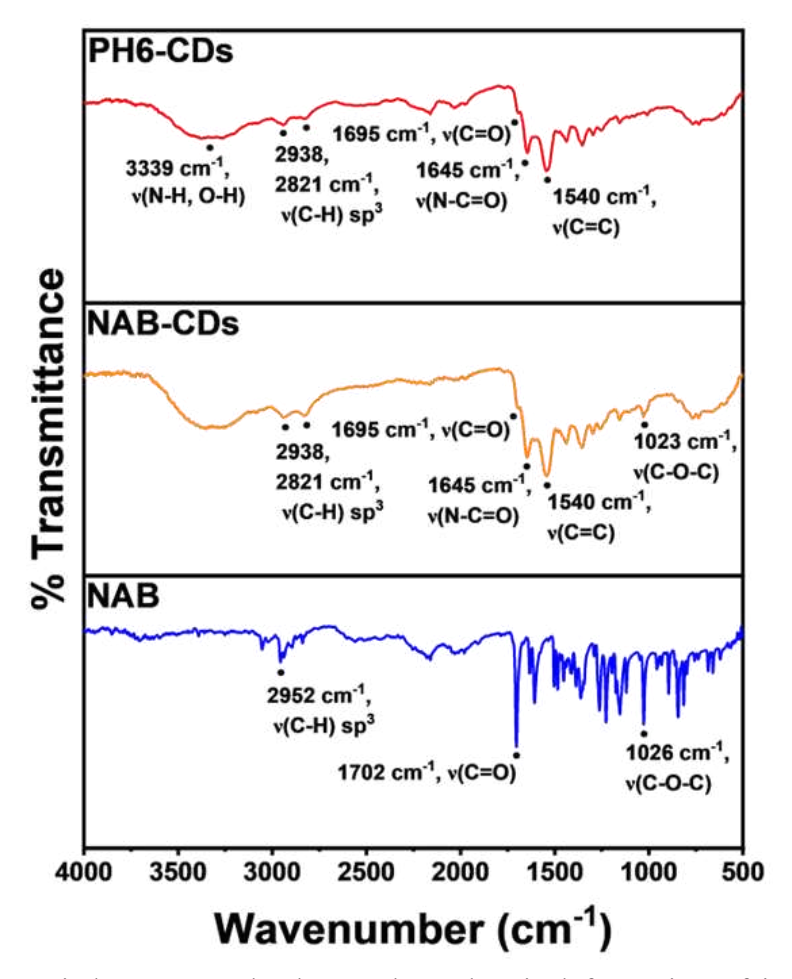


Figure 26. FTIR carried out to study the mechanochemical formation of imine bonds on the surfaces of PH6-CDs (20 mg PH6-CDs, 40 mg NAB, three stainless steel 10 mm diameter beads, 30 minutes, 60 Hz, three 10 mL acetone washes).

FTIR proved challenging to assess successful drug conjugation due to the absence of noticeable differences between the FTIR of CDs before and after NAB conjugation. Nonetheless, some degree of association was evident due to the presence of a new ether stretch at 1023 cm⁻¹ and a slight increase in the relative intensity of C-H sp³ stretches at around 2800-2900 cm⁻¹ following NAB conjugation. Interestingly enough, the most intense carbonyl stretch for NAB, at 1702 cm⁻¹, is absent following conjugation suggesting the possibility of an imine bond. ¹H-NMR spectroscopy was then carried out to confirm if an imine bond was indeed formed (**Figure 27**).

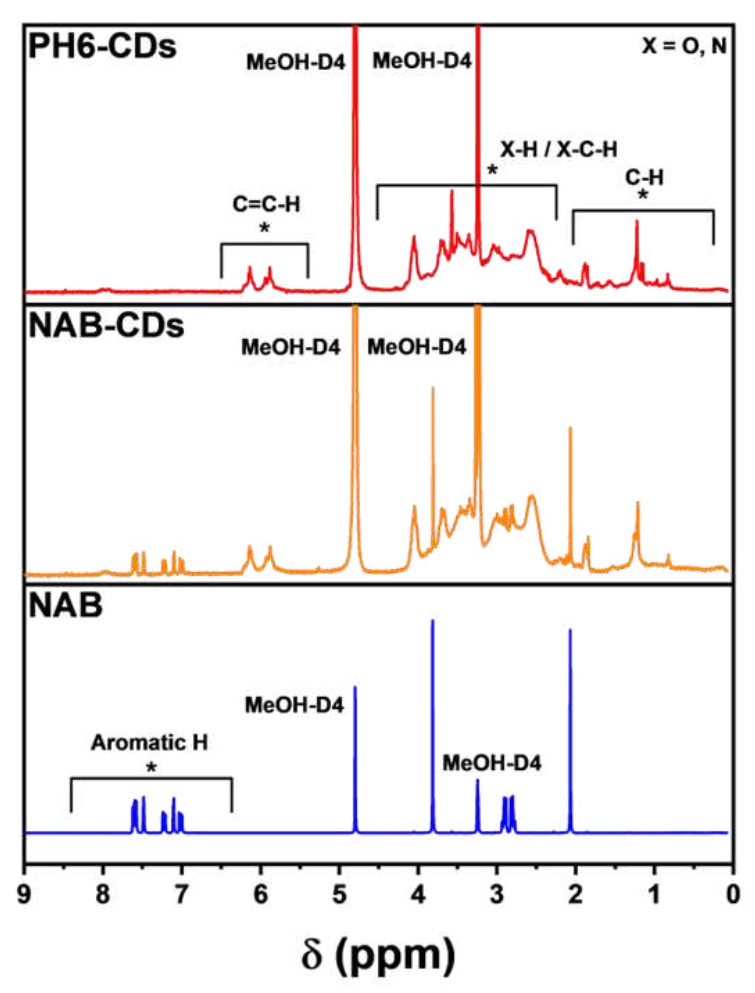


Figure 27. ¹H-NMR (300MHz, MeOH-D4) carried out to study the unassisted formation of imine bonds on the surfaces of PH6-CDs (20 mg PH6-CDs, 40 mg NAB, three stainless steel 10 mm diameter beads, 30 minutes, 60 Hz, three 10 mL acetone washes).

Similar to the ¹H-NMR spectrum for the unassisted conjugation of NAB shown in **Figure 25**, all of the chemical shifts of NAB are present before and after conjugation, however, none of them shift downfield or up field after conjugation specifically the protons for the carbon atoms of the ketone motif at 2.15 ppm indicating that a covalent bond such as the imine bond did not form. Nonetheless, successful association of a molecule with CDs via mechanochemistry has never been done before, therefore this experiment propelled additional studies to investigate more reactive molecules such as aldehydes in order to achieve the goal of forming covalent imine bonds on the surfaces of PH6-CDs. As mentioned earlier, ketone molecules such as NAB can form imine bonds,

however, they are typically much less reactive than aldehyde molecules. Thus a different model aldehyde molecule, Vanillin (VAN), was chosen to maximize the possibility of forming imine bonds.

Figure 28. Chemical structure of VAN

VAN was chosen as a model aldehyde molecule due to a mostly inert chemical structure with the most reactive functional group being the aldehyde group highlighted in red in

Figure 28. Furthermore, VAN also exhibits therapeutic effects. It is often described as having antioxidant and anticarcinogenic potential and thus apart from acting as a model molecule, VAN is also applicable to the field of drug delivery. Following similar mechanochemical conjugation procedures, VAN was successfully conjugated to the surfaces of CDs via imine bonds. FTIR spectra (Figure 29), before and after conjugation, were very similar with no noticeable differences indicating that this technique would not be sensitive enough to ascertain the conjugation of VAN. The only conclusion one might make is the most intense stretching vibration at 1658 cm⁻¹ associated with the carbonyl from the aldehyde group is missing following conjugation and indirectly hinting towards the possibility of a possible reaction involving the transformation of the aldehyde group to an imine bond. Further evidence was obtained using ¹H-

NMR analysis, which not only confirmed the conjugation of VAN, but also shows for the first time, the formation of imine bonds on the surfaces of CDs via mechanochemistry (**Figure 30**).

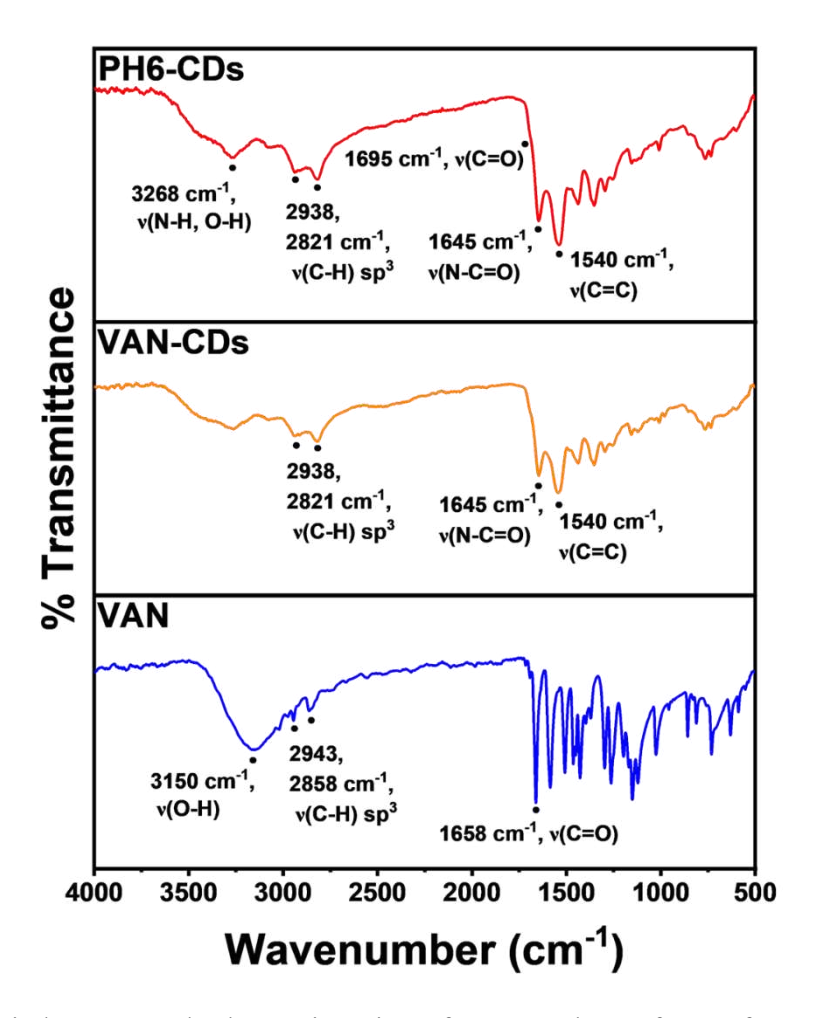


Figure 29. FTIR carried out to study the conjugation of VAN to the surfaces of PH6-CDs (60 mg PH6-CDs, 90 mg VAN, three stainless steel 10 mm diameter beads, 30 minutes, 60 Hz, three 25 mL acetone washes).

A clear disappearance of the aldehyde singlet proton at 9.80 ppm could be observed coupled with the appearance of a new broad singlet at 8.10 ppm after conjugation of VAN to PH6-CDs corresponding to the imine protons. It should also be noted that new broad aromatic protons can also be observed spanning 6.50-7.50 ppm and slightly shifted up field in comparison to the aromatic protons of native VAN. This slight change in chemical shift is also to be expected because

covalent bond formation is expected to change the chemical environment surrounding such protons influencing their respective chemical shifts.

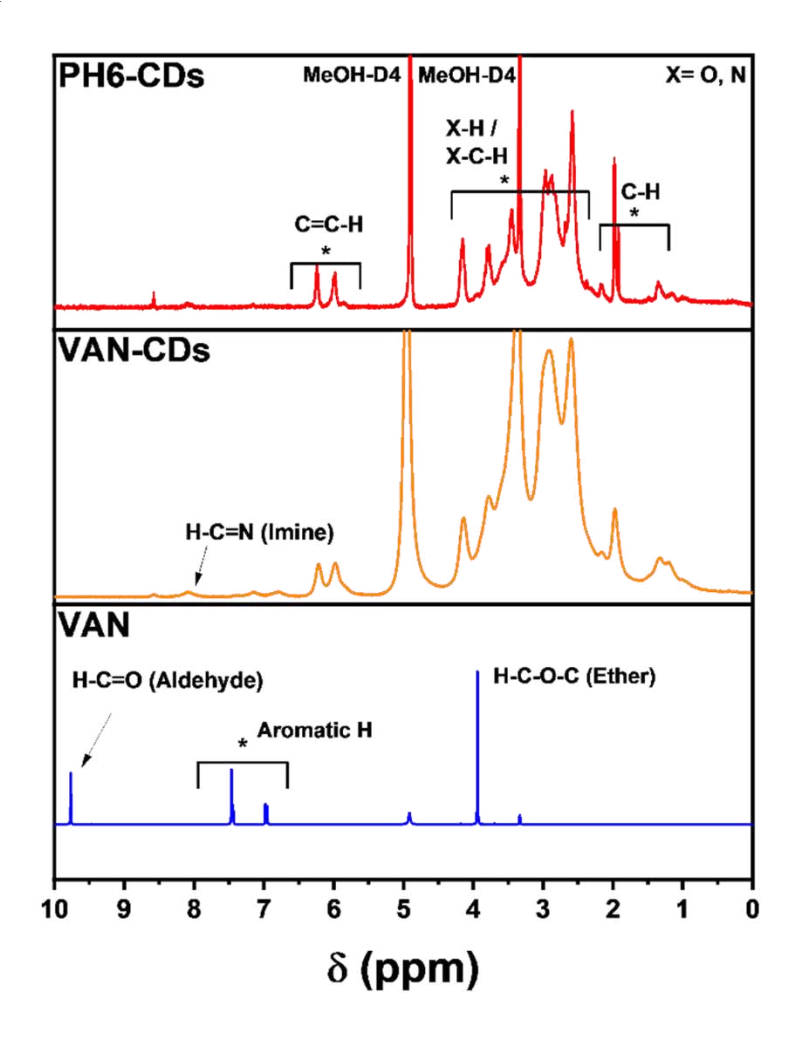


Figure 30. ¹H-NMR (300MHz, MeOH-D4) depicting the formation of imine bonds when mechanochemically conjugating VAN to the surfaces of PH6-CDs (20 mg PH6-CDs, 40 mg NAB, three stainless steel 10 mm diameter beads, 30 minutes, 60 Hz, three 10 mL acetone washes).

A zoomed-in portion of the downfield region can also be seen in **Figure 31** and further emphasizes the formation of imine bonds. It can be clearly observed that the aldehyde protons are no longer present, and that the imine/aromatic protons are now quite evident. The corresponding integrations match our expectations. The aldehyde of VAN contains 1 proton and therefore integrates for 1.00 while the aromatic motif has 3 corresponding protons and integrates as 3.09.

The conversion into an imine bond results in similar integrations with the imine proton (highlighted in red in **Figure 32**) integrating as 1.00 since this bond contains 1 proton and the corresponding aromatic protons integrate for 3.05 as VAN has 3 aromatic protons as previously mentioned.

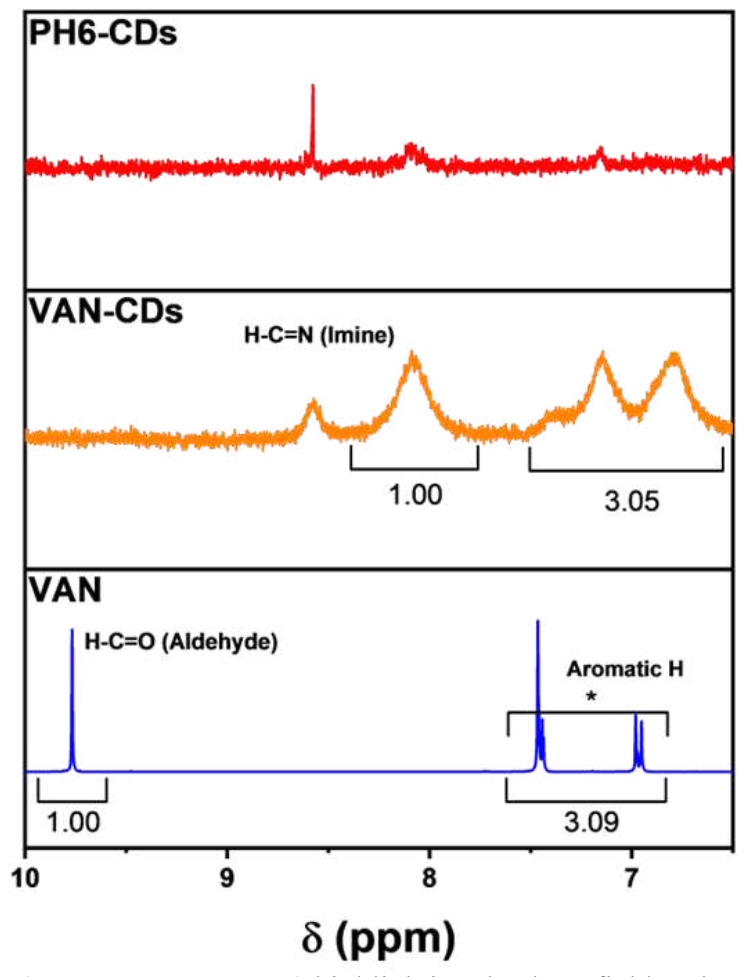


Figure 31. ¹H-NMR (300MHz, MeOH-D4) highlighting the downfield region of the imine bonded VAN model (20 mg PH6-CDs, 40 mg NAB, three stainless steel 10 mm diameter beads, 30 minutes, 60 Hz, three 10 mL acetone washes).

The broader nature of the NMR signals post conjugation was also to be expected as the chemical environment surrounding each imine bond is slightly different. PH6-CDs are complex macromolecular structures decorated with many amines on their surfaces. Every single surface amine will differ depending on the neighboring atoms and functional groups. This can lead to

multiple signals around the same chemical shift appearing as a singular broad response. A general schematic of imine-bonded VAN can be found in **Figure 32**.

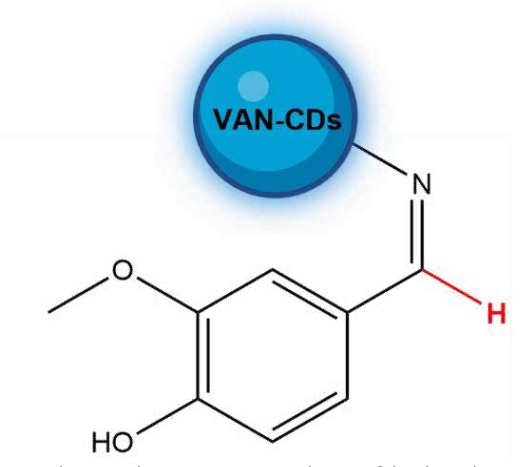


Figure 32. Schematic representation of imine bonded VAN to CDs

While these results proved to be extremely promising, appropriate controls were carried out to ensure that the broad singlet at 8.10 ppm associated with a proton of the newly formed imine bond does not arise from a self-induced reaction between only the CDs, or only VAN. To confirm this, PH6-CDs were ball milled under identical reaction conditions. The ¹H-NMR can be seen in **Figure 33**, and shows that ball milling CDs does not induce a significant imine signal. It should be noted that a broad singlet already exists at 8.10 ppm since PH6-CDs have imine bonds already incorporated in their structure. There is no noticeable increase in the intensity of this signal after ball milling and there is an absence of the broad multiplet spanning 6.50-7.50 ppm associated with aromatic protons. Furthermore, the ¹H-NMR of ball milled VAN also does not seem to suggest a self-induced reaction. There is a clear absence of imine protons at 8.10 ppm and the aromatic protons that are present are shifted down field and are much more resolved in comparison to when the molecule is conjugated to the dots. These controls show that the conjugation of VAN to the

surfaces of PH6-CDs arises from imine bonds and is not an artifact induced by CDs or VAN reacting by themselves.

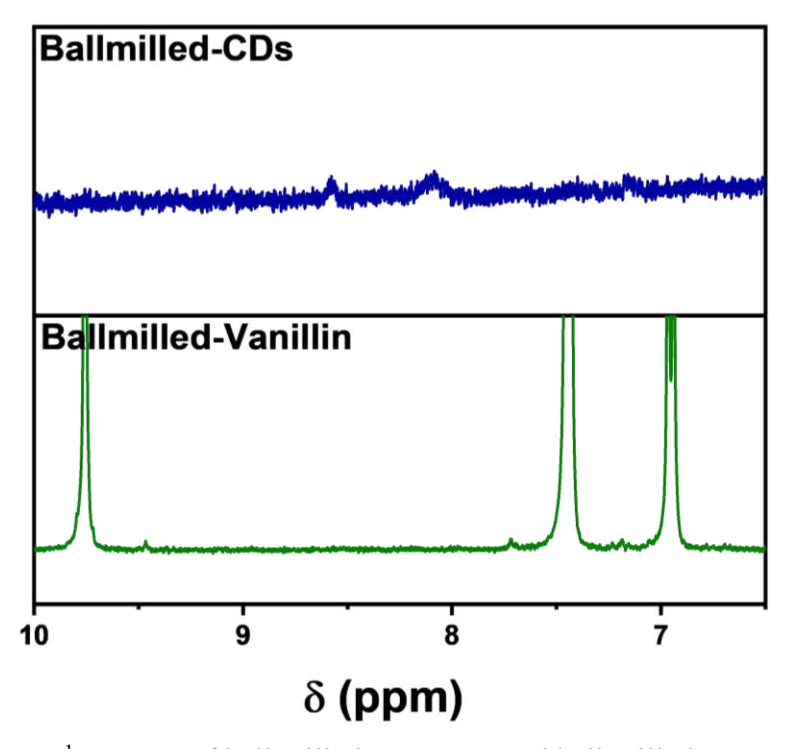


Figure 33. ¹H-NMR of ball milled PH6-CDs and ball milled VAN controls.

Further characterization of the CD-drug complex was carried out after confirmation of successful conjugation of VAN via imine bonds. PXRD was performed (Figure 34) and as expected, PH6-CDs which were amorphous materials prior to ball milling, remain so even after conjugation with VAN. This result aligns with previous findings as it demonstrates that bulk vanillin is crystalline, however, during the conjugation process, individual molecules of VAN are taken apart from the crystal and conjugate to the surfaces of the CDs. Thus, no Bragg's reflections are observed post conjugation. This finding depicts how crystals of VAN do not interact with CDs but rather individual molecules, which are facilitated due to the mechanochemical reaction

between the aldehyde group of VAN and the amine groups of PH6-CDs leading to the formation of imine bonds.

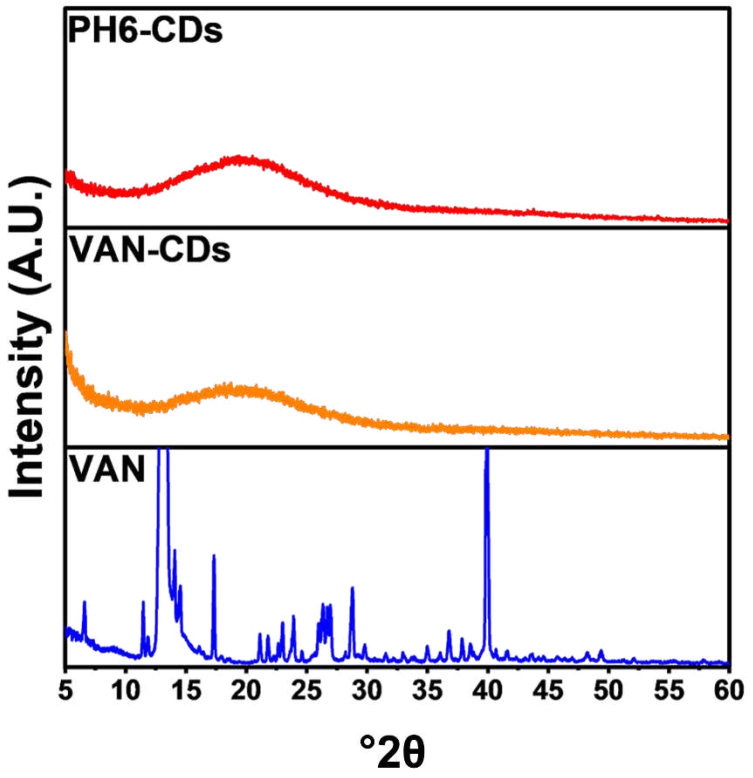


Figure 34. PXRD carried out to assess the crystallinity of PH6-CDs after drug conjugation (20 mg PH6-CDs, 40 mg NAB, three stainless steel 10 mm diameter beads, 30 minutes, 60 Hz, three 10 mL acetone washes).

XPS was also carried out to further assess the surface of PH6-CDs before and after VAN conjugation (**Figure 35**). Survey scans of PH6-CDs and VAN-CDs show that the elemental surface composition does not significantly change. This is to be expected as previous analyses such as FTIR have shown that the amount of VAN conjugated is quite small. Further high-resolution scans of carbon, nitrogen and oxygen elements were then carried out to assess differences in surface functional groups. Deconvolution of the C1s (carbon) and O1s (oxygen) spectra show that these

functional groups do not evidence any significant changes before and after conjugation. A stark difference, however, is noted in the deconvolution of the N1s (nitrogen) spectrum of PH6-CDs in comparison to VAN-CDs (**Figure 35D, G**). An imine bond signal at ~398.5 eV increases drastically from 38.9% to 61.9% further confirming their successful formation.

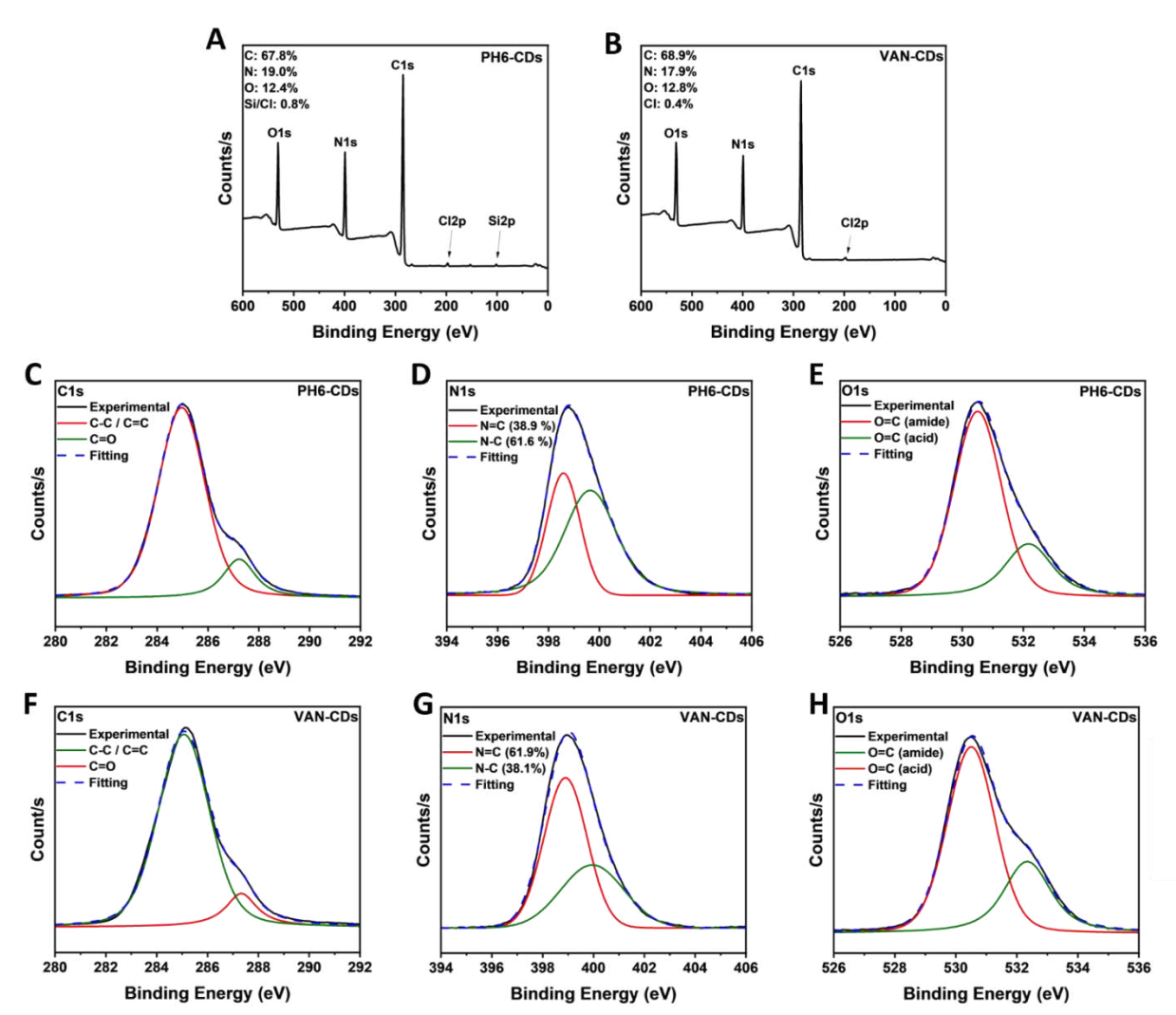


Figure 35. XPS Surface Elemental Composition Analysis of PH6-CDs before and after van conjugation. (A) Survey scan for PH6-CDs. (B) Survey scan of VAN-CDS. (C) Deconvoluted high resolution C1S spectrum of PH6-CDs. (D) Deconvoluted high resolution N1S spectrum of PH6-CDs. (E) Deconvoluted high resolution O1S spectrum of PH6-CDs. (F) Deconvoluted high resolution C1S spectrum of VAN-CDs. (G) Deconvoluted high resolution N1S spectrum of VAN-CDs. (H) Deconvoluted high resolution O1S spectrum of VAN-CDs.

3.3.2 Drug Loading

Following a full characterization of VAN-CDs, the drug loading capacity (DLC) was assessed. TGA was first carried out to determine whether a decomposition event corresponding to iminebonded VAN can be distinguished. By subjecting each sample to high temperatures, weight loss events occur and are quantified to determine the mass composition of the given sample. **Figure 36A-C** show the TGA of PH6-CDs, VAN-CDs and VAN, respectively. Starting with PH6-CDs, three main decomposition events can be observed with the first weight loss event (4.5%) due to the loss of moisture, the second weight loss (72.9%) originating from the surface functional groups of the CDs and the third (9.0%) is due to the final decomposition of the carbon core. These three weight loss events are also present in the TGA of VAN-CDs and in very similar percentages. Furthermore, no individual weight loss event around the decomposition temperature of VAN (185°C) is noted for conjugated VAN indicating that the DLC is likely quite low.

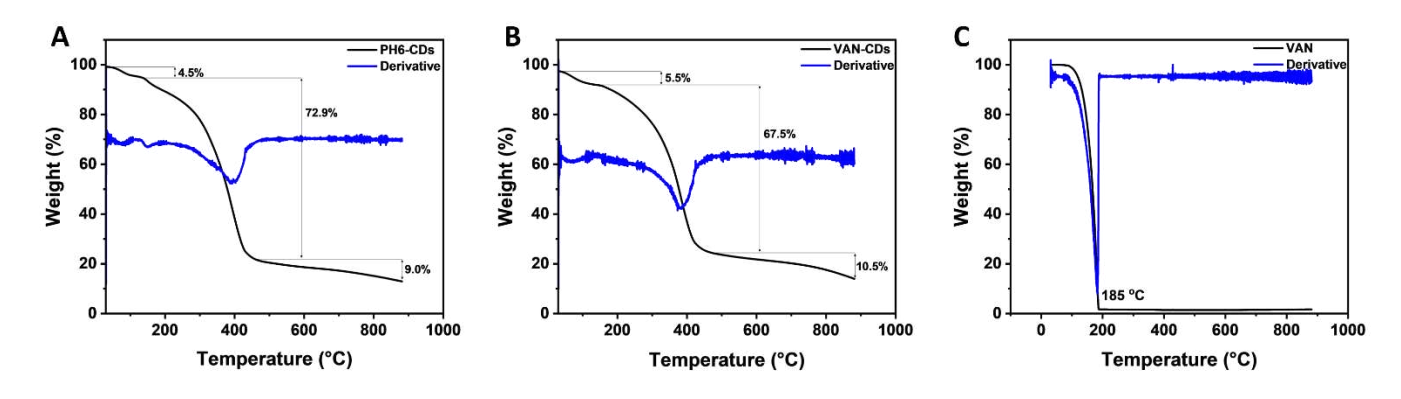


Figure 36. TGA carried out to investigate drug loading. (A) TGA of native VAN-CDs before drug conjugation. (B) TGA of VAN conjugated CDs. (C) TGA of VAN.

While TGA proved to be non-conclusive, quantitative nuclear magnetic resonance (qNMR) provided much higher sensitivity and success for determining the DLC. qNMR makes use of introducing an internal standard with a known concentration to determine the concentration of the analyte (**Figure 37**). It should be noted that 3-(trimethylsilyl)propionic-2,2,3,3-D4 acid, sodium

salt (TSP-D4) is a water-soluble internal standard often used with deuterium oxide (D₂O) as the deuterated solvent. Additionally, D₂O can hydrolyze imine bonds and is the reason for why some aldehyde content is present in the ¹H-NMR (**Figure 37**). To ensure the accuracy of the calculated DLC, a second ¹H-NMR was carried out using tetramethysilane (TMS) as an internal standard and MeOH-D4 as the deuterated solvent.

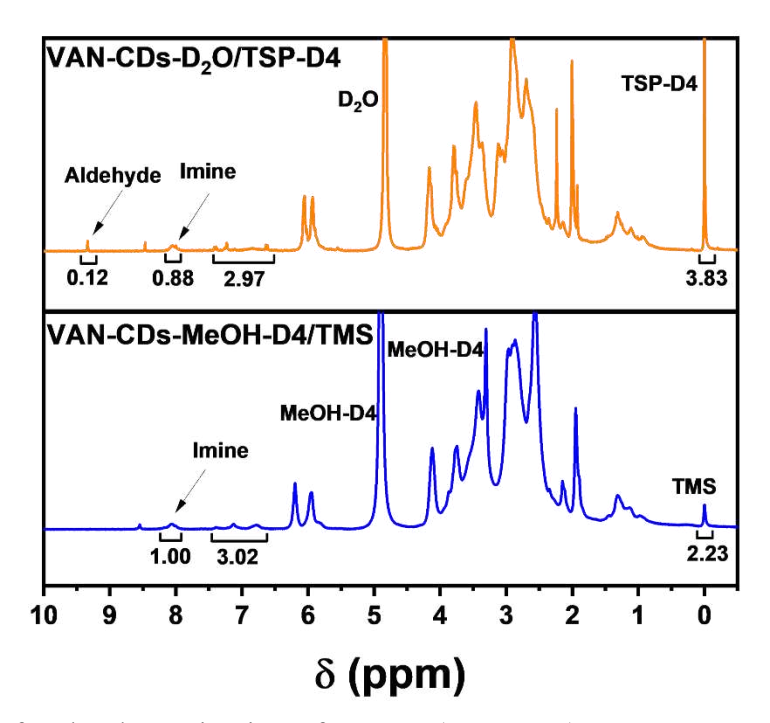


Figure 37. qNMR for the determination of a DLC (300 MHz). 27 mg VAN-CDs and 16.8 mg VAN-CDs dispersed in 0.75mL MeOH-D4 containing 0.03% v/v TMS and 0.75 mL D_2O containing 0.05 wt.% TSP-D4 respectively.

A DLC of 5.02% was determined using TMS and a DLC of 5.10% was determined using TSP-D4 for an average DLC of 5.06% +/- 0.06% according to the following adapted qNMR formula: 134,135

(1)
$$(m_{drug} = \frac{S_{drug}}{S_{std}} * \frac{N_{std}}{N_{drug}} * \frac{M_{drug}}{M_{std}} * m_{std})$$

(2)
$$(DLC \%) = \frac{m_{drug}}{m_{drug+CDS}} * 100$$

Where m_{drug} : Mass of drug S_{drug} : Signal area of drug S_{std} : Signal area of standard

 N_{std} : Number of resonating protons of the standard N_{drug} : Number of resonating protons of the drug

 M_{drug} : Molar mass of the drug M_{std} : Molar mass of the standard m_{std} : Mass of the standard

A lower DLC can be advantageous in many cases such as administering medication with narrow therapeutic indices. ¹³⁶ Administering such medication can often have fatal consequences if the dosage is above the therapeutic dose and thus precision dosing is necessary. ¹³⁷ A formulation with a lower DLC can allow for precise control on the amount of medication released and thus administered. In this case the obtained DLC was low in comparison to other NMs such as polymeric nanoparticles and mesoporous silica nanoparticles whose DLCs can reach as high as 66 and 69%, respectively. ^{138,139}

3.3.3 Drug Release

Drug release studies were carried out in different biologically relevant pH-adjusted aqueous media to investigate release behavior. As previously mentioned, nanocarriers often encounter changes in pH ranging from a pH of 7.4 (blood stream) to a pH of 6.0 (early endosome) and finally a pH of 5.0 (late endosome/lysosome), when uptaken in cells through endocytosis.¹²²

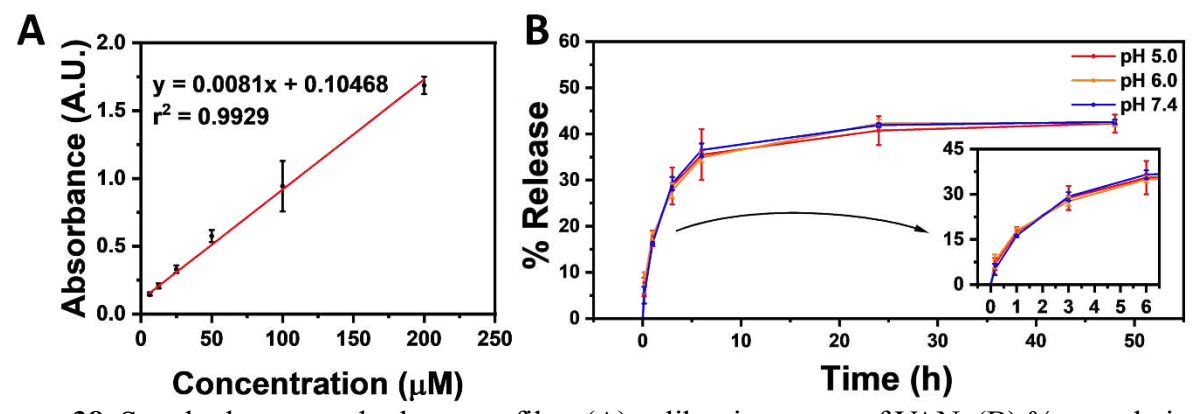


Figure 38. Standard curve and release profiles. (A) calibration curve of VAN. (B) % cumulative release of VAN from conjugated CDs at pH 7.4, 6.0 and 5.0.

Prior to carrying out release studies, a standard curve corresponding to absorbance readings at a λ_{max} of 275 nm for different concentrations of VAN was generated (**Figure 38A**). The obtained trend line depicts a linear relationship confirmed by an r^2 value >0.99. The generated calibration equation was then utilized to quantify the release of VAN from the surfaces of CDs in aqueous environments of differing pH values. The release profiles showed a cumulative release occurring over a period of 24 hours until a plateau was reached (**Figure 38B**).

To the best of our knowledge, this experiment demonstrates the first ever covalent conjugation of a molecule to the surfaces of CDs in a reversible manner via mechanochemistry. Release over several hours can be quite advantageous as the need to administer a subsequent dose is diminished. A longer release period can help maintain the drug concentration within the therapeutic window avoiding the need to re-administer medication. Moreover, it addresses the limitations associated with the commonly used covalent amide bonds, which is commonly not hydrolyzed under physiological conditions and necessitates the use of harmful coupling agents to form. Amide bonds, being one of the most used covalent linkages, are limited by the fact that they cannot be cleaved under mild conditions. As mentioned earlier, this can be quite problematic as the pharmacophore of the drug can be involved in the conjugation process hindering subsequent therapeutic effects. Imine bonds provide a covalent alternative which can easily form and hydrolyze as shown by VAN-CDs. It is also interesting to note that release does not change with response to change in pH. This can be quite advantageous for applications such as wound healing where pH fluctuations are commonly found between healthy, or damaged/infected tissue. 140 A delivery system which does not change in the presence of such fluctuations can ensure consistent and predictable dosing, allowing for efficient healing. Indeed, this study confirms the reversible nature of imine bonds which may require further optimization and fine tuning to render them pH

responsive. Nonetheless, a foundation has been laid out for the proper formation and characterization of such bonds.

3.3.4 Cytotoxicity

In vitro studies were carried out to confirm that the mechanochemical approach did not induce any acute harmful biological effects relative to the control (PBS), CDs or VAN alone (Figure 39). Human A549 lung epithelial cells were used as a model system, and treated with PBS, PH6-CDs, VAN-CDs and VAN for 72 hours, or three cell division cycles, in order to provide strong evidence for a lack of acute toxicity in vitro. The CDs used herein have been previously confirmed by Clermont-Paquette et al. to be non-toxic in vitro up to 10,000 mg/mL.⁴² While VAN is a model molecule, it also exhibits anticarcinogenic properties in certain cell lines. 132 In addition to possessing fast replication times and being easily accessible, A549 cells were used in this study as VAN does not induce any cytotoxic behavior in these cells. In choosing this cell line, we have made sure that any toxicity observed is solely attributed to the mechanochemical modification of CDs rather than from the model drug itself. Wells treated with CDs contained 100 µL of a 500 μg/mL dispersion of CDs (50 μg) corresponding to the upper limit of the NM dosage range commonly employed (10-60 μg). ^{141,142} Wells treated with VAN contained 100 μL of 70.5 μM VAN solutions corresponding to the maximum amount of VAN released from the CDs. As expected, the metabolic activity observed for all of the treatment conditions, was well above the standard 70% toxicity threshold. 143,144 However, there was a drop in metabolic activity to 91.8 % for VAN-CDs, which shows statistically significant differences when compared to the other treatment conditions (p < 0.001). Slight differences in toxicity are to be expected as chemical modifications are occurring at the surfaces of the dots, which can alter properties such as their cellular behaviour. In

spite of that, these changes are not expected to induce significant toxicity. As such, we can conclude that mechanochemical conjugation of VAN does not render the CDs toxic to cells.

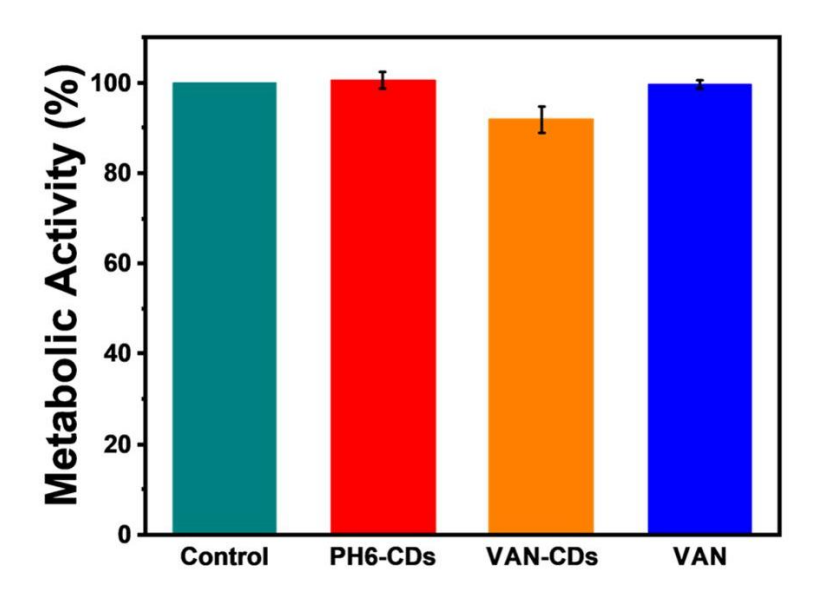


Figure 39. Resazurin cell viability assay of A549 lung cancer cells treated with PBS (control), PH6-CDs, VAN-CDs and VAN.

Chapter 4. Conclusions and Future Works

4.1 Concluding Remarks

To the best of our knowledge, we have reported for the first time the successful mechanochemical formation of imine bonds on the surfaces of PH6-CDs. This works has allowed us to shed light on greener conjugation strategies and alternative covalent linkages that can open up new avenues in nanodiagnostics and therapeutics. This approach addresses the limitations associated with the popular robust amide bond approach, particularly their inability to cleave and release molecules, as well as the need for hazardous coupling agents. VAN was used as a model aldehyde containing molecule allowing for a condensation reaction to occur with primary amines located on the surface of CDs. In depth characterization was carried out to determine the manner of conjugation confirming the formation of imine bonds. A clear conversion of the starting material's aldehyde proton into the imine proton was evident through ¹H-NMR analysis. Additionally, the clearly resolved chemical shifts allowed for the use of qNMR to quantify a DLC of 5.06% +/- 0.06%. After determining the conjugation method and DLC, release studies were then carried out and confirmed the reversible nature of the formed bonds. VAN was released over a period of 24 hours before reaching a plateau at the three tested pH values (7.4, 6.0 and 5.0). While no notable differences in release were observed between the pH values, these findings lay a solid foundation for future optimization and fine tuning, which can allow for pH-responsive release. Finally, the cytotoxicity before and after mechanochemical surface modification of the CDs was deemed to be low, highlighting the advantages of this novel CD conjugation strategy.

4.2 Future Works

Future studies for this work should firstly focus on rendering the formed imine bonds responsive to changes in environment pH. We hypothesize that the unique surface chemistry of PH6-CDs may be playing a role in hindering the pH responsiveness of the formed imine bonds. A citric acid precursor introduces many carboxylic acid functionalities on the surfaces of the CDs, which can play a role in the relative stability of neighboring imine bonds due to their electron withdrawing nature. This may explain why the cleavage at pH 7.4 is similar to that at pH 6.0 and pH 5.0. Selection of a different CD with lower to no carboxylic acid content can likely lead to imine bond stability at a physiological pH and cleavage in slightly more acidic environments. Secondly, optimization of the mechanochemical parameters used for conjugation such as the frequency, milling time and amount of milling media should be a focus to render the process more efficient. Lastly, this research can also benefit from scaling up the conjugation procedure in order to allow for a single batch to be used for all future experiments.

Chapter 5. References

- 1 F. Findik, *Period. Eng. Nat. Sci*, 2021, **9**, 62–75.
- N. Baig, I. Kammakakam and W. Falath, *Mater Adv*, 2021, **2**, 1821–1871.
- 3 E. Roduner, *Chem Soc Rev*, 2006, **35**, 583–592.
- 4 F. Eker, H. Duman, E. Akdaşçi, E. Bolat, S. Sarıtaş, S. Karav and A. M. Witkowska, *Molecules*, 2024, **29**, 3482.
- 5 K. J. Hughes, M. Ganesan, R. Tenchov, K. A. Iyer, K. Ralhan, L. L. Diaz, R. E. Bird, J. Ivanov and Q. A. Zhou, *ACS Omega*, 2025, 10, 7530–7548.
- 6 I. V. Gürsel, T. Noël, Q. Wang and V. Hessel, *Green Chemistry*, 2015, **17**, 2012–2026.
- M. Farhang, A. R. Akbarzadeh, M. Rabbani and A. M. Ghadiri, *Polyhedron*, 2022, **227**, 116124.
- 8 X. Zhou, X. Guo, F. Jian and G. Wei, ACS Omega, 2018, 3, 4418–4422.
- 9 M. Khalil, G. T. M. Kadja and M. M. Ilmi, *Journal of Industrial and Engineering Chemistry*, 2021, **93**, 78–100.
- 10 A. Shetty, D. Sunil, T. Rujiralai, S. P. Maradur, A. N. Alodhayb and G. Hegde, *Nanoscale Adv*, 2024, **6**, 2516–2526.
- 11 M. Sui, S. Kunwar, P. Pandey and J. Lee, *Sci Rep*, 2019, **9**, 16582.
- 12 M. A. Darwish, W. Abd-Elaziem, A. Elsheikh and A. A. Zayed, *Nanoscale Adv*.
- 13 Z.-L. Zhou, T.-F. Kang, Y. Zhang and S.-Y. Cheng, *Microchimica Acta*, 2009, **164**, 133–138.
- 14 H. S. Lahoti, S. D. Jogdand and H. Lahoti, *Cureus*.
- 15 S. Siddique and J. C. L. Chow, *Nanomaterials*, 2020, **10**, 1700.

- Y. Zhong, Z. Ma, F. Wang, X. Wang, Y. Yang, Y. Liu, X. Zhao, J. Li, H. Du, M. Zhang, Q. Cui, S. Zhu, Q. Sun, H. Wan, Y. Tian, Q. Liu, W. Wang, K. C. Garcia and H. Dai, *Nat Biotechnol*, 2019, 37, 1322–1331.
- O. Esim, S. Kurbanoglu, A. Savaser, S. A. Ozkan and Y. Ozkan, in *New developments in nanosensors for pharmaceutical analysis*, Elsevier, 2019, pp. 273–301.
- 18 M. L. Etheridge, S. A. Campbell, A. G. Erdman, C. L. Haynes, S. M. Wolf and J. McCullough, *Nanomedicine*, 2013, **9**, 1–14.
- 19 M. Palombo, M. Deshmukh, D. Myers, J. Gao, Z. Szekely and P. J. Sinko, *Annu Rev Pharmacol Toxicol*, 2014, **54**, 581–598.
- J. Safari and Z. Zarnegar, Journal of Saudi Chemical Society, 2014, 18, 85–99.
- 21 H. Ragelle, D. Fabienne, P. Véronique, L. Robert and D. G. and Anderson, *Expert Opin Drug Deliv*, 2017, **14**, 851–864.
- M. Tuerhong, X. U. Yang and Y. I. N. Xue-Bo, *Chinese Journal of Analytical Chemistry*, 2017, **45**, 139–150.
- 23 X. Xu, R. Ray, Y. Gu, H. J. Ploehn, L. Gearheart, K. Raker and W. A. Scrivens, *J Am Chem Soc*, 2004, **126**, 12736–12737.
- 24 Y. Ando and X. Zhao, New diamond and frontier carbon technology, 2006, 16, 123–138.
- A. Jorio and G. Dresselhaus, in *Encyclopedia of Physical Science and Technology (Third Edition)*, ed. R. A. Meyers, Academic Press, New York, 2003, pp. 315–335.
- Y.-P. Sun, B. Zhou, Y. Lin, W. Wang, K. A. S. Fernando, P. Pathak, M. J. Meziani, B. A. Harruff, X. Wang and H. Wang, *J Am Chem Soc*, 2006, 128, 7756–7757.
- S. Zhu, Q. Meng, L. Wang, J. Zhang, Y. Song, H. Jin, K. Zhang, H. Sun, H. Wang and B. Yang, *Angewandte Chemie International Edition*.

- A. Clermont-Paquette, D.-A. Mendoza, A. Sadeghi, A. Piekny and R. Naccache, *Sensors*, 2023, **23**, 5200.
- 29 K. J. Mintz, M. Bartoli, M. Rovere, Y. Zhou, S. D. Hettiarachchi, S. Paudyal, J. Chen, J. B. Domena, P. Y. Liyanage and R. Sampson, *Carbon N Y*, 2021, **173**, 433–447.
- 30 M. Jorns and D. Pappas, *Nanomaterials*, 2021, **11**, 1448.
- 31 F. Yan, Y. Jiang, X. Sun, Z. Bai, Y. Zhang and X. Zhou, *Microchimica Acta*, 2018, **185**, 1–34.
- 32 S. Li, D. Amat, Z. Peng, S. Vanni, S. Raskin, G. De Angulo, A. M. Othman, R. M. Graham and R. M. Leblanc, *Nanoscale*, 2016, **8**, 16662–16669.
- Disha, P. Kumari, M. K. Patel, P. Kumar and M. K. Nayak, *Biosensors (Basel)*, 2022, **12**, 993.
- P. R. Sreenath, S. Mandal, H. Panigrahi, P. Das and K. D. Kumar, *Nano-Structures & Nano-Objects*, 2020, **23**, 100477.
- Y. Zhang, Y. Wang, X. Feng, F. Zhang, Y. Yang and X. Liu, *Appl Surf Sci*, 2016, 387, 1236–1246.
- 36 H. Tang, Y. Tang, M. Xiao, H. Zhu and M. Guo, Colloids Surf A Physicochem Eng Asp, 2022, 651, 129564.
- L. Bao, Z. Zhang, Z. Tian, L. Zhang, C. Liu, Y. Lin, B. Qi and D. Pang, *Adv Mater*, 2011,23, 5801–5806.
- 38 L. Bao, C. Liu, Z. Zhang and D. Pang, *Advanced Materials*, 2015, **27**, 1663–1667.
- 39 C. Kang, Y. Huang, H. Yang, X. F. Yan and Z. P. Chen, *Nanomaterials*, 2020, **10**, 2316.
- 40 M. Liu, Nanoarchitectonics, 2020, 1–12.

- 41 M.-H. Chan, B.-G. Chen, L. T. Ngo, W.-T. Huang, C.-H. Li, R.-S. Liu and M. Hsiao, *Pharmaceutics*, 2021, **13**, 1874.
- 42 A. Clermont-Paquette, K. Larocque, A. Piekny and R. Naccache, *Mater Adv*, 2024, **5**, 3662–3674.
- 43 S.-T. Yang, X. Wang, H. Wang, F. Lu, P. G. Luo, L. Cao, M. J. Meziani, J.-H. Liu, Y. Liu and M. Chen, *The Journal of Physical Chemistry C*, 2009, **113**, 18110–18114.
- W. Kasprzyk, T. Świergosz, P. P. Romańczyk, J. Feldmann and J. K. Stolarczyk, *Nanoscale*, 2022, 14, 14368–14384.
- 45 M. K. Mahto, D. Samanta, M. Shaw, M. A. S. Shaik, R. Basu, I. Mondal, A. Bhattacharya and A. Pathak, *ACS Appl Nano Mater*, 2023, **6**, 8059–8070.
- S. Ganguly, P. Das, S. Banerjee and N. C. Das, *Functional Composites and Structures*, 2019,1, 022001.
- 47 Z. Han, L. He, S. Pan, H. Liu and X. Hu, *Luminescence*, 2020, **35**, 989–997.
- 48 P. Zhao, X. Li, G. Baryshnikov, B. Wu, H. Ågren, J. Zhang and L. Zhu, *Chem Sci*, 2018, **9**, 1323–1329.
- 49 R. Gedye, F. Smith, K. Westaway, H. Ali, L. Baldisera, L. Laberge and J. Rousell, Tetrahedron Lett, 1986, 27, 279–282.
- 50 C. O. Kappe, Angewandte Chemie International Edition, 2004, 43, 6250–6284.
- T. V. De Medeiros, J. Manioudakis, F. Noun, J. R. Macairan, F. Victoria and R. Naccache, *J Mater Chem C Mater*, 2019, **7**, 7175–7195.
- 52 H. K. M. Ng, G. K. Lim and C. P. Leo, *Microchemical Journal*, 2021, **165**, 106116.
- 53 Y. Zhuo, Y.-G. Zhao and Y. Zhang, *Molecules*, 2024, **29**, 4854.

- 54 S. Zhang, Q. Fu, Y. Zhang, J. Pan, L. Zhang, Z. Zhang and Z. Liu, *Acta Pharmacol Sin*, 2021, 42, 1040–1054.
- A. O. Elzoghby, W. M. Samy and N. A. Elgindy, *Journal of controlled release*, 2012, **157**, 168–182.
- 56 S. M. FINEGOLD, Ann Intern Med, 1980, **93**, 585–587.
- 57 S. M. Ibrahim, A. S. Al-Mizraqchi and J. Haider, *Antibiotics*, 2023, **12**, 1288.
- 58 Z. Wang, Z. Wang and F. Wu, *ChemMedChem*, 2022, **17**, e202200003.
- 59 S. M. Ardekani, A. Dehghani, P. Ye, K.-A. Nguyen and V. G. Gomes, *J Colloid Interface Sci*, 2019, 552, 378–387.
- 60 B. A. Weaver, How Taxol/Paclitaxel Kills Cancer Cells. MBoC 25, 2677-2681. doi: 10.1091/mbc, E14-04-0916, 2014.
- E. Bernabeu, M. Cagel, E. Lagomarsino, M. Moretton and D. A. Chiappetta, *Int J Pharm*, 2017, **526**, 474–495.
- 62 I. J. Gomez, B. Arnaiz, M. Cacioppo, F. Arcudi and M. Prato, *J Mater Chem B*, 2018, **6**, 5540–5548.
- 63 Q. Zeng, D. Shao, X. He, Z. Ren, W. Ji, C. Shan, S. Qu, J. Li, L. Chen and Q. Li, *J Mater Chem B*, 2016, **4**, 5119–5126.
- V. Ejigah, O. Owoseni, P. Bataille-Backer, O. D. Ogundipe, F. A. Fisusi and S. K. Adesina, *Polymers (Basel)*, 2022, **14**, 2601.
- F. Everaerts, M. Torrianni, M. Hendriks and J. Feijen, Journal Of Biomedical Materials Research Part A: An Official Journal Of The Society For Biomaterials, The Japanese Society For Biomaterials, And The Australian Society For Biomaterials And The Korean Society For Biomaterials, 2008, 85, 547–555.

- S. D. Hettiarachchi, R. M. Graham, K. J. Mintz, Y. Zhou, S. Vanni, Z. Peng and R. M. Leblanc, *Nanoscale*, 2019, **11**, 6192–6205.
- 67 M. Ciaccia and S. Di Stefano, *Org Biomol Chem*, 2015, **13**, 646–654.
- 68 K. Norwich, Front Physiol, 2010, 1, 1760.
- 69 M. E. Belowich and J. F. Stoddart, *Chem Soc Rev*, 2012, **41**, 2003–2024.
- S. A. Rackley, in *Carbon Capture and Storage*, ed. S. A. Rackley, Butterworth-Heinemann, Boston, 2010, pp. 353–372.
- 71 L. J. Silverberg, D. J. Coyle, K. C. Cannon, R. T. Mathers, J. A. Richards and J. Tierney, J. Chem Educ, 2016, 93, 941–944.
- J. McMurry, Organic Chemistry, OpenStax, 10th edn., 2023.
- G. Bosica, R. Abdilla, K. Demanuele and J. Fiteni, *PeerJ Organic Chemistry*, 2022, 4, e7.
- V. Yadav, J. Reang, V. Sharma, J. Majeed, P. C. Sharma, K. Sharma, N. Giri, A. Kumar and R. K. Tonk, *Chem Biol Drug Des*, 2022, 100, 389–418.
- I. L. Aleksanyan and L. P. Hambardzumyan, Russian Journal of Organic Chemistry, 2024,60, 1585–1590.
- 76 M. Ciaccia and S. Di Stefano, *Org Biomol Chem*, 2015, **13**, 646–654.
- 77 M. Dalal, A Textbook of Organic Chemistry–Volume 1, Dalal Institute, 2019.
- 78 A. Hejl, M. W. Day and R. H. Grubbs, *Organometallics*, 2006, **25**, 6149–6154.
- 79 E. Nwoye, S. Raghuraman, M. Costales, J. Batteas and J. R. Felts, *Physical Chemistry Chemical Physics*, 2023, **25**, 29088–29097.
- 80 E. Boldyreva, *Chem Soc Rev*, 2013, **42**, 7719–7738.
- M. Nic, L. Hovorka, J. Jirat, B. Kosata and J. Znamenacek, *IUPAC compendium of chemical terminology-the gold book*, International Union of Pure and Applied Chemistry, 2005.

- M. Banerjee, P. C. Panjikar, D. Das, S. Iyer, A. A. Bhosle and A. Chatterjee, *Tetrahedron*, 2022, **112**, 132753.
- 83 C. F. Burmeister and A. Kwade, *Chem Soc Rev*, 2013, **42**, 7660–7667.
- 84 C. Espro and D. Rodríguez-Padrón, Curr Opin Green Sustain Chem, 2021, 30, 100478.
- 85 T. Seo, K. Kubota and H. Ito, *J Am Chem Soc*, 2020, **142**, 9884–9889.
- V. Sereikaitė, T. M. T. Jensen, C. R. O. Bartling, P. Jemth, S. A. Pless and K. Strømgaard, *Chembiochem*, 2018, **19**, 2136–2145.
- F. Garzón-Posse, Y. Quevedo-Acosta and D. Gamba-Sánchez, *J Chem Educ*, 2022, **99**, 2385–2391.
- 88 L. Zhu, L. Deng, Y. Xie, L. Liu, X. Ma and R. Liu, Results Chem, 2023, 5, 100882.
- 89 S. Han, J. Lee, E. Jung, S. Park, A. Sagawa, Y. Shibasaki, D. Lee and B.-S. Kim, *ACS Appl Bio Mater*, 2021, **4**, 2465–2474.
- 90 G. A. Ozin and A. Arsenault, *Nanochemistry: a chemical approach to nanomaterials*, Royal Society of Chemistry, 2015.
- 91 P. Bergese and K. Hamad-Schifferli, *Nanomaterial Interfaces in Biology*, Springer, 2013, vol. 1025.
- 92 J. Yao, Y. Sun, M. Yang and Y. Duan, *J Mater Chem*, 2012, **22**, 14313–14329.
- 93 C. T. Matea, T. Mocan, F. Tabaran, T. Pop, O. Mosteanu, C. Puia, C. Iancu and L. Mocan, Int J Nanomedicine, 2017, 5421–5431.
- A. Bagheri, H. Arandiyan, C. Boyer and M. Lim, *Advanced Science*, 2016, **3**, 1500437.
- 95 X. Wang, D. Niu, C. Hu and P. Li, *Curr Pharm Des*, 2015, **21**, 6140–6156.
- 96 Y. Tian, Z. Gao, N. Wang, M. Hu, Y. Ju, Q. Li, F. Caruso, J. Hao and J. Cui, *J Am Chem Soc*, 2022, **144**, 18419–18428.

- 97 L. He, Z. Shang, H. Liu and Z. Yuan, *Biomed Res Int*, 2020, **2020**, 1487259.
- 98 L. Xing, Y.-T. Fan, L.-J. Shen, C.-X. Yang, X.-Y. Liu, Y.-N. Ma, L.-Y. Qi, K.-H. Cho, C.-S. Cho and H.-L. Jiang, *Int J Biol Macromol*, 2019, **141**, 85–97.
- 99 A. Samad, Y. Sultana and M. Aqil, *Curr Drug Deliv*, 2007, **4**, 297–305.
- 100 R. H. Müller, K. Mäder and S. Gohla, European journal of pharmaceutics and biopharmaceutics, 2000, **50**, 161–177.
- 101 Q. Wang, X. Huang, Y. Long, X. Wang, H. Zhang, R. Zhu, L. Liang, P. Teng and H. Zheng, Carbon N Y, 2013, 59, 192–199.
- G. Calabrese, G. De Luca, G. Nocito, M. G. Rizzo, S. P. Lombardo, G. Chisari, S. Forte, E.
 L. Sciuto and S. Conoci, *Int J Mol Sci*, 2021, 22, 11783.
- 103 W. Li, Y. Ma, L. Ou, C. Xu, Y. Wei, K. Yang and B. Yuan, J Hazard Mater, 2024, 465, 133382.
- 104 C. Kong, K. Wang, L. Sun, H. Zhao, T. Wang, W. Zhou, D. Wu and F. Xu, *Int J Nanomedicine*, 2024, 3611–3622.
- 105 D. M. Arvapalli, A. T. Sheardy, K. Allado, H. Chevva, Z. Yin and J. Wei, ACS Appl Bio Mater, 2020, 3, 8776–8785.
- W. Luo, L. Zhang, X. Li, J. Zheng, Q. Chen, Z. Yang, M. Cheng, Y. Chen, Y. Wu and W. Zhang, *Nano Res*, 2022, 15, 9274–9285.
- 107 J. Li, Q. Li, Q. Yang, Q. Tang, X. Hu, Q. Liu and L. Zhang, *Mater Today Nano*, 2024, 100532.
- 108 H. Zhao, J. Duan, Y. Xiao, G. Tang, C. Wu, Y. Zhang, Z. Liu and W. Xue, *Chemistry of Materials*, 2018, 30, 3438–3453.
- 109 T. Feng, X. Ai, G. An, P. Yang and Y. Zhao, ACS Nano, 2016, **10**, 4410–4420.

- 110 F. Yarur, J. R. Macairan and R. Naccache, Environ Sci Nano, 2019, 6, 1121–1130.
- 111 Y.-Y. Yao, G. Gedda, W. M. Girma, C.-L. Yen, Y.-C. Ling and J.-Y. Chang, *ACS Appl Mater Interfaces*, 2017, **9**, 13887–13899.
- Z. Wang, H. Liao, H. Wu, B. Wang, H. Zhao and M. Tan, *Analytical Methods*, 2015, 7, 8911–8917.
- 113 T. Feng, X. Ai, H. Ong and Y. Zhao, ACS Appl Mater Interfaces, 2016, **8**, 18732–18740.
- J. Qi, R. Zhang, X. Liu, Y. Liu, Q. Zhang, H. Cheng, R. Li, L. Wang, X. Wu and B. Li, ACS Appl Nano Mater, 2023, 6, 9071–9084.
- 115 C. Hogarth, K. Arnold, A. McLauchlin, S. P. Rannard, M. Siccardi and T. O. McDonald, *J Mater Chem B*, 2021, **9**, 9874–9884.
- S. D. Hettiarachchi, E. K. Cilingir, H. Maklouf, E. S. Seven, S. Paudyal, S. Vanni, R. M. Graham and R. M. Leblanc, *Nanoscale*, 2021, **13**, 5507–5518.
- 1-Ethyl-3-(3-Dimethylaminopropyl)carbodiimide, Hydrochloride, Thermo Fisher Scientific, https://www.thermofisher.com/order/catalog/product/E2247, (accessed 23 April 2025).
- 1-Ethyl-3-(3-Dimethylaminopropyl)carbodiimide, Hydrochloride, SDS Cat No. E2247,
 Thermo Fisher Scientific, https://assets.thermofisher.com/TFS-Assets/LSG/SDS/E2247_MTR-NALT_EN.pdf, (accessed 23 April 2025).
- 119 X. Qu and Z. Yang, Chemistry—An Asian Journal, 2016, 11, 2633–2641.
- 120 Y. Tao, S. Liu, Y. Zhang, Z. Chi and J. Xu, *Polym Chem*, 2018, **9**, 878–884.
- 121 H. Ding, P. Tan, S. Fu, X. Tian, H. Zhang, X. Ma, Z. Gu and K. Luo, *Journal of Controlled Release*, 2022, **348**, 206–238.

- 122 C. C. Scott, F. Vacca and J. Gruenberg, in *Seminars in cell & developmental biology*, Elsevier, 2014, vol. 31, pp. 2–10.
- 123 J.-L. Do and T. Friščić, ACS Cent Sci, 2017, 3, 13–19.
- 124 X. Liu, Y. Li, L. Zeng, X. Li, N. Chen, S. Bai, H. He, Q. Wang and C. Zhang, *Advanced Materials*, 2022, **34**, 2108327.
- 125 J. Qu, Y. Wang, X. Mu, J. Hu, B. Zeng, Y. Lu, M. Sui, R. Li and C. Li, *Advanced Materials*, 2022, **34**, 2203320.
- J. Xing, K. Takeuchi, K. Kamei, T. Nakamuro, K. Harano and E. Nakamura, *Proceedings of the National Academy of Sciences*, 2022, **119**, e2114432119.
- D. Ozyurt, M. Al Kobaisi, R. K. Hocking and B. Fox, Carbon Trends, 2023, 12, 100276.
- 128 R. Alam, A. Das, G. Huang, L. Eriksson, F. Himo and K. J. Szabó, *Chem Sci*, 2014, **5**, 2732–2738.
- E. A. Boyle, P. C. Freemanm, F. R. Mangan and M. J. Thomson, *Journal of Pharmacy and Pharmacology*, 1982, **34**, 562–569.
- 4-(6-methoxy-2-napthalenyl)-2-butanone, Cayman Chemical, https://www.caymanchem.com/product/20251?srsltid=AfmBOorffZhElt1uWYRWqtqybn-5VLUxyYGfIAyQe2Ajv1G7hJxj14M5, (accessed 5 May 2025).
- 131 Firmenich S. A., World Intellectual Property Organization, 2006.
- D. P. Bezerra, A. K. N. Soares and D. P. de Sousa, Oxid Med Cell Longev, 2016, 2016, 9734816.
- 133 A. Macina, T. V. De Medeiros and R. Naccache, *J Mater Chem A Mater*, 2019, **7**, 23794–23802.

- T. Miura, N. Sugimoto, S. Bhavaraju, T. Yamazaki, Y. Nishizaki, Y. Liu, A. Bzhelyansky, C. Amezcua, J. Ray and E. Zailer, *Chem Pharm Bull (Tokyo)*, 2020, **68**, 868–878.
- W. Xin, W. Yumei, G. Xianmou, G. Kaijun, L. Jing, L. Sanming, Z. Lin and H. and Li, *Int J Nanomedicine*, 2020, **15**, 7451–7468.
- D. Gonzalez, G. G. Rao, S. C. Bailey, K. L. R. Brouwer, Y. Cao, D. J. Crona, A. D. M. Kashuba, C. R. Lee, K. Morbitzer and J. H. Patterson, *Clin Transl Sci*, 2017, **10**, 443.
- 137 J. Tamargo, J.-Y. Le Heuzey and P. Mabo, *Eur J Clin Pharmacol*, 2015, **71**, 549–567.
- 138 S. Shen, Y. Wu, Y. Liu and D. Wu, *Int J Nanomedicine*, 2017, 4085–4109.
- 139 G. Yang, Y. Liu, S. Jin, Y. Hui, X. Wang, L. Xu, D. Chen, D. Weitz and C. Zhao, *Aggregate*, 2023, 4, e314.
- S. Saghazadeh, C. Rinoldi, M. Schot, S. S. Kashaf, F. Sharifi, E. Jalilian, K. Nuutila, G. Giatsidis, P. Mostafalu and H. Derakhshandeh, *Adv Drug Deliv Rev*, 2018, **127**, 138–166.
- J. Ortenzio, L. Degn, A. Goldstein-Plesser, J. K. McGee, J. Navratilova, K. Rogers, R. M. Zucker and W. K. Boyes, *NanoImpact*, 2019, 14, 100156.
- H. Sahin, O. Yucel, P. Holloway, E. Yildirim, S. Emik, G. Gurdag, G. Tanriverdi and G. Erkanli Senturk, *Pharmaceuticals*, 2024, **17**, 1567.
- A. Azqueta, H. Stopper, B. Zegura, M. Dusinska and P. Møller, *Mutation Research/Genetic Toxicology and Environmental Mutagenesis*, 2022, **881**, 503520.
- M. R. Romano, C. Gatto, L. Giurgola, E. Ragazzi and J. D. Tóthová, *Transl Vis Sci Technol*,2021, 10, 24.

Chapter 6. Appendix

The following is a list of published manuscripts which are not directly related to the topic of this thesis but are included as a record of the research outputs achieved throughout the MSc program.

Adeola, A. O.; Paramo, L.; **Fuoco, G**.; Naccache, R. Emerging Hazardous Chemicals and Biological Pollutants in Canadian Aquatic Systems and Remediation Approaches: A Comprehensive Status Report. *Science of The Total Environment* **2024**, 176267. https://doi.org/10.1016/j.scitotenv.2024.176267.

While drug delivery is a core interest, it is also important to recognize that pharmaceuticals make up a large portion of pollutants found in aquatic ecosystems, for this reason a lignin-derived magnetic carbon-based material was developed and implemented for the removal of pharmaceutical mixtures from water through adsorption.

Duarte, M. P.; Adeola, A. O.; Fuoco, G.; Jargaille, T. J.; Naccache, R. Efficient Decaffeination with Recyclable Magnetic Microporous Carbon from Renewable Sources: Kinetics and Isotherm Analysis. *Environ Res* 2024, 258, 119446. https://doi.org/10.1016/j.envres.2024.119446.

Similar to CDs, many carbon-based materials exist and exhibit desirable properties. In this manuscript, a microporous activated carbon material and its magnetic derivative were synthesized and exhibited high adsorption efficiency for caffeine suggesting a potentially effective remediation tool for water containing high levels of caffeine contaminants.

Adeola, A. O.; **Fuoco, G.**; Adegoke, K. A.; Adeleke, O.; Oyebamiji, A. K.; Paramo, L.; Naccache, R. Experimental, Machine-Learning, and Computational Studies of the Sequestration of Pharmaceutical Mixtures Using Lignin-Derived Magnetic Activated Carbon.

ACS Sustainable Resource Management **2025**, 2 (1), 219–230. https://doi.org/10.1021/acssusresmgt.4c00451.

Lastly, a review article was published surrounding emerging contaminants found within Canadian water systems. As a Canadian born scientist, this review shed light on the need for research surrounding novel and effective water polishing tools as our water systems are not immune from pollution.

ELSEVIER

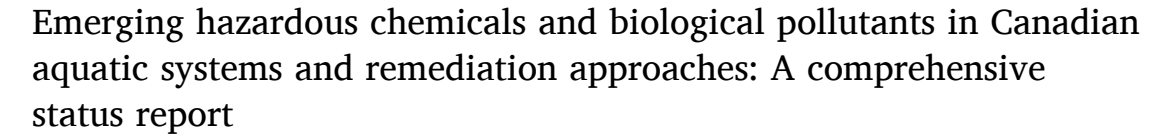
Contents lists available at ScienceDirect

Science of the Total Environment

journal homepage: www.elsevier.com/locate/scitotenv



Review



Adedapo O. Adeola*, Luis Paramo¹, Gianluca Fuoco¹, Rafik Naccache

Department of Chemistry and Biochemistry and the Centre for NanoScience Research, Concordia University, Montreal, QC H4B 1R6, Canada Quebec Centre for Advanced Materials, Department of Chemistry and Biochemistry, Concordia University, Montreal, QC H4B 1R6, Canada

HIGHLIGHTS

- Emerging contaminants, natural or synthetic, pose threats to water systems.
- Canada with 7 % of the global freshwater supply, faces rising contamination.
- Pharmaceuticals, pesticides, heavy metals, and hydrocarbons pose public health risks.
- Wastewater surveillance reveals risks from antibiotic-resistant and SARS-CoV-2 genes.
- Canadian researchers are investigating remediation and preventive measures.

G R A P H I C A L A B S T R A C T



ARTICLE INFO

Editor: Jay Gan

Keywords:
Emerging contaminants
Heavy metals
Pharmaceuticals
Pesticides
Remediation
SARS-COV-2 virus

ABSTRACT

Emerging contaminants can be natural or synthetic materials, as well as materials of a chemical, or biological origin; these materials are typically not controlled or monitored in the environment. Canada is home to nearly 7 % of the world's renewable water supply and a wide range of different kinds of water systems, including the Great Lake, rivers, canals, gulfs, and estuaries. Although the majority of these pollutants are present in trace amounts (μ g/L - η g/L concentrations), several studies have reported their detrimental impact on both human health and the biota. In Canadian aquatic environments, concentrations of pharmaceuticals (as high as $115 \, \mu$ g/L), pesticides (as high as $1.95 \, \mu$ g/L), bioavailable heavy metals like dissolved mercury (as high as $135 \, \eta$ g/L), and hydrocarbon/crude oil spills (as high as $4.5 \, m$ illion liters) have been documented. Biological threats such as genetic materials of the contagious SARS-CoV-2 virus have been reported in the provinces of Québec, Ontario, Saskatchewan and Manitoba provinces, as well as in the Nunavut territory, with a need for more holistic research. These toxins and emerging pollutants are associated with nefarious short and long-term health effects, with the potential for bioaccumulation in the environment. Hence, this Canadian-focused report provides the footprints for water and environmental sustainability, in light of this emerging threat to the environment and society. Several remediation pathways/tools that have been explored by Canadian researchers, existing challenges and prospects are also

E-mail addresses: adedapo.adeola@concordia.ca (A.O. Adeola), rafik.naccache@concordia.ca (R. Naccache).

^{*} Corresponding authors.

¹ These authors contributed equally and share the second authorship of this publication.

1. Introduction

Water pollution has become a worldwide challenge and it is estimated that several million tons of human waste is expelled into aquatic systems per annum (Bell et al., 2011; Sami Ullah and Umara, 2021). Thus, the emphasis of the United Nations' Sustainable Development Goal (SDG) #6, is the need to facilitate access to safe water sources and sanitation (UNSDG, 2018). The quality and sustainability of water supplies must be addressed, as they are vital to human and environmental safety (Bhaduri et al., 2016; UNSDG, 2018). Aquatic systems may be exposed to contaminants due to various anthropogenic activities such as deforestation, transportation, and construction activities, as well as agricultural, industrial, and domestic activities (Bashir et al., 2020). Emerging pollutants (EPs) go by various names, such as "contaminants of emerging concern (CEC)", "emerging contaminants (ECs)", "micropollutants (MPs), emerging pollutants (EPs), or "trace organic compounds (TrOCs)". EPs are described as chemically fabricated or naturally occurring substances that are not typically monitored, but have the potential to emerge into natural environments and cause adverse effects for many biological organisms (Adeola and Forbes, 2021b; Geissen et al., 2015). Most of these pollutants are organic in nature, and they normally exist in trace amounts at concentrations between parts per trillion (ppt or ng/L) to parts per billion (ppb or µg/L) (Bashir et al., 2020; Schwartz et al., 2021a). Emerging pollutants in our environment raise substantial concern due to implications to human health and the well-being of flora and fauna in our natural environments, as a result of the potential for bioaccumulation due to continuous exposure, or one-time exposure to pollutant concentrations that surpass environmental safety limits.

In Canada, EPs such as pharmaceuticals, cosmetics, personal care items, industrial additives, surfactants, hormones, antibiotic-resistant genes, and aromatic hydrocarbons, have been discovered in waste-,

ground-, drinking and surface waters (Cuprys et al., 2019; Fernando et al., 2016; Neudorf et al., 2017; Schwartz et al., 2021a). The presence of foreign substances or chemicals in aquatic systems amounts to contamination, and the buildup of these contaminants may lead to pollution and its resulting challenges. Numerous avenues allow chemicals to infiltrate the aquatic environment, such as surface runoff containing fertilizers, processed sludge/wastewater, and other pollutants from urban or agricultural regions (Fig. 1). Other pathways are the direct discharge of treated or raw wastewater from municipalities, industrial and hospital wastewater treatment plants (WWTPs), and/or accidental spillage (Oluwole et al., 2020; Rodriguez-Narvaez et al., 2017). Although there is growing attention to the increasing concentrations of contaminants in aquatic systems in Canada, there are no comprehensive reports/reviews, directed towards the occurrence and impacts of chemical and biological contaminants in Canada, yet it is vital to address these knowledge gaps, review scientific strides in the identification of EPs in Canada, and propose preventive measures for public health safety and protection.

2. Emerging pollutants and classifications

Various unregulated chemical compounds, including pharmaceuticals, household products, and industrial chemicals, pose risks to humans and animals in Canada's water bodies, harming aquatic life and potentially impacting human health (Femi-Oloye et al., 2023; Lei et al., 2015; Lishman et al., 2006; Petrie et al., 2015). Although pollutants can be organized according to the listed categories (Table 1), the examples of compounds assigned to each category are quite extensive and may overlap. It is for this reason that a global general classification of emerging contaminants has yet to be recognized. These substances can typically consist of poly/per-fluoroalkyls, microplastics, nanoparticles,



Fig. 1. A broad categorization of emerging chemical pollutants in various hydrogeological compartments.

parabens, bisphenols, antibiotics, antiviral/antiretrovials, among many others; their origins are often attributed to industrial additives, constituents of pharma products, personal care items, or disinfectants (Adeola and Forbes, 2021b; Ganesan et al., 2022; Sun et al., 2016; Tang et al., 2022; Vale et al., 2022; Viaroli et al., 2022). Table 1 highlights the variety of global emerging contaminants, including those found in Canadian aquatic systems.

3. Nature of water systems in Canada

Canada is home to nearly 7 % of the world's renewable water supply and a wide range of different kinds of water systems, including lakes, rivers, canals, gulfs, and estuaries [ECCC, 2013]. Canada boasts a vast array of aquatic systems, with five of them officially recognized as part of the country's Great Lakes system on a global scale. This is because the largest collection of connected freshwater lakes in the world—Lakes Erie, Superior, Huron, and Ontario—occupy slightly >20 % of the planet's fresh surface water (Ghosh, 2021). The total surface area of all surface freshwater originating from the Great Lakes is an astounding 244,106 km² with a total volume of 22,671 km³ (Krushelnicki, 1995). The Great Lakes of Canada hosts a large and diverse population of flora and fauna, including 150 different species of fish within the aquatic bodies (Grady, 2007).

The water systems in Canada represent a complex and interconnected network where rivers from Southern Ontario drain into the St. Lawrence River system, the Great Lakes, and ultimately the Atlantic Ocean. Rivers in Northern Ontario empty into Hudson Bay and James Bay, while the Ottawa River, which originates in western Quebec and naturally divides Ontario and Quebec, is one of the major rivers that flows towards the Atlantic Ocean. The St. Lawrence River, its estuary, and the gulf are the most significant waterway and geographical features in the province of Quebec. The Richelieu, Yamaska, Chaudière, and Matapédia rivers on the southern shore are the principal tributaries of the St. Lawrence River while the Saint-Maurice, Saguenay, Manicouagan, and Ottawa rivers are located on the north shore of the province. With the exception of the Petitot River, which empties into the Mackenzie River directly after passing through the Liard River and avoiding the Great Slave Lake, all of Alberta's rivers that are part of the Arctic Ocean watershed drain into the Mackenzie River. The province's northern rivers discharge at a somewhat faster pace than its southern rivers, which flow through a drier region. The northern rivers empty into the Arctic Ocean. Apart from the Milk River and its tributaries, which flow south through the Missouri and Mississippi Rivers to the Gulf of Mexico, the majority of the southern half of Alberta is covered by waterways that flow towards Hudson Bay. Many significant rivers, including the Fraser, Columbia, Peace, and Skeena Rivers, drain various regions of British Columbia. In addition, the Coast Mountains yield a number of small rivers that flow westward into the Pacific Ocean, while others empty onto Vancouver Island and the Queen Charlotte Islands.

Historically, the variety and amount of fish residing within bodies of water in Canada were indicative of how healthy the environment was. The same can be attributed to the flora residing in these water systems, including but not limited to Bartonia paniculata, Eleocharis tricostata, Panicum verrucosum, and Xyris torta (Reznicek, 1994). As important as these great water systems are to humans and aquatic life, it is currently subjected to increasingly higher levels of pollution arising from anthropogenic activities and the rise in mercury-containing compounds leading to the near extinction of several species. In a study conducted by Gandhi et al., an analysis of >200,000 samples of fish by the Ontario Ministry of the Environment revealed that mercury levels in fish fall between 0.01 and 0.07 μ g/g. However, the analysis also showed a trend of increased mercury content (between 0.01 and 0.27 µg/g) in fish species found in water bodies in Walleve and Pike located in northern Ontario between 1995 and 2012 (Gandhi et al., 2014). In a related study by Depew et al., an analysis of data collected by the Canadian fish mercury database revealed that mercury levels ranged between 0.11 and 10.9 μg/g wet mass, for analysis carried out on different fish species. However, it was determined that increased mercury levels were related to the species' trophic level, whereas the highest mercury levels corresponded to predatory species. Median concentrations like 0.42, 0.41, 0.38, and 0.33 were found in species like sauger, walleye, northern pike, and smallmouth bass, respectively (Depew et al., 2013). While these concentrations are relatively low, the potential for bioaccumulation/ bioconcentration upon repeated exposures to trace-level contaminants poses latent risk.

Moreover, chemicals, including microplastics, have been detected in fish populations in alarming concentrations which has now raised concerns about how human health will be affected upon consumption (Arnnok et al., 2017; Munno et al., 2022). According to Alimi et al., most of the plastics that end up in the ocean are transported by rivers, and their sources can be ascribed to land, agriculture, or wastewater treatment plants (Alimi et al., 2018). In water bodies like the Saint Lawrence

Table 1Classification of emerging pollutants that are often reported in aquatic systems.

Classification	Description	Examples	Reference
Personal care products	Typically composed of a combination of chemical compounds, including pigments, emollients, surfactants, and preservatives used for the enhancement or changing of one's physical appearance	2-(p-nonylphenoxy) ethanol, 2-nonylphenol, 4-tert-octylphenol, 2-amino musk ketone, civetone, 2-ethylhexyl-p-methoxycinnamate, 4-methylbenzylidenecamphor, ethylparaben, methylparaben, etc.	(Montes-Grajales et al., 2017)
Pharmaceuticals	Chemicals are specifically formulated for preventing, treating, or alleviating medical conditions, diseases, or symptoms in humans or animals.	Sulfamethoxazole, ciprofloxacin Penicillin, methotrexate, daunorubicin, estrone, estriol, nevirapine, efavirenz, etc.	(Abdallat et al., 2022; Schwartz et al., 2021b)
Synthetic/industrial chemicals	Compounds produced by chemical reactions or processes, and manufactured for a wide range of industrial, commercial, scientific, and technological applications.	Dyes, triphenylmethane, anthraquinone, triethyl citrate, butylated hydroxyanisole, camphor, citral, polyfluoroalkyls, etc.	(Singh et al., 2021; Stuart et al., 2012)
Water treatment byproducts	Chemical substances that are generated from the treatment of water or wastewater for safe consumption or discharge as effluents.	Bromodichloromethane, chloroacetic acid, dichloroacetaldehyde, 2-chlorophenol, bromoacetonitrile, iodoacetonitrile, mucochloric acid, etc.	(Gilca et al., 2020; Koley et al., 2024)
Algae-derived toxins	Toxic compounds are produced by various types of algae, particularly certain species of microalgae and cyanobacteria (blue-green algae). These toxins can have harmful effects on aquatic ecosystems, marine life, and even humans.	Cytotoxin, oscillatoxin, anatoxin, axitoxin, hemolysins, lyngbyatoxin, debromoaplysiatoxin, etc.	(Qian et al., 2015)
Biocides/pesticides	Agents are used to prevent the growth or proliferation of various types of microorganisms, including bacteria, fungi, algae, viruses, and other unwanted pests.	Malathion, temephos, propoxur, bendiocarb, carbaryl, cyfluthrin, permethrin, etc.	(Femi-Oloye et al., 2023; Hassaan and El Nemr, 2020)
Steroid hormones and biological agents	Natural and synthetic biological agents that may disrupt the optimal function of the endocrine system, affect reproductive functions and other adverse effects.	Testoterone, progesterone, norgestrel, cortisol, estrogen, aldosterone, Spironolactone, etc.	(Ojoghoro et al., 2021; Xie et al., 2022)

River, a multiple site analysis revealed that there is a presence of microplastics, where plastic with sizes ranging from 20 to 300 mm maintained a concentration between 0 and 1.4 items/L; on the other hand, smaller microplastics of 300 to 3200 mm had concentration ranging from 0.001 to 0.0032 items/L. The concentration of these microplastics depends on the sampling site, where a higher concentration was determined at downstream surface water compared to upstream (Rowenczyk et al., 2022).

4. Occurrence of water contaminants in Canadian environments

Many water systems in Canada suffer consequences due to the discharge of EPs including the Grand River in southern Ontario which receives wastewater from nearly 30 different treatment plants originating from a population consisting of nearly 1 million people (Gillis et al., 2014). In general, the mechanisms of toxicity of ECPs depend on the characteristics and type of contaminant, but the overwhelming consensus that exposures and associated adverse effects arise from the high reactivity and bioactivity of EPs, even at low concentrations (Mezzelani et al., 2018; Mohapatra and Kirpalani, 2019). Therefore, it is essential to recognize the presence of these compounds to improve our understanding of the fate of these pollutants, elucidate the threat they pose, and the strategies that can be adopted to curb or reduce contaminants and exposure.

4.1. Pharmaceuticals and their potential toxicities

These molecules can be classified based on their therapeutic activities in categories that include antidepressants, antibiotics, anti-inflammatories, analgesics, synthetic hormones, antacids, anti-anxiety, antiarrhythmics, anticoagulants, and antivirals/antiretrovirals, among others (Adeola and Forbes, 2021b; Adeola et al., 2022c; Valdez-Carrillo et al., 2020; Vaudin et al., 2022). A total of 40 general categories have been reported by the Federal Drug Administration of the United States, with the most prevalent contaminants being anti-inflammatory drugs, analgesics, and antibiotics (Adeleye et al., 2022; Ortúzar et al., 2022).

Drugs are designed to act on the receptors found in humans, or animals (in the case of veterinary drugs); however, this is further exacerbated due to their ability to act on the receptors of other non-target species whose share similar receptors (Patel et al., 2019). This makes different fish species, amphibians, reptiles, and even microorganisms, such as bacteria and algae vulnerable to pharmaceutical-related contamination in water (Arnold et al., 2014). In humans, it has been observed that exposure to pharmaceuticals, personal care products, or pesticides can lead to effects that can vary from infertility, hormonal alterations, to cancer, or organ toxicities (Chaturvedi et al., 2021; Rathi et al., 2021). Drugs have various routes of entry into aquatic environments. When consumed, drugs can go through multiple processes to be metabolized, transforming into other types of molecules, known as metabolites. These metabolites, along with the unmetabolized fraction, may be excreted through urine or feces and constitute sewage wastes (Hejna et al., 2022). On the other hand, unused or expired drugs, which are indiscriminately discarded without adherence to disposal guidelines can cause pollution and find their way in the water system if disposed of through sanitation plumbing (Fig. 2).

Due to limitations in existing wastewater treatment systems, particularly in the handling of trace levels, these drug compounds and metabolites are re-introduced into the ecosystem, via irrigation of vegetables/plants with treated water, wastewater treatment effluents, etc. (Masanabo et al., 2023). The persistence of drugs varies, and factors such as the action of sunlight and organisms present in media containing contaminants can cause their decomposition and transformation into various metabolites (Parezanović et al., 2019). However, it is highly inadvisable to continuously burden the environment with the hopes that it will naturally remedy itself. The toxicity of pharmaceutical compounds is strongly dependent on their concentration in the environment. Likewise, their effects will depend on what type of organism interacts with a specific drug substance (Arnold et al., 2014).

Several reports on different organisms exposed to pharmaceuticals, such as carbamazepine, erythromycin, fluoxetine, metoprolol, naproxen, and sulfamethoxazole, in concentrations ranging from mg/L to μ g/L, revealed the most common toxic effects that include behavioral

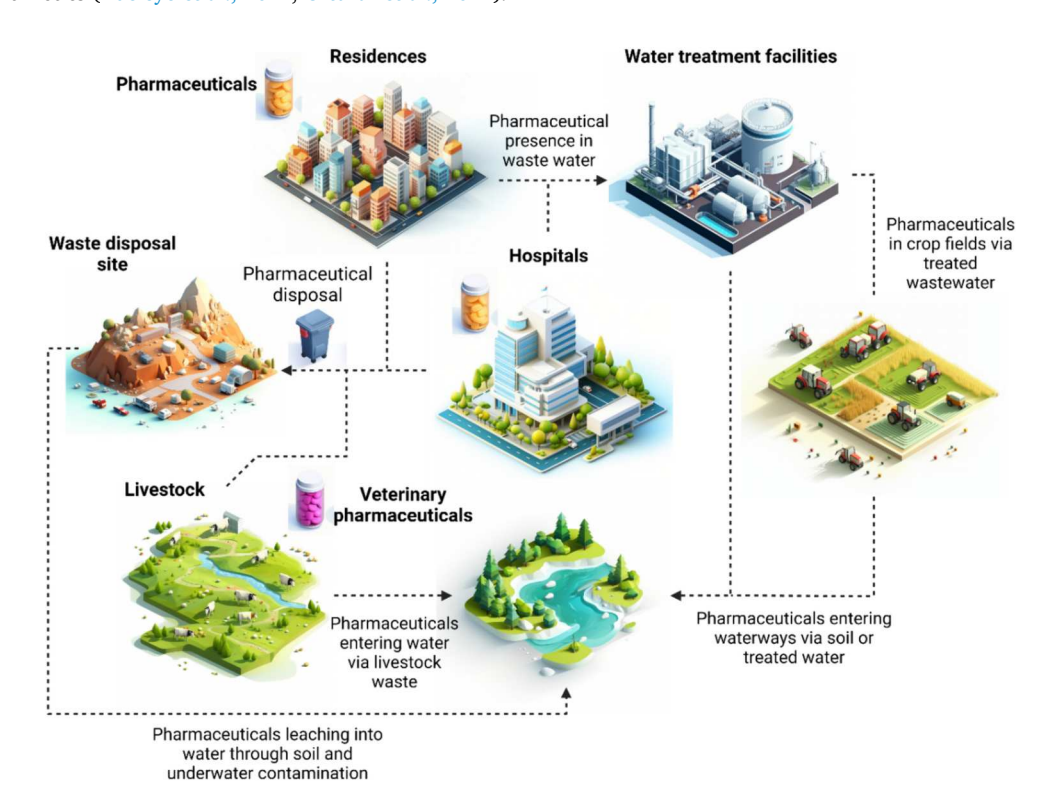


Fig. 2. Commonly reported pathways for the release of pharmaceuticals in water resources.

alterations, modifications in their biochemical responses, cytotoxic and genotoxic phenomena (Srain et al., 2021). The negative impacts on the environment are different according to the bioactive effect of the drugs. However, exposure of aquatic organisms to drug compounds above acceptable limits may cause genetic and histological alterations, oxidative stress, growth defects, changes in hatching processes, as well as metabolic alterations (Yang et al., 2020). Table 2 shows the exposure effects in some aquatic species.

4.1.1. Pharmaceuticals in Canadian water systems

Canada is one of the countries with the highest expenditure in the pharmaceutical market, with several billion dollars annually spent on drugs (Mezzelani et al., 2018). The high consumption of pharmaceutical-related products has led to the ubiquitous detection of various types of pharmacological molecules (human and veterinary drugs) in water bodies (Lissemore et al., 2006). Lissemore et al. determined that the drugs with the highest frequency of detection were lincomycin (human and livestock antibiotic), monensin (livestock antibiotic), carbamazepine (anticonvulsant), sulfamethazine (livestock antimicrobial), and trimethoprim (human and livestock antibiotic). However, a total of fourteen (14) pharmacological analytes were detected in the samples collected, where drugs such as lincomycin HCl in a range of concentrations of 0.2–355 ng/L, had the most frequency of detection of 91.2 % in the 1225 samples analyzed (Lissemore et al., 2006).

In the province of Nova Scotia, a total of seven (7) high-consumption drugs were found throughout the various sampling regions, revealing the presence of metformin, acetaminophen, paraxanthine, cotinine, caffeine, naproxen, venlafaxine with concentrations ranging from 2.65 to 115 μ g/L. However, 13 compounds were detected, with the occurrence of higher concentrations of pharmaceuticals in regions close to effluent treatment plants, compared to rural areas (Ghoshdastidar et al., 2015). In Quebec, Husk et al. reported the presence of pharmaceuticals in different parts of Québec, such as Estrie, Centre-du-Québec, and

Montérégie, including some surface watersheds located in St. Francis, Yamaska, and Nicolet Rivers (Husk et al., 2019). The group of researchers reported the detection of naproxen, ofloxacin, acetaminophen, and caffeine. However, nine pharmaceuticals were also found in the samples recollected, with mefenamic acid (pain reliever) having the highest concentration (1.848 $\mu g/L$) (Husk et al., 2019). The above examples show how the level of detected contaminants may vary depending on the region studied, with Québec showing significantly lesser concentrations of pharmaceutical-related compounds.

A recent study conducted by Schwartz et al. has also highlighted the spread of pharmaceutical contaminants across various provinces in Canada including British Columbia, Alberta, Saskatchewan, Manitoba, Ontario, Quebec, and Atlantic Canada. By analyzing multiple sampling locations, such as fishing sites and water intakes near recreational sites, Schwartz et al. identified 35 different drug compounds. Among these, Atenolol, caffeine, and metformin were the most prominent in the sampling sites, with a detection frequency of >20 % and average concentrations of 22.6, 120.9, and 716 ng/L, respectively (Schwartz et al., 2021a). In southern Ontario, drugs such as ibuprofen, naproxen, venlafaxine, and carbamazepine, as well as other antiandrogenic products such as triclosan, were detected in the Grand River watershed, south of Ontario. The concentration level of these drugs varied from one location to the other, where the highest concentrations were detected in areas downstream of treatment plants (Arlos et al., 2015).

Other regions containing contaminants including their location, compound(s) detected, and concentrations are shown in Table 3. It is important to mention that most reported concentrations are at trace levels, which may not impose a significant impact on aquatic life. However, there have been cases where high concentrations of pharmaceuticals like ibuprofen and its metabolite hydroxy ibuprofen at concentrations of 860 ng/L and 3.6–1800 ng/L, respectively, have been measured in samples collected from St Lawerence River. Moreover, caffeine concentrations in the range of 12–7200 ng/L have been reported (Vaudreuil et al., 2024). Although most concentrations are

Table 2
Toxic effects of selected pharmaceuticals to aquatic organisms.

Pharmaceutical	Organisms	Effect	Exposure Concentration	References
Carbamazepine	Thamnocephalus platyurus	Increase of enzyme activity such as hemoxidase, and glutathione-s-transferase. Inhibition of cytochrome P450 3A. <i>T platyurus</i> had an accumulation of 128.6 mg of CBZ per gram of dry biomass after 24 h exposure to algae containing carbamazepine	0.1–0.5 ng/L	(Vernouillet et al., 2010)
	Hydra attenuata	Increase activity of cytochrome. Inhibition of glutathione-S-transferase.	Hydra attenuate was exposed to carbamazepine with <i>T. platyrus</i> , which was previously exposed to carbamazepine through algae.	
Norsertraline	Rudd (Scardinius erythrophthalmus)	Accumulation of Norsertraline in rudd liver (647 ng/g)	Rudd exposed to water obtained from wastewater treatment plants, Norsentraline concentration (200 ng/mL)	(Arnnok et al. 2017)
lbuprofen Diclofenac	Rainbow trout	Increases oxidative stress. Organ affectations in kidneys and liver. Inflammatory deformities in gills. Change in mRNA biochemical markers.	Rainbow trout exposed to a diet including ibuprofen and diclofenac in concentrations of 2 µg kg and 200 µg/kg for each drug.	(Hodkovicova et al., 2022)
Paracetamol, irbesartan carbamazepine, diclofenac, naproxen mixture	Rainbow trout Oncorhynchus mykiss	IBRv2 levels increased at the highest concentration tested. Increased levels of lysozyme after 42 days of exposure. Changes in brain serotonin.	Paracetamol (0, 0.1, 1, 10 μg/L) Irbesartan (0, 0.05, 0.5 μg/mL) Carbamazepine (0.025, 0.25, 2.5 μg/mL) Diclofenac (0, 0.025, 0.25, 2.5 μg/mL) Naproxen (0, 0.025, 0.25, 0.25 μg/mL)	(Beghin et al., 2021)
Clotrimazole	Rainbow trout	Histopathological alterations	0.01, 1.0, 10 μg/L	(Burkina et al 2016)
Amitriptyline, amlodipine, azithromycin, diltiazem, diphenhydramine, fluocinonide, fluoxetine, gemfibrozil, metformin, miconazole, PFDA, PFOS, PFOSA, sertraline, triclocarban triclosan mixture	Chinook salmon Oncorhynchus tshawytscha	Liver mitochondrial content was reduced. Increased mitochondrial protein carbonyls. Increases expression of glutathione peroxidase. Reduction of oxidative phosphorylation.	Fish were exposed to a dietary mixture of 16 analytes (0.3-, 1-, and 10-fold of each analyte) in concentrations of ng/ml.	(Yeh et al., 2017)

Table 3Locations where pharmaceutical contaminants were detected in Canada and range of concentrations.

Location	Compound detected	Concentration determined	References
Grand River	Carbamazepine	0.16–24 ng/L	(Lissemore
Watershed,	Chlortetracycline	192 ng/L	et al., 2006)
Southern	Doxycycline	2.7-73 ng/L	
Ontario	Erythromycin	0.9-51 ng/L	
	Lincomycin HCl	0.2–355 ng/L	
	Monensin sodium salt	6.2–1172 ng/L	
	Roxithromycin	0.7 ng/L	
	Sulfachloropyridazine	0.5–7 ng/L	
	Sulfadimethoxine	0.2–56 ng/L	
	Sulfamethazine	0.3–408 ng/L	
	Sulfamethoxazole	0.3–9 ng/L	
	Sulfathiazole	1.3–16 ng/L	
	Trimethoprim	0.2–15 ng/L	
Nova Scotia	Acetaminophen	28.9 μg/L	(Ghoshdastidar
	Caffeine	115 μg/L	et al., 2015)
	Cotinine	$3.1~\mu g/L$	
	Metmorfin	10.6 μg/L	
	Naproxen	29.1 μg/L	
	Paraxanthine	18.2 μg/L	
	Venlafaxine	2.65 μg/L	
Quebec	Acetaminophen	147 ng/L	(Husk et al.,
Estrié, Centre-	Bezafibrate	79 ng/L	2019)
du-Quebec,	Caffeine	285 ng/L	
Montérégie,	Carbamazepine	30 ng/L	
St Francis,	Cyclophosphamide	1233 ng/L	
Yamaska and	Ibuprofen	97 ng/L	
Nicolet Rivers	Mefenamic acid	1848 ng/L	
	Naproxen	404 ng/L	
	Ofloxacin	177 ng/L	
Grand River	Naproxen	3–323 ng/L	(Arlos et al.,
watershed in	Venlafaxine	1-202 ng/L	2015)
southern	Carbamazepine	39-106 ng/L	
Ontario	Ibuprofen	71–1457 ng/L	
Kugluktuk	Atenolol	45.4-268 ng/L	(Stroski et al.,
Nunavut	Carbamazepine	514-1810 ng/L	2020)
	Metoprolol	52.5–398 ng/L	
	Naproxen	422–1080 ng/L	
St. Lawrence	Carbamazepine	0.03-1.2 ng/L	(Picard et al.,
Estuary and Gulf	Venlafaxine	0.03-4.1 ng/L	2021)
between Quebec	Sucralose	0.56-226 ng/L	
City and the	Caffeine	1.4–143 ng/L	
Cabot Strait			
Medicine Hat	Ethinylestradiol	<50 ng/L	(Basiuk et al.,
Alberta	Avermectins	2293 ng/L	2017)
(Wastewater	Caffeine	15,982 ng/L	
treatment plant)	Sulfamethazine	<50 ng/L	
	Sulfamethoxazole	1112 ng/L	
Red Deer and	a-Zearalenol	5.19 ng/L	(Jeffries et al.,
Oldman Rivers,			2010)
Alberta Canada			
Cambridge bay,	Atenolol	97 ng/L	(Chaves-
Nunavut	Carbamazepine	<100 ng/L	Barquero et al.,
	Sulfamethoxazole	274 ng/L	2016)
	Trimethoprim	<30 ng/L	

relatively low, the presence of these compounds in the water bodies is worth mentioning and the role of bioaccumulation cannot be ruled out. Based on the data presented, the most abundant types of pharmaceuticals present in the locations analyzed are antibiotics which include chlortetracycline, doxycycline, erythromycin, lincomycin HCl, roxithromycin, sulfachloropyridazine, sulfadimethoxine, sulfamethazine, sulfamethoxazole, sulfathiazole trimethoprim and ofloxacin. The second most prominent category corresponds to analgesics such as acetaminophen, ibuprofen, and naproxen. The rest of the pharmaceuticals detected belong to classes cardiovascular drugs (atenolol, metoprolol, bezafibrate), antidiabetics (metformin), stimulants (caffeine, cotinine), hormones (ethinylestradiol), antiparasitics (avermectins) and growth promoters (a-zeranol). Furthermore, in terms of the ubiquity of specific compounds in different provinces, carbamazepine was detected in

Ontario, Quebec, and Nunavut; sulfamethazine in Ontario and Alberta; caffeine in Nova Scotia, Ontario, and Quebec; and naproxen in Nova Scotia, Quebec, Ontario, and Nunavut. This may point to the need for closer attention should be paid to carbamazepine, sulfamethazine, naproxen and the proliferation of caffeinated substances in Canada. Industry, hospital waste, over-prescription of drugs, along with household and commercial consumption may all be contributors to the observed levels of pollution.

The presence of pharmaceuticals (including antibiotics) in the environment may pose risks that could negatively impact both human and animal health (Bunce and Hellyer, 2018; Granados-Chinchilla and Rodríguez, 2017; Koch et al., 2021). Therefore, indiscriminate disposal and widespread usage of drugs need to be carefully managed, and urgent sensitization about the proper handling of pharma-related wastes is vital.

4.2. Pesticides and their negative impacts

Pesticides are renowned for their ability to limit the growth and spread of pests in essential crops, one of the biggest causes of low agricultural yield and threat to food security globally (Savary et al., 2019). Their use is not only restricted to agriculture; some of these products are also available to people for pest control at home and for gardening purposes (Md Meftaul et al., 2020). Based on data collected in 2020, approximately 78,893 tons of pesticides have been used in Canada; where about 75.33 % were herbicides, 10 % were fungicides and bactericides, 4.32 % were insecticides, and the rest were pesticides for rodent control; with an estimated usage of 2.05 kg per hectare (Ritchie et al., 2022). Pesticides have one of the most direct routes of entry into the environment; via direct application through irrigation systems or being sprayed on plants or crops. In both ways, pesticides can contaminate soil and water, causing disruption in the development of other plants and organisms that inhabit the surrounding environment (Kumar et al., 2023).

Pesticides have multiple classifications, the broadest of which relates them to their target species/organism, such as birds, plants, fish, mammals, insects, fungi, viruses, and bacteria. However, its most straightforward classification is related to its chemical structure, having a total of 6 categories: organochlorine, organophosphorus, carbamate, pyrethrin, azadirachtin, and pyrethroid (Hassaan and El Nemr, 2020; Ore et al., 2023). The classification of pesticides can also depend on the level of hazard they pose. The World Health Organization provides a classification guide based on factors such as LD50 in rats, classifying them into 6 categories. Category 1a includes extremely harmful pesticides, with an oral LD₅₀ of <5 mg/kg. This is followed by Category 1b, which covers those highly risky, with an LD₅₀ of 5-50 mg/kg. Category II includes those that are moderately risky (50-2000 mg/kg), while Category III consists of those that are less risky (> 2000 mg/kg). Finally, Category U describes those pesticides that are unlikely to pose any acute hazard, with an $LD_{50} > 5000$ mg/kg (World Health Organisation, 2020).

The mechanisms by which pesticides generate toxicity vary and will depend on the pesticide used. However, common mechanisms are linked to the generation of oxidative stress, alteration of nucleus receptors, or mitochondrial dysfunctions. In turn, because the presence of multiple combinations of pesticides has been reported in the environment, synergistic or antagonistic effects may occur, modifying the toxicity mechanisms caused by these molecules (Hernández et al., 2017). The toxicity of pesticides also depends on the concentration of exposure and the type of species as well. An example of this is the study carried out where the exposure of several chemicals for pest control was monitored in Ontario Canada (Salerno et al., 2018). Neonicotinoids, carbamates organophosphates, and butanolides were introduced to mussels Villosa iris and Lamsilis siliquoidea organisms, of importance in the ecosystem. The study showed that the organisms in their different stages of development did not display adverse effects when exposed to pesticides in both acute toxicity and subchronic toxicity tests. The concentrations

used for the test were higher than those found in the Ontario flows, indicating that these concentrations do not pose any risk to this species (Salerno et al., 2018). However, the roles of bioaccumulation and prolonged exposures were not factored in, which is quite important for toxicity studies relating to emerging contaminants. In another study with zebra fish as the test subject, fungicides like thiram have been shown to cause eye, tail, heart, yolk sacs, and spine deformities in embryos and larvae of zebrafish at different concentrations (Vasamsetti et al., 2022). Table 4 shows the toxic effects of pesticides determined in some aquatic organisms.

4.2.1. Pesticides in Canadian water systems

The problems associated with aquatic systems containing pesticides are somewhat similar to those of pharmaceuticals. Most pesticides are highly soluble, and their presence in water occurs primarily from treated soils which are transported to surface waters by action of rainfall, erosion, irrigation and groundwater movements, among other mechanisms (Bashir et al., 2020; Sultana et al., 2018). Although some pesticides are designed to affect particular species populations such as insects or plants, they also have harmful effects on non-target species, including humans (Pathak et al., 2022; Sultana et al., 2018). The transport of these pesticides, as well as their concentration, depends on the regional meteorological conditions. In Canada, specifically Nova Scotia for example, the transport of pesticides from agricultural areas to the maritime regions is mainly facilitated by rainfall and/or snow melt (Lalonde and Garron, 2020; Schwartz et al., 2021a).

Table 5 shows the maximum acceptable concentrations of some pesticides according to Canadian water quality guidelines. Pesticides are not only found in untreated water samples; these compounds are even present in drinking water samples from water treatment plants, as demonstrated by the presence of thiamethoxam, clothianidin, and imidacloprid in both treated and untreated water samples (Sultana et al., 2018). The concentration of thiamethoxam detected (at a mean concentration of 0.28 $\mu g/L$) is above the permissible level for consumption as drinking water (European Union directive on pesticide levels < 0.1 µg/L) (Sultana et al., 2018). In a related study, pesticides with concentrations above those recommended have been reported for atrazine, chlorpyrifos, clothianidin, metribuzin, and thiamethoxan, found in samples throughout Nova Scotia, Prince Edward Island, and New Brunswick (Lalonde and Garron, 2020). In several regions of Ontario, the presence of compounds such as atrazine, metolachlor, hexazinone, and terbuthylazine was detected in drinking water samples in the partper-billion concentration range (Husk et al., 2019). Although many of the concentrations reported are below permissible levels and often below the detection limit of instruments, the potential for bioaccumulation of pesticides makes their presence in aquatic environments and drinking water a potential threat to the ecosystem.

Table 6 provides information regarding the presence of pesticides reported in various regions in Canada. To limit some of the risks of pesticides, it may be advisable for agri-businesses to adopt more natural fertilizers like manure, compost, and peat. In addition, care should be taken to prevent excessive use of fertilizer and pesticides, which may lessen the amount of chemical runoff into surrounding water sources.

4.3. Heavy metals and their negative impacts

The primary source of exposure of water bodies to heavy metals is from anthropogenic sources, i.e., industrial processes related to the processing of products composed of these metals. Mining is one of the main contributors to the increase of heavy metal levels in the environment (Zamora-Ledezma et al., 2021). To a lesser extent, domestic wastes can also contribute to heavy metals pollution (Kumar et al., 2019). Hence, heavy metals' presence in the environment is primarily due to industrial wastes and improper disposal of materials containing heavy metals. Industries that deal with textiles, dyes, paint, electroplating, mining, pesticides, among others, are significant sources of heavy metal

pollution (Mishra et al., 2019). An emerging contributor to metal pollution is electronic waste, also called e-waste, and has become a new anthropogenic source of soil and water contamination by heavy metals (Wu et al., 2015). In aquatic environments such as rivers, heavy metals are distributed by water flow to other areas, spreading their presence in different areas (Zamora-Ledezma et al., 2021). In addition, crop irrigation with water containing contaminants leads to pollution of soils and possibly groundwater bodies via soil leaching. However, the exposure of these bodies will depend on multiple factors, such as soil type, organic matter, and reactive metal oxides, which can hinder the transfer of these metals to the subsoil (Raja et al., 2015). In aquatic environments, heavy metals mainly interact with organic matter, inorganic matter, aquatic species, and microorganisms via absorption and adsorption, depending on factors such as the pH of the medium or even salinity levels (Miranda et al., 2021). In prolonged exposure, heavy metals go through a process of adsorption to sediments, progressively accumulating heavy metals (Kumar et al., 2019).

The bioavailable fraction of heavy metals influences their interaction with organisms and different chemical species of heavy metals will have different degrees of mobility in the environment (Ore and Adeola, 2021; Xu et al., 2022). Thus, bioavailability plays a role in processes like biosorption, precipitation, biomethylation, complexation, oxidationreduction, pH, microbial activity, ion competition, or redox potential (Etteieb et al., 2021). Heavy metals can be present in water in several forms and varying in size. Dissolved fractions consist of the smallest available form of heavy metals with sizes <1 kD and thus possessing the highest mobility and bioavailability; these are followed by colloidal forms (1 kD - $0.45 \mu m$) where the bioavailability and mobility are decreased. However, colloids can still act as soluble matter, or be more available to certain types of filter-feeding organisms (de Paiva Magalhães et al., 2015). The heaviest type consists of particulate heavy metals surpassing 0.45 µm; and due to their relatively large size, they tend to accumulate on sediments (Liu et al., 2024). Furthermore, some aquatic physicochemical characteristics, such as pH variation, can cause the solubilization of metal particulates and lead to the formation of various metal species (de Paiva Magalhães et al., 2015). For example, selenium can exist in various aquatic media as elemental Se, selenite, selenide, selenate, or organic Se, depending on the nature of the aqueous media. However, the selenate species has been determined as the most bioavailable form of selenium and potentially the most toxic selenium species in sediments in Northern Quebec, Canada (Etteieb et al., 2021).

Heavy metal compounds like mercuric chloride have shown adverse effects on fish species like zebrafish, showing morphological alteration in essential organs such as gills (Macirella and Brunelli, 2017). These morphological alterations were observed at concentrations of 7.7 µg/L, causing detachment of epithelium from the connective tissue, hypertrophy of epithelial cells, and hypertrophy of epithelial cells (Fig. 3a, b) In another study using zebrafish, assessment of the exposure effects of lead at concentrations of 2.5 and 5 µg/L revealed that although lead did not cause a difference in mortality rate, fish exposed to lead exhibited a hatching delay compared to control, and suffered from development impairments like spinal and tail deformity (Fig. 3c, d), as well as pericardial edema and yolk swelling that showed an increment based on exposure time and lead concentration (Curcio et al., 2021). Cadmium exposure, on the other hand, also reveals adverse effects on several organs of fish like the gills causing inflammation, apoptosis, necrosis, change in gill cell structure, ion transport enzyme activity, and ion transport, lamellae bending, aneurysm, cell shedding, and oxidative damage. After entering through the gills, cadmium can relocate to organs like the liver, causing endoplasmic reticulum expansion, nuclear deformation, swelling, and granulation, impacting growth, reproduction, and survival (Fig. 3e) (Liu et al., 2022).

Although some heavy metals are part of cofactors that sustain life in many organisms, high concentrations often lead to nefarious effects, either through acute toxicity or chronic exposure. Humans may be exposed to heavy metals through various sources, such as aquaculture,

Table 4Toxic effects of pesticides on aquatic organisms.

Pesticide	Species	Exposure concentrations	Effect	References
The mixture of atrazine, linuron, and metolachlor	Juvenile rainbow trout (Oncorhynchus mykiss)	Concentrations based on 2007 highest concentration found in the Adour- Garonne River basin	Behavior alterations: exposed fish tended to exhibit hypoactivity and lower-height swimming	(Shinn et al., 2015)
Diquat dibromide (Reward®)	Rainbow trout (Oncorhynchus mykiss)	Final nominal concentrations: atrazine $(10 \mu\text{g/L})$, linuron $(15 \mu\text{g/L})$, metolachlor $(45 \mu\text{g} /\text{L})$ Continuous exposure 56 d post-hatch $(0, 0.37, 0.80, 1.8, 4.0, 8.7 \text{mg/L})$ 85 days post-hatch $(0, 6.5, 10, 15, 23 \text{mg/L})$	Exposure to pesticides altered body morphometrics at embryo and alevin stages. Reward® produces changes in RNA/mRNA processes, enzyme activity, and energy homeostasis	(McCuaig et al., 2020)
Fungicides (azoxystrobin, boscalid, metalaxyl, myclobutanil). Neonicotinoids (clothianidin, imidacloprid, thiamethoxam).	Lampsilis siliquoidea and Villosa iris glochidia	Discontinuous/pulse exposure to embryos 0.015, 0.074, 0.37, 1.9, 9.3 mg/L Discontinuous/pulse juvenile exposure 0.12, 0.37, 1.1, 3.3, 10 mg/L Nominal concentrations for <i>Villosa iris glochidia</i> tests 0–21,200 µg/L Nominal concentrations for <i>Lampsilis gliqueidae</i> tests	Species were insensitive to the tested pesticides in their life stages, where the tested compounds possessed a median effect and lethal concentration above 161 $\mu g/L$.	(Salerno et al., 2018)
Carbamates (carbaryl and malathion). Organophosphate (chlorpyrifos). Butenolide (flupyradifurone). Chlorpyrifos	Postlarval American	siliquoidea tests 0–10,000 μg/L 0.375, 0.47, 0.56, 0.75, and1.5 μg/L	The median lethal concentration at stage IV of	(Taylor et al.,
	Lobster (Homarus americanus)		H. americanus was determined to be 1.56 μg/L at 24 h and 1.33 μg/L at 48 h. Cessation of normal movement was caused using 0.66 μg/L in 48 h. Acetylcholinesterase activity was inhibited in concentrations above 0.50 μg/L, recoverable in clean seawater for 9–15 days. Exposure to chlorpyrifos at concentrations of 0.82 μg/L led to an increased intermolt period, decreased growth rate, and decreased molt increment.	2019)
Clothianidin and thiamethoxam	Early-life stage copper redhorse and river redhorse (Moxostoma carinatum)	Contaminated river water with concentrations of clothianidin and thiamethoxam exceeding water quality guidelines concentration (>20 ng/L)	Copper redhorse appeared more sensitive to pesticide exposure, hatching in 10.7 cumulative degree days earlier than controls and exhibiting a longer survival (73 %) than controls (93 %). Copper redhorse larvae possessed 18 differentially expressed genes after 14 days of exposure, with upregulated genes related to immune functions and downregulation of genes	(Marchand et al., 2022)
Atrazine and chlorothalonil	Pacific sockeye salmon (Oncorhynchus nerka)	Nominal concentrations: Atrazine (25 and 250 $\mu g/L$) Chlorothalonil (0.5 an 5 $\mu g/L$)	related to ingestions and nutrient uptake. Reduced survival compared to control. A 24 % increase in finfold deformity was associated with chlorothalonil exposure. Atrazine exposure led to a premature hatch, and chlorothalonil led to a delayed hatch. Chlorothalonil led to increased triglyceride levels.	(Du Gas et al., 2017)
Thiamethoxam and clothianidin	Wood frog (Lithobates sylvaticus)	2.5 and 250 μg/L	Chronic exposure led to an impact on blood cell profiles and conticotisone concentrations. Compared to controls, exposed organisms suffered from anemia in all treatments except tadpoles exposed with 2.5 µg/L of clothianidin. Frogs exposed to 250 µg/L of thiamethoxam exhibited an elevated neutrophil-to-leukocyte and neutrophil-to-lymphocyte ratio. Tadpoles exposed to 250 µg/L of thiamethoxam showed lower corticosterone than other treatments.	(Gavel et al., 2019)
Imidacloprid and thiamethoxam	Wood frog (Lithobates sylvaticus)	1, 10, and 100 μg/L	Imidacloprid exposure at 10 µg/L and 100 µg/L increased survival and delayed completion of metamorphosis compared to controls.	(Robinson et al., 2017)
Imidacloprid or thiamethoxam	Wood frog (Lithobates sylvaticus)	1, 10, and 100 μg/L	Pesticide exposure to wood frogs revealed affectations in danger perceptions and responses to predators. Frogs exposed to imidacloprid at 10 and 100 showed less response to a simulated predator attack and less response to leaving the attack area compared to unexposed frogs.	(Lee-Jenkins and Robinson, 2018)

Table 5The maximum acceptable concentration of selected pesticides in drinking water based on Canadian water quality guidelines.

Compound	Maximum acceptable concentration
	(μg/L)
Atrazine	0.005
Bromoxynil	0.03
Chlorpyrifos	0.09
Dicamba	0.11
2,4- Dichlorophenoxy acetic acid (2,4-D)	0.1
Dimethoate and omethoate	0.02
Diquat	0.05
Glyphosate	0.28
Malathion	0.19
2-Methyl-4- chlorophenoxyacetic acid	0.35
(MCPA)	
Metribuzin	0.08
1,4- Dichlorobenzene	0.005

(https://www.canada.ca/content/dam/hc-sc/migration/hc-sc/ewh-semt/alt_formats/pdf/pubs/water-eau/sum_guide-res_recom/summary-tables-sept-2022-eng.pdf.)

and consuming food and water containing contaminants (Hama Aziz et al., 2023). Although heavy metals are not biodegradable, they can undergo biotransformation in the environment by interacting with organisms such as bacteria (Jaishankar et al., 2014). This biotransformation often leads to methylated derivatives that are more dangerous due to enhanced reactivity and bioavailability. For example, methylated arsenic can cause cardiac dysfunction, liver damage, and neurotransmitter impairment, among other effects (Balali-Mood et al., 2021; Ore and Adeola, 2021). Mercury is also a metal capable of being methylated, which increases its toxicity, being more toxic than metallic mercury and its ionic species, such as Hg^{2+} and Hg^{+} (Jaishankar et al., 2014). High mercury concentrations cause renal dysfunction, hepatotoxicity, and enzyme inhibition, not to mention the production of reactive oxygen species (ROS), such as superoxide ion, hydrogen peroxide, and hydroxyl radical. Such reactive species in high concentrations can cause damage at the cellular level and DNA damage (Balali-Mood et al., 2021; Jaishankar et al., 2014; Ore and Adeola, 2021). Chromium, in its various oxidative states such as Cr(III) and Cr(VI), are highly oxidative species that promote the generation of ROS, which leads to organ malfunction such as kidney, cancer, or skin diseases (Balali-Mood et al., 2021; Ore and Adeola, 2021). Similarly, lead in biological mediums generates ROS; however, the most notorious mechanism of toxicity of lead is the transmetallation substitution with other ions such as Ca²⁺, Mg²⁺, and Fe²⁺ in the metabolic system of cells, disturbing cellular stability, inactivating enzymes, such as ferrochelatase or decreasing the levels of antioxidant enzymes, such as catalase or superoxidodimutase, as well as elevating the levels of inflammatory cytokines (Balali-Mood et al., 2021; Jaishankar et al., 2014; Ore and Adeola, 2021).

In summary, the effects of heavy metals on living organisms, whether terrestrial or aquatic, depend significantly on the species and the degree of exposure. Table 7 summarizes some harmful effects reported in various aquatic species, with a focus on species found in North America, especially in Canada. In Canada, studies conducted in British Columbia show that heavy metals such as mercury are still below the consumption guidelines for various species of salmon and are still a safe food source (Kelly et al., 2008). There are cases where metal concentrations were alarmingly high in specific regions and certain species, such as Greenland shark, Ivory gulls, and arctic char with a mercury content of 0.5–1.0 $\mu g/g$ (wet weight) (Scheuhammer et al., 2015). Although most studies reveal that concentrations remain below levels of concern, there is a need for periodic monitoring, and more research in these areas is required.

4.3.1. Heavy metals in Canadian water systems

Bioavailable concentrations of heavy metals are of concern due to

Table 6Pesticides contaminants reported in Canadian aquatic systems.

Location	Compound	Concentration	Ref
Southern Ontario	Thiamethoxam	79.2 ng/L	(Sultana
Drinking water treatment	Clothianidin	86.9 ng/L	et al., 2018)
plants in the Lake Erie	Imidacloprid	13.5 ng/L	
watershed (raw samples)	Thiacloprid	2.7 ng/L	
Quebec	Atrazine	606 ng/L	(Husk et al.,
Estrie, Centre-du-Québec	Metolachlor	856 ng/L	2019)
and Montérégie	Hexazinon	21 ng/L	
Surface watersheds (St.	Terbuthylazine	287 ng/L	
Francis, Yamaska and	Thiabenzadole	125 ng/L	
Nicolet Rivers	Carbendazim	71 ng/L	
South Saskatchewan River	2,4-D	0.354 μg/L	(Sheedy
Basin in southern Alberta,	Dicamba	0.077 μg/L	et al., 2019)
Canada	Mecoprop	0.060 μg/L	
	Clopyralid	0.039 μg/L	
	Bentazone	0.030 μg/L	
	Atrazine	0.041 μg/L	
	+ 11 other		
	pesticides		
Grand River watershed in southern Ontario	Atrazine	108–499 ng/L	(Arlos et al., 2015)
St. Lawrence Estuary and	Atrazine	0.54-34 ng/L	(Picard
Gulf between Quebec	Dimethenamid	0.01-0.10 ng/	et al., 2021)
City and the Cabot Strait	Fomesafen	L	
	Glyphosate	0.17-1.9 ng/L	
	Hexazinone	0.07-0.60 ng/	
	Hydroxyatrazine	L	
	(S)-metolachlor	0.002-0.06	
	Metolachlor-ESA	ng/L	
	Simazine	0.21-12 ng/L	
	Tebuconazole	0.03-5.3 ng/L	
		0.48-80 ng/L	
		0.35-7.7 ng/L	
		0.009-0.38	
		ng/L	
Nova Scotia, Prince Edward	Atrazine	18,800 ng/L	(Lalonde
Island and New	Chlorpyrifos	601 ng/L	and Garron,
Brunswick (NB)	Clothianidin	204 ng/L	2020)
	Metribuzin	1160 ng/L	
	Thiamethoxam	838 ng/L	
	+6 other	Ü	
	pesticides		
Medicine Hat Alberta	2,4-D	<2000 ng/L	(Basiuk
(Wastewater treatment	Glyphosate	1952 ng/L	et al., 2017)
plant)	• •		

their harmful effects, affecting simple organisms such as bacteria, and complex organisms such as humans, potentially causing both cellular and systemic damage (Balali-Mood et al., 2021). Since these pollutants are not biodegradable, they are more prevalent in the environment (Zamora-Ledezma et al., 2021). The classification of heavy metals includes those elements whose atomic number exceeds 20 and whose density exceeds 5 g/cm³ (Mishra et al., 2019). Among the most common heavy metals whose harmful effects are widely studied are cadmium, arsenic, mercury, lead, copper, zinc, nickel, and chromium, which are highly toxic even at low concentrations (Mishra et al., 2019).

The problem caused by heavy metals has been a subject of scientific discussion for many years, yet their impact continues to grow, especially in developing countries, whose regulations concerning the use and exposure to heavy metals are still flawed (Adebiyi et al., 2021; Baby et al., 2022; Järup, 2003; Mishra et al., 2018; Muhammad and Usman, 2021; Shil et al., 2017). In Canada, most information corresponding to the presence of heavy metals in drinking water or raw water is provided by the Ministry of Health, in the form of technical guides for the quality of drinking water. In these guides, the permissible limits or maximum acceptable concentration (MAC) are determined regarding water quality for some selected toxic heavy metals. The data was recently updated in 2022 and are provided in Table 8 for different types of heavy metals. However, it needs to be mentioned that the values are based on total concentrations and not dissolved fractions of the heavy metals.

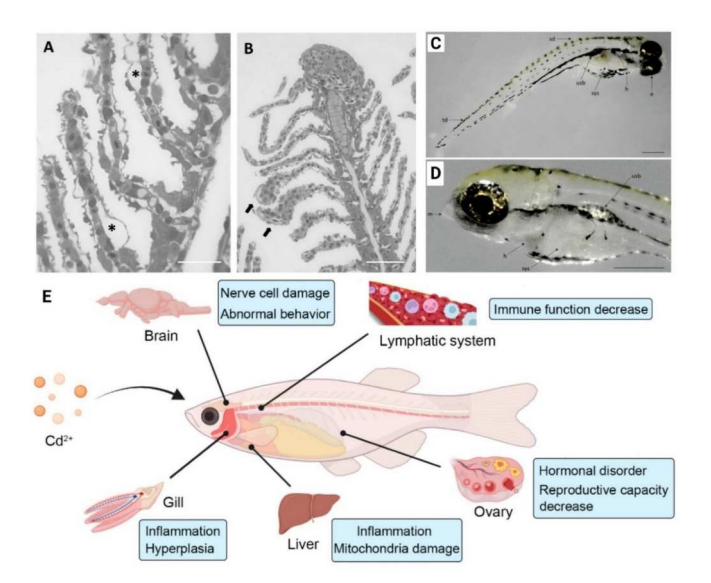


Fig. 3. Gill apparatus in *Danio rerio* after 96 h of exposure to 7.7 μ g/L of HgCl₂: (a) detachment of epithelium (b) hypertrophy in endothelial cells and blood congestion, adapted from (Macirella and Brunelli, 2017). Zebrafish embryos and larvae after exposure to 2.5 μ g/L of Pb (c,d) after 144 h of exposure to Pb (Curcio et al., 2021). (e) Toxic effects of Cd on fish organs, adapted from (Liu et al., 2022) *Open Access*.

Therefore, it may not reflect the toxic fraction present in water compared to US EPA guidelines for the protection of aquatic life (Shotyk et al., 2017). Although commonly measured, total metal concentration does not fully describe the toxicity levels of a contaminated water body. Speciation of the heavy metals in the water body will define its availability to interact with organisms and dissolved metals will have a faster and easier interaction with aquatic life due to a reduced size compared to species bound to organic matter (Borgmann et al., 2004; Guéguen et al., 2011).

The Ministry of Health provides technical guides for heavy metals such as arsenic, cadmium, chromium, and lead. These technical guides have studies where the concentration of the metals of interest has been determined in various water sources, as well as in the different provinces of Canada, 2016; Canada, 2019; Canada, 2020). Table 9 provides a compilation of the information provided in these technical guides, showing the regions where the quantification of heavy metals was carried out, the range of determined concentrations, and the sampling period. It is important to note that no information on the bioavailable fraction of the detected concentrations is mentioned in the technical guidelines. In essence, heavy metals have been reported widely in Canada, even in sub-arctic areas (Kirk et al., 2008). Studies have shown various concentrations of the deadly methylated mercury compounds in ng/L concentrations. Considering various sea depths during sampling and analysis, it was established that the concentrations of methylated mercury compounds are higher in deeper zones than those on the surfaces, suggesting that bioaccumulation may have played a major role (Kirk et al., 2008).

Furthermore, the concentration of these metals depends on anthropogenic activities around the sampling location. For example, areas close to mining operations revealed higher concentrations of heavy metals in comparison to more remote areas (Sprague and Vermaire, 2018). In Ontario, arsenic levels at various sites in the region of the town of Cobalt and around the Silver Center mining field revealed concentrations ranging from 972 μ g/L in surface waters and 10,800 mg/kg in lake sediments. In lakes close to mining activity, the range of arsenic concentrations was 431 µg/L and 1704 mg/kg, while control lakes with no mining activity in the area had a concentration of 2.2 µg/L and 11 mg/kg, in water and sediments, respectively (Sprague and Vermaire, 2018). In a study conducted by Etteieb et al., mine effluent discharge rich in Se with a total Se concentration of 65 \pm 0.9 $\mu g/L$ and bioavailable Se chemical species like selenate and selenite at 7.2 \pm 0.5 $\mu g/L$ and 57 \pm 6.8 $\mu g/L$ respectively was evaluated in Northern Quebec and sediment concentrations as high as 321 mg/kg were found. Typha latifolia plants exposed to the contaminated sediment showed a high concentration of Se amounting to 534 mg/kg (roots) and 92 mg/kg (leaves). Se speciation demonstrated that several Se compounds were bioavailable for

Table 7Toxic effects of some heavy metals on aquatic organisms.

Heavy metals	Aquatic species	Effects/toxicity	Exposure concentrations	References
Нg	Beluga whale (Delphinapterus leucas)	Bioaccumulation of methylated mercury on tissue. Reduced lymphocyte proliferation. Decreased intracellular thiol levels. Induction of metallothionein.	0, 0.03, 0.1, 0.33, 1, 3.3 or 10 μM	(Frouin et al., 2012)
As	Rainbow trout (Oncorhynchus mykiss)	Reduced growth. Slower feeding rate. Reduced food conversion efficiency. Liver cell abnormalities. Digestive effects.	26–77 mg As/g dm	(Erickson et al., 2010)
Cd	Rainbow trout (Oncorhynchus mykiss)	Olfactory dysfunctions	Nominal concentrations of cadmium (0.05 µg/L), copper (3.6 µg/L total, 2 µg/L added), nickel (136.6 µg/L), zinc (30 µg/L)	(Dew et al., 2016)
Cd	Common carp (Cyprinus carpio)	Reduced activity of enzymes such as acetylcholinesterase and gamma-glutamyl-transferase. Increase activity of aminotransferase and alanine aminotransferase, lactate dehydrogenase, and alkaline phosphatase. Modifications of plasma total protein, albumin, and globulin content.	Cd exposures 250 and 500 µg/L Exposure of Cd and microplastics also conducted in various ratios of Cd/Microplastics	(Banaee et al., 2019)
Cd	Rainbow trout (<i>Oncorhynchus mykiss</i>) White sturgeon	Increased sensitivity to Cd in rainbow trout at later life stages compared to the sturgeon. Greater disturbance of calcium uptake in rainbow trout compared to white sturgeon. Lower affinity to Cd in white sturgeons compared to rainbow trout.	Trout exposed to 0, 0.625, 1.25, 2.5, 5, 10 and 20 $\mu g/L$ Sturgeon exposed to 0, 5, 10, 20, 40, 80 and 160 $\mu g/L$	(Shekh et al., 2018)
Zn, Cd	Rainbow trout (Oncorhynchus mykiss)	Zinc accumulation on fish gills. Zinc accumulation on gills was reduced in exposure to cadmium, indicating competitive uptake.	Zn (1 mg/L), Zn (1 mg/L) + Cd (20 µg/L), and Zn (1 mg/L) + Cu (100 µg/L).	(Saibu et al., 2018)

Table 8Maximum acceptable concentration of certain heavy metals based on Canadian water quality guidelines.

Heavy metal	Maximum acceptable concentration for drinking water ($\mu g/L$)
Antimony	0.006
Arsenic	0.010
Cadmium	0.007
Chromium	0.05
Copper	2
Lead	0.005
Manganese	0.12
Mercury	0.001
Selenium	0.05

absorption like selenate and selenite (<1 mg/kg) and other species bound to carbonates, mineral oxides, and organic matter (Etteieb et al., 2021). A study by Borgmann et al. determined that sediments collected from Rouyn Noranda Lake in Quebec contain increased levels of metals like Cd, Cu, Pb, and Zn. Sediments were exposed to *Hyalella* and it revealed a high bioaccumulation of metals like Cd. Although metal absorption could indicate bioavailability, these models may not be reliable indicators for physiologically regulated metals like Cu and Zn (Borgmann et al., 2004).

Speciation models like WHAM (Windermere Humic Aqueous Model) can serve to identify the metal species present in an aquatic media. In a study performed by Bhavsar et al., WHAM was used to determine the fate of several metal species like Cd, Cu, Ni, Pb, and Zn in Ross Lake located in Manitoba, Kelly Lake located in Ontario, and Lake Tantaré in Quebec. By employing the model, it is possible to estimate that Cu's colloidal and particulate phases corresponded to 1, 84, and 15 % for Ross, Kelly, and Tantarpe Lakes. On the other hand, Pb colloidal fractions correspond to 65–95 % in both Kelly and Tantare Lake. In Lake Tantaré, Cd and Zn, in dissolved forms, corresponded to 55 and 65 %, respectively, while colloidal phases accounted for 30–37 % (Bhavsar et al., 2008).

In a study conducted by Donner et al., Se content was analyzed in the lower Athabasca River watershed. A quadrupole inductively coupled plasma mass spectrometer was employed to analyze the dissolved Se concentration. In the main stem of Athabasca River, the concentration of dissolved Se in 2014 was $0.11 \pm 0.02~\mu g/L$ while in 2015, the concentration was $0.16 \pm 0.02~\mu g/L$; in other tributaries, concentrations ranged from 0.02 to $0.27~\mu g/L$ (Donner et al., 2018). Based on US EPA guidelines, the Se content in the Athabasca River and the tributaries are below acceptable thresholds of $3.1~\mu g/L$. Speciation analysis determined that in the Athabasca River, Se(VI) accounted for a concentration of $0.11~\pm~0.015~\mu g/L$ while Se(IV) concentration was approximately $0.012~\mu g/L$. Analysis of fish species such as Trout-perch in the Athabasca River revealed that the concentration of Se at $2.2 \pm 0.4~m g/kg$ in fish muscle is lower than the US EPA guidelines of 11.3~m g/kg (Donner et al., 2018).

Another analysis of the Athabasca River conducted by Donner et al. focused on Arsenic content and speciation. They reported the dissolved As concentration in 2014 was 0.37 \pm 0.01 µg/L with no apparent increase in 2015 (0.34 \pm 0.01 $\mu g/L$) (Donner et al., 2017). The total As content in Athabasca River corresponded to 12.7 \pm 2.8 $\mu g/L$ in 2014 and $3.3\pm0.65~\mu\text{g}/$ in 2015. On another sample near mountain headwater, the dissolved As concentrations were as low as 0.08 \pm 0.005 $\mu g/L$ with similar content in two upstream sites. As speciation determined that the redox state As(V) and As(III) were consistent in the Athabasca River, where As(V) accounted for concentrations of 0.18 \pm 0.09 μ g/L and 0.18 \pm 0.02 µg/L in 2014 and 2015, respectively. On the other hand, arsenite was present in trace amounts at concentrations <60 ng/L. Redox conditions were also relatable to the speciation of As in water, where As(III) concentrations were higher in water with lower redox potential, while As(V) was more abundant in water with elevated dissolved oxygen and redox potential (Donner et al., 2017). More studies evaluating dissolved

Table 9Total heavy metals concentration ranges in different Canadian provinces based on the data provided by Canada's Ministry of Health (Health Canada, 2016, 2019, 2020).

Provinces	Heavy metals	Concentration range in µg/L	Sample type	Sampling period
Newfoundland	Arsenic	6–288	Public water supplies	2002
	Cadmium	0.01-3.5	Source water	2011-2016
	Chromium	2-26	Surface water	2004-2010
			and	
	Y 4	0.1.60	groundwater	2005 2016
N. 0 .:	Lead	0.1–60	Not specified	2005–2010
Nova Scotia	Arsenic	> 25	Well water sample	1991–1997
	Cadmium	0.01-4.0	Raw water	2002–2016
	Chromium	2.5–5	Raw water	2004 2009
Quebec	Arsenic	1.0-25.0	Surface water	1990-2002
	Cadmium	0.002-3.4	Distributed water	2013–2017
	Chromium	4-992	Drinking water	2005-2010
	Lead	0.01-997	Tap water	2013 2014
Ontario	Arsenic	2.5-68	Treated, raw,	1999-2002
			and drinking water	
	Cadmium	0.003-10.0	Raw, treated,	2012-2019
	Gaaman	0.000 10.0	and distributed water	2012 201
	Chromium	1.2-41.3		2009–201
	Lead	< 0.01–359	Drinking water	
Manitoba	Lead Cadmium	< 0.01-359 0.01-1.0	Not specified	2000 2007
Manitoba	Cadmium	0.01-1.0	Raw, treated,	2009–2017
			and distributed water	
	Chromium	3–14	Raw water	2009 2010
	Lead	0.1–36	Not specified	2008–2009
Saskatchewan	Arsenic	0.5–105.0	Treated wáter	1976–2002
	Cadmium	0.01–5.9	Raw treated and distributed	2007–2017
	Chromium	5.4-29.0	Not specified	2002 2010
	Lead	0.1–60	Not specified	Not specified
Alberta	Arsenic	0.1–1000	Groundwater	1980–2002
			and surface water	
	Cadmium	1.0-3.1	Well water	2012-2017
	Chromium	_	_	_
	Lead	< 0.5	Not specified	Not
				specified
Prince Edward	Arsenic	0.1-26.0	Groundwater	1986-2002
Island	Cadmium	2.0-6.0	Tap water	2013-201
	Chromium	60-234	well water	2005 2010
	Lead	2-335	Not specified	2005-2010
Yukon	Arsenic	-	_	-
	Cadmium	0.003-3.41	Not specified	Not specified
	Chromium	0.7-1.2	Drinking water	2007–2010
	Lead	0.1–7.6	Tap water	2005 2010
British	Arsenic	580	Groundwater	Not
Columbia	Cadmium	0.005-100	Raw and	specified 2007–201
	Chromium	< 1–5	treated water Not specified	2004 2010
	Lead	_	_	_

metal content in multiple water bodies located in Canada are summarized in Table $10. \,$

4.4. Oil spillage in Canadian water systems

Canada has been affected by fuel spill events on several occasions dating back to 1970 (Feng et al., 2021). An example is the Pacific Ocean spill in the Nestucca, which released approximately 874 $\rm m^3$ of material. Although it occurred near Washington State, the coast of Vancouver Island was affected (Feng et al., 2021). This spill triggered environmental consequences that resulted in the death of $\sim\!56,000$ seabirds and

affected crustacean and crab species. Most of the spills that have affected Canada have been recorded in the Pacific, Atlantic, and the Arctic regions and the majority are of bunker C kind (fuel oil used aboard water vessels), diesel, or crude oil (Feng et al., 2021). Another major spill in Canada was the sinking of the Arrow tanker, where approximately 2000 m³ of Bunker C was released and spread up to 300 km (Yang et al., 2018).

The persistence of the released contaminants related to this spill was studied in the region of Chedabucto Bay, Nova Scotia, where it was determined that there was no significant change in the chemistry of the spilled oil due to the environment, indicating that this type of contaminant can persist for a long time. However, it has been recorded that depending on the weather conditions, certain constituents of the released fuels can be transformed either chemically or physically in processes, such as photooxidation, aerosolization, and emulsification (Zhang et al., 2019). Table 10 presents a selection of reported accidents that have led to the release of fuels in Canada; two cases of pipeline spills are presented, however, up to 11 accidents have been reported between Alberta and Saskatchewan, which have released between 60,000 L to 15 million liters of fuel between the years 2008 to 2017 [89].

Based on density, oils can be categorized into light oils - comprising chemicals such as gasoline and jet fuels, and heavy-density oils which include compounds such as fuel oil crudes and bitumen (Adeola et al., 2022b; Zhang et al., 2019). The impact and difficulties of oil spill remediation will depend on factors like the type of oil released, location, and weather conditions, among others (White and Molloy, 2003). Oil spills that consist of light products such as gasoline, diesel, and light crude are considered non-persistent because the constituents have high volatility and greater dispersion. When the released product possesses lower volatility and higher viscosity, like crude and heavy oils, it is considered persistent since it stays longer in the aquatic media and travels larger distances (Ore and Adebiyi, 2021; White and Molloy, 2003).

Due to the variety of constituents in crude oils, their toxicity varies and factors such as product density help to define the environmental impact. It has been observed that the most significant toxicity is generally exerted by the constituents with higher volatility, while those with higher density are considered to have less impact (Chen et al., 2022). In Canada, the negative impact of oil spills includes the destruction of the natural aesthetics of the environment, adverse climate changes, and organisms that come into contact with regions exposed to crude oil spills have consequences that may result in death (Little et al., 2021). Marine mammals such as seals or sea lions may inhale toxic fumes or suffer skin irritations. Seabirds lose the insulation in their feathers, making them susceptible to hypothermia due to low temperatures (Feng et al., 2021; Thakur and Koul, 2022). In general, the loss of biodiversity, genotoxicity/mutations, shortage of clean/potable water, and climate change remain the major challenges associated with hydrocarbon pollution of aquatic environments.

5. Emergence of SARS-CoV-2 in Canadian water systems

Wastewater surveillance for the RNA of the SARS-CoV-2 virus, which causes COVID-19, has brought wastewater-based epidemiology (WBE) back into the spotlight in 2020 (Oloye et al., 2022). While some researchers have successfully linked WBE results with clinical assessments of human infections, many others were unable to do so due to limitations in clinical outcomes and inaccurate population size estimations to which to normalize their data (Lapolla et al., 2020; Wu et al., 2020). Regardless, the genetic material of the coronavirus disease (COVID-19) virus has been reported in wastewater, indicating that water monitoring may be able to detect an epidemic outbreak (de Llanos et al., 2022; Lastra et al., 2022; Reynolds et al., 2022; Wu et al., 2020). Normalizing the pathogen loads to the population that contributes waste to the wastewater influent is crucial, to account for seasonal fluctuations or variations in loadings and treatments between different locations and times (Olove et al., 2022). Finding the appropriate bio-indicators and extracting the genetic materials from wastewater using the right technique has always been a difficult task. A substance must meet certain criteria to be utilized for normalizing the viral load. These characteristics include stability in water, rapidly and safely quantifiable, uniqueness to human metabolic activities, and consistent excretion rate (Asadi et al., 2023a; Senta et al., 2015).

The first major research carried out in Canada to quantify SARS-CoV-2 in wastewater was a collaborative inter-laboratory study using wastewater grab samples collected from the Winnipeg Wastewater Treatment Plant on August 31, 2020 (Chik et al., 2021). The method of analysis used was reverse transcription-quantitative polymerase chain reaction (RT-qPCR), which at the time was unstandardized globally. Results provided by different laboratories were consistently within a range of 1.0-log₁₀, and low- and high-spikes were identified by each laboratory. SARS-CoV-2 RNA concentration estimations for each spiking condition typically stayed within 1.0-log₁₀ ranges. SARS-CoV-2 RNA was either non-detectable or in trace quantities (<20 gene copies/mL) in the no-spike wastewater aliquots that were supplied. The detections seem associated with techniques that involved, or concentrated, on the wastewater solid matrix and could indicate the presence of in-situ SARS-CoV-2 in the wastewater sample (Chik et al., 2021).

In a more comprehensive study, the daily per capita trends of SARS-CoV-2 in wastewater were determined for three Canadian cities: North Battleford, Prince Albert, and Saskatoon (Asadi et al., 2023b). The three Saskatchewan communities' Wastewater Viral Load Risk Index (WWVLRI) provided a straightforward tool for interpreting wastewater surveillance data. The development of the index took into account the correlations among clinical data, weekly viral load change rate, daily per capita amount of virus materials in wastewater, and reproduction rate. The limits for daily per capita efficiency adjusted viral loads of 85×10^6 and 200×10^6 Nucleocapsid gene counts (gc)/population day (pd) were established, along with the effective reproduction rate (Rt) (Asadi et al., 2023b). These values along with their change rates were utilized to classify the likelihood of COVID-19 breakouts and the declines that

 Table 10

 Bioavailable heavy metals concentration determination in different Canadian provinces.

Location	Metals	Technique	Bioavailable concentration	References
Lake 658 Experimental lakes area (Ontario)	MeHg dissolved and bound to dissolved organic matter	Diffuse gradient thin film	The concentration of dissolved MeHg showed dependency on the depth of analysis at the Epilmnion (<3 m). Concentrations of 0.07 ± 0.02 ng/L were determined, while at higher depths (>9 m), the highest concentration was 1.8 ng/L. At 7 m, 43 % of the MeHg consisted of the free ion or ion species bounded to small inorganic complexes	(Clarisse et al., 2009)
Churchill River estuary (Manitoba)	Dissolved Vanadium	Diffuse gradients in thin films	Dissolved vanadium concentrations appeared to be five times higher during summer base (27.3 nM) flow compared to spring high flow (4.8 nM); this was related to a change between the levels of dissolved organic matter, suggesting that dissolved organic matter played a high role, in vanadium bioavailability.	(Shi et al., 2016)
Athabasca River (Alberta)	Dissolved Ag, Cd, Pb, Sb, and Tl	ICP quadrupole mass spectrometry	Concentrations of metal below US EPA and Canadian water quality guidelines. Metal concentrations resemble background levels	(Shotyk et al., 2017)

followed. When the per capita viral load was 85×10^6 N2 gc/pd. (N2 signifies the number of nucleocapsid gene mutations), the weekly average was deemed "low risk". When the per capita copies were between 85×10^6 and 200×10^6 N2 gc/pd. with a rate of change <100 %, this was referred to as a "medium risk." A "medium-high" risk rating denoted the beginning of an outbreak when the amount of viral material concentrations was >85 \times 10⁶ N2 gc/pd. and the week-over-week rate of change was >100 %. The study concluded that a viral load >200 \times 10⁶ N2 gc/pd. was considered "high risk". Decision-makers and health authorities can benefit greatly from this methodology, especially considering the limitations of COVID-19 surveillance that continues to rely on clinical data (Asadi et al., 2023b; Oloye et al., 2022; Xie et al., 2022).

Although, numerous studies have been conducted to measure SARS-CoV-2 in wastewater in other parts of the World (Barril et al., 2021; Cervantes-Avilés et al., 2021; Philo et al., 2021; Rusiñol et al., 2020), there has not been wide-spread surveillance of SARS-CoV-2 in wastewater in Canada. The major works in literature are those carried out in Saskatchewan and Manitoba (Asadi et al., 2023b; Chik et al., 2021). If wastewater data is to be used for the prediction of future pandemics, the dependability, repeatability, and sensitivity of these approaches need to be validated using results collected from other provinces in Canada.

6. Recent remediation approaches to emerging contaminants in Canada

Due to the vast quantities of hazardous chemicals that find their way into water sources on a daily basis, environmental pollution stands as one of the foremost challenges confronting society today (Alimi et al., 2018). Efforts to purify water containing contaminants are continuously evolving through ongoing research into cost-effective methods, as well as the development of novel and efficient materials/tools. In the development of materials for environmental remediation, key considerations include simple design, cost-effective production, toxicity, biocompatibility, reusability, and regenerative potential (Adeola et al., 2023b). In the advancement of environmental remediation, nanomaterials have garnered a lot of attention among a plethora of materials due to their large surface area to volume ratio at the nanoscale, ease of functionalization, tunability, etc. (Roy et al., 2021). Nanomaterials can be altered to provide unique functionality for target-specific applications (Adeola et al., 2024; Clermont-Paquette et al., 2024; Clermont-Paquette et al., 2023). Consequently, several studies have focused on integrating green chemistry principles with physicochemical surface modifications of nanomaterials to generate solutions capable of addressing the complexities of contaminant remediation (Zhang et al., 2023). In the last two decades, the notion of "green chemistry" arose from a shift in focus within material research, moving towards utilizing waste materials and implementing waste reduction (Dev et al., 2021). This transition has directed the chemical industry and scientists towards advocating and adhering to sustainable and eco-friendly approaches, guided by the twelve principles of green chemistry (DeVierno et al., 2017).

Recent works have evaluated the possibility of utilizing ligninderived sorbents for the remediation of dye contamination (Adeola et al., 2023a). In a series of experiments, low-cost lignin-based sorbents were developed through microwave and acid-precipitation treatments of raw lignin for Rhodamine-B removal from water. The models of adsorption utilized suggest complex interactions between the pollutant and synthesized sorbent, potentially driven by various mechanisms, including Van der Waals attraction and π - π stacking. Under optimal conditions, we recorded 97 % removal efficiency and findings suggest lignin valorization as an economically viable and sustainable water purification method (Adeola et al., 2023a). Similarly, ammonium in water systems has been investigated due to the significant risks it poses to the ecosystems, and biochar derived from digested sludge pyrolysis has been reported in Canada as a remediation tool (Tang et al., 2019). Pyrolysis temperatures between 350 and 550 $^{\circ}$ C were used to produce biochar from anaerobic digester sludge in Alberta, Canada. Biochar produced at 450 $^{\circ}$ C showed the highest ammonium removal capacity due to increased surface area and functional groups. The adsorption pattern followed a monolayer mechanism with an ammonium removal capacity in municipal wastewater was 1.2 mg/g and 1.4 mg/g in distilled water due to less competition with other contaminants (Tang et al., 2019).

Furthermore, advanced carbon-based materials have been prepared using the self-assemblage method to transform 2D materials such as graphene oxide (GO) nanosheets into 3D sponges (Rao et al., 2021). These materials have been reported to offer a promising strategy for efficient contaminant removal in Canada and other parts of the world (Kubheka et al., 2022; Yousefi et al., 2018). Yousefi et al. reported the synthesis of highly porous 3D sponges using GO, vitamin C, and cellulose nanocrystals isolated from wood pulp. This architecture enhances the specific surface area of GO, enabling effective adsorption of various contaminants (such as diclofenac, sulfamethoxazole, 17-α-ethynylestradiol, tetracycline, and microcystin-LR) from water. Another class of advanced materials that have been reported in Canada for water treatment is polymer-based materials (Bonenfant et al., 2012; Bonenfant et al., 2010; Mohamed et al., 2008; Orprecio and Evans, 2003; Pratt et al., 2010). Orprecio et al. reported that β-cyclodextrin polymers crosslinked with epichlorohydrin were formed into beads and utilized to pack a column intended for capturing organic contaminants in flowing water. The contaminants targeted include naphthalene, naproxen, and 2-naphthol. The polymeric material demonstrated a high % naphthalene removal efficiency of 98 %, while 70 % removal efficiency was recorded for 2-naphthol; however, naproxen adsorption was notably lower at 18 %. The variation in the performance of the material suggests that ionized species cannot be efficiently trapped by β-cyclodextrin polymers. This could ultimately restrict the utilization of the polymer adsorbent to clean up flowing waterways when the pH is high enough to ionize contaminants (Orprecio and Evans, 2003). Nonetheless, many notable medicinal compounds are hydrophobic, unlike pesticides, hence these chemical species, along with aromatic hydrocarbons should adhere easily to β -cyclodextrin polymeric materials (Table 11).

Researchers in Canada and around the world have also explored the use of filtration media for the removal of chemical and biological contaminants (Adeola and Forbes, 2021a; Cescon and Jiang, 2020; Mohamed et al., 2008; Qiu et al., 2015). Most commonly, sand, anthracite and granular activated carbon (GAC) filters have been used (Papineau et al., 2013). Papineau et al. analyzed Cryptosporidium parvum removal in granular filters with sand, anthracite, and GAC and it was discovered that aging improved sand and GAC performance by 26 % and 31 %, respectively, but had no effect on anthracite. Enhanced removal correlated with biofilm development, notably in aged GAC, suggesting media aging enhances the removal of biological pollutants in the filtration process. Similarly, Escherichia coli, Pseudomonas aeruginosa, Bacillus subtilis and Staphylococcus aureus present have been remediated using an electrochemical method with the aid of zinc oxide nanopillars hydrothermally synthesized on stainless steel (ZnOSS) (Lin et al., 2023). Results indicate effectiveness varies based on bacterial species and biofouling conditions. The treatment efficiently removes microcolonies in 30 s but struggles with concentrated Staphylococcus aureus accumulations. During the treatment, the process of removing biofouling can be explained by a dual mechanism that includes the formation of bubbles on the surface, which dislodges attached bacteria, alongside the generation of antibacterial oxidants through electrolysis. However, this treatment suits low bacterial concentrations but may not fully restore heavily contaminated media (Lin et al., 2023).

Overall, cost-effectiveness, facile synthesis, green chemistry, non-toxicity, target-specificity, biodegradability, recyclability, and regenerability are some of the key challenges that must be considered when developing new nano/materials for environmental remediation (Adeola et al., 2023b; Guerra et al., 2018). Several studies have focused on

employing the principles of nanotechnology and waste valorization, in combination with physicochemical modifications of nanomaterials/ composites to develop functional materials that can overcome existing limitations (Pokrajac et al., 2021). Yet, some challenges persist as some of the materials are inherently unstable under environmental conditions and their preparation requires complex/tedious techniques at a nanoscale. More research is needed to prevent agglomeration and enhance monodispersity and stability while maintaining high efficiency and reusability. The potential toxicity and ecotoxicological impact of nanoparticles/nanomaterials utilized for environmental remediation is largely unknown, and recovery costs from the remediation site are factors that may impose limitations (Martínez et al., 2021). Therefore, an understanding of the material platforms, their fabrication process, performance optimization, and ecotoxicological studies of residues are required for full-scale and real-world applications of various advanced materials/composites/nanomaterials. (See Table 12.)

6.1. Other remediation approaches

Biodegradation is considered an eco-friendly mechanism for removing emerging contaminants (ECs) and various methods have been explored to enhance the biodegradation of persistent emerging contaminants using algae, oxidoreductase enzymes, nitrifying agents, and fungal cultures (Li et al., 2023). Certain ECs have been effectively removed utilizing techniques including anaerobic membranes, aerobic membranes, and anoxic membrane reactors; untreated ECs are dealt with using a combination of conventional and non-traditional approaches (Ahmed et al., 2021). For instance, xenoestrogens can be removed up to 92 % by traditional treatment using activated sludge, 80 % by two oxidation ditch approaches, 70 % by several bioreactors, and 64 % by a sequence of ten lagoons (Jatoi et al., 2023). Metabolites and co-metabolites are formed during the biodegradation of pollutants. Caffeine, estradiol, acetaminophen, and ibuprofen are examples of pollutants with high biodegradation constants that break down quickly. In contrast, because of their low biodegradation constants, carbamazepine and iopamidol exhibit greater resistance to biodegradation (Bilal et al., 2019). Temperature, molecular nature, redox potential, and the physicochemical and biophysical characteristics of the contaminants are among the many factors that are crucial in the effective degradation of

Table 11Major oil spill events reported in Canadian environments.

Event	Region	Volume spilled	Chemicals released	References
T/V Odyssey 1998	Coast of Nova Scotia	132,000 t	Oil	(Feng et al., 2021)
Arrow spill 1970	Chedabucto Bay	11,000 m ³	Bunker C	
T/V Kurdistan spill	Cabot Strait	d 7700 m ³	Bunker C	
Westridge spill 2007	Burnaby British Columbia	224 m ³	Crude oil	
Little Buffalo pipeline spill 2011	Little Buffalo Northwest Alberta	4.5 million liters	Crude Oil	(Datta and Hurlbert, 2020)
Husky Oil Spill 2016	Paynton Ferry, Saskatchewan,	225 m ³	Heavy crude oil Resins Asphaltenes Aromatics Saturates	(DeBofsky et al., 2020)
Anthan E Stewart sinking 2017	British Columbia o Seaforth Channel	235,000 L	Diesel fuel	(Eykelbosh et al., 2018)
Judy Creek Pipeline Spill 2017	Judy Creek Alberta	1.9 million liters	Not specified	(Datta and Hurlbert, 2020)

pollutants. The biodegradation process is limited to biodegradable contaminants, and requires extensive monitoring due to its specificity and sensitivity regarding environmental growth conditions, microorganism type, and nutrient requirements. It presents the possibility of producing unknown and potentially toxic byproducts, making it a comparatively time-consuming process.

Advanced oxidation processes (AOP) involve the formation of highly reactive and non-selective reactive oxygen species, capable of partial or 100 % mineralization of contaminants into CO2 and inorganic ions (Priyadarshini et al., 2022). These processes can significantly reduce pollutant concentrations from hundreds of parts per million (ppm) to just a few parts per billion (ppb). Recent advancements in wastewater treatment have introduced techniques such as metal oxide-based photocatalysis, as well as Fenton, and photo-Fenton approaches (Adeola et al., 2022a; Fatimah et al., 2024). Several reactive radicals and methods have been investigated in relation to AOP such as peroxymonosulphate (HSO₅), persulphate ($S_2O_8^{2-}$), catalytic ozonation (O_3), ultrasonication and hydrodynamic cavitation (OH), gamma radiation (*OH and H*), electrochemical oxidation (Cl*, Cl2*, ClO*), modified Fenton (Fe²⁺ and H₂O₂ to generate OH), and plasma-assisted AOPs (O, H^o, OH, O₂^{o-}) (Privadarshini et al., 2022; Wang and Wang, 2020). The main obstacle to full-scale AOP adoption is their high running costs; consequently, techno-economic analyses are required to identify the most viable AOPs for operation and scale-up with actual wastewater. Optimizing reactor design and configuration, using solar radiation rather than UV light, creating waste-derived catalysts, and enhancing the reuse of catalytic materials are other ongoing advancements that are necessary.

Although more research is required to develop smart and adaptable materials for environmental remediation, it should be noted that the adsorption technique holds great potential when compared to other methods in terms of efficiency and cost-effectiveness (El-sayed, 2020). Electrochemical treatment for example makes use of the application of an electric current to drive chemical reactions at specific electrodes in turn separating chemical species such as metals (Wang et al., 2022). However, it is a relatively expensive method in comparison to using adsorbents derived from renewable sources (Adeola et al., 2023a). Boron-doped diamond (BDD) electrodes are often employed as they are better suited to oxidize contaminants than metal oxide anodes with prices reaching a staggering 17,850-26,800 \$ CAD/m² (Radjenovic and Sedlak, 2015). In comparison, 100 g of lignin alkali is ~145 \$ CAD as of June 2024 (Sigma-Aldrich) and is a green and renewable carbonaceous material used for the synthesis of carbon-based adsorbents. While price is one advantage, energy consumption is also a great topic of interest. The typical adsorption process is driven mechanically, whereas electrochemical methods require a constant input of electricity to drive electrochemical reactions. The typical energy associated with such operations is usually in the range of 22-95 kWh kg/contaminant, depending on the current efficiency and density (Radjenovic and Sedlak, 2015). Adsorption offers many advantages over other methods in terms of cost, lower energy consumption, and high removal efficiency with minimum secondary sludge generation (Sophia and Lima, 2018).

The first principle of green chemistry principle states that it is always better to entirely prevent the generation of waste than trying to clean it up after it has been created (Etzkorn, 2019). This principle should be applied by industries and research institutions towards making strides at reducing waste products generated during synthesis or manufacturing processes. Previously many organic solvents were used for the synthesis of sertraline (Zoloft) such as toluene, hexane, methylene chloride, and tetrahydrofuran, however, its modern-day synthesis has introduced ethanol as a sole solvent, thereby reducing solvent usage from 250 to 25 L/Kg drug (Sheldon, 2011). Reducing the amount of solvent used in the mass production of such compounds reduces the chances of environmental contamination and highlights the importance of waste prevention. Another notable example of preventing waste stems from the greener synthesis of ibuprofen, one of the most widely used non-

Table 12

Methods and materials developed by various Canadian researchers for remediation of pollutants.

Material	Method/Approach	Target pollutant	Removal capacity/% efficiency	References
Reduced graphene oxide-cellulose nanocrystal sponges	Adsorption	Diclofenac, sulfamethoxazole, 17- α-ethynylestradiol, tetracycline and microcystin-LR	~850 mg/g	(Yousefi et al., 2018)
Granular filters (GAC, sand, and anthracite)	Filtration	Cryptosporidium parvum	39–56 %	(Papineau et al., 2013)
Granular activated carbon	Nanofiltration, Adsorption	Naphthenic acids	100–160 mg/g	(Mohamed et al., 2008)
Zinc oxide nanopillars-stainless steel	Electrochemical treatment	Escherichia coli, Pseudomonas aeruginosa, Bacillus subtilis and Staphylococcus aureus	~90 %	(Lin et al., 2023)
Biochar derived from digested sludge	Adsorption	Ammonium	48-58 % / 1.4 mg/g	(Tang et al., 2019)
Epichlorohydrin-crosslinked β-cyclodextrin polymers	Adsorption	Naphthalene 2-naphthol	Naph (98 %), 2-Naph (70 %),	(Orprecio and Evans, 2003)
p-cyclodextriii polymers		naproxen	NPX (18 %)	
β-Cyclodextrin-carboxymethylcellulose	Adsorption	Nonylphenol ethoxylate	NE 83–92 w%, NE	(Bonenfant et al., 2012;
polymer		Fluoxetine hydrochloride	1.1–6.8 mg/g FH 5.076 mg/g	Bonenfant et al., 2010)
β-cyclodextrin with epichlorohydrin- mesoporous silica	Nanofiltration, Adsorption	Naphthenic acids	20-30 mg/g	(Mohamed et al., 2008)
β-Cyclodextrin copolymer materials	Adsorption	p-nitrophenol	~ 58 %	(Pratt et al., 2010)
Carbon nanotubes	Adsorption	norfloxacin and 17α-ethinylestradiol	24.5–48.9 mg/g 76–98 %	(Duarte et al., 2022)
Acid-precipitated and microwave- treated softwood lignin	Adsorption	Rhodamine B	\sim 2766 mg/g	(Adeola et al., 2023a)

steroidal anti-inflammatory drugs (NSAIDs) worldwide. The classical route for ibuprofen production consists of six synthetic steps using stoichiometric reagents, leading to poor atom economy and generating large quantities of inorganic salts as byproducts. The modern synthesis of ibuprofen has been substantially improved to utilize three steps, yielding 100 % atom economy with a significant reduction in impurities/by-products that have the potential to reach and pollute the environment.

7. Preventive measures, recommendations and conclusion

Water pollution results from inadequate sanitation and infrastructure, and it is widely accepted that preventive measures are superior to end-of-pipe treatment (Adeola and Forbes, 2021b; Mueller and Gasteyer, 2021). In light of the pervasiveness of contamination linked to pharmaceuticals, hospital waste management systems need to be standardized to ensure the maintenance of environmental safety in Canada. There is a need for more emphasis on how important it is to efficiently sort, collect, package, store, and dispose of municipal and hospital waste materials. Inefficient collection and transportation are among the main causes of inadequate waste management around the world (Abubakar et al., 2022; Kumar et al., 2017). Key preventive approaches may include ensuring strict compliance with existing regulations with regard to the disposal of hazardous chemicals and biological agents, and isolating contaminant sources. The improvement of existing technology in WWTPs, and incorporating new tools in WWTPs may also be required for handling trace-level contaminants.

The most widely used remediation techniques for biological and chemical contaminants in aqueous systems include adsorption, membrane filtration, coagulation, chemical precipitation, ion exchange, aerobic biodegradation, and photocatalytic clean-ups (Ahmed et al., 2022). These methods can be categorized into physical, chemical, biological, ecological, and engineering techniques. The most economical way to remediate contaminants in environmental matrices is still to use carbon-based adsorbents (Militao et al., 2021). Carbon-based adsorbents, such as agricultural waste-derived carbon materials, graphene-based materials, carbon nanotubes, and granular or powdered activated carbon, have been applied to absorb a variety of environmental pollutants (Adeola et al., 2023a; Ighalo et al., 2023). In comparison to alternative adsorbents, activated carbon is a reasonably cheap and ecofriendly option.

However, in the case of heavily polluted sites, single techniques are

often ineffective; instead, integrated systems or hybrid procedures that entail the integration of two or more approaches are better (Adeola and Forbes, 2021a; Rajendran et al., 2022; Xiang et al., 2022). The physical-engineering approach is one example of an integrated/hybrid technique. Aeration is a popular and effective way to promote the growth and activity of bacteria that may eventually break down organic contaminants in the environment (Capodaglio and Olsson, 2020). Similar methods that use plant and microorganism-based solutions to clean organic pollutants from surface water or diffuse sources of pollution include ecological floating beds, wetlands, and biofilm reactors (Md Anawar and Chowdhury, 2020). Other techniques that promote sedimentation, aeration, photolysis by sunlight, and anoxic reactions are hydraulic structures, riverbank filtration, stormwater diversion, and dredging.

In practical terms, environmental protection is a collective responsibility, hence from an individualistic perspective, it is advisable to dispose of waste properly instead of throwing trash away on the beach, riverbank, or near other bodies of water. Federal or provincial regulations are needed to improve waste collection, processing, and valorization strategies for the collective good of the environment, animals, and humans. Furthermore, it is advisable to purchase eco-friendly cleaning agents, such as detergents with low or no phosphate content, to prevent the eutrophication of water bodies. Green chemistry practices should not be limited to research laboratories as there is a need for industries producing various chemicals, to seek out precursors and alternatives that are less hazardous, self-degrading, and non-persistent in the environment upon incidental release.

In a bid to achieve the United Nations Sustainable Development Goals, the water treatment sectors (both private and government) should ensure that WWTPs are properly maintained and upgraded to handle the rapidly growing environmental and economic demands for clean and safe water. There is an urgent need to ensure water reusability due to the increasing demand for clean water. To reduce the danger of exposure and its effects, the development of better and more effective ways for treating sewage, drinking water, and wastewater is germane. Membrane technology, adsorption, and integrated systems are examples of more compact, economical, adaptable, and efficient treatment techniques that warrant further investigation due to their ability to purify wastewater without requiring a significant amount of chemical intervention.

In conclusion, future research into the environmental toxicology of emerging pollutants should take into account both human exposures and environmental concentrations to establish a valuable correlation between dose-related effects (IC_{50}/EC_{50}), total bioavailable fractions, environmental exposure, and biological effects of emerging contaminants. There is a paucity of information regarding relevant ecotoxicological endpoints for human and biota lethal dose/exposure for most emerging and potentially hazardous contaminants in Canada. Hence, for public health protection and environmental safety, more public-private partnerships between government agencies, healthcare providers, industries, and institutions of higher learning are necessary to promote research and development.

CRediT authorship contribution statement

Adedapo O. Adeola: Writing – review & editing, Writing – original draft, Validation, Project administration, Investigation, Formal analysis, Data curation, Conceptualization. Luis Paramo: Writing – original draft, Software, Investigation, Formal analysis, Data curation. Gianluca Fuoco: Writing – original draft, Visualization, Validation. Rafik Naccache: Writing – review & editing, Supervision, Resources, Project administration, Investigation.

Declaration of competing interest

The authors declare that they have no known competing financial interests or personal relationships that could have appeared to influence the work reported in this paper.

Data availability

No data was used for the research described in the article.

Acknowledgment

The authors are grateful to the funding agencies for financial support. RN is grateful to the Natural Sciences and Engineering Research Council of Canada (NSERC) for funding through the Discovery Grant Program. RN is also thankful to Concordia University for funding through the Research Chair Program. AA is grateful for financial support from Concordia University.

References

- Abdallat, G.A., Salameh, E., Shteiwi, M., Bardaweel, S., 2022. Pharmaceuticals as emerging pollutants in the reclaimed wastewater used in irrigation and their effects on plants, soils, and groundwater. Water 14, 1560.
- Abubakar, I.R., Maniruzzaman, K.M., Dano, U.L., AlShihri, F.S., AlShammari, M.S., Ahmed, S.M.S., et al., 2022. Environmental sustainability impacts of solid waste management practices in the global south. Int. J. Environ. Res. Public Health 19.
- Adebiyi, F.M., Ore, O.T., Adeola, A.O., Durodola, S.S., Akeremale OF, Olubodun, K.O., et al., 2021. Occurrence and remediation of naturally occurring radioactive materials in Nigeria: a review. Environ. Chem. Lett. 19, 3243–3262.
- Adeleye, A.S., Xue, J., Zhao, Y., Taylor, A.A., Zenobio, J.E., Sun, Y., et al., 2022. Abundance, fate, and effects of pharmaceuticals and personal care products in aquatic environments. J. Hazard. Mater. 424, 127284.
- Adeola, A.O., Forbes, P.B.C., 2021a. Advances in water treatment technologies for removal of polycyclic aromatic hydrocarbons: existing concepts, emerging trends, and future prospects. Water Environ. Res. 93, 343–359.
- Adeola, A.O., Forbes, P.B.C., 2021b. Antiretroviral drugs in African surface waters: prevalence, analysis, and potential remediation. Environ. Toxicol. Chem. 41 (2), 247–262.
- Adeola, A.O., Abiodun, B.A., Adenuga, D.O., Nomngongo, P.N., 2022a. Adsorptive and photocatalytic remediation of hazardous organic chemical pollutants in aqueous medium: a review. J. Contam. Hydrol. 248, 104019.
- Adeola, A.O., Akingboye, A.S., Ore, O.T., Oluwajana, O.A., Adewole, A.H., Olawade, D.
 B., et al., 2022b. Crude oil exploration in Africa: socio-economic implications, environmental impacts, and mitigation strategies. Environ. Syst. Decis. 42, 26–50.
- Adeola, A.O., Ore, O.T., Fapohunda, O., Adewole, A.H., Akerele, D.D., Akingboye, A.S., et al., 2022c. Psychotropic drugs of emerging concerns in aquatic systems: ecotoxicology and remediation approaches. Chem. Afr. 5, 481–508.
- Adeola, A.O., Cui, M., Naccache, R., 2023a. Rhodamine B sequestration using acidprecipitated and microwave-treated softwood lignin: comparative isotherm, kinetics and thermodynamic studies. Environ. Technol. Innov. 32, 103419.

- Adeola, A.O., Duarte, M.P., Naccache, R., 2023b. Microwave-assisted synthesis of carbon-based nanomaterials from biobased resources for water treatment applications: emerging trends and prospects. Frontiers in Carbon 2.
- Adeola, A.O., Clermont-Paquette, A., Piekny, A., Naccache, R., 2024. Advances in the design and use of carbon dots for analytical and biomedical applications. Nanotechnology 35, 012001.
- Ahmed, M., Mavukkandy, M.O., Giwa, A., Elektorowicz, M., Katsou, E., Khelifi, O., et al., 2022. Recent developments in hazardous pollutants removal from wastewater and water reuse within a circular economy. npj Clean Water 5, 12.
- Ahmed, S.F., Mofijur, M., Nuzhat, S., Chowdhury, A.T., Rafa, N., Uddin, M.A., et al., 2021. Recent developments in physical, biological, chemical, and hybrid treatment techniques for removing emerging contaminants from wastewater. J. Hazard. Mater. 416, 125012
- Alimi, O.S., Farner Budarz, J., Hernandez, L.M., Tufenkji, N., 2018. Microplastics and nanoplastics in aquatic environments: aggregation, deposition, and enhanced contaminant transport. Environ. Sci. Technol. 52, 1704–1724.
- Arlos, M.J., Bragg, L.M., Parker, W.J., Servos, M.R., 2015. Distribution of Selected Antiandrogens and Pharmaceuticals in a Highly Impacted Watershed. Occurrence, Fate, Removal and Assessment of Emerging Contaminants in Water in the Water Cycle (From Wastewater to Drinking Water), 72, pp. 40–50.
- Arnnok, P., Singh, R.R., Burakham, R., Pérez-Fuentetaja, A., Aga, D.S., 2017. Selective uptake and bioaccumulation of antidepressants in fish from effluent-impacted Niagara River. Environ. Sci. Technol. 51, 10652–10662.
- Arnold, K.E., Brown, A.R., Ankley, G.T., Sumpter, J.P., 2014. Medicating the environment: assessing risks of pharmaceuticals to wildlife and ecosystems. Philos. Trans. R. Soc. B 369, 20130569.
- Asadi, M., Hamilton, D., Shomachuk, C., Oloye, F.F., De Lange, C., Pu, X., et al., 2023a.
 Assessment of rapid wastewater surveillance for determination of communicable disease spread in municipalities. Sci. Total Environ. 901, 166541.
- Asadi, M., Oloye, F.F., Xie, Y., Cantin, J., Challis, J.K., McPhedran, K.N., et al., 2023b.
 A wastewater-based risk index for SARS-CoV-2 infections among three cities on the Canadian Prairie. Sci. Total Environ. 876, 162800.
- Baby, T.P.N., Vineethkumar, V., Shimod, K.P., Vishnu, C.V., Jayadevan, S., 2022. Heavy metal contamination in water sources of Thaliparamba municipality, Kerala, India. Radiat. Prot. Environ. 45, 54–61.
- Balali-Mood, M., Naseri, K., Tahergorabi, Z., Khazdair, M.R., Sadeghi, M., 2021. Toxic mechanisms of five heavy metals: mercury, Lead, chromium, cadmium, and arsenic. Front. Pharmacol. 12.
- Banaee, M., Soltanian, S., Sureda, A., Gholamhosseini, A., Haghi, B.N., Akhlaghi, M., et al., 2019. Evaluation of single and combined effects of cadmium and micro-plastic particles on biochemical and immunological parameters of common carp (Cyprinus carpio). Chemosphere 236, 124335.
- Barril, P.A., Pianciola, L.A., Mazzeo, M., Ousset, M.J., Jaureguiberry, M.V., Alessandrello, M., et al., 2021. Evaluation of viral concentration methods for SARS-CoV-2 recovery from wastewaters. Sci. Total Environ. 756, 144105.
- Bashir, I., Lone, F.A., Bhat, R.A., Mir, S.A., Dar, Z.A., Dar, S.A., 2020. Concerns and threats of contamination on aquatic ecosystems. In: Hakeem, K.R., Bhat, R.A., Qadri, H. (Eds.), Bioremediation and Biotechnology: Sustainable Approaches to Pollution Degradation. Springer International Publishing, Cham, pp. 1–26.Basiuk, M., Brown, R.A., Cartwright, D., Davison, R., Wallis, P.M., 2017. Trace organic
- Basiuk, M., Brown, R.A., Cartwright, D., Davison, R., Wallis, P.M., 2017. Trace organic compounds in rivers, streams, and wastewater in southeastern Alberta, Canada. Inland Waters 7, 283–296.
- Beghin, M., Schmitz, M., Betoulle, S., Palluel, O., Baekelandt, S., Mandiki, S.N.M., et al., 2021. Integrated multi-biomarker responses of juvenile rainbow trout (Oncorhynchus mykiss) to an environmentally relevant pharmaceutical mixture. Ecotoxicol. Environ. Saf. 221, 112454.
- Bell, K.Y., Wells, M.J.M., Traexler, K.A., Pellegrin, M.-L., Morse, A., Bandy, J., 2011. Emerging Pollutants. Water Environ. Res. 83, 1906–1984.
- Bhaduri, A., Bogardi, J., Siddiqi, A., Voigt, H., Vörösmarty, C., Pahl-Wostl, C., et al., 2016. Achieving sustainable development goals from a water perspective. Frontiers in Environmental Science 4.
- Bhavsar, S.P., Gandhi, N., Diamond, M.L., Lock, A.S., Spiers, G., de la Torre, M.C.A., 2008. Effects of estimates from different geochemical models on metal fate predicted by coupled speciation-fate models. Environ. Toxicol. Chem. 27, 1020–1030.
- Bilal, M., Adeel, M., Rasheed, T., Zhao, Y., Iqbal, H.M.N., 2019. Emerging contaminants of high concern and their enzyme-assisted biodegradation – a review. Environ. Int. 124, 336–353.
- Bonenfant, D., Niquette, P., Mimeault, M., Hausler, R., 2010. Adsorption and recovery of nonylphenol ethoxylate on a crosslinked β -cyclodextrin-carboxymethylcellulose polymer. Water Sci. Technol. 61, 2293–2301.
- Bonenfant, D., Mimeault, M., Niquette, P., Hausler, R., 2012. Adsorption study of a commonly used antidepressant drug, fluoxetine hydrochloride, onto a crosslinked β -cyclodextrin-carboxymethylcellulose polymer. Water Sci. Technol. 66, 224–230.
- Borgmann, U., Nowierski, M., Grapentine, L.C., Dixon, D.G., 2004. Assessing the cause of impacts on benthic organisms near Rouyn-Noranda, Quebec. Environ. Pollut. 129, 20, 48
- Bunce, J.T., Hellyer, P., 2018. Antibiotic resistance and antibiotic prescribing by dentists in England 2007–2016. Br. Dent. J. 225, 81–84.
- Burkina, V., Zamaratskaia, G., Oliveira, R., Fedorova, G., Grabicova, K., Schmidt-Posthaus, H., et al., 2016. Sub-lethal effects and bioconcentration of the human pharmaceutical clotrimazole in rainbow trout (Oncorhynchus mykiss). Chemosphere 159, 10–22.
- Canada, H., 2016. Guidelines for Canadian Drinking Water Quality: Guideline Technical Document Chromium, Ottawa, Ontario.
- Canada, H., 2019. Guidelines for Canadian Drinking Water Quality: Guideline Technical Document Lead, Ottawa, Ontario.

- Canada, H., 2020. Guidelines for Canadian Drinking Water Quality: Guideline Technical Document — Cadmium, Ottawa, Ontario.
- Capodaglio, A.G., Olsson, G., 2020. Energy issues in sustainable urban wastewater management: use, demand reduction and recovery in the urban water cycle. Sustainability 12, 266.
- Cervantes-Avilés, P., Moreno-Andrade, I., Carrillo-Reyes, J., 2021. Approaches applied to detect SARS-CoV-2 in wastewater and perspectives post-COVID-19. Journal of Water Process Engineering 40, 101947.
- Cescon, A., Jiang, J.-Q., 2020. Filtration process and alternative filter media material in water treatment. Water 12, 3377.
- Chaturvedi, P., Shukla, P., Giri, B.S., Chowdhary, P., Chandra, R., Gupta, P., et al., 2021. Prevalence and hazardous impact of pharmaceutical and personal care products and antibiotics in environment: a review on emerging contaminants. Environ. Res. 194, 110664.
- Chaves-Barquero, L.G., Luong, K.H., Mundy, C.J., Knapp, C.W., Hanson, M.L., Wong, C. S., 2016. The release of wastewater contaminants in the Arctic: a case study from Cambridge Bay, Nunavut, Canada. Environ. Pollut. 218, 542–550.
- Chen, X., Bi, H., Yue, R., Chen, Z., An, C., 2022. Effects of oil characteristics on the performance of shoreline response operations: A review. Frontiers in Environmental Science 10
- Chik, A.H.S., Glier, M.B., Servos, M., Mangat, C.S., Pang, X.-L., Qiu, Y., et al., 2021. Comparison of approaches to quantify SARS-CoV-2 in wastewater using RT-qPCR: results and implications from a collaborative inter-laboratory study in Canada. J. Environ. Sci. 107, 218–229.
- Clarisse, O., Foucher, D., Hintelmann, H., 2009. Methylmercury speciation in the dissolved phase of a stratified lake using the diffusive gradient in thin film technique. Environ. Pollut. 157, 987–993.
- Clermont-Paquette, A., Mendoza, D.-A., Sadeghi, A., Piekny, A., Naccache, R., 2023. Ratiometric sensing of glyphosate in water using dual fluorescent carbon dots. Sensors 23, 5200.
- Clermont-Paquette, A., Larocque, K., Piekny, A., Naccache, R., 2024. Shining a light on cells: amine-passivated fluorescent carbon dots as bioimaging nanoprobes. Materials Advances 35, 012001.
- Cuprys, A., Lecka, J., Proulx, F., Brar, S.K., Drogui, P., 2019. Appearance of ciprofloxacin/chlortetracycline-resistant bacteria in waters of Québec City in Canada. J. Infect. Public Health 12, 897–899.
- Curcio, V., Macirella, R., Sesti, S., Pellegrino, D., Ahmed, A.I.M., Brunelli, E., 2021. Morphological and molecular alterations induced by lead in embryos and larvae of Danio rerio. Appl. Sci. 11.
- Datta, R., Hurlbert, M.A., 2020. Pipeline spills and indigenous energy justice. Sustainability 12.
- DeBofsky, A., Xie, Y., Jardine, T.D., Hill, J.E., Jones, P.D., Giesy, J.P., 2020. Effects of the husky oil spill on gut microbiota of native fishes in the North Saskatchewan River, Canada. Aquat. Toxicol. 229, 105658.
- Depew, D.C., Burgess, N.M., Anderson, M.R., Baker, R., Bhavsar, S.P., Bodaly, R.A., et al., 2013. An overview of mercury concentrations in freshwater fish species: a national fish mercury dataset for Canada. Can. J. Fish. Aquat. Sci. 70, 436–451.
- DeVierno, Kreuder A., House-Knight, T., Whitford, J., Ponnusamy, E., Miller, P., Jesse, N., et al., 2017. A method for assessing greener alternatives between chemical products following the 12 principles of green chemistry. ACS Sustain. Chem. Eng. 5, 2927–2935.
- Dew, W.A., Veldhoen, N., Carew, A.C., Helbing, C.C., Pyle, G.G., 2016. Cadmiuminduced olfactory dysfunction in rainbow trout: effects of binary and quaternary metal mixtures. Aquat. Toxicol. 172, 86–94.
- Dey, T., Bhattacharjee, T., Nag, P., Ritika, Ghati A., Kuila, A., 2021. Valorization of agrowaste into value added products for sustainable development. Bioresource Technology Reports 16, 100834.
- Donner, M.W., Javed, M.B., Shotyk, W., Francesconi, K.A., Siddique, T., 2017. Arsenic speciation in the lower Athabasca River watershed: a geochemical investigation of the dissolved and particulate phases. Environ. Pollut. 224, 265–274.
- Donner, M.W., Cuss, C.W., Poesch, M., Sinnatamby, R.N., Shotyk, W., Siddique, T., 2018. Selenium in surface waters of the lower Athabasca River watershed: chemical speciation and implications for aquatic life. Environ. Pollut. 243, 1343–1351.
- Du Gas, L.M., Ross, P.S., Walker, J., Marlatt, V.L., Kennedy, C.J., 2017. Effects of atrazine and chlorothalonil on the reproductive success, development, and growth of early life stage sockeye salmon (Oncorhynchus nerka). Environ. Toxicol. Chem. 36, 1354–1364.
- Duarte, M.P., Silva, R.C.F., Medeiros, TpVd, Ardisson, J.D., Cotta, A.A.C., Naccache, R., et al., 2022. Carbon nanotubes derived from waste cooking oil for the removal of emerging contaminants. New J. Chem. 46, 11315–11328.
- ECCC, 2013. Environment and Climate Change Canada. Water in Canada. https://www.canada.ca/en/environment-climate-change/services/water-overview/publications/water-in-canada.html.
- El-sayed, M.E.A., 2020. Nanoadsorbents for water and wastewater remediation. Sci. Total Environ. 739, 139903.
- Erickson, R.J., Mount, D.R., Highland, T.L., Hockett, J.R., Leonard, E.N., Mattson, V.R., et al., 2010. Effects of copper, cadmium, lead, and arsenic in a live diet on juvenile fish growth. Can. J. Fish. Aquat. Sci. 67, 1816–1826.
- Etteieb, S., Magdouli, S., Komtchou, S.P., Zolfaghari, M., Tanabene, R., Brar, K.K., et al., 2021. Selenium speciation and bioavailability from mine discharge to the environment: a field study in Northern Quebec, Canada. Environ. Sci. Pollut. Res. 28, 50799–50812.
- Etzkorn, F.A., 2019. Prevent Waste. Green Chemistry: Principles and Case Studies. The Royal Society of Chemistry, pp. 0.

- Eykelbosh, A., Slett, C.M., Wilson, P., Pillsworth, L., Luttrell, G., Reid, D., 2018. Supporting indigenous communities during environmental public health emergencies. Environmental Health Review 61, 9–11.
- Fatimah, I., Ramanda, G.D., Sagadevan, S., Suratno, Tamyiz M., Doong, R.-a., 2024. One-pot synthesis of nickel nanoparticles-embedded biochar and insight on adsorption, catalytic oxidation and photocatalytic oxidation of dye. Case Studies in Chemical and Environmental Engineering 10, 100767.
- Femi-Oloye, O.P., Oloye, F.F., Daneshamouz, S., Jones, P.D., Giesy, J.P., 2023. Toxicity of individual and combined effect of Mefenpyr di-ethyl safener and its co-herbicide, Fenoxaprop-P-ethyl, to zebrafish. Journal of Hazardous Materials Advances 11, 100334.
- Feng, Q., An, C., Cao, Y., Chen, Z., Owens, E., Taylor, E., et al., 2021. An analysis of selected oil spill case studies on the shorelines of Canada. Journal of Environmental Informatics Letters 5 (1), 39–47.
- Fernando, D.M., Tun, H.M., Poole, J., Patidar, R., Li, R., Mi, R., et al., 2016. Detection of antibiotic resistance genes in source and drinking water samples from a first nations community in Canada. Appl. Environ. Microbiol. 82, 4767–4775.
- Frouin, H., Loseto, L.L., Stern, G.A., Haulena, M., Ross, P.S., 2012. Mercury toxicity in beluga whale lymphocytes: limited effects of selenium protection. Aquat. Toxicol. 109, 185–193.
- Gandhi, N., Tang, R.W.K., Bhavsar, S.P., Arhonditsis, G.B., 2014. Fish mercury levels appear to be increasing lately: a report from 40 years of monitoring in the province of Ontario, Canada. Environ. Sci. Technol. 48, 5404–5414.
- Ganesan, S., Chawengkijwanich, C., Gopalakrishnan, M., Janjaroen, D., 2022. Detection methods for sub-nanogram level of emerging pollutants – per and polyfluoroalkyl substances. Food Chem. Toxicol. 168, 113377.
- Gavel, M.J., Richardson, S.D., Dalton, R.L., Soos, C., Ashby, B., McPhee, L., et al., 2019. Effects of 2 neonicotinoid insecticides on blood cell profiles and corticosterone concentrations of wood frogs (Lithobates sylvaticus). Environ. Toxicol. Chem. 38, 1273–1284.
- Geissen, V., Mol, H., Klumpp, E., Umlauf, G., Nadal, M., van der Ploeg, M., et al., 2015. Emerging pollutants in the environment: a challenge for water resource management. International Soil and Water Conservation Research 3, 57–65.
- Ghosh, D., 2021. Bodies of Water. 2023.
- Ghoshdastidar, A.J., Fox, S., Tong, A.Z., 2015. The presence of the top prescribed pharmaceuticals in treated sewage effluents and receiving waters in Southwest Nova Scotia, Canada. Environ. Sci. Pollut. Res. 22, 689–700.
- Gilca, A.F., Teodosiu, C., Fiore, S., Musteret, C.P., 2020. Emerging disinfection byproducts: a review on their occurrence and control in drinking water treatment processes. Chemosphere 259, 127476.
- Gillis, P.L., Gagné, F., McInnis, R., Hooey, T.M., Choy, E.S., André, C., et al., 2014. The impact of municipal wastewater effluent on field-deployed freshwater mussels in the Grand River (Ontario, Canada). Environ. Toxicol. Chem. 33, 134–143.
- Grady, W., 2007. The Great Lakes. Vancouver: Greystone Books and David Suzuki Foundation, 13, 21–26, 42–43.
- Granados-Chinchilla, F., Rodríguez, C., 2017. Tetracyclines in food and feedingstuffs: from regulation to analytical methods, bacterial resistance, and environmental and health implications. J. Anal. Methods Chem. 2017, 1315497.
- Guéguen, C., Clarisse, O., Perroud, A., McDonald, A., 2011. Chemical speciation and partitioning of trace metals (Cd, Co, Cu, Ni, Pb) in the lower Athabasca river and its tributaries (Alberta, Canada). J. Environ. Monit. 13, 2865–2872.
- Guerra, F.D., Attia, M.F., Whitehead, D.C., Alexis, F., 2018. Nanotechnology for environmental remediation: materials and applications. Molecules 23, 1760.
- Hama Aziz, K.H., Mustafa, F.S., Omer, K.M., Hama, S., Hamarawf, R.F., Rahman, K.O., 2023. Heavy metal pollution in the aquatic environment: efficient and low-cost removal approaches to eliminate their toxicity: a review. RSC Adv. 13, 17595–17610.
- Hassaan, M.A., El Nemr, A., 2020. Pesticides pollution: classifications, human health impact, extraction and treatment techniques. The Egyptian Journal of Aquatic Research 46, 207–220.
- Hejna, M., Kapuścińska, D., Aksmann, A., 2022. Pharmaceuticals in the aquatic environment: a review on eco-toxicology and the remediation potential of algae. Int. J. Environ. Res. Public Health 19.
- Hernández, A.F., Gil, F., Lacasaña, M., 2017. Toxicological interactions of pesticide mixtures: an update. Arch. Toxicol. 91, 3211–3223.
- Hodkovicova, N., Hollerova, A., Blahova, J., Mikula, P., Crhanova, M., Karasova, D., et al., 2022. Non-steroidal anti-inflammatory drugs caused an outbreak of inflammation and oxidative stress with changes in the gut microbiota in rainbow trout (Oncorhynchus mykiss). Sci. Total Environ. 849, 157921.
- Husk, B., Sanchez, J.S., Leduc, R., Takser, L., Savary, O., Cabana, H., 2019. Pharmaceuticals and pesticides in rural community drinking waters of Quebec, Canada–a regional study on the susceptibility to source contamination. Water Quality Research Journal 54, 88–103.
- Ighalo, J.O., Ojukwu, V.E., Umeh, C.T., Aniagor, C.O., Chinyelu, C.E., Ajala, O.J., et al., 2023. Recent advances in the adsorptive removal of 2,4-dichlorophenoxyacetic acid from water. Journal of Water Process Engineering 56, 104514.
- Jaishankar, M., Tseten, T., Anbalagan, N., Mathew, B.B., Beeregowda, K.N., 2014. Toxicity, mechanism and health effects of some heavy metals. Interdiscip. Toxicol. 7, 60–72.
- Järup, L., 2003. Hazards of heavy metal contamination. Br. Med. Bull. 68, 167–182.
 Jatoi, A.S., Ahmed, J., Akhter, F., Sultan, S.H., Chandio, G.S., Ahmed, S., et al., 2023.
 Recent advances and treatment of emerging contaminants through the bio-assisted method: a comprehensive review. Water Air Soil Pollut. 234, 49.
- Jeffries, K.M., Jackson, L.J., Ikonomou, M.G., Habibi, H.R., 2010. Presence of natural and anthropogenic organic contaminants and potential fish health impacts along two river gradients in Alberta, Canada. Environ. Toxicol. Chem. 29, 2379–2387.

- Kelly, B.C., Ikonomou, M.G., Higgs, D.A., Oakes, J., Dubetz, C., 2008. Mercury and Other Trace Elements in Farmed and Wild Salmon From British Columbia, Canada.
- Kirk, J.L., St. Louis, V.L., Hintelmann, H., Lehnherr, I., Else, B., Poissant, L., 2008. Methylated mercury species in marine waters of the Canadian High and Sub Arctic. Environ. Sci. Technol. 42, 8367–8373.
- Koch, N., Islam, N.F., Sonowal, S., Prasad, R., Sarma, H., 2021. Environmental antibiotics and resistance genes as emerging contaminants: methods of detection and bioremediation. Current Research in Microbial Sciences 2, 100027.
- Koley, S., Dash, S., Khwairakpam, M., Kalamdhad, A.S., 2024. Perspectives and understanding on the occurrence, toxicity and abatement technologies of disinfection by-products in drinking water. J. Environ. Manag. 351, 119770.
- Krushelnicki, L.B.B., 1995. The Great Lakes: An Environmental Atlas and Resource Book: Government of Canada Toronto, Ontario and United States Environmental Protection Agency Great Lakes National Program Office, Chicago, Illinois.
- Kubheka, G., Adeola, A.O., Forbes, P.B.C., 2022. Hexadecylamine functionalised graphene quantum dots as suitable nano-adsorbents for phenanthrene removal from aqueous solution. RSC Adv. 12, 23922–23936.
- Kumar, S., Smith, S.R., Fowler, G., Velis, C., Kumar, S.J., Arya, S., et al., 2017. Challenges and opportunities associated with waste management in India. R. Soc. Open Sci. 4, 160764
- Kumar, V., Parihar, R.D., Sharma, A., Bakshi, P., Singh Sidhu, G.P., Bali, A.S., et al., 2019. Global evaluation of heavy metal content in surface water bodies: a meta-analysis using heavy metal pollution indices and multivariate statistical analyses. Chemosphere 236, 124364.
- Kumar, V., Sharma, N., Sharma, P., Pasrija, R., Kaur, K., Umesh, M., et al., 2023. Toxicity analysis of endocrine disrupting pesticides on non-target organisms: a critical analysis on toxicity mechanisms. Toxicol. Appl. Pharmacol. 474, 116623.
- Lalonde, B., Garron, C., 2020. Temporal and spatial analysis of surface water pesticide occurrences in the maritime region of Canada. Arch. Environ. Contam. Toxicol. 79, 12–22.
- Lapolla, P., Lee, R., Mingoli, A., 2020. Wastewater as a red flag in COVID-19 spread. Public Health 185, 26.
- Lastra, A., Botello, J., Pinilla, A., Urrutia, J.I., Canora, J., Sánchez, J., et al., 2022. SARS-CoV-2 detection in wastewater as an early warning indicator for COVID-19 pandemic. Madrid region case study. Environ. Res. 203, 111852.
- Lee-Jenkins, S.S.Y., Robinson, S.A., 2018. Effects of neonicotinoids on putative escape behavior of juvenile wood frogs (Lithobates sylvaticus) chronically exposed as tadpoles. Environ. Toxicol. Chem. 37, 3115–3123.
- Lei, M., Zhang, L., Lei, J., Zong, L., Li, J., Wu, Z., et al., 2015. Overview of emerging contaminants and associated human health effects. Biomed. Res. Int. 2015, 404796.
- Li S, Yang Y, Yang S, Zheng H, Zheng Y, M J, et al. Recent advances in biodegradation of emerging contaminants - microplastics (MPs): feasibility, mechanism, and future prospects. Chemosphere 2023; 331: 138776.
- Lin, N., Nguyen, B., Omanovic, S., Moraes, C., Tufenkji, N., 2023. Electrochemical removal of Bacteria from zinc oxide nanopillars synthesized on stainless steel. ACS Applied Engineering Materials 1, 1524–1534.
- Lishman, L., Smyth, S.A., Sarafin, K., Kleywegt, S., Toito, J., Peart, T., et al., 2006. Occurrence and reductions of pharmaceuticals and personal care products and estrogens by municipal wastewater treatment plants in Ontario, Canada. Sci. Total Environ. 367, 544–558.
- Lissemore, L., Hao, C., Yang, P., Sibley, P.K., Mabury, S., Solomon, K.R., 2006. An exposure assessment for selected pharmaceuticals within a watershed in Southern Ontario. Chemosphere 64, 717–729.
- Little, D.I., Sheppard, S.R.J., Hulme, D., 2021. A perspective on oil spills: what we should have learned about global warming. Ocean Coast. Manag. 202, 105509.
- Liu, X., Sheng, Y., Liu, Q., Li, Z., 2024. Suspended particulate matter affects the distribution and migration of heavy metals in the Yellow River. Sci. Total Environ. 912, 169537.
- Liu, Y., Chen, Q., Li, Y., Bi, L., Jin, L., Peng, R., 2022. Toxic effects of cadmium on fish. Toxics 10.
- de Llanos, R., Cejudo-Marín, R., Barneo, M., Pérez-Cataluña, A., Barberá-Riera, M., Rebagliato, M., et al., 2022. Monitoring the evolution of SARS-CoV-2 on a Spanish university campus through wastewater analysis: a pilot project for the reopening strategy. Sci. Total Environ. 845, 157370.
- Macirella, R., Brunelli, E., 2017. Morphofunctional alterations in zebrafish (Danio rerio) gills after exposure to mercury chloride. Int. J. Mol. Sci. 18.
- Marchand, H., Barst, B.D., Boulanger, E., Vachon, N., Houde, M., Xia, J., et al., 2022. Exposure to contaminated river water is associated with early hatching and dysregulation of gene expression in early life stages of the endangered copper redhorse (Moxostoma hubbsi). Environ. Toxicol. Chem. 41, 1950–1966.
- Martínez, G., Merinero, M., Pérez-Aranda, M., Pérez-Soriano, E.M., Ortiz, T., Villamor, E., et al., 2021. Environmental impact of nanoparticles' application as an emerging technology: a review. Materials 14, 166.
- Masanabo, N., Orimolade, B., Idris, A.O., Nkambule, T.T.I., Mamba, B.B., Feleni, U., 2023. Advances in polymer-based detection of environmental ibuprofen in wastewater. Environ. Sci. Pollut. Res. 30, 14062–14090.
- McCuaig, L.M., Martyniuk, C.J., Marlatt, V.L., 2020. Morphometric and proteomic responses of early-life stage rainbow trout (Oncorhynchus mykiss) to the aquatic herbicide diquat dibromide. Aquat. Toxicol. 222, 105446.
- Md Anawar, H., Chowdhury, R., 2020. Remediation of polluted river water by biological, chemical, ecological and engineering processes. Sustainability 12, 7017.
- Md Meftaul, I., Venkateswarlu, K., Dharmarajan, R., Annamalai, P., Megharaj, M., 2020. Pesticides in the urban environment: a potential threat that knocks at the door. Sci. Total Environ. 711, 134612.

- Mezzelani, M., Gorbi, S., Regoli, F., 2018. Pharmaceuticals in the aquatic environments: evidence of emerged threat and future challenges for marine organisms. Mar. Environ. Res. 140, 41–60.
- Militao, I.M., Roddick, F.A., Bergamasco, R., Fan, L., 2021. Removing PFAS from aquatic systems using natural and renewable material-based adsorbents: a review. J. Environ. Chem. Eng. 9, 105271.
- Miranda, L.S., Wijesiri, B., Ayoko, G.A., Egodawatta, P., Goonetilleke, A., 2021. Water-sediment interactions and mobility of heavy metals in aquatic environments. Water Res. 202. 117386.
- Mishra, S., Kumar, A., Yadav, S., Singhal, M.K., 2018. Assessment of heavy metal contamination in water of Kali River using principle component and cluster analysis, India. Sustainable Water Resources Management 4, 573–581.
- Mishra, S., Bharagava, R.N., More, N., Yadav, A., Zainith, S., Mani, S., et al., 2019. Heavy metal contamination: an alarming threat to environment and human health. In: Sobti, R.C., Arora, N.K., Kothari, R., Sobti, R.C., Arora, N.K., Kothari, R. (Eds.), Environmental Biotechnology: For Sustainable Future. Singapore, pp. 103–125.
- Mohamed, M.H., Wilson, L.D., Headley, J.V., Peru, K.M., 2008. Novel materials for environmental remediation of tailing pond waters containing naphthenic acids. Process. Saf. Environ. Prot. 86, 237–243.
- Mohapatra, D.P., Kirpalani, D.M., 2019. Advancement in treatment of wastewater: fate of emerging contaminants. Can. J. Chem. Eng. 97, 2621–2631.
- Montes-Grajales, D., Fennix-Agudelo, M., Miranda-Castro, W., 2017. Occurrence of personal care products as emerging chemicals of concern in water resources: a review. Sci. Total Environ. 595, 601–614.
- Mueller, J.T., Gasteyer, S., 2021. The widespread and unjust drinking water and clean water crisis in the United States. Nat. Commun. 12, 3544.
- Muhammad, S., Usman, Q.A., 2021. Heavy metal contamination in water of Indus River and its tributaries, Northern Pakistan: evaluation for potential risk and source apportionment. Toxin Rev. 41, 380–388.
- Munno, K., Helm, P.A., Rochman, C., George, T., Jackson, D.A., 2022. Microplastic contamination in Great Lakes fish. Conserv. Biol. 36, e13794.
- Neudorf, K.D., Huang, Y.N., Ragush, C.M., Yost, C.K., Jamieson, R.C., Truelstrup, Hansen L., 2017. Antibiotic resistance genes in municipal wastewater treatment systems and receiving waters in Arctic Canada. Sci. Total Environ. 598, 1085–1094.
- Ojoghoro, J.O., Scrimshaw, M.D., Sumpter, J.P., 2021. Steroid hormones in the aquatic environment. Sci. Total Environ. 792, 148306.
- Oloye, F.F., Xie, Y., Asadi, M., Cantin, J., Challis, J.K., Brinkmann, M., et al., 2022. Rapid transition between SARS-CoV-2 variants of concern Delta and Omicron detected by monitoring municipal wastewater from three Canadian cities. Sci. Total Environ. 841, 156741.
- Oluwole, A.O., Omotola, E.O., Olatunji, O.S., 2020. Pharmaceuticals and personal care products in water and wastewater: a review of treatment processes and use of photocatalyst immobilized on functionalized carbon in AOP degradation. BMC Chemistry 14, 62.
- Ore, O.T., Adebiyi, F.M., 2021. A review on current trends and prospects in the pyrolysis of heavy oils. Journal of Petroleum Exploration and Production 11, 1521–1530.
- Ore, O.T., Adeola, A.O., 2021. Toxic metals in oil sands: review of human health implications, environmental impact, and potential remediation using membrane-based approach. Energy Ecol. Environ. 6, 81–91.
- Ore, O.T., Adeola, A.O., Bayode, A.A., Adedipe, D.T., Nomngongo, P.N., 2023.
 Organophosphate pesticide residues in environmental and biological matrices:
 occurrence, distribution and potential remedial approaches. Environmental
 Chemistry and Ecotoxicology 5, 9–23.
- Orprecio, R., Evans, C.H., 2003. Polymer-immobilized cyclodextrin trapping of model organic pollutants in flowing water streams. J. Appl. Polym. Sci. 90, 2103–2110.
- Ortúzar, M., Esterhuizen, M., Olicón-Hernández, D.R., González-López, J., Aranda, E., 2022. Pharmaceutical pollution in aquatic environments: a concise review of environmental impacts and bioremediation systems. Front. Microbiol. 13.
- de Paiva Magalhães, D., da Costa Marques, M.R., Baptista, D.F., Buss, D.F., 2015. Metal bioavailability and toxicity in freshwaters. Environ. Chem. Lett. 13, 69–87.
- Papineau, I., Tufenkji, N., Servais, P., Barbeau, B., 2013. Impact of media aging on the removal of Cryptosporidium in granular media filters. J. Environ. Eng. 139, 603–611
- Parezanović, G.Š., Lalic-Popovic, M., Golocorbin-Kon, S., Vasovic, V., Milijašević, B., Al-Salami, H., et al., 2019. Environmental transformation of pharmaceutical formulations: a scientific review. Arch. Environ. Contam. Toxicol. 77, 155–161.
- Patel, M., Kumar, R., Kishor, K., Mlsna, T., Pittman Jr., C.U., Mohan, D., 2019.
 Pharmaceuticals of emerging concern in aquatic systems: chemistry, occurrence, effects, and removal methods. Chem. Rev. 119, 3510–3673.
- Pathak, V.M., Verma, V.K., Rawat, B.S., Kaur, B., Babu, N., Sharma, A., et al., 2022. Current status of pesticide effects on environment, human health and it's eco-friendly management as bioremediation: a comprehensive review. Front. Microbiol. 13, 962619.
- Petrie, B., Barden, R., Kasprzyk-Hordern, B., 2015. A review on emerging contaminants in wastewaters and the environment: current knowledge, understudied areas and recommendations for future monitoring. Water Res. 72, 3–27.
- Philo, S.E., Keim, E.K., Swanstrom, R., Ong, A.Q.W., Burnor, E.A., Kossik, A.L., et al., 2021. A comparison of SARS-CoV-2 wastewater concentration methods for environmental surveillance. Sci. Total Environ. 760, 144215.
- Picard, J.-C., Munoz, G., Vo Duy, S., Sauvé, S., 2021. Longitudinal and vertical variations of waterborne emerging contaminants in the St. Lawrence Estuary and Gulf during winter conditions. Sci. Total Environ. 777, 146073.
- Pokrajac, L., Abbas, A., Chrzanowski, W., Dias, G.M., Eggleton, B.J., Maguire, S., et al., 2021. Nanotechnology for a sustainable future: addressing global challenges with the International Network4Sustainable nanotechnology. ACS Nano 15, 18608–18623.

- Pratt, D.Y., Wilson, L.D., Kozinski, J.A., Mohart, A.M., 2010. Preparation and sorption studies of β-cyclodextrin/epichlorohydrin copolymers. J. Appl. Polym. Sci. 116, 2982–2989
- Priyadarshini, M., Das, I., Ghangrekar, M.M., Blaney, L., 2022. Advanced oxidation processes: performance, advantages, and scale-up of emerging technologies. J. Environ. Manag. 316, 115295.
- Qian, Z.-J., Kang, K.-H., Ryu, B., 2015. Chapter 35 microalgae-derived toxic compounds. In: Kim, S.-K. (Ed.), Handbook of Marine Microalgae. Academic Press, Boston, pp. 527–537.
- Qiu, Y., Lee, B.E., Neumann, N., Ashbolt, N., Craik, S., Maal-Bared, R., et al., 2015. Assessment of human virus removal during municipal wastewater treatment in Edmonton, Canada. J. Appl. Microbiol. 119, 1729–1739.
- Radjenovic, J., Sedlak, D.L., 2015. Challenges and opportunities for electrochemical processes as next-generation technologies for the treatment of contaminated water. Environ. Sci. Technol. 49, 11292–11302.
- Raja, S., Cheema, H.M.N., Babar, S., Khan, A.A., Murtaza, G., Aslam, U., 2015. Socio-economic background of wastewater irrigation and bioaccumulation of heavy metals in crops and vegetables. Agric. Water Manag. 158, 26–34.
- Rajendran, S., Priya, T.A.K., Khoo, K.S., Hoang, T.K.A., Ng, H.-S., Munawaroh, H.S.H., et al., 2022. A critical review on various remediation approaches for heavy metal contaminants removal from contaminated soils. Chemosphere 287, 132369.
- Rao, N., Singh, R., Bashambu, L., 2021. Carbon-based nanomaterials: synthesis and prospective applications. Materials Today: Proceedings 44, 608–614.
- Rathi, B.S., Kumar, P.S., Show, P.-L., 2021. A review on effective removal of emerging contaminants from aquatic systems: current trends and scope for further research. J. Hazard. Mater. 409, 124413.
- Reynolds, L.J., Sala-Comorera, L., Khan, M.F., Martin, N.A., Whitty, M., Stephens, J.H., et al., 2022. Coprostanol as a population biomarker for SARS-CoV-2 wastewater surveillance studies. Water 14, 225.
- Reznicek, A.A., 1994. The disjunct coastal plain flora in the Great Lakes region. Biol. Conserv. 68, 203–215.
- Ritchie, H., Roser, M., Rosado, P., 2022. Pesticides. Our World in Data.
- Robinson, S.A., Richardson, S.D., Dalton, R.L., Maisonneuve, F., Trudeau, V.L., Pauli, B. D., et al., 2017. Sublethal effects on wood frogs chronically exposed to environmentally relevant concentrations of two neonicotinoid insecticides. Environ. Toxicol. Chem. 36, 1101–1109.
- Rodriguez-Narvaez, O.M., Peralta-Hernandez, J.M., Goonetilleke, A., Bandala, E.R., 2017. Treatment technologies for emerging contaminants in water: a review. Chem. Eng. J. 323, 361–380.
- Rowenczyk, L., Cai, H., Nguyen, B., Sirois, M., Côté-Laurin, M.C., Toupoint, N., et al., 2022. From freshwaters to bivalves: microplastic distribution along the saint-Lawrence river-to-sea continuum. J. Hazard. Mater. 435, 128977.
- Roy, A., Sharma, A., Yadav, S., Jule, L.T., Krishnaraj, R., 2021. Nanomaterials for remediation of environmental pollutants. Bioinorg. Chem. Appl. 2021, 1764647.
- Rusiñol, M., Martínez-Puchol, S., Forés, E., Itarte, M., Girones, R., Bofill-Mas, S., 2020. Concentration methods for the quantification of coronavirus and other potentially pandemic enveloped virus from wastewater. Current Opinion in Environmental Science & Health 17, 21–28.
- Saibu, Y., Jamwal, A., Feng, R., Peak, D., Niyogi, S., 2018. Distribution and speciation of zinc in the gills of rainbow trout (Oncorhynchus mykiss) during acute waterborne zinc exposure: interactions with cadmium or copper. Comp. Biochem. Physiol., Part C: Toxicol. Pharmacol. 206-207, 23–31.
- Salerno, J., Bennett, C.J., Holman, E., Gillis, P.L., Sibley, P.K., Prosser, R.S., 2018.
 Sensitivity of multiple life stages of 2 freshwater mussel species (Unionidae) to various pesticides detected in Ontario (Canada) surface waters. Environ. Toxicol. Chem. 37, 2871–2880.
- Sami Ullah, B., Umara, Q., 2021. Implications of sewage discharge on freshwater ecosystems. In: Tao, Z. (Ed.), Sewage. IntechOpen, Rijeka pp. Ch. 6.
- Savary, S., Willocquet, L., Pethybridge, S.J., Esker, P., McRoberts, N., Nelson, A., 2019. The global burden of pathogens and pests on major food crops. Nature Ecology & Evolution 3, 430–439.
- Scheuhammer, A., Braune, B., Chan, H.M., Frouin, H., Krey, A., Letcher, R., et al., 2015. Recent progress on our understanding of the biological effects of mercury in fish and wildlife in the Canadian Arctic. Special Issue: Mercury in Canada's North 509-510, 91-103.
- Schwartz, H., Marushka, L., Chan, H.M., Batal, M., Sadik, T., Ing, A., et al., 2021a. Pharmaceuticals in source waters of 95 First Nations in Canada. Can. J. Public Health 112, 133–153.
- Schwartz, H., Marushka, L., Chan, L., Batal, M., Sadik, T., Ing, A., et al., 2021b. Pharmaceuticals in source waters of 95 First Nations in Canada. Can. J. Public Health 112, 133–153.
- Senta, I., Gracia-Lor, E., Borsotti, A., Zuccato, E., Castiglioni, S., 2015. Wastewater analysis to monitor use of caffeine and nicotine and evaluation of their metabolites as biomarkers for population size assessment. Water Res. 74, 23–33.
- Sheedy, C., Kromrey, N., Nilsson, D., Armitage, T., 2019. From peaks to prairies: a time-of-travel synoptic survey of pesticides in watersheds of southern Alberta, Canada. Inland Waters 9, 438–452.
- Shekh, K., Tang, S., Hecker, M., Niyogi, S., 2018. Investigating the role of ionoregulatory processes in the species- and life-stage-specific differences in sensitivity of rainbow trout and white sturgeon to cadmium. Environ. Sci. Technol. 52, 12868–12876.
- Sheldon, R.A., 2011. Utilisation of biomass for sustainable fuels and chemicals: molecules, methods and metrics. Catal. Today 167, 3–13.
- Shi, Y.X., Mangal, V., Guéguen, C., 2016. Influence of dissolved organic matter on dissolved vanadium speciation in the Churchill River estuary (Manitoba, Canada). Chemosphere 154, 367–374.

- Shil, S.C., Islam, M.S., Irin, A., Tusher, T., Hoq, M.E., 2017. Heavy metal contamination in water and sediments of Passur River near the Sundarbans Mangrove of Bangladesh. Journal of Environmental Science and Natural Resources 10, 15–19.
- Shinn, C., Santos, M.M., Lek, S., Grenouillet, G., 2015. Behavioral response of juvenile rainbow trout exposed to an herbicide mixture. Ecotoxicol. Environ. Saf. 112, 15–21.
- Shotyk W, Bicalho B, Cuss CW, Donner MW, Grant-Weaver I, Haas-Neill S, et al. Trace metals in the dissolved fraction ($<0.45\mu m$) of the lower Athabasca River: Analytical challenges and environmental implications. Sci. Total Environ. 2017; 580: 660–669.
- Singh, J., Gupta, P., Das, A., 2021. Dyes from textile industry wastewater as emerging contaminants in agricultural fields. In: Kumar Singh, V., Singh, R., Lichtfouse, E. (Eds.), Sustainable Agriculture Reviews 50: Emerging Contaminants in Agriculture. Springer International Publishing, Cham, pp. 109–129.
- Sophia, A.C., Lima, E.C., 2018. Removal of emerging contaminants from the environment by adsorption. Ecotoxicol. Environ. Saf. 150, 1–17.
- Sprague, D.D., Vermaire, J.C., 2018. Legacy arsenic pollution of lakes near cobalt, Ontario, Canada: arsenic in lake water and sediment remains elevated nearly a century after mining activity has ceased. Water Air Soil Pollut. 229, 87.
- Srain, H.S., Beazley, K.F., Walker, T.R., 2021. Pharmaceuticals and personal care products and their sublethal and lethal effects in aquatic organisms. Environ. Rev. 29, 142–181.
- Stroski, K.M., Luong, K.H., Challis, J.K., Chaves-Barquero, L.G., Hanson, M.L., Wong, C. S., 2020. Wastewater sources of per- and polyfluorinated alkyl substances (PFAS) and pharmaceuticals in four Canadian Arctic communities. Sci. Total Environ. 708, 134494
- Stuart, M., Lapworth, D., Crane, E., Hart, A., 2012. Review of risk from potential emerging contaminants in UK groundwater. Sci. Total Environ. 416, 1–21.
- Sultana, T., Murray, C., Kleywegt, S., Metcalfe, C.D., 2018. Neonicotinoid pesticides in drinking water in agricultural regions of southern Ontario, Canada. Chemosphere 202, 506–513.
- Sun, M., Arevalo, E., Strynar, M., Lindstrom, A., Richardson, M., Kearns, B., et al., 2016. Legacy and emerging perfluoroalkyl substances are important drinking water contaminants in the cape fear river watershed of North Carolina. Environ. Sci. Technol. Lett. 3, 415–419.
- Tang, Y., Alam, M.S., Konhauser, K.O., Alessi, D.S., Xu, S., Tian, W., et al., 2019. Influence of pyrolysis temperature on production of digested sludge biochar and its application for ammonium removal from municipal wastewater. J. Clean. Prod. 209, 927–936
- Tang, Y., Li, Y., Zhan, L., Wu, D., Zhang, S., Pang, R., et al., 2022. Removal of emerging contaminants (bisphenol A and antibiotics) from kitchen wastewater by alkalimodified biochar. Sci. Total Environ. 805, 150158.
- Taylor, L.J., Mann, N.S., Daoud, D., Clark, K.F., van den Heuvel, M.R., Greenwood, S.J.,
 2019. Effects of sublethal chlorpyrifos exposure on postlarval American lobster
 (Homarus americanus). Environ. Toxicol. Chem. 38, 1294–1301.
 Thakur, A., Koul, B., 2022. Chapter 7 impact of oil exploration and spillage on marine
- Thakur, A., Koul, B., 2022. Chapter / impact of oil exploration and spillage on marine environments. In: Das, P., Manna, S., Pandey, J.K. (Eds.), Advances in Oil-Water Separation. Elsevier, pp. 115–135.
- UNSDG, 2018. Sustainable Development Goal 6. Synthesis Report on Water and Sanitation. https://sustainabledevelopment.un.org/content/documents/19901SD G6 SR2018 web 3.ndf.
- Valdez-Carrillo, M., Abrell, L., Ramírez-Hernández, J., Reyes-López, J.A., Carreón-Diazconti, C., 2020. Pharmaceuticals as emerging contaminants in the aquatic environment of Latin America: a review. Environ. Sci. Pollut. Res. 27, 44863–44891.
- Vale, F., Sousa, C.A., Sousa, H., Santos, L., Simões, M., 2022. Parabens as emerging contaminants: environmental persistence, current practices and treatment processes. J. Clean. Prod. 347, 131244.
- Vasamsetti, B.M., Chon, K., Kim, J., Oh, J.-A., Yoon, C.-Y., Park, H.-H., 2022. Developmental toxic effects of Thiram on developing zebrafish (Danio rerio) embryos. Toxics 10.
- Vaudin, P., Augé, C., Just, N., Mhaouty-Kodja, S., Mortaud, S., Pillon, D., 2022. When pharmaceutical drugs become environmental pollutants: potential neural effects and underlying mechanisms. Environ. Res. 205, 112495.
- Vaudreuil, M.-A., Munoz, G., Vo Duy, S., Sauvé, S., 2024. Tracking down pharmaceutical pollution in surface waters of the St. Lawrence River and its major tributaries. Sci. Total Environ. 912, 168680.
- Vernouillet, G., Eullaffroy, P., Lajeunesse, A., Blaise, C., Gagné, F., Juneau, P., 2010.
 Toxic effects and bioaccumulation of carbamazepine evaluated by biomarkers measured in organisms of different trophic levels. Chemosphere 80, 1062–1068.
- Viaroli, S., Lancia, M., Re, V., 2022. Microplastics contamination of groundwater: current evidence and future perspectives. A review. Sci. Total Environ. 824, 153851.
- Wang, J., Wang, S., 2020. Reactive species in advanced oxidation processes: formation, identification and reaction mechanism. Chem. Eng. J. 401, 126158.
- Wang, Z., Tan, Z., Li, H., Yuan, S., Zhang, Y., Dong, Y., 2022. Direct current electrochemical method for removal and recovery of heavy metals from water using straw biochar electrode. J. Clean. Prod. 339, 130746.
- White, I.C., Molloy, C.F., 2003. Factors that determine the cost of oil spills. International Oil Spill Conference Proceedings 2003, 1225–1229.
- Wu, F., Zhang, J., Xiao, A., Gu, X., Lee, W.L., Armas, F., et al., 2020. SARS-CoV-2 titers in wastewater are higher than expected from clinically confirmed cases. mSystems 5. https://doi.org/10.1128/msystems.00614-20.
- World Health Organisation, 2020. WHO Recommended Classification of Pesticides by Hazard and Guidelines to Classification, 2019 edition. Geneva.
- Wu, Q., Leung, J.Y.S., Geng, X., Chen, S., Huang, X., Li, H., et al., 2015. Heavy metal contamination of soil and water in the vicinity of an abandoned e-waste recycling site: implications for dissemination of heavy metals. Sci. Total Environ. 506-507, 217–225.

- Xiang, L., Harindintwali, J.D., Wang, F., Redmile-Gordon, M., Chang, S.X., Fu, Y., et al., 2022. Integrating biochar, bacteria, and plants for sustainable remediation of soils contaminated with organic pollutants. Environ. Sci. Technol. 56, 16546–16566.
- Xie, Y., Challis, J.K., Oloye, F.F., Asadi, M., Cantin, J., Brinkmann, M., et al., 2022. RNA in municipal wastewater reveals magnitudes of COVID-19 outbreaks across four waves driven by SARS-CoV-2 variants of concern. ACS ES&T Water 2, 1852–1862.
- Xu, D., Shen, Z., Dou, C., Dou, Z., Li, Y., Gao, Y., et al., 2022. Effects of soil properties on heavy metal bioavailability and accumulation in crop grains under different farmland use patterns. Sci. Rep. 12, 9211.
- Yang, C., Song, G., Lim, W., 2020. A review of the toxicity in fish exposed to antibiotics. Comparative Biochemistry and Physiology Part C: Toxicology & Pharmacology 237, 108240
- Yang, Z., Shah, K., Laforest, S., Hollebone, B.P., Lambert, P., Brown, C.E., et al., 2018. A study of the 46-year-old arrow oil spill: persistence of oil residues and variability in oil contamination along Chedabucto Bay, Nova Scotia, Canada. J. Clean. Prod. 198, 1459–1473.
- Yeh, A., Marcinek, D.J., Meador, J.P., Gallagher, E.P., 2017. Effect of contaminants of emerging concern on liver mitochondrial function in Chinook salmon. Aquat. Toxicol. 190, 21–31.
- Yousefi, N., Wong, K.K.W., Hosseinidoust, Z., Sørensen, H.O., Bruns, S., Zheng, Y., et al., 2018. Hierarchically porous, ultra-strong reduced graphene oxide-cellulose nanocrystal sponges for exceptional adsorption of water contaminants. Nanoscale 10, 7171–7184.
- Zamora-Ledezma, C., Negrete-Bolagay, D., Figueroa, F., Zamora-Ledezma, E., Ni, M., Alexis, F., et al., 2021. Heavy metal water pollution: a fresh look about hazards, novel and conventional remediation methods. Environ. Technol. Innov. 22, 101504.
- Zhang, B., Matchinski, E.J., Chen, B., Ye, X., Jing, L., Lee, K., 2019. Chapter 21 marine oil spills—oil pollution, sources and effects. In: Sheppard, C., Sheppard, C. (Eds.), World Seas: An Environmental Evaluation, Second edition, pp. 391–406.
- Zhang, M., Day, E.L., McFall-Boegeman, H., Petritis, S.J., Cooper, M.M., 2023. Incorporation of green chemistry into undergraduate organic laboratory using cooperative project-based experiments and case studies. Green Chem. Lett. Rev. 16, 2183781.

ELSEVIER

Contents lists available at ScienceDirect

Environmental Research

journal homepage: www.elsevier.com/locate/envres





Efficient decaffeination with recyclable magnetic microporous carbon from renewable sources: Kinetics and isotherm analysis

Michelle P. Duarte ^{a,b,1}, Adedapo O. Adeola ^{a,b,**,1}, Gianluca Fuoco ^{a,b}, Tyler J. Jargaille ^{a,b}, Rafik Naccache ^{a,b,*}

ARTICLE INFO

Keywords:
Adsorption
Activated carbon
Caffeine
Emerging contaminants
Water treatment

ABSTRACT

Rapid global urbanization and population growth have ignited an alarming surge in emerging contaminants in water bodies, posing health risks, even at trace concentrations. To address this challenge, novel water treatment and reuse technologies are required as current treatment systems are associated with high costs and energy requirements. These drawbacks provide additional incentives for the application of cost-effective and sustainable biomass-derived activated carbon, which possesses high surface area and low toxicity. Herein, we synthesized microporous activated carbon (MAC) and its magnetic derivative (m-MAC) from tannic acid to decaffeinate contaminated aqueous solutions. Detailed characterization using SEM, BET, and PXRD revealed a very high surface area (>1800 m²/g) and a highly porous, amorphous, heterogeneous sponge-like structure. Physicochemical and thermal analyses using XPS, TGA, and EDS confirmed thermal stability, unique surface moieties, and homogeneous elemental distribution. High absorption performance (>96 %) and adsorption capacity (287 and 394 mg/g) were recorded for m-MAC and MAC, respectively. Mechanistic studies showed that the sorption of caffeine is in tandem with multilayer and chemisorptive mechanisms, considering the models' correlation and error coefficients. π-π stacking and hydrogen bonding were among the interactions that could facilitate MAC-Caffeine and m-MAC-Caffeine bonding interactions. Regeneration and reusability experiments revealed adsorption efficiency ranging from 90.5 to 98.4 % for MAC and 88.6-93.7 % for m-MAC for five cycles. Our findings suggest that MAC and its magnetic derivative are effective for caffeine removal, and potentially other organic contaminants with the possibility of developing commercially viable and cost-effective water polishing tools.

1. Introduction

Emerging chemical pollutants (ECPs) encompass various substances, including cosmetics, pharmaceuticals, surfactants, manufacturing additives, plasticizers, and pesticides, which have been detected within our ecosystem. While we are aware of their presence, the full extent of their environmental hazards and the threat to animal life, and human health remains inadequately understood (Petrie et al., 2015). One of the pressing concerns with ECPs is their persistence in water sources. Conventional wastewater treatment and purification facilities struggle to eliminate these compounds, resulting in trace amounts persisting in our

ecosystem and drinking water (Adeola and Forbes, 2021; Menya et al., 2023; Richardson and Kimura, 2017). Caffeine is one example of these persistent ECPs and is a recalcitrant chemical that is frequently detected in potable water, groundwater, sewage, wastewater effluents, lakes, rivers, remote mountain lakes, and even Antarctic waters (Buerge et al., 2003; Gogoi et al., 2018; Heberer, 2002; Philip et al., 2018). Caffeine is the most ubiquitous psychotropic substance in the world (Gardinali and Zhao, 2002). It is a chemical molecule belonging to the methylxanthines family and a stimulant of the central nervous system, with addictive tendencies (Bruton et al., 2010). Remarkably, caffeine has been detected in water systems of nations where it is not even cultivated but is

a Department of Chemistry and Biochemistry and the Centre for NanoScience Research, Concordia University, Montreal, QC, H4B 1R6, Canada

b Quebec Centre for Advanced Materials, Department of Chemistry and Biochemistry, Concordia University, Montreal, QC, H4B 1R6, Canada

^{*} Corresponding author.

^{**} Corresponding author. Department of Chemistry and Biochemistry and the Centre for NanoScience Research, Concordia University, Montreal, QC, H4B 1R6, Canada.

 $[\]textit{E-mail addresses:} \ a dedapo. a deola@concordia. ca\ (A.O.\ Adeola),\ rafik. naccache@concordia. ca\ (R.\ Naccache).$

 $^{^{1}\,}$ These authors contributed equally and share the first authorship of this publication.

consumed. This raises significant concerns regarding unintended exposure and potential impact on aquatic fauna, a concern that has yet to be adequately addressed.

In light of the growing negative effects on the aquatic environment, amongst other sources of water pollution, remediation steps are needed to reduce the impact of caffeine on aquatic systems. In environmental sciences, biomass-derived carbonaceous architectures are widely utilized because they often possess large specific surface areas, relatively low toxicity, high sorption affinity, biocompatibility, biodegradability, sustainability, affordability, carbon neutrality, and natural abundance (Adeola et al., 2023). These precursors can originate from naturally occurring minerals, industrial, agricultural, plant, and fruit wastes. Numerous precursors, including date pits, vermiculata plants, coconut shells and husks, bamboo waste, rice husks, ground nut shells, olive stones, oil palm fiber and shell, corncob, olive seed waste, fir wood, Euphorbia rigida bio plant, roots of vetiver, sugars, seeds of Rosa canina, apricot and peach stones can be effectively employed for the production of activated carbon, according to literature (Sambo et al., 2024; Tyagi, 2024). In particular, adsorption techniques with the aid of biomass-derived materials have been explored as a useful tool for caffeine removal from contaminated water. While few studies have endeavored to rid water of caffeine using biomass materials (Batista et al., 2016; Couto et al., 2015; Galhetas et al., 2014), there has been no investigation of magnetic carbon-based composites derived from renewable sources, boasting an unparalleled surface area, high adsorption capability, and potential for recovery and reusability. Yet such innovation would greatly reinforce the principles of sustainability, significantly curbing secondary waste and contamination.

Herein, we synthesized renewable and eco-friendly microporous activated carbon (MAC) and its magnetic derivative (m-MAC) from tannic acid using pyrolysis and solvothermal techniques. Investigations were carried out on the role of process variables such as initial concentrations of caffeine, reaction time (sorption kinetics), pH of solution in achieving the maximum caffeine sorption, the model organic contaminant. Comparative isothermal and kinetic modeling equations were used to elucidate the possible mechanisms of sorbate-sorbent interactions. Furthermore, regeneration and reusability tests of the sorbents over five cycles were carried out to elucidate their potential for sustainable applications.

2. Experimental

2.1. Materials and reagents

Caffeine (98%), tannic acid, hydrochloric acid (HCl), iron(III) acetylacetonate (Fe(acac)₃), sodium hydroxide (NaOH), calcium chloride (CaCl₂), potassium carbonate (K₂CO₃), potassium chloride (KCl), oleylamine, oleic acid, acetone and ethanol were supplied by Sigma-Aldrich. ChemScience supplied the 0.45 μm syringe PTFE filters used in the study. Ultra-pure water (Milli-Q® Water Systems, Sigma-Aldrich) was used for the preparation of the solutions.

2.2. Preparation of microporous activated carbon (MAC) and magnetic functionalization of MAC sorbent

The synthesis of the activated carbon was conducted following the established methodology with a slight modification (Díez et al., 2019). Briefly, a mixture consisting of tannic acid (0.5 g), K_2CO_3 (0.5 g), and KCl (3 g) was prepared and thoroughly mixed through grinding. Subsequently, the resulting mixture was introduced into an alumina boat and placed into a horizontal furnace. The pyrolysis process took place under a N_2 atmosphere (100 mL/min) at a temperature of 750 °C (5 °C/min) for 1 h. Upon completion, the system was cooled to ambient temperature while keeping the nitrogen flow. The product was rinsed with hot deionized water and filtered to eliminate any residual unreacted potassium salts, after which the sample was oven-dried at

85 °C for 24 h. The product obtained in step 1, described above, was functionalized by doping with magnetic iron oxide nanoparticles (FeONPs) (Fig. 1). A solution made of 3.8 mL oleic acid and 15 mL oleylamine was used to dissolve Fe(acac) $_3$ and MAC (0.5 g each). The mixture was placed in a hydrothermal reactor and heated with stirring at 200 °C for 2 h. After cooling to ambient temperature, the product was washed with ethanol and dried in the oven at 85 °C, and pyrolyzed at 600 °C under N $_2$ atmosphere (100 mL/min) for 1 h.

2.3. Material characterization

The Rigaku MiniFlex 6G diffractometer (Cu K α source; $\lambda = 1.54$ Å) was used to acquire the powder X-ray diffraction (PXRD) patterns in the 2θ range from 10° to 80° at a rate of scan of 10 $^{\circ}\text{C/min}.$ The Thermo Scientific Nicolet iS5 equipped with an iD5 ATR accessory was used to collect the Fourier-transformed infrared spectroscopy (FTIR) spectra in the range of 400–4000 cm⁻¹ wavenumber range. Data were analyzed with the Omnic 9 software. A Phenom ProXdesktop G6 (Thermofisher Scientific) was used for scanning electron microscopy (SEM) and energy dispersive X-ray spectroscopy (EDS) analyses at 5 kV. The TGA Q500 analyzer aided the thermogravimetric analyses (TGA) of the samples. The sample temperature was raised from 25 to 900 °C at a rate of 10 °C/ min under an oxidizing atmosphere with a flow of 50 mL/min. The Micromeritics® TriStar II Plus facilitated the analysis of the samples' specific surface area (SSA) and pore size distribution by nitrogen adsorption/desorption isotherms at 77 K. The samples were previously activated for 24 h at 100 °C. The Brunauer-Emmett-Teller (BET) was used to determine the SSA while the non-local density functional theory (NLDFT) method was employed for the pore size distribution analysis. The pH of the point of zero charge of each sorbent was investigated by adding 15.0 mL of 0.1 M NaCl solution to multiple vials, and adjusting the solution pH between 2 and 12, using a trace amount of 0.1 M HCl or NaOH. Afterwards, 10 mg of each material was added to the vials. The vials were stirred for 48 h using an orbital shaker. The solutions were filtered and the final pH values were obtained using a pH meter (AB150, accumet®, Fisher Scientific). The pHPZC was obtained by plotting a graph of ΔpH (pH_{final}-pHi_{nitial}) versus pHi_{nitial}.

2.4. Adsorption kinetics and isotherm studies

The materials synthesized were evaluated for the adsorption of caffeine using 50 mL screw-capped polypropylene vials with $CaCl_2$ (0.01 mol/L) as electrolyte at 25 °C. The contact time and by extension the adsorption kinetics studies were performed placing 10 mg of both materials in contact with 100 mg/L and 500 mg/L caffeine solutions. The reaction vessels were shaken at 300 rpm (Thermo Scientific 2314 Multi-Purpose Lab Rotator) for 24 h (Kubheka et al., 2022). For the adsorption isotherm studies, initial caffeine concentrations ranged from 20 to 500 mg/L. The vials were shaken for 1 h following the optimized contact time obtained from kinetic studies. After each study, the solution was filtered and supernatants were analyzed to quantify the caffeine adsorption. Furthermore, the pH effect on caffeine removal was investigated by using 0.1 M HCl or NaOH to vary the solution pH between 2 and 12. Measurements were obtained in duplicates to ensure the reproducibility of the results.

Caffeine concentration at equilibrium was analyzed using UV-visible absorption spectroscopy (Cary 5 Series – Agilent Technologies). A calibration curve was obtained using the maximum absorption wavelength (273 nm) of caffeine and varying the concentration from 1 to 20 mg/L (Fig. S1). Furthermore, caffeine removal was evaluated using Eq. (1), while the adsorption capacity was calculated using Eq. (2).

Removal efficiency (%) =
$$\frac{(C_0 - C_e)}{C_0} \times 100$$
 (1)

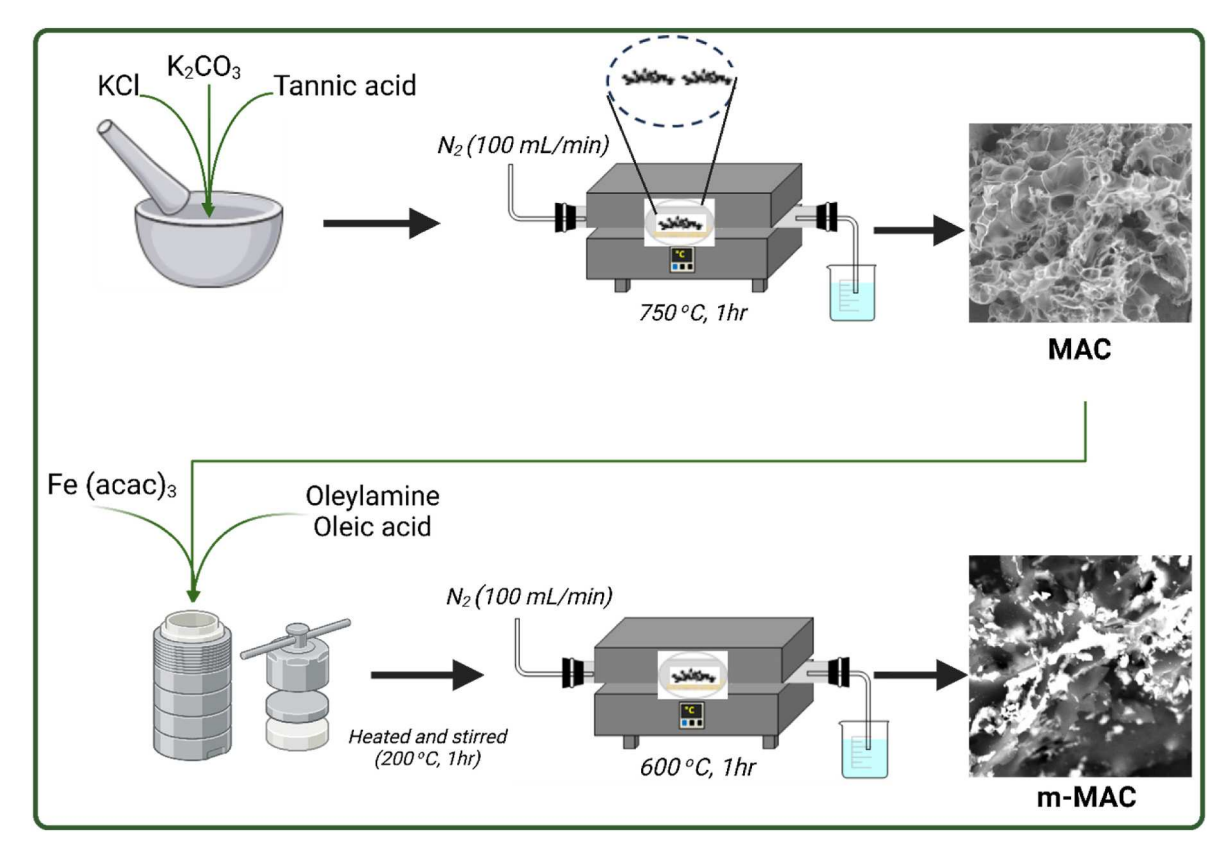


Fig. 1. Schematic of the synthesis of MAC and m-MAC.

$$q_e = \frac{(C_0 - C_e)V_0}{m} \tag{2}$$

Where C_0 is the pre-adsorption caffeine concentration (mg/L), Ce is the equilibrium caffeine concentration (mg/L), q_e is the sorption capacity (mg/g), V_0 is the initial solution volume (L), and m is the mass (g) of the adsorbents.

2.5. Kinetics and isotherm modelling

The data obtained from batch experiments were fitted to the Weber-Morris intraparticle diffusion (eq. (3)), pseudo-first-order (PFO) (eq. (4)), and pseudo-second-order (PSO) (eq. (5)) models (Fig. 5 and S3). The initial sorption rate and half-life were evaluated using eqs. (6) and (7), and the best-fit model was validated using the sum of squares of errors (SSE) and the chi-square test (χ^2) (eqs. (8) and (9)) (Anthony et al., 2020; Duarte et al., 2022).

$$q_t = K_{id}t^{0.5} + C \tag{3}$$

$$q_t = q_e \, \left(1 \, - \, e^{-K_1 t} \right) \tag{4}$$

$$q_t = \frac{q_e^2 K_2 t}{q_e K_2 t + 1} \tag{5}$$

$$h = K_2 q_e^2 \tag{6}$$

$$t_{0.5} = \frac{1}{K_2 q_e} \tag{7}$$

$$\sum\nolimits_{i=1}^{n} \left(q_{e,\text{cal}} - q_{e,\text{exp}} \right)_{i}^{2} \tag{8}$$

$$\chi^2 = \sum \frac{\left(q_{exp} - q_{calc}\right)^2}{q_{calc}} \tag{9}$$

Where q_t and q_e are caffeine adsorbed per sorbent mass (mg/g) per time (t) and at equilibrium, respectively, K_I (1/min) and K_2 (g/mg × min) are rate constants for pseudo-first-order and pseudo-second-order, K_{id} (mg/g × min^{1/2}) and C (mg/g) are the rate constant for intraparticle diffusion and constant linked to the thickness of boundary layer, respectively, and h (mg/g × min) and $t_{0.5}$ are the initial rate of sorption and half-life, respectively.

In isotherm studies, the Freundlich model is commonly used to describe multilayer adsorption of chemical pollutants onto heterogeneous surfaces (eq. (10)), while the Langmuir model (eq. (11)) is based on a monolayer sorption mechanism on homogeneous surfaces with a site-limiting sorption (Inyinbor et al., 2017). The complex interactions between sorbent and sorbate are described by the Sips model (eq. (12)). It may be reduced to the Langmuir or Freundlich model due to changes in pollutant concentration and surface interactions with the sorbents (Adeola and Forbes, 2019; Kubheka et al., 2022). The Sips model has three main parameters, while Langmuir and Freundlich models have two key parameters. The best-fitted model was confirmed by using the sum of squared errors (SSE) and the chi-square test (χ^2) (eqs. (8) and (9)) (Mozaffari Majd et al., 2022; Unuabonah et al., 2019).

$$q_e = K_f C_e^N$$
 (10)

$$q_{e} = \frac{q_{\text{max}} K_{L} C_{e}}{1 + K_{L} C_{e}} \tag{11}$$

$$q_{e} = \frac{q_{m}K_{s} C_{e}^{ms}}{1 + K_{s} \cdot C_{e}^{ms}}$$
(12)

Where Ce is caffeine unadsorbed (mg/L) and q_e is the amount of caffeine

adsorbed (mg/g). K_F is the adsorption capacity-related parameter, K_L is the Langmuir constant, N & ms are heterogeneity indicators, and q_{\max} & q_m are the maximum adsorption capacities.

3. Results and discussion

3.1. Sorbent characterization

Scanning electron microscopy (SEM) revealed a porous structure for MAC (Fig. 2a and b) and m-MAC (Fig. 2c and d) with the pores presenting a sponge-like morphology, composed of carbon layers. K₂CO₃ has been widely applied as a chemical activating agent in the production of various activated carbons (Adinata et al., 2007; Kılıç et al., 2012; Márquez-Montesino et al., 2020; Wu et al., 2023). The activation process using K₂CO₃ occurs in several steps. First, the precursors are impregnated with K₂CO₃, followed by carbonization at high temperatures under an inert atmosphere. During the carbonization, char is formed, which then reacts with K₂CO₃, rendering the reduction of carbon and the formation of CO as shown in eq. (13)-(15). The gas is responsible for creating internal pressure, promoting the creation of the pores, and consequently, resulting in materials with a high surface area. Moreover, the porosity is further explained by the formation of potassium compounds (K2O and K), which expand the existing pores and create new ones. (Adinata et al., 2007; Heidarinejad et al., 2020; Lobato-Peralta et al., 2023; Mu et al., 2019; Okman et al., 2014).

$$K_2CO_{3(s)} + 2C_{(s)} \rightarrow 2K_{(s)} + 3CO_{(g)}$$
 (13)

$$K_2CO_{3(a0)} \rightarrow K_2O_{(s)} + CO_{2(g)}$$
 (14)

$$K_2O_{(s)} + C_{(s)} \rightarrow 2K_{(s)} + CO_{(g)}$$
 (15)

Moreover, inorganic salts are known to act as hard templates, which control the morphology of the carbon material, such as the shape and size of the pores. Thus, the sponge-like structure observed for MAC can be associated with the presence of KCl (Díez et al., 2021). Díez et al. (2019) synthesized porous carbon materials using K_2CO_3 and KCl as salt templates. The authors observed that materials created without KCl presented a porous structure that was not sponge-like. However, when KCl was employed, the sponge-like structure was evident.

The impregnation of the resultant microporous materials (MAC) with FeONPs endowed it with magnetic properties (m-MAC). It can be seen that the process created more heterogeneous morphological characteristics as supported by TEM and SEM analyses (Fig. 2). The higher contrast FeONPs can be seen distributed around the surface and pores of MAC substrate in the m-MAC. EDS analysis confirmed the dominant presence of carbon and oxygen, with trace amounts of potassium from the reacted precursors MAC salts (Fig. S2), while the successful incorporation of FeONPs for the m-MAC was confirmed considering the relative abundance of the elements, showing increased amounts of oxygen, as well as the presence of iron (Figs. S2 and 3). EDS mapping images of m-MAC showed that C, O, and Fe elements were present throughout the structures (Fig. 2e–h).

PXRD patterns were obtained for both materials (Fig. 3a and b) and it is possible to observe broad and weak reflection at $\sim 22^{\circ}$ 20 assigned to the graphite carbon phase (JCPDS-1-640) for MAC (Fig. 3a). Moreover, the broad halo under these peaks evidences the amorphous nature of the material (Díez et al., 2019; Lobato-Peralta et al., 2023). For m-MAC (Fig. 3b), the characteristic diffraction peaks of magnetite (Fe₃O₄) were observed (JCPDS-1-1111), which confirms the inclusion of the magnetic

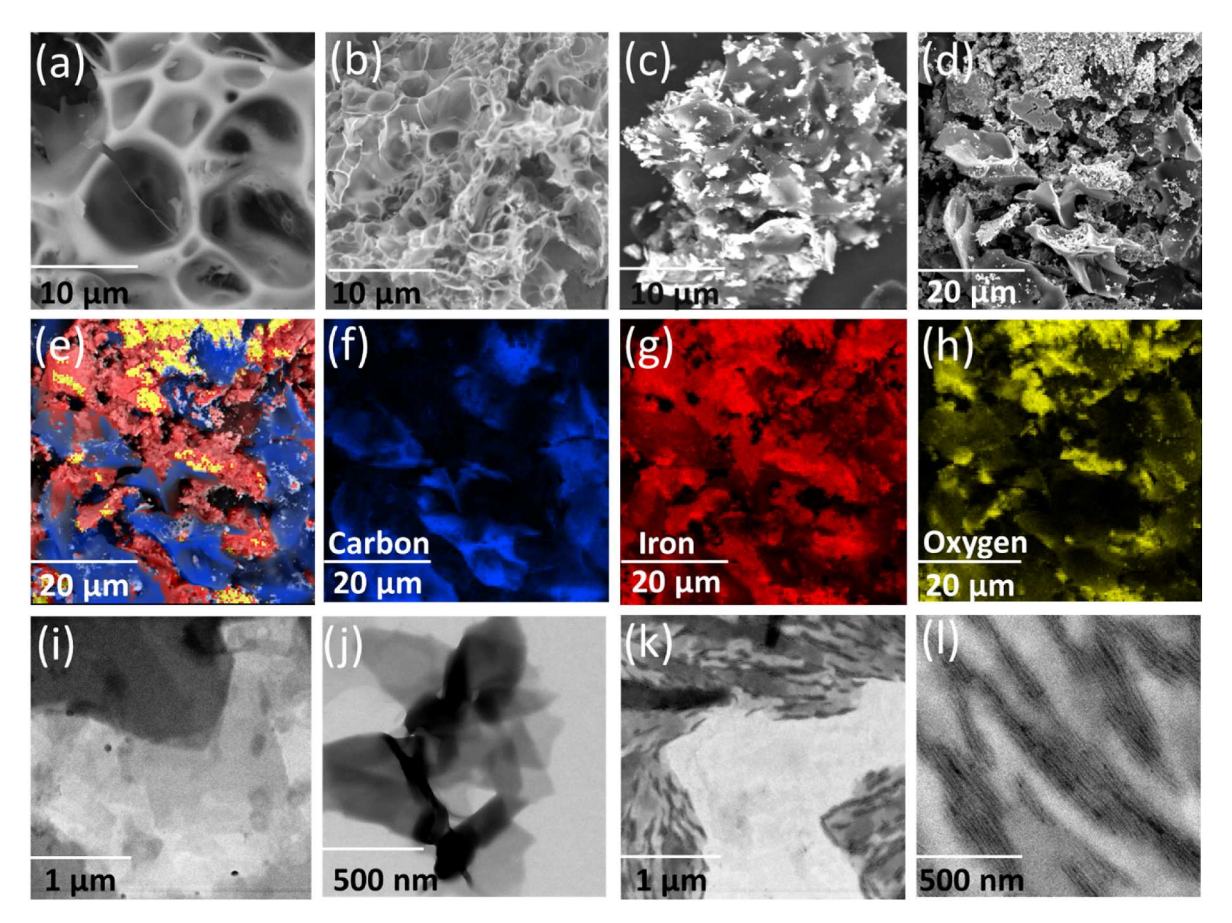


Fig. 2. SEM, EDS mapping, and TEM images of MAC and m-MAC (a,b) MAC 10 μ m @x1000 and \times 5000 magnification, (c,d) m-MAC 10 μ m@x1000 and 20 μ m@ \times 5000 magnification. (e-h) SEM-EDS mapping shows the distribution of carbon (blue), oxygen (yellow), and iron (red) in m-MAC. (i-l) TEM of pristine MAC sheets (I & j) and m-MAC (k & l) showing the magnetic iron oxide particles grafted over the sheet.

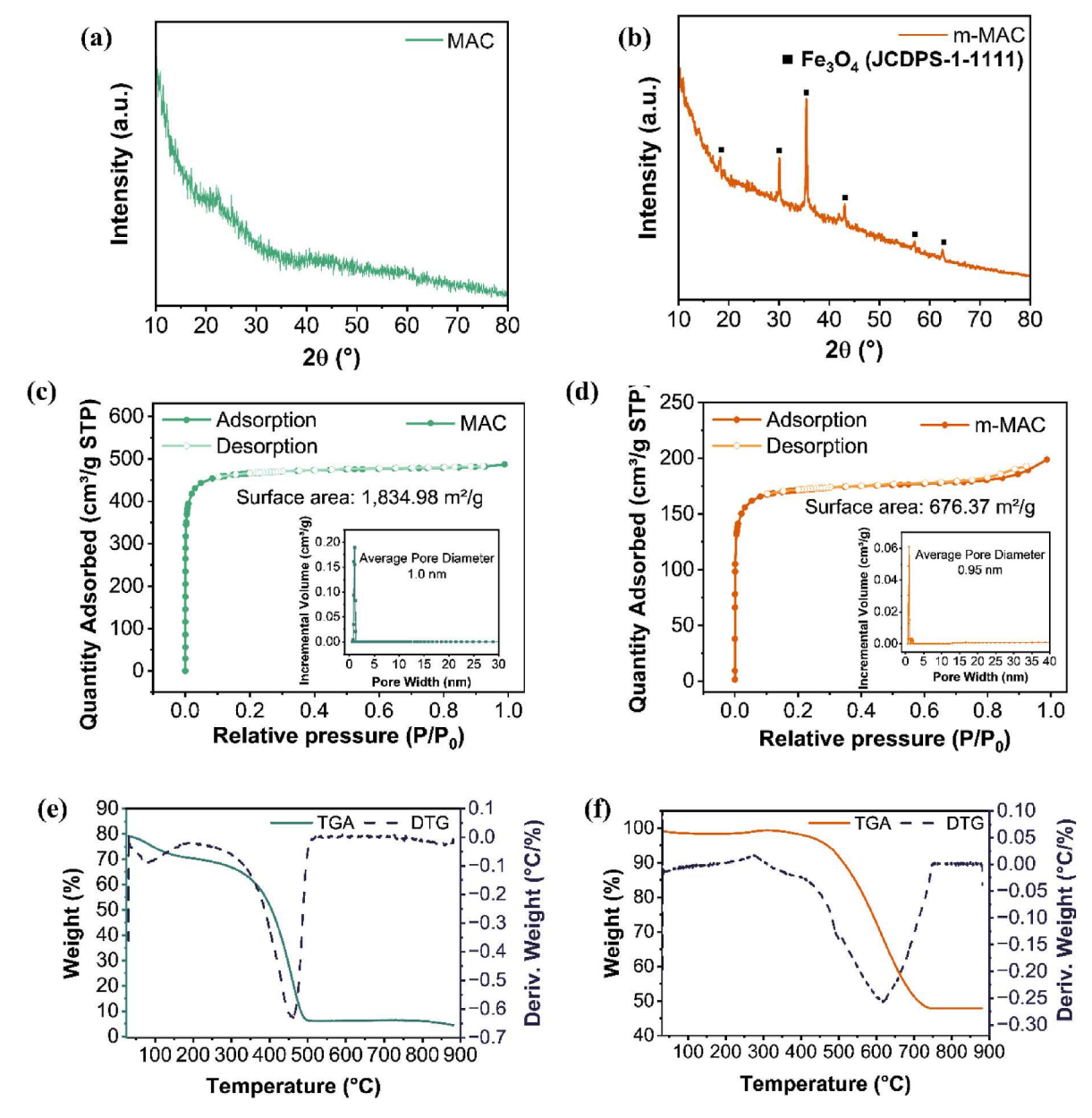


Fig. 3. PXRD diffractograms of MAC and m-MAC (a,b), N₂ sorption isotherm curves of MAC and m-MAC with inset showing the pore size distribution, average pore diameter, and specific surface area (c,d), TGA and DTG analysis of adsorbents showing thermal transitions and stability of the materials over the range of 100–900 °C (a,f).

nanoparticles (Rocha et al., 2020). This result is consistent with EDS analysis, which showed the presence of iron uniformly distributed throughout the material's structure. The surface areas of MAC and m-MAC were determined using N2 adsorption/desorption isotherms and calculated using the BET method (Fig. 3c and d). Both materials displayed type I(a) isotherms, often associated with microporous materials, with narrow micropores (Thommes et al., 2015). It is possible to observe for m-MAC, at high relative pressure, a slight deviation in the isotherm type with a small increase in the adsorbed quantities noted in lieu of the expected plateau. According to Khuong et al. (2022), this deviation may correspond to the presence of meso/macropores in the material. BET SSA value of MAC is $1834 \text{ m}^2/\text{g}$, while m-MAC presented a value of 676 m^2/g . The high surface area of the materials may be associated with the use of K₂CO₃ as a chemical activating agent, as it plays a crucial role in the formation of high pore volumes and, consequently, high surface areas (Heidarinejad et al., 2020; Okman et al., 2014; Zhang et al., 2016). The lower SSA value of m-MAC sorbent may be attributed to the presence of the iron oxide nanoparticles, as confirmed by the PRXD analysis. These nanoparticles are encapsulated in the carbon structure, which decreases the sites available for N_2 adsorption (Silva et al., 2020). The pore diameter distribution evaluated by NLDFT revealed an average pore diameter of 1.0 nm for MAC and 0.95 nm for m-MAC. This reflects the microporous nature of both materials and buttresses the type of BET isotherm observed (Thommes et al., 2015). In addition, it is possible to note the presence of small amounts of pores with a size greater than 15 nm for m-MAC. This is in agreement with the slight deviation of the type I(a) isotherm and ascribed to the presence of large pores.

The thermogravimetric analysis presented the thermal stability of the synthesized adsorbents (Fig. 3e and f). The TGA curve for MAC (Fig. 3e) presented two thermal degradation events. Initially, a mass loss of nearly 10% at 80 $^{\circ}\text{C}$ was shown, corresponding with loss of moisture and volatiles. A second weight loss was noted, with a maximum decomposition temperature of 460 $^{\circ}\text{C}$, and is related to carbon oxidation (Sudha et al., 2019). Lastly, a residue mass of 4.5% was observed which

can be attributed to the remaining potassium originating from the precursors (Liu et al., 2020). In contrast, a single weight-loss event assigned to carbon oxidation, with a maximum decomposition temperature of 614 °C is noted in the TGA curve for m-MAC (Fig. 3f), indicating higher thermal stability for this material. A slight increase in weight was also observed at 274 °C likely due to the oxidation of available iron particles (Chen et al., 2002). In addition, a residue mass of 48% is observed for m-MAC, attributed to the iron oxides present in the sample, as confirmed by EDS and PXRD analyses (Chen et al., 2002; Kumar et al., 2022).

XPS analysis was performed to evaluate the chemical composition of the surface of both materials. The survey spectra (Fig. 4a) showed peaks with binding energies associated with C 1s (284.5 eV), K2s (378.2 eV), and O 1s (533.3 eV). Moreover, a peak with binding energy attributed to Fe2p (710.8 eV) was observed for m-MAC. The C1s spectra that have

been deconvoluted for MAC and m-MAC (Fig. 4b–d), presented peaks at 284.4 eV, 285.0 eV, and 286.9 eV related to C]C, C–O/C–OH and C]O bonds, respectively (Chen et al., 2020). Furthermore, peaks at 293.1 eV and 296.1 eV, associated with K2s were also noted due to the use of potassium salts during the synthesis of the materials (Kim et al., 2021). The presence of potassium is consistent with the TGA results for MAC, which showed a residue mass of 4.5%. Given its composition, which includes C, O, and K, this residue is likely potassium oxide. The O 1s spectra also showed peaks at $\sim\!531.0$ eV and $\sim\!533.0$ eV, assigned to C]O and C–O bonds, respectively (Duarte et al., 2022; Jain et al., 2021). A peak centered at 535.0 eV was observed for MAC which can be attributed to COOH or sorbed $\rm H_2O$ on the surface, while a peak at 530.1 eV associated with O–Fe was noticed for m-MAC (Pereira et al., 2023). Finally, the deconvoluted high-resolution spectrum of Fe2p for m-MAC

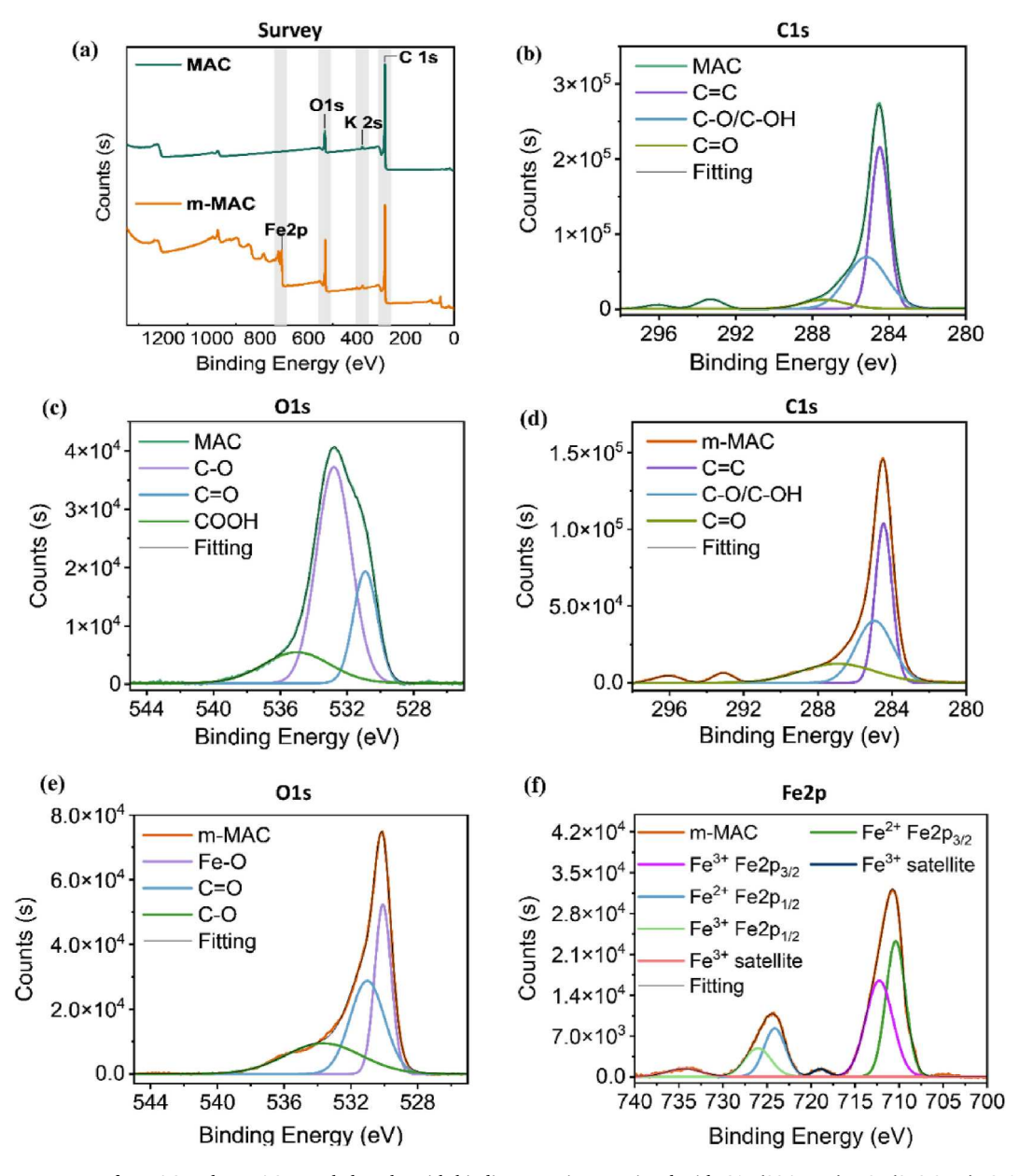


Fig. 4. (a) XPS survey spectra for MAC and m-MAC revealed peaks with binding energies associated with C1s (284.5 eV), K2s (378.2 eV), O 1s (533.3 eV), and (710.8 eV). (b) The deconvoluted high-resolution spectra of C1s for MAC presented peaks related to C]C, C-O/C-OH, and C]O bonds. (c) The deconvoluted high-resolution spectra of O1s for MAC showed peaks attributed to C]O and C-O bonds, and a peak associated with COOH bonds or adsorbed water on the surface of the material. (d) The deconvoluted high-resolution spectra of C1s for m-MAC presented peaks related to C]C, C-O/C-OH, and C]O bonds. (e) The deconvoluted high-resolution spectra of O1s for m-MAC showed peaks attributed to Fe-O, C]O, and C-O bonds. (f) The deconvoluted high-resolution spectra of Fe2p for m-MAC showed peaks assigned to Fe2p3/2, Fe2p1/2, and their respective satellite peaks, proving the presence of magnetite on the surface of the material.

(Fig. 4f) exhibited peaks centered at 710.4 eV, 712.2 eV, 718.9 eV, 724.1 eV, 726.0 eV, and 734.4 eV, related to $2p_{3/2}$ of Fe^{2+} and Fe^{3+} , Fe^{3+} $2p_{3/2}$ satellite, $2p_{1/2}$ of Fe^{2+} and Fe^{3+} , and Fe^{3+} $2p_{1/2}$ satellite, respectively (Guo et al., 2012; Pereira et al., 2023). This result confirms the formation of Fe_3O_4 species, consistent with the findings of EDS, PXRD, and TGA analyses, which have also demonstrated its presence in the material's structure.

3.2. Sorption kinetics and effect of contact time

Kinetics studies are essential to comprehend the sorption mechanism and the sorption rate owing to their dependence on contact time between sorbate and sorbent. These parameters can be inferred using timeconcentration data produced by the interaction of the sorbate and sorbent before reaching equilibrium (Adeola et al., 2021; Akpomie et al., 2022). The kinetic variables obtained by applying the models are reported in Table 1 and S1. It was revealed that caffeine adsorption is best suited to the PSO kinetic model, considering the lowest values of SSE, chi-square, and R^2 . Hence, the PSO model suggests that MAC and m-MAC interactions with caffeine may be facilitated by chemical adsorption, which also influences the adsorption rate and mechanism for caffeine removal from aqueous solutions. It can be observed by the correlation and error coefficients presented in Table 1 that the Weber-Morris diffusion model, which is used to explain the role of external and intraparticle diffusion within the pores of the porous materials, does not fit the respective sorbate-sorbent interactions. This is not surprising since mass-transfer processes in porous substances are inherently challenging due to diffusional and molecular effects (Gil et al., 2019; Rosli et al., 2019).

Fig. 5 displays multiple linearities depicting other sorptive processes contributing to the sorbent-sorbate interaction. As can be noticed, the boundary layer constant (C) is greater than zero for both MAC-Caffeine and m-MAC-Caffeine, and it is known that the larger the value of C, the more significant the effect of the solid-solution boundary thickness (Sahoo and Prelot, 2020). Thus, it implies that during the adsorption process, mechanisms other than film diffusion took place. The sorption process may have commenced with film diffusion between the adsorbent-solution interphase, followed by strong interactions, such as electrostatic and covalent bonding, between caffeine molecules and the sorbent's surface, as suggested by the PSO kinetic model (Adeola et al., 2021; Anthony et al., 2020; Iwuozor et al., 2022).

The steepness of the curve observed in the first 10 min of sorbate-sorbent interaction and the >60 % caffeine removal within 30 s reflects ultrafast initial adsorption due to the availability of binding sites,

Table 1Adsorption kinetic parameters for caffeine adsorption by MAC and m-MAC.

Adsorption kinetics	Parameters	Caffeine	
		MAC	m-MAC
First order	q_e (mg/g)	95.13	94.46
	K_1 (1/min)	0.05	7.51
	SSE	1.122	1.023
	χ^2	3051.78	1.26
	R^2	0.9317	0.9831
Second order	q_e (mg/g)	92.42	95.44
	K_2 (mg/g.min)	2.12	0.37
	h (mg/g.min)	19.2e03	3.30e03
	Half-life (t _{0.5})	4.96e-	28.6e-
		03	03
	SSE	1.057	1.017
	χ^2	23.56	1.07
	R^2	0.9925	0.9856
Weber-Morris intraparticle	K_{id} (mg/g.min ^{1/}	4.80	4.58
diffusion	2)		
	C	46.88	68.79
	SSE	6.568	6.777
	χ^2	3733.3	6282.6
	R^2	0.2543	0.5302

after which equilibrium and site saturation also occurred quickly (Fig. 5a and b). The MAC-Caffeine and m-MAC-Caffeine reached equilibrium after 20 min, adsorbing >96% which is relatively fast compared to other activated carbon materials obtained from other sources (Gil et al., 2019; Rosli et al., 2019). The initial rate constant (h) reveals a faster sorption rate for MAC than m-MAC (Table 1), which may be due to unbound electrons, higher surface area, and unaltered pore structures in the pristine MAC adsorbent. This is further supported by the PSO overall rate constant (K_2) which equally indicates a faster rate of chemisorption governing MAC-Caffeine interactions.

3.3. Sorption isotherm

Sorption isotherm models are used to explain the interactions between sorbate and sorbents at a constant temperature as the adsorption process reaches equilibrium. Among the various process factors, the sorption capacity of adsorbents is significantly influenced by the sorbate concentration (Perveen et al., 2022). Thus, mass transport between the contaminated aqueous phase and the solid phase comprised of adsorbents is primarily driven by the quantity or concentration of pollutants in the solution. The caffeine adsorption isotherms using the synthesized adsorbents are presented in Fig. 6a and b. The data obtained from the adsorption batch experiments were fitted with Freundlich, Langmuir, and Sips models, and the parameters are presented in Table 2.

The correlation and error coefficients served as indicators of the bestfit model for the sorbate-sorbent interactions. The Freundlich isotherms model has the highest R^2 values, and least chi-square and SSE values in comparison to Sips and Langmuir models, for MAC-Caffeine and m-MAC-Caffeine interactions respectively (Table 2). This suggests that the overarching mechanism of interaction between the synthesized material and the target pollutant is multilayer adsorption on a heterogeneous surface. Tannic acid, which contains aromatics, is the carbon source for the synthesis of MAC and m-MAC. Tannic acid also increases the possibility of several mechanisms of interaction, including hydrogen bonding and π - π attractions with the aromatic structure of caffeine which has two carbonyl groups and four tertiary amines. Inner-sphere surface complexes are formed as a result of electron sharing between pollutants and carbonaceous materials in π -complexation interactions. π -complexation or π - π interactions are also brought about by the overlap of π electrons between sorbate and aromatic-containing carbon-based materials (Adeola et al., 2023; Thakuria et al., 2019). The sorption maximal as predicted by Langmuir and Sips suggests that MAC has better caffeine removal capacity, approximately 394 and 296 mg/g (MAC) as opposed to 287 and 286 mg/g reported for m-MAC (Table 2). The BET sorption isotherm revealed a larger specific surface area and average pore diameter for the pristine MAC sample compared with m-MAC. This has a positive correlation with the binding capacity/maximum adsorption capacity of MAC and m-MAC. The larger the surface area and pore size, the better the adsorption capacity of the synthesized and functionalized materials. However, both materials showed very good caffeine removal efficiency >99%, with m-MAC's magnetic property providing an advantage for ease of recovery and regeneration for enhanced process sustainability.

3.4. Effect of solution pH

The solution pH is crucial to the adsorption process as it can alter not only the net surface charge of the materials but also the charge of the sorbate molecule, consequently affecting the adsorbent-adsorbate interactions (Kubheka et al., 2022; Wei et al., 2022). Hence, there is a need to investigate the role of pH in these processes, as the composition and character of aquatic systems have a direct impact on the pH of these systems (Bhateria and Jain, 2016). Therefore, the point of zero charge (pHpzc) for MAC and m-MAC was determined to understand the surface charge of the materials under variable solution pH. As can be seen in Fig. 6c and d, MAC and m-MAC presented pHpzc equal to 8 and 8.3,

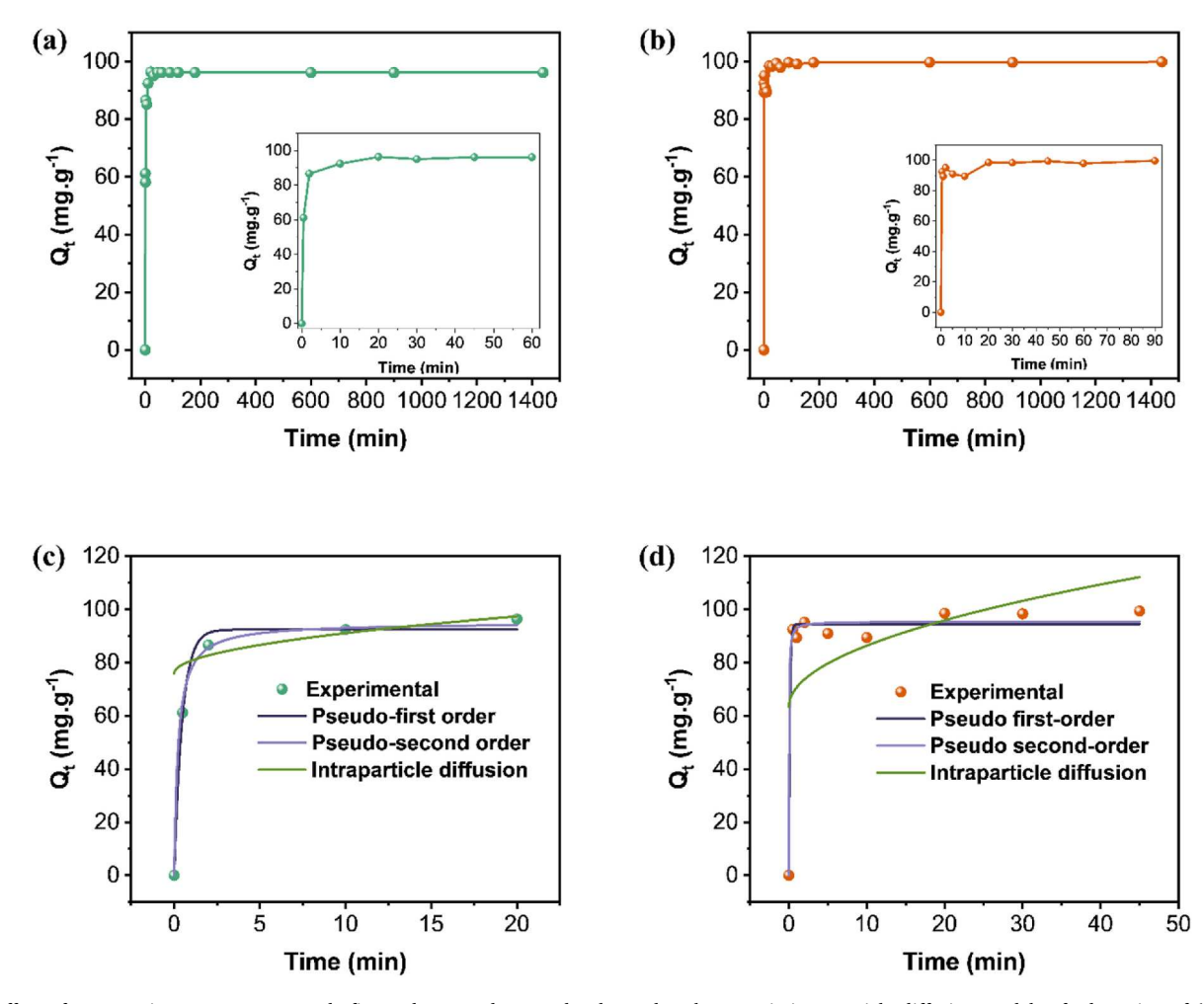


Fig. 5. Effect of contact time, Lagergren pseudo-first-order, pseudo-second-order and Weber-Morris intraparticle diffusion models of adsorption of (a, c) MAC-Caffeine and (b, d) m-MAC-Caffeine (process parameters: Co = 100 mg/L; dosage = 1 mg/mL; solution pH $= 5.8 \pm 0.2$; mixing rate = 300 rpm; $T = 25 \pm 1 \,^{\circ}\text{C}$).

respectively. This suggests that the surface charge was not significantly altered by the magnetic iron oxides, trapped within the heterostructure and/or sparingly on the surface of m-MAC. Based on the concept of PZC, the MAC and doped MAC materials are negatively charged when solution pH is above the pHpzc, and predominantly positively charged when the solution pH is below the pHpzc (da Silva Vasconcelos de Almeida et al., 2021). The pH effect on caffeine removal using the prepared adsorbents was investigated by altering the solutions' pH between 3 and 12 (Fig. 6e and f). The results obtained suggest that acidic pH relatively favors the adsorption of caffeine when compared to basic pH media, which can be associated with the enhanced role of hydrogen bonding between the sorbents and caffeine at a pH less than 7 (Sotelo et al., 2012). This is consistent with other reports where coconut-activated carbon (Couto et al., 2015), grape stalk-activated carbon (Portinho et al., 2017), and pine needles biochar (Anastopoulos et al., 2020) were utilized. A pH ranging from 5 to 7 can be regarded as optimal for caffeine removal from aqueous systems using MAC and m-MAC adsorbents, similar to graphene (Yang and Tang, 2016), modified clay (Cabrera-Lafaurie et al., 2012), carbon xerogels (Álvarez et al., 2015), active biochar from açai seed (da Silva Vasconcelos de Almeida et al., 2021) and peach stone activated carbon (Torrellas et al., 2015). Interestingly, although there appear to be slight variations in the amount adsorbed in basic and acidic mediums for MAC and m-MAC, these variations are insignificant offering no uniform trend. This may be partly attributed to the pka of caffeine, which is 14, meaning that it maintains the same molecular form throughout the pH scale (1-14), hence limiting the role of protonation/deprotonation and electrostatics on the part of the adsorbate. Xiong et al. [8] have earlier reported that electrostatic interactions may play a minor role in some adsorption processes. Therefore, it may be inferred that the impact of pH variations on the overall performance of MAC and m-MAC is not significant enough to warrant pH adjustments, hence adopting a neutral pH (often reported as the best for caffeine removal (Quintero-Jaramillo et al., 2021)), or working at the natural pH of caffeine in water (pH 5.8 \pm 0.2), will suffice. Overall, the amount adsorbed, Qe, regardless of solution pH shows a relatively higher performance for MAC over m-MAC.

3.5. Regeneration and reusability tests

MAC and m-MAC were regenerated via a facile approach of mild rinsing with DI water and acetone. The sorbents were filtered and washed using vacuum filtration and reused in five successive adsorption cycles. The adsorption caffeine efficiency of the MAC (98.4–90.5%) and m-MAC (93.7–88.6%) in the cycles of adsorption-regeneration are shown in Fig. 7. Irreversible pore deformation and changes in the thermodynamic state and morphology of the material due to regeneration cycles, as well as sorbate or solvent-induced alteration of the sorbent, are several factors that may be responsible for the slight decline in caffeine removal over several cycles. However, the regeneration and reusability test showed that MAC/m-MAC can be adopted for the treatment of caffeine-contaminated water for at least five cycles without a negligible decrease in removal performance. The regeneration test further revealed that m-MAC with its magnetic properties was easily recovered from solution and thus recorded a minimal loss in mass over

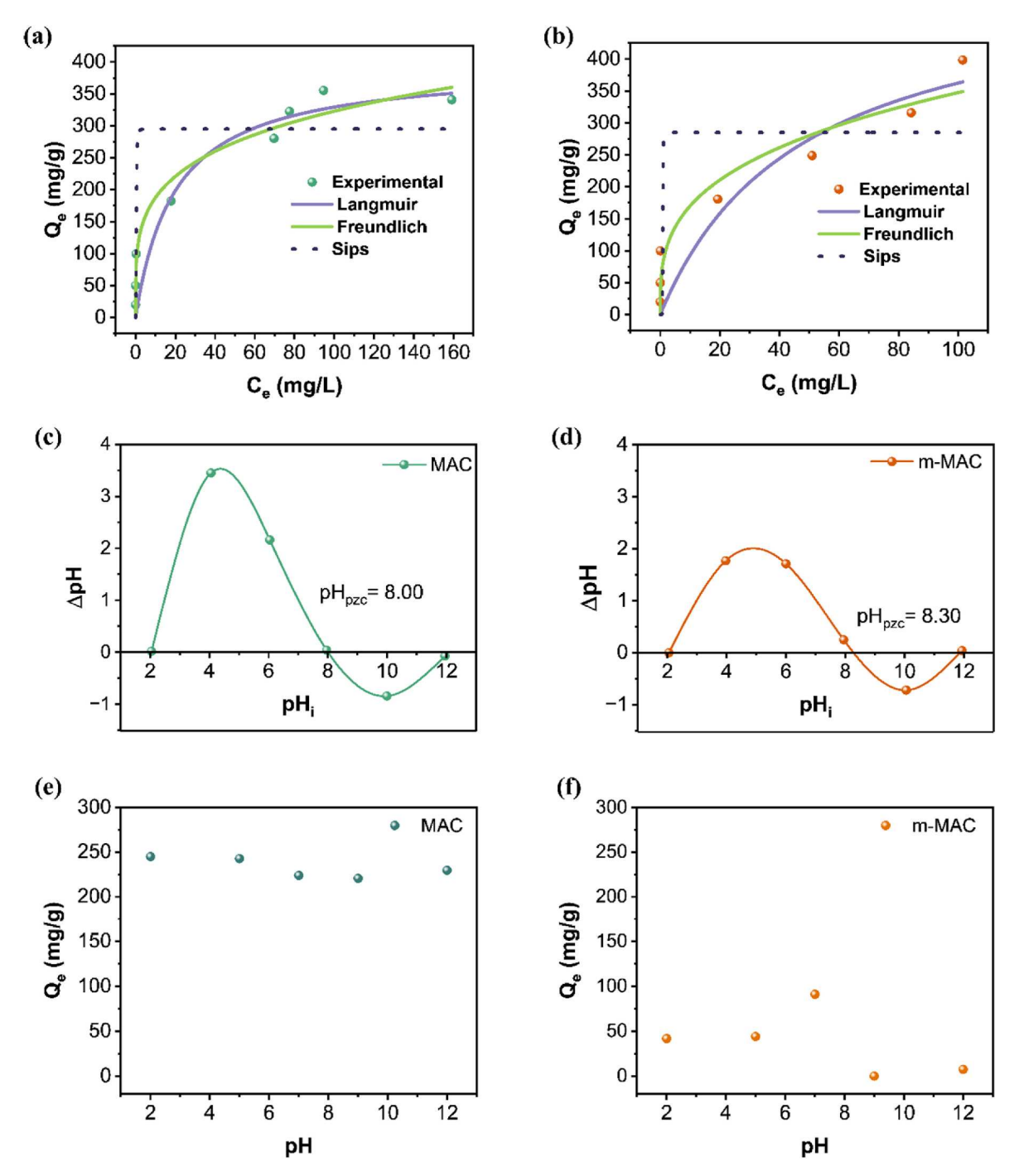


Fig. 6. (a, b) Adsorption isotherm and modeling for MAC-Caffeine and m-MAC-Caffeine [process parameters: Co = 20-500 mg/L; sorbent dosage Cont = 1 mg/mL, solution pH $Cont = 5.8 \pm 0.2$; mixing rate Cont = 300 rpm, Cont = 10 mg/L; dosage Cont = 10 mg/mL, solution pH C

several cycles. Sorbent recovery was more complex for MAC samples due to its dispersibility. In this case, vacuum filtration was the only viable route to recover the MAC solids. Furthermore, sorbent loss was slightly higher for MAC than m-MAC, which in contrast revealed negligible reduction in sorbent mass over five cycles. Acetone/water rinsing and drying under vacuum pressure replaced the need for solid-phase extraction and thermal regeneration that has been previously reported in the literature (Adeola and Forbes, 2019; Huang et al., 2022; Oesterle et al., 2020). This adds to process sustainability and minimizes regeneration costs.

4. Comparison of caffeine removal using biobased-based activated carbon (AC) adsorbents

The developmental strides in waste valorization and sustainable preparation of AC adsorbents with high SSA from agricultural waste and plant-derived materials are summarized in Table 3. The various adsorption characteristics such as the best-fit isotherm and kinetic models, maximum adsorption capacity, and optimum contact time are also included. In this study, BET results revealed the exceptionally high surface area of the MAC adsorbent synthesized from tannic acid, often commercially derived from Tara pods (*Caesalpinia spinosa*), gallnuts from *Rhus semialata*, *Quercus infectoria* or Sicilian sumac leaves (*Rhus*

Table 2Sorption isotherm models for caffeine by the MAC and m-MAC sorbents.

Isotherm models	Parameter	MAC	m-MAC
Freundlich	K_f	109.02	83.05
	N	4.24	3.22
	SSE	0.55	0.32
	χ^2	57.21	128.68
	R^2	0.9491	0.9040
Langmuir	$q_{\rm max}$ (mg/g)	394.08	287.26
	$K_L (L/mg)$	0.05	0.02
	SSE	2.79	0.14
	χ^2	7201.32	12,907.72
	R^2	0.8965	0.8657
Sips	K_s	15.09	5.83
	$q_m (mg/g)$	296.24	285.99
	m_s	0.34	0.06
	SSE	0.53	0.33
	χ^2	6486.48	3.11E+19
	R^2	0.8267	0.6743

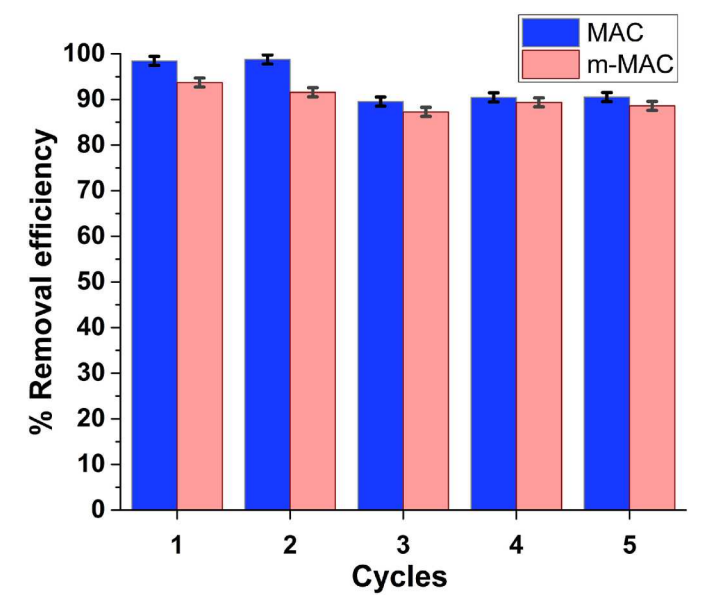


Fig. 7. Reusability test of MAC and m-MAC for aqueous decaffeination (experimental conditions: $25\,^{\circ}$ C; sorbent dosage: 20 mg; caffeine concentration: 500 mg/L, acetone/water volume: 10 mL (1:1), n = 2).

coriaria) (Huang et al., 2018). Our literature search revealed that pristine AC has been reported with high SSAs, ranging from ${\sim}400$ to 1500 m²/g with excellent morphological characteristics such as porosity, tunability, stability, and hydrophobicity, amongst others. The MAC adsorbent has a SSA value > 1800 m²/g with 100% adsorption efficiency for caffeine removal.

The adsorption capacity for caffeine ranges from \sim 2.5 to 500 mg/g in the literature with MAC/m-MAC, from this study, showing the highest maximum adsorption capacity, except for pine-AC. Furthermore, while it requires other sorbents between 40 min and 24 h for optimum adsorption to be attained, MAC and m-MAC reached their adsorption maxima in less than 20 min. Hence, ultrafast adsorption, large SSA, high adsorption capacity, and the added advantage of magnetic properties for ease of post-adsorption recovery, make MAC and m-MAC potentially more suitable for water treatment applications.

5. Conclusion

Microporous activated carbon (MAC) and its magnetic derivative (m-MAC) were prepared via a facile two-step process involving hydrothermal treatment and pyrolysis, for decaffeination of water. The characterization of both sorbents affirmed their porous surface with very high specific surface areas. Freundlich isotherm and pseudo-secondorder kinetics predicted the formation of multiple layers of caffeine over the surface of the adsorbents, and that the sorbate-sorbent interactions were mainly facilitated by chemisorption, and sorption equilibrium was reached very fast. While MAC and the magnetic derivative are differently impacted by variations in solution pH, this impact is not significant and adsorption at the natural pH of caffeine in water or neutral pH sufficed for effective removal of caffeine. Overall, MAC and m-MAC proved to be effective adsorbents for caffeine removal. The doping of MAC with FeONPs facilitated the convenient recovery of m-MAC with the aid of a magnetic field. The findings of the study suggest that the presence of other emerging organic contaminants in aqua systems may be remediated using these functionalized carbon-based materials. Future works may focus on the investigation of the competitive adsorption of organic pollutants (i.e., pharmaceuticals, pesticides, etc.) using the m-MAC composites, and the impact of natural organic matter on the performance of the biomass-derived material. This will provide further insight into the impact of the molecular structure of different organics on the sorption process, particularly in a complex mixture, similar to environmental samples and industrial effluents.

CRediT authorship contribution statement

Michelle P. Duarte: Writing - original draft, Software,

Table 3Summary of various agricultural waste-derived activated carbons as adsorbent for caffeine removal in aqueous media.

Activated carbon source	SSA (m ² /g)	Adsorption capacity (mg/g)	Isotherm model	Kinetic model	Contact time (min.)	References
Pine	945	500.0	Langmuir	PSO	240	Galhetas et al. (2014)
Biodiesel production waste	1165	296.3	Langmuir	PSO	240	Batista et al. (2016)
Coconut shells	755-980	186.9-212.3	Langmuir	PSO	120	Couto et al. (2015)
Pineapple leaves	1031	155.5	Langmuir	PSO	90	Beltrame et al. (2018)
Treated cork	750	153.4	_	PSO	1440	Mestre et al. (2014)
Kanlow switchgrass	1373	102.0	Langmuir	PSO	300	Oginni et al. (2019)
Sponge gourd	_	59.9	Langmuir	PSO	80	Anastopoulos and Pashalidis
						(2019)
Oil palm	408	13.0	Langmuir	PSO	300	Melo et al. (2020)
Water hyacinth	_	2.49	Langmuir	PSO	_	Emily Chelangat et al. (2016)
Coconut leaf	678.03	70.5–73.8	Redlich-	PSO	40	Oliveira et al. (2022)
			Peterson			
Argan Fruit Shells	1007	210.65	Langmuir	PSO	90	Bouhcain et al. (2022)
Tannic acid	1835	394.1	Freundlich	PSO	5	This study
Tannic acid and iron oxide nanoparticles	676	287.3	Freundlich	PSO	20	This study

Methodology, Investigation, Formal analysis, Data curation, Conceptualization. Adedapo O. Adeola: Writing – review & editing, Writing – original draft, Validation, Software, Project administration, Methodology, Investigation, Formal analysis, Data curation, Conceptualization. Gianluca Fuoco: Visualization, Methodology, Investigation, Formal analysis, Data curation. Tyler J. Jargaille: Methodology, Investigation. Rafik Naccache: Writing – review & editing, Visualization, Validation, Supervision, Project administration, Funding acquisition, Formal analysis.

Declaration of competing interest

The authors declare that they have no known competing financial interests or personal relationships that could have appeared to influence the work reported in this paper.

Data availability

Data will be made available on request.

Acknowledgment

The authors are grateful for the funding provided by the Natural Sciences and Engineering Research Council (NSERC) through the Discovery Grant Program, and Concordia University (Montreal, Canada) for funding through the Research Chair Program. MPD is grateful to Concordia University for the Concordia International Tuition Award of Excellence. XPS studies were performed at McGill University (MIAM Facilities in the Department of Mining and Materials Engineering) with the assistance of Dr. Lihong Shang. The authors are also grateful to Mr. Christopher Copeman and Ms. Clara Vieira for their assistance with the PXRD and N_2 adsorption and desorption analyses.

Appendix A. Supplementary data

Supplementary data to this article can be found online at https://doi.org/10.1016/j.envres.2024.119446.

References

- Adeola, A.O., de Lange, J., Forbes, P.B.C., 2021. Adsorption of antiretroviral drugs, efavirenz and nevirapine from aqueous solution by graphene wool: kinetic, equilibrium, thermodynamic and computational studies. Applied Surface Science Advances 6, 100157.
- Adeola, A.O., Duarte, M.P., Naccache, R., 2023. Microwave-assisted synthesis of carbon-based nanomaterials from biobased resources for water treatment applications: emerging trends and prospects. Frontiers in Carbon 2.
- Adeola, A.O., Forbes, P.B.C., 2019. Optimization of the sorption of selected polycyclic aromatic hydrocarbons by regenerable graphene wool. Water Sci. Technol. 80, 1931–1943.
- Adeola, A.O., Forbes, P.B.C., 2021. Antiretroviral drugs in African surface waters: prevalence, analysis, and potential remediation. Environ. Toxicol. Chem. n/a.
- Adinata, D., Wan Daud, W.M.A., Aroua, M.K., 2007. Preparation and characterization of activated carbon from palm shell by chemical activation with K2CO3. Bioresour. Technol. 98, 145–149.
- Akpomie, K.G., Conradie, J., Adegoke, K.A., Oyedotun, K.O., Ighalo, J.O., Amaku, J.F., et al., 2022. Adsorption mechanism and modeling of radionuclides and heavy metals onto ZnO nanoparticles: a review. Appl. Water Sci. 13, 20.
- Álvarez, S., Ribeiro, R.S., Gomes, H.T., Sotelo, J.L., García, J., 2015. Synthesis of carbon xerogels and their application in adsorption studies of caffeine and diclofenac as emerging contaminants. Chem. Eng. Res. Des. 95, 229–238.
- Anastopoulos, I., Katsouromalli, A., Pashalidis, I., 2020. Oxidized biochar obtained from pine needles as a novel adsorbent to remove caffeine from aqueous solutions. J. Mol. Liq. 304, 112661.
- Anastopoulos, I., Pashalidis, I., 2019. The application of oxidized carbon derived from Luffa cylindrica for caffeine removal. Equilibrium, thermodynamic, kinetic and mechanistic analysis. J. Mol. Liq. 296, 112078.
- Anthony, E.T., Ojemaye, M.O., Okoh, A.I., Okoh, O.O., 2020. Synthesis of CeO2 as promising adsorbent for the management of free-DNA harboring antibiotic resistance genes from tap-water. Chem. Eng. J. 401, 125562.
- Batista, M.K.S., Mestre, A.S., Matos, I., Fonseca, I.M., Carvalho, A.P., 2016. Biodiesel production waste as promising biomass precursor of reusable activated carbons for caffeine removal. RSC Adv. 6, 45419–45427.

- Beltrame, K.K., Cazetta, A.L., de Souza, P.S.C., Spessato, L., Silva, T.L., Almeida, V.C., 2018. Adsorption of caffeine on mesoporous activated carbon fibers prepared from pineapple plant leaves. Ecotoxicol. Environ. Saf. 147, 64–71.
- Bhateria, R., Jain, D., 2016. Water quality assessment of lake water: a review. Sustainable Water Resources Management 2, 161–173.
- Bouhcain, B., Carrillo-Peña, D., El Mansouri, F., Ez Zoubi, Y., Mateos, R., Morán, A., et al., 2022. Removal of emerging contaminants as diclofenac and caffeine using activated carbon obtained from argan fruit shells. Appl. Sci. 12, 2922.
- Bruton, T., Alboloushi, A., de la Garza, B., Kim, B.-O., Halden, R.U., 2010. Fate of caffeine in the environment and ecotoxicological considerations. Contaminants of emerging concern in the environment: ecological and human health considerations. Am. Chem. Soc. 1048, 257–273.
- Buerge, I.J., Poiger, T., Müller, M.D., Buser, H.-R., 2003. Caffeine, an anthropogenic marker for wastewater contamination of surface waters. Environ. Sci. Technol. 37, 691–700
- Cabrera-Lafaurie, W.A., Román, F.R., Hernández-Maldonado, A.J., 2012. Transition metal modified and partially calcined inorganic-organic pillared clays for the adsorption of salicylic acid, clofibric acid, carbamazepine, and caffeine from water. J. Colloid Interface Sci. 386, 381–391.
- Chen, X., Wang, X., Fang, D., 2020. A review on C1s XPS-spectra for some kinds of carbon materials. Fullerenes, Nanotub. Carbon Nanostruct. 28, 1048–1058.
- Chen, X.H., Chen, C.S., Chen, Q., Cheng, F.Q., Zhang, G., Chen, Z.Z., 2002. Non-destructive purification of multi-walled carbon nanotubes produced by catalyzed CVD. Mater. Lett. 57, 734–738.
- Couto, Jr OM., Matos, I., da Fonseca, I.M., Arroyo, P.A., da Silva, E.A., de Barros, M.A.S. D., 2015. Effect of solution pH and influence of water hardness on caffeine adsorption onto activated carbons. Can. J. Chem. Eng. 93, 68–77.
- da Silva Vasconcelos de Almeida, A., Vieira, W.T., Bispo, M.D., de Melo, S.F., da Silva, T. L., Balliano, T.L., et al., 2021. Caffeine removal using activated biochar from açaí seed (Euterpe oleracea Mart): experimental study and description of adsorbate properties using Density Functional Theory (DFT). J. Environ. Chem. Eng. 9, 104891.
- Díez, N., Ferrero, G.A., Sevilla, M., Fuertes, A.B., 2019. A sustainable approach to hierarchically porous carbons from tannic acid and their utilization in supercapacitive energy storage systems. J. Mater. Chem. A 7, 14280–14290.
- Díez, N., Fuertes, A.B., Sevilla, M., 2021. Molten salt strategies towards carbon materials for energy storage and conversion. Energy Storage Mater. 38, 50–69.
- Duarte, M.P., Silva, R.C.F., Medeiros, TPVd, Ardisson, J.D., Cotta, A.A.C., Naccache, R., et al., 2022. Carbon nanotubes derived from waste cooking oil for the removal of emerging contaminants. New J. Chem. 46, 11315–11328.
- Emily Chelangat, N., Francis, O., Lilechi Danstone, B., Victor Odhiambo, S., Selly Jemutai, K., 2016. Adsorption of caffeine and ciprofloxacin onto pyrolitically derived water hyacinth biochar: isothermal, kinetic and thermodynamic studies. Journal of Chemistry and Chemical Engineering 10.
- Galhetas, M., Mestre, A.S., Pinto, M.L., Gulyurtlu, I., Lopes, H., Carvalho, A.P., 2014. Chars from gasification of coal and pine activated with K2CO3: acetaminophen and caffeine adsorption from aqueous solutions. J. Colloid Interface Sci. 433, 94–103.
- Gardinali, P.R., Zhao, X., 2002. Trace determination of caffeine in surface water samples by liquid chromatography-atmospheric pressure chemical ionization-mass spectrometry (LC-APCI-MS). Environ. Int. 28, 521–528.
- Gil, A., Taoufik, N., García, A.M., Korili, S.A., 2019. Comparative removal of emerging contaminants from aqueous solution by adsorption on an activated carbon. Environ. Technol. 40, 3017–3030.
- Gogoi, A., Mazumder, P., Tyagi, V.K., Tushara Chaminda, G.G., An, A.K., Kumar, M., 2018. Occurrence and fate of emerging contaminants in water environment: a review. Groundwater for Sustainable Development 6, 169–180.
- Guo, J., Wang, R., Tjiu, W.W., Pan, J., Liu, T., 2012. Synthesis of Fe nanoparticles@graphene composites for environmental applications. J. Hazard Mater. 225–226, 63–73.
- Heberer, T., 2002. Tracking persistent pharmaceutical residues from municipal sewage to drinking water. J. Hydrol. 266, 175–189.
- Heidarinejad, Z., Dehghani, M.H., Heidari, M., Javedan, G., Ali, I., Sillanpää, M., 2020. Methods for preparation and activation of activated carbon: a review. Environ. Chem. Lett. 18, 393–415.
- Huang, F., Liu, W., Chen, S., Tian, Z., Wei, J., 2022. Thermal desorption characteristics of the adsorbate in activated carbon based on a two-dimensional heat and mass transfer model. Appl. Therm. Eng. 214, 118775.
- Huang, Q., Liu, X., Zhao, G., Hu, T., Wang, Y., 2018. Potential and challenges of tannins as an alternative to in-feed antibiotics for farm animal production. Animal Nutrition 4, 137–150.
- Inyinbor, A.A., Adekola, F.A., Olatunji, G.A., 2017. Liquid phase adsorptions of Rhodamine B dye onto raw and chitosan supported mesoporous adsorbents: isotherms and kinetics studies. Appl. Water Sci. 7, 2297–2307.
- Iwuozor, K.O., Akpomie, K.G., Conradie, J., Adegoke, K.A., Oyedotun, K.O., Ighalo, J.O., et al., 2022. Aqueous phase adsorption of aromatic organoarsenic compounds: a review. J. Water Proc. Eng. 49, 103059.
- Jain, A., Ghosh, M., Krajewski, M., Kurungot, S., Michalska, M., 2021. Biomass-derived activated carbon material from native European deciduous trees as an inexpensive and sustainable energy material for supercapacitor application. J. Energy Storage 34, 102178.
- Khuong, D.A., Trinh, K.T., Nakaoka, Y., Tsubota, T., Tashima, D., Nguyen, H.N., et al., 2022. The investigation of activated carbon by K2CO3 activation: micropores- and macropores-dominated structure. Chemosphere 299, 134365.
- Kılıç, M., Apaydın-Varol, E., Pütün, A.E., 2012. Preparation and surface characterization of activated carbons from Euphorbia rigida by chemical activation with ZnCl2, K2CO3, NaOH and H3PO4. Appl. Surf. Sci. 261, 247–254.

- Kim, J.H., Park, G.D., Kang, Y.C., 2021. Synthesis of yolk-shell-structured iron monosulfide-carbon microspheres and understanding of their conversion reaction for potassium-ion storage. Int. J. Energy Res. 45, 14910–14919.
- Kubheka, G., Adeola, A.O., Forbes, P.B.C., 2022. Hexadecylamine functionalised graphene quantum dots as suitable nano-adsorbents for phenanthrene removal from aqueous solution. RSC Adv. 12, 23922–23936.
- Kumar, A., Patra, C., Kumar, S., Narayanasamy, S., 2022. Effect of magnetization on the adsorptive removal of an emerging contaminant ciprofloxacin by magnetic acid activated carbon. Environ. Res. 206, 112604.
- Liu, X., Zhang, S., Wen, X., Chen, X., Wen, Y., Shi, X., et al., 2020. High yield conversion of biowaste coffee grounds into hierarchical porous carbon for superior capacitive energy storage. Sci. Rep. 10, 3518.
- Lobato-Peralta, D.R., Duque-Brito, E., Orugba, H.O., Arias, D.M., Cuentas-Gallegos, A.K., Okolie, J.A., et al., 2023. Sponge-like nanoporous activated carbon from corn husk as a sustainable and highly stable supercapacitor electrode for energy storage. Diam. Relat. Mater. 138, 110176.
- Márquez-Montesino, F., Torres-Figueredo, N., Lemus-Santana, A., Trejo, F., 2020.
 Activated carbon by potassium carbonate activation from pine sawdust (pinus montezumae lamb. Chem. Eng. Technol. 43, 1716–1725.
- Melo, L.L.A., Ide, A.H., Duarte, J.L.S., Zanta, C.L.P.S., Oliveira, L.M.T.M., Pimentel, W.R. O., et al., 2020. Caffeine removal using Elaeis guineensis activated carbon: adsorption and RSM studies. Environ. Sci. Pollut. Control Ser. 27, 27048–27060.
- Menya, E., Jjagwe, J., Kalibbala, H.M., Storz, H., Olupot, P.W., 2023. Progress in deployment of biomass-based activated carbon in point-of-use filters for removal of emerging contaminants from water: a review. Chem. Eng. Res. Des. 192, 412–440.
- Mestre, A.S., Pires, R.A., Aroso, I., Fernandes, E.M., Pinto, M.L., Reis, R.L., et al., 2014. Activated carbons prepared from industrial pre-treated cork: sustainable adsorbents for pharmaceutical compounds removal. Chem. Eng. J. 253, 408–417.
- Mozaffari Majd, M., Kordzadeh-Kermani, V., Ghalandari, V., Askari, A., Sillanpää, M., 2022. Adsorption isotherm models: a comprehensive and systematic review (2010–2020). Sci. Total Environ. 812, 151334.
- Mu, J., Li, Q., Kong, X., Wu, X., Sunarso, J., Zhao, Y., et al., 2019. Characterization of hierarchical porous carbons made from bean curd via K2CO3 activation as a supercapacitor electrode. Chemelectrochem 6, 4022–4030.
- Oesterle, P., Lindberg, R.H., Fick, J., Jansson, S., 2020. Extraction of active pharmaceutical ingredients from simulated spent activated carbonaceous adsorbents. Environ. Sci. Pollut. Res. Int. 27, 25572–25581.
- Oginni, O., Singh, K., Oporto, G., Dawson-Andoh, B., McDonald, L., Sabolsky, E., 2019. Effect of one-step and two-step H3PO4 activation on activated carbon characteristics. Bioresour. Technol. Rep. 8, 100307.
- Okman, I., Karagöz, S., Tay, T., Erdem, M., 2014. Activated carbons from grape seeds by chemical activation with potassium carbonate and potassium hydroxide. Appl. Surf. Sci. 293, 138–142.
- Oliveira, E.N., Meneses, A.T., de Melo, S.F., Dias, F.M.R., Perazzini, M.T.B., Perazzini, H., et al., 2022. Highly effective adsorption of caffeine by a novel activated carbon prepared from coconut leaf. Environ. Sci. Pollut. Control Ser. 29, 50661–50674.
- Pereira, D., Gil, M.V., Esteves, V.I., Silva, N.J.O., Otero, M., Calisto, V., 2023. Ex-situ magnetic activated carbon for the adsorption of three pharmaceuticals with distinct physicochemical properties from real wastewater. J. Hazard Mater. 443, 130258.
- Perveen, S., Nadeem, R., Nosheen, F., Asjad, M.I., Awrejcewicz, J., Anwar, T., 2022. Biochar-mediated zirconium ferrite nanocomposites for tartrazine dye removal from textile wastewater. Nanomaterials 12.
- Petrie, B., Barden, R., Kasprzyk-Hordern, B., 2015. A review on emerging contaminants in wastewaters and the environment: current knowledge, understudied areas and recommendations for future monitoring. Water Res. 72, 3–27.
- Philip, J.M., Aravind, U.K., Aravindakumar, C.T., 2018. Emerging contaminants in Indian environmental matrices a review. Chemosphere 190, 307–326.
- Portinho, R., Zanella, O., Féris, L.A., 2017. Grape stalk application for caffeine removal through adsorption. J. Environ. Manag. 202, 178–187.

- Quintero-Jaramillo, J.A., Carrero-Mantilla, J.I., Sanabria-González, N.R., 2021. A review of caffeine adsorption studies onto various types of adsorbents. Sci. World J. 2021, 9998924.
- Richardson, S.D., Kimura, S.Y., 2017. Emerging environmental contaminants: challenges facing our next generation and potential engineering solutions. Environ. Technol. Innovat. 8, 40–56.
- Rocha, L.S., Pereira, D., Sousa, É., Otero, M., Esteves, V.I., Calisto, V., 2020. Recent advances on the development and application of magnetic activated carbon and char for the removal of pharmaceutical compounds from waters: a review. Sci. Total Environ. 718, 137272.
- Rosli, M.A., Daud, Z., Ridzuan, M.B., Abd Aziz, N.A., Awang, H.B., Oyekanmi Adeleke, A., et al., 2019. Equilibrium isotherm and kinetic study of the adsorption of organic pollutants of leachate by using micro peat-activated carbon composite media. Desalination Water Treat. 160, 185–192.
- Sahoo, T.R., Prelot, B., 2020. Chapter 7 adsorption processes for the removal of contaminants from wastewater: the perspective role of nanomaterials and nanotechnology. In: Bonelli, B., Freyria, F.S., Rossetti, I., Sethi, R. (Eds.), Nanomaterials for the Detection and Removal of Wastewater Pollutants. Elsevier, pp. 161-222.
- Sambo, GsN., Adeola, A.O., Muhammad, S.A., 2024. Oil palm waste-derived adsorbents for the sequestration of selected polycyclic aromatic hydrocarbon in contaminated aqueous medium. Appl. Water Sci. 14, 113.
- Silva, R.C.F., Ardisson, J.D., Cotta, A.A.C., Araujo, M.H., Teixeira, APdC., 2020. Use of iron mining tailings from dams for carbon nanotubes synthesis in fluidized bed for 17α-ethinylestradiol removal. Environ. Pollut. 260, 114099.
- Sotelo, J.L., Rodríguez, A.R., Mateos, M.M., Hernández, S.D., Torrellas, S.A., Rodríguez, J.G., 2012. Adsorption of pharmaceutical compounds and an endocrine disruptor from aqueous solutions by carbon materials. Journal of Environmental Science and Health, Part B 47, 640–652.
- Sudha, V., Senthil Kumar, S.M., Thangamuthu, R., 2019. Hierarchical porous carbon derived from waste amla for the simultaneous electrochemical sensing of multiple biomolecules. Colloids Surf. B Biointerfaces 177, 529–540.
- Thakuria, R., Nath, N.K., Saha, B.K., 2019. The nature and applications of π - π interactions: a perspective. Cryst. Growth Des. 19, 523–528.
- Thommes, M., Kaneko, K., Neimark, A.V., Olivier, J.P., Rodriguez-Reinoso, F., Rouquerol, J., et al., 2015. Physisorption of gases, with special reference to the evaluation of surface area and pore size distribution (IUPAC Technical Report). Pure Appl. Chem. 87, 1051–1069.
- Torrellas, S.Á., García Lovera, R., Escalona, N., Sepúlveda, C., Sotelo, J.L., García, J., 2015. Chemical-activated carbons from peach stones for the adsorption of emerging contaminants in aqueous solutions. Chem. Eng. J. 279, 788–798.
- Tyagi, U., 2024. Sustainable and low-cost biomass derived adsorbents for the removal of toxic contaminants from wastewater: approaches and future perspective. Waste Management Bulletin.
- Unuabonah, E.I., Omorogie, M.O., Oladoja, N.A., 2019. 5 modeling in adsorption: fundamentals and applications. In: Kyzas, G.Z., Mitropoulos, A.C. (Eds.), Composite Nanoadsorbents. Elsevier, pp. 85–118.
- Wei, F., Zhu, Y., He, T., Zhu, S., Wang, T., Yao, C., et al., 2022. Insights into the pH-dependent adsorption behavior of ionic dyes on phosphoric acid-activated biochar. ACS Omega 7, 46288–46302.
- Wu, W., Wu, C., Zhang, G., Liu, J., Li, Y., Li, G., 2023. Synthesis and characterization of magnetic K2CO3-activated carbon produced from bamboo shoot for the adsorption of Rhodamine b and CO2 capture. Fuel 332, 126107.
- Yang, G.C.C., Tang, P.-L., 2016. Removal of phthalates and pharmaceuticals from municipal wastewater by graphene adsorption process. Water Sci. Technol. 73, 2268–2274.
- Zhang, S., Tao, L., Zhang, Y., Wang, Z., Gou, G., Jiang, M., et al., 2016. The role and mechanism of K2CO3 and Fe3O4 in the preparation of magnetic peanut shell based activated carbon. Powder Technol. 295, 152–160.





pubs.acs.org/acssrm Article

Experimental, Machine-Learning, and Computational Studies of the Sequestration of Pharmaceutical Mixtures Using Lignin-Derived Magnetic Activated Carbon

Adedapo O. Adeola,* Gianluca Fuoco, Kayode A. Adegoke, Oluwatobi Adeleke, Abel K. Oyebamiji, Luis Paramo, and Rafik Naccache*



Cite This: ACS Sustainable Resour. Manage. 2025, 2, 219-230



ACCESS I

Metrics & More

Article Recommendations

s Supporting Information

ABSTRACT: Pharmaceutical pollutants pose significant risks to human health and aquatic ecosystems. This study investigates lignin-derived magnetic carbon composite (L-MAC) for removing atenolol (ATN), carbamazepine (CBZ), diclofenac (DCF), and sulfamethoxazole (SMZ) from aqueous media. Characterization of L-MAC's physicochemical properties, along with isotherm and kinetic studies, revealed that the Langmuir and pseudo-second-order models best describe sorbent—sorbate interactions, with maximum adsorption capacities ranging from 11.30 to 27.97 mg/g. The adsorption efficiency followed the order ATN < SMZ < CBZ < DCF, achieving over 99% removal under optimal conditions of 1–4 h contact time and pH 2–7. Strong π – π interactions, hydrogen bonding, and chemisorption contributed to sorption irreversibility. Artificial intelligence models predicted a material performance with high accuracy. The adaptive neuro-fuzzy inference system model outperformed others, achieving error coefficients of 5.745, 3.125, and 11.085 during training and 6.123, 4.974, and 12.456 during testing. Density functional theory analysis examined reactivity and binding strength using



descriptors like HOMO-LUMO energy gaps. DCF showed the highest electron-donor capacity, followed by CBZ, ATN, and SMZ, confirming L-MAC's high efficacy in removing pharmaceuticals. This study demonstrates L-MAC's robustness for the adsorptive removal of contaminant mixtures.

KEYWORDS: adsorption, density functional theory, lignin-derived magnetic carbon composite, pharmaceutical mixtures, machine learning

1. INTRODUCTION

Recent environmental awareness and pollution concerns have driven the search for sustainable resources to create ecofriendly materials for environmental reclamation. Water pollution poses a significant global threat, harming ecosystems and human health by spreading diseases and disrupting food chains. Research in continents like the Americas, Europe, and Asia identifies pharmaceutical compounds as major contributors to this issue. 1,2 Specifically, atenolol (ATN), carbamazepine (CBZ), diclofenac (DCF), and sulfamethoxazole (SMZ) are among the molecules most commonly found in aquatic systems.³⁻⁷ ATN is a β -blocker medication commonly prescribed for conditions such as angina, high blood pressure (hypertension), and heart rhythm irregularities.8 Approximately 90% of the administered ATN dose remains unmetabolized in the human body and is excreted unchanged via urine. Consequently, it has been frequently identified in wastewater and hospital sewage, with concentrations ranging from approximately 0.78 to 6.6 μ g/L. On the other hand, CBZ is categorized as an endocrine-disrupting chemical, utilized as an antiepileptic medication.^{7,10} It has a tricyclic dibenzazepine structure comprising two fused benzene rings and an azepine group, which poses risks to human health, even

in trace amounts in aquatic systems. 11 DCF belongs to the class of nonsteroidal antiinflammatory drugs and is frequently recommended as a pain-relieving medication and for treatment of various conditions such as dysmenorrhea and inflammatory disorders. 12 Prolonged exposure to DCF has detrimental effects on aquatic organisms, while in humans, it can induce thyroid tumors and hemodynamic alterations. 13 Furthermore, the sulfonamide antibiotic SMZ, selected for this study, has been widely used to combat livestock diseases. It is often excreted unchanged into the environment, 14 which is a common feature of the compounds selected for this study. SMZ has a half-life of 85-100 days in the environment and has been associated with hepatic cancer, as well as genetic alterations. 15 Given the widespread prescription and usage of ATN, CBZ, DCF, and SMZ, they have been detected globally in both wastewater and natural water sources, such as surface,

Received: November 1, 2024
Revised: December 30, 2024
Accepted: December 31, 2024
Published: January 8, 2025





ground, and even drinking water. ¹⁶ Thus, their effective removal is imperative due to their environmental persistence and health risks.

Current sorbent technologies utilize materials comprising petrochemical-based products, organometallic nanocomposite, 17 polymeric composite, 18 and advanced carbon nanomaterials like carbon nanotubes and graphene. 19,20 Raw materials polymeric adsorbents could cost as much as US\$259 per gram,²¹ and the manufacturing cost of advanced carbon nanomaterials such as graphene and carbon nanotubes could range from US\$700 to 1000 per gram as of 2022.²² In addition to high costs, these materials pose challenges related to sustainability and toxicity. Biomass utilization, as a precursor for carbon material production, has garnered significant attention due to its widespread availability and abundance compared to conventional petroleum-derived materials, known for their pollution, toxicity, and nonbiodegradability.²³ There is an increasing focus on using plant biomass as a key material, drawing interest from industries seeking cost-effective biobased products from renewable sources.²⁴ As a result, converting biomass into activated carbon has become a key area of research with significant potential and an estimated cost of less than US\$1 per gram as of 2022. 25-27 Lignin comprises a very high content of aromatics, which offer diverse interaction mechanisms, including hydrogen bonding, electrostatic interactions, van der Waals forces, and $\pi - \pi$ stacking.²⁸ The incorporation of magnetic properties into lignin enhances their regenerability and reusability, significantly lowering the costs associated with the disposal of spent adsorbents.²⁹ Additionally, many studies focus on single pollutants, limiting our understanding of interactions and competitive adsorption among different pharmaceuticals in water.

To address these challenges, recent advancements in machine-learning and molecular simulations via density functional theory (DFT) present a promising approach. Unlike empirical models, which often struggle to predict outcomes and link operating conditions to adsorption capacity, machine learning offers a reliable approach to bridge knowledge gaps in adsorption processes. To overcome the empirical pitfalls, it is desirable to model and comprehend how pharmaceutical contaminants bind to agro-derived carbon materials using artificial intelligence (AI) and DFT techniques. By the use of high-quality machine-learning models and DFT techniques, the complexity, number of experiments, and reaction times required to predict the efficiency of adsorption processes can be significantly reduced. Furthermore, it can be used to demonstrate a mathematical relationship, specifically a nonlinear connection between dependent and independent input variables.30

Herein, we synthesized lignin-based magnetic activated carbon (L-MAC) via a facile one-step pyrolytic process and evaluated the influence of process conditions such as the initial pollutant concentrations and solution pH for optimal ATN, CBZ, DCF, and SMX sorption. The sorbent was characterized using X-ray photoelectron spectroscopy (XPS), X-ray diffraction, scanning electron microscopy, energy-dispersive X-ray spectroscopy, and Brunauer–Emmett–Teller analysis, among others. Moreover, process interactions were modeled and optimized by using DFT and AI techniques. In addition, the study investigated the preferential adsorption of four model ubiquitous pharmaceuticals in relation to the chemistry of the compounds and sorbent characteristics. To the best of our knowledge, the combination of experimental studies with AI

and computational modeling has not been reported previously for the magnetic carbon capture of pharmaceutical mixtures in aqueous systems.

2. MATERIALS AND METHODS

2.1. Materials. Softwood lignin was acquired from Laboratoire Des Technologies De La Biomass, Centre de mise à l'échelle (CME), 3000 boul. de l'université (P3 pavillon), Sherbrooke, Québec, Canada. Softwood comprises cellulose, hemicellulose, and lignin as the primary components. The technique for extracting lignin involves the breakdown of cellulose and hemicelluloses. Atenolol (ATN, 98% purity), carbamazepine (CBZ, 98% purity), diclofenac (DCF, 98% purity), sulfamethoxazole (SMZ, 98% purity), iron(III) acetylacetonate (Fe(acac)₃, 97% purity), hydrochloric acid (HCl, 96% purity), sodium hydroxide (NaOH, 98% purity), calcium chloride (CaCl₂, 97% purity), and methanol (99% purity) were purchased from Sigma-Aldrich. The 0.45 μm syringe PTFE filters utilized in the study were purchased from ChemScience. Ultrapure water from Milli-Q Water Systems (Sigma-Aldrich) was used in this study.

2.2. One-Pot Synthesis of Lignin-Based Magnetic Activated Carbon (L-MAC). L-MAC was synthesized using a previously established method with minor modifications. ²⁰ Briefly, lignin powder (0.5 g) and $\text{Fe}(\text{acac})_3$ (0.5 g) were homogenized, transferred into an alumina boat, and placed in a tube furnace (Figure S1). Pyrolysis was conducted in a nitrogen (N_2) environment at a flow rate of 100 mL/min, with a temperature ramp to $600 \, ^{\circ}\text{C}$ at a rate of $5 \, ^{\circ}\text{C/min}$. The sample was maintained at this temperature for 1 h. Subsequently, the product was cooled to ambient temperature and stored in screwcapped scintillation vials for both analytical characterization and various sorption experiments.

2.3. Material Characterization. X-ray diffraction (XRD) patterns were obtained using a Rigaku MiniFlex 6G diffractometer with a Cu K α source (λ = 1.54 Å), scanning within the 2 θ range of 10-80° at a rate of 10°/min.31 Fourier transform infrared spectra were acquired over the wavenumber range of 400-4000 cm⁻¹ using a Thermo Scientific Nicolet iS5 equipped with an iD5 ATR accessory and *Omnic* 9 software.³² Scanning electron microscopy (SEM) and energy-dispersive X-ray spectroscopy (EDS) analyses were performed at 5 kV using a Phenom ProX desktop G6 (ThermoFisher Scientific).³³ Thermogravimetric analysis (TGA) was conducted using a TGA Q500 analyzer with the temperature ramped from 25 to 900 °C at a rate of 10 °C/min under an oxidant flow of 50 mL/ min. The specific surface area (SSA) and pore-size distribution were analyzed using N2 adsorption/desorption isotherms at 77 K on a Micromeritics TriStar II Plus instrument, after sample activation for 24 h at 100 °C. The SSA was calculated using the Brunauer-Emmett-Teller (BET) method, while the pore-size distribution was determined by the nonlocal density functional theory (NLDFT) method.³⁴ The point of zero charge (pH_{PZC}) for L-MAC was determined by the addition of 15 mL of a 0.1 M NaCl solution to several vials and adjustment of the pH between 2 and 12 with 0.1 M NaOH or HCl. Subsequently, each vial received 10 mg of L-MACl and was mixed for 48 h with a rotating shaker, followed by filtration and pH measurement (AB150, Accumet, Fisher Scientific). The pH_{PZC} was determined by plotting ΔpH (pH_{final} – $pH_{initial}$) versus pH_{initial}.

2.4. Adsorption Kinetics and Isotherm Studies. L-MAC was evaluated for the adsorption of pharmaceutical mixtures (ATN, CBZ, DCF, and SMZ) in 40 mL screw-capped polypropylene vials with 0.01 mol/L CaCl₂ as the electrolyte at 25 °C. The sorption kinetics and contact time studies were carried out with 20 mg of L-MAC interacting with 50 mg/L of the combined pollutants. Using a Thermo Scientific 2314 multipurpose lab rotator, the reaction vessels were shaken for 24 h at 300 rpm. The initial doses of the mixture of contaminants for the adsorption isotherm study varied from 10 to 80 mg/L. Beyond the minimum contact time determined by kinetic studies, the vials were shaken for 12 h to facilitate complete equilibration. Following equilibration, the residual amount of

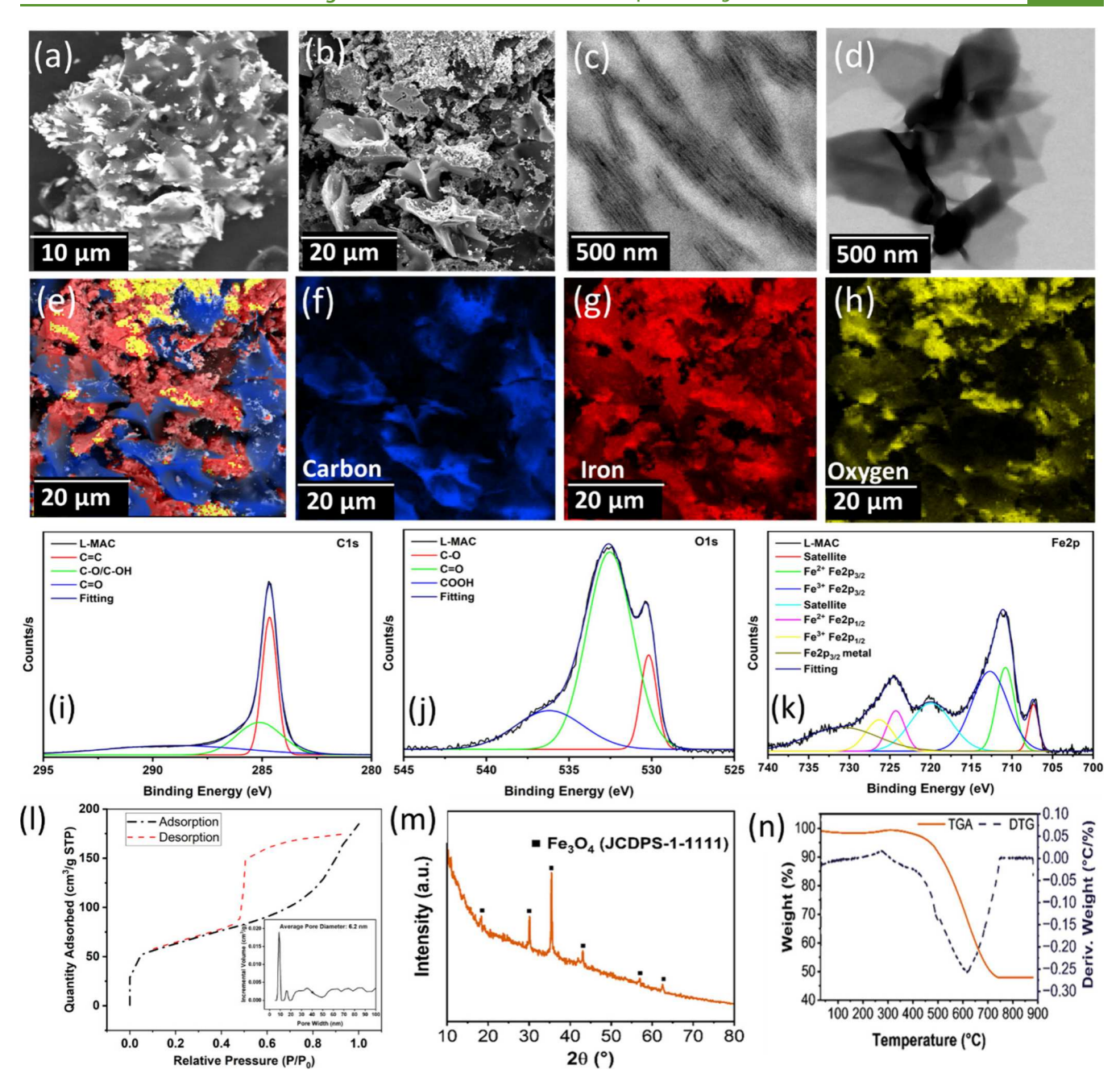


Figure 1. (a and b) SEM images of L-MAC at 10 and 20 μ m magnification. (c and d) TEM images highlight the magnetic iron oxide particles grafted onto the sheet. (e–h) SEM–EDS mapping reveals the distribution of carbon (blue), oxygen (yellow), and iron (red) in L-MAC. (i–k) XPS spectra showing peaks corresponding to the binding energies of C 1s (284.5 eV), O 1s (533.3 eV), and Fe 2p (711.8 eV) and satellite peaks confirming the presence of magnetic iron species. (l) BET plot of L-MAC showing sorption hysteresis, with the inset highlighting the pore-size distribution and average pore diameter. (m) Powder XRD diffractogram of L-MAC. (n) TGA and dynamic thermal gravimetry analysis of L-MAC demonstrating thermal transitions and stability over the 100–900 °C temperature range.

pollutants in the solutions was measured by filtering the solution and analyzing the supernatants.

2.5. High-Performance Liquid Chromatography (HPLC)/UV Analysis. Adsorption and desorption analysis of each pollutant was carried out using HPLC. Separation of each compound was achieved using an Agilent Technologies, Inc. 1200 series high-performance liquid chromatograph equipped with an ACE C18 column (5 μ m particle size, 150 mm length × 4.6 mm internal diameter). Separation was achieved through an isocratic elution method using 70% HPLC-grade water (0.1% TFA, solvent A) and 30% HPLC-grade acetonitrile (solvent B). A flow rate of 1 mL/min was used for each run followed by a total run time of 27 min. Each injection was performed with the help of an autosampler set to inject 10 μ L every run; each standard

and sample was analyzed in duplicate (n=2). The system was equipped with a diode-array detector, and peaks were separated and analyzed through their respective absorptions at 220 nm. Calibration curves were generated from stock solutions of the pharmaceutical mixture, yielding a regression coefficient $(R^2) > 0.98$. The working standards ranged from 0 to 1000 mg/L, equilibrium concentrations (C_e) were determined using the curve equation, and the amount adsorbed was calculated using the following mass-balance equations:

removal efficiency (%) =
$$\frac{C_0 - C_e}{C_0} \times 100$$
 (1)

$$q_{\rm e} = \frac{C_0 - C_{\rm e}}{m} \tag{2}$$

where C_0 (mg/L) is the initial concentration of each pharmaceutical compound, C_e (mg/L) is the equilibrium solute concentration, V_0 is the initial volume (L), and m is the mass (g) of L-MAC.

2.6. Machine-Learning Model. *2.6.1. Artificial Neural Network (ANN).* ANNs are soft computing cornerstones of machine learning and AI that can recognize patterns, learn from experimental/raw data, and make decisions/predict results. ANN draws inspiration from the brain and nervous system, as seen in Figure S2. These networks simulate a biological neural network, although they employ a limited set of principles derived from biological brain systems. These algorithms are designed to recognize patterns in data and make predictions or decisions based on those patterns. The output error of the network is calculated and used to update the weights through the backpropagation process. This cycle is repeated several times to improve the network's performance and minimize errors. Mathematically, the structure of the neural network can be simplified as illustrated in eq 3.

$$y(t) = F \left[\sum_{i=0}^{m} w_i(t) \ x_i(t) + b \right]$$
 (3)

where $w_i(t)$ is the weight value in discrete time t, b is the bias, and F is the transfer function.

2.6.2. Adaptive Neuro-Fuzzy Inference System (ANFIS). ANFIS is a hybrid soft computing method that provides accelerated learning and interpretation capabilities to model complex patterns and draw correlations between nonlinear relationships in experimental data. ANFIS integrates the numerical advantages of ANNs with the linguistic elements of fuzzy logic (Figures S3 and S4). By addressing the limitations of traditional fuzzy control while preserving its benefits, ANFIS creates a fuzzy control system that offers enhanced accuracy and faster response times³⁶ In the ANFIS modeling approach, the input and output components of the Takagi—Sugeno fuzzy inference system are connected through fuzzy rules.³⁷ See the Supporting Information for details (section 1.1).

2.6.3. Model Training and Development. This section presents the training and development of the ANN and ANFIS models for the adsorption rate prediction. To make accurate predictions with these models, the approach involves data preprocessing, network architecture design, and optimization. Furthermore, to verify model efficacy, hyperparameter selection and performance evaluation are prioritized. The data needed for the neuro-fuzzy modeling was extracted from the experimental procedure using the operational variables on the adsorption of pharmaceutical mixtures (ATN, CBZ, DCF, and SMZ). To prepare the data for the model, preprocessing (normalization) was carried out to ensure that the training data were standardized to a uniform scale, thereby reducing the influence of features with larger magnitudes and facilitating more efficient training convergence. In this study, the neural network inputs consist of the following operation parameters, namely, effects of the initial concentration, contact time, and solution pH. The output is referred to as the adsorption (i.e., adsorption capacity). The input and output values have been normalized within the range of 0 and 1 using eq 4.

$$x_{\text{norm}} = \frac{x - x_{\text{min}}}{x_{\text{max}} - x_{\text{min}}} \tag{4}$$

where x_{norm} is the normalized variable and x is the mean of the variables. x_{max} and x_{min} are the maximum and the minimum variables, respectively. The architectural structure of the neural network model in this study is depicted in Figure S3. See the Supporting Information for details (section 1.2). Common statistical metrics were utilized to evaluate the model's accuracy and robustness. These are the mean absolute deviation (MAD), mean absolute percent error (MAPE), root mean square error (RMSE), and R, which were employed and computed using eqs 5–8.

$$RMSE = \sqrt{\frac{\sum_{k=1}^{N} [y_k - \widehat{y_k}]}{N}}$$
 (5)

$$MAD = \frac{1}{N} \sum_{k=1}^{N} |y_k - \overline{y}|$$
(6)

MAPE =
$$\frac{1}{N} \sum_{k=1}^{N} \left| \frac{y_k - \widehat{y_k}}{y_k} \right| \times 100\%$$
 (7)

$$R = \frac{\sum_{k=1}^{N} (\widehat{y_k} - y_k)}{\sqrt{\sum_{k=1}^{N} \widehat{y_k}^2}}$$
(8)

2.7. DFT Studies. The two-dimensional structures of the studied pharmaceutical mixtures (ATN, CBZ, DCF, and SMZ) were modeled using the *ChemDraw* 22.2.0.3300 version, ³⁸ and the modeled structures were converted to 3D using *Spartan* '14 software before subjecting it to optimization. The optimization was executed via 6-31G* as the basis set using the DFT method. The compounds were optimized in a vacuum at neutral total charge and zero unpaired electrons. Also, completion of the optimization calculation was based on the nature of individual atoms present in the molecule, and this indicates that the time for completion of individual compounds varied compared to each other. In this work, a series of descriptors were obtained from the optimized compounds, and the descriptors were the highest occupied molecular orbital energy (HOMO), lowest unoccupied molecular orbital energy (LUMO), energy gaps, and binding affinities.

3. RESULTS AND DISCUSSION

3.1. Sorbent Characterization. Morphological characterization of L-MAC was performed by using SEM (Figure 1). A porous structure was evident in L-MAC (Figure 1a,b), with a spongelike or honeycomb surface structure comprising carbon layers. The impregnation of iron oxide in L-MAC via a one-pot synthesis rendered the material magnetic, leading to the heterogeneous composite characteristics of the mesoporous adsorbent. Parts c and d of Figure 1 show tiny rods of magnetic Fe₃O₄ that were grafted onto the sheet. The higher contrast iron oxide deposition is evident on the surface and pores of L-MAC, along with EDS analysis, confirming a predominant presence of carbon and oxygen, while the successful incorporation of iron was ascertained based on the element's relative abundance. Mapping images of L-MAC collected with EDS revealed the presence of C, O, and Fe elements distributed throughout the structures (Figure 1e-h). Moreover, XPS analysis was conducted to assess the chemical composition of the L-MAC surface. The peaks shown by the survey spectra (Figure 1i-k) are associated with binding energies of C 1s (284.5 eV), O 1s (533.3 eV), and Fe 2p (711.8 eV). The deconvoluted C 1s spectra for L-MAC (Figure 1i) showed binding energies at 284.4, 285.0, and 286.9 eV associated with C=C, C-O/C-OH, and C=O bonds, respectively.³⁹ The O 1s spectra revealed binding energies of ~531.0 and ~533.0 eV, attributed to C=O and C-O bonds, respectively. ^{40,41} A peak at 535.0 eV was ascribed to COOH or adsorbed H2O on the L-MAC's surface, while the peak at 530.1 eV corresponded to the O-Fe binding energy.⁴² Additionally, the deconvoluted high-resolution Fe 2p spectrum (Figure 1k) displayed peaks at 710.4, 712.2, 718.9, 724.1, 726.0, and 734.4 eV, corresponding to $2p_{3/2}$ of Fe^{2+} and Fe^{3+} , Fe^{3+} $2p_{3/2}$ satellite, $2p_{1/2}$ of Fe^{2+} and Fe^{3+} , and Fe^{3+} $2p_{1/2}$ satellite, respectively. These results confirm that iron oxide species were formed.

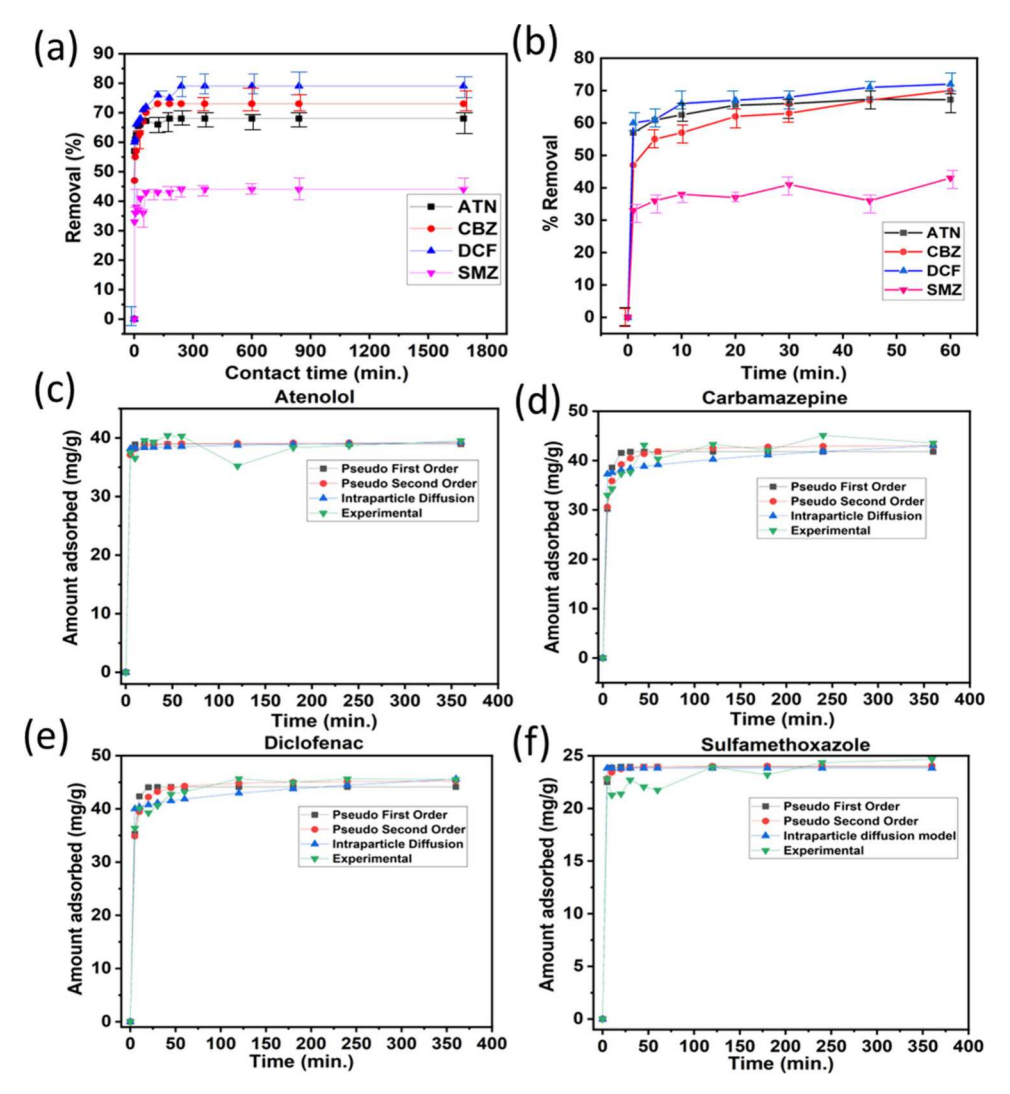


Figure 2. (a and b) Effect of contact time (24 h and 60 min). Lagergren PFO and PSO and Weber–Morris intraparticle diffusion models of adsorption of pharmaceutical mixtures containing (c) ATN, (d) CBZ, (e) DCF, and (f) SMZ (process parameters: [Co] = 80 mg/L; dosage = 1 mg/mL; solution pH = 5.8 \pm 0.2; mixing rate = 300 rpm; $T = 25 \pm 1$ °C).

The magnetic carbon composite displayed type IV(a) isotherms, often associated with meso/macroporous materials, with pores greater than 4 nm. 44,45 A BET SSA value for L-MAC of 221.1 m²/g and an average pore diameter of 6.2 nm were obtained, as evaluated by NLDFT (Figure 1m). It is likely that iron oxide particles potentially limit the accessibility for N₂ adsorption by clogging the pores. 46 XRD patterns revealed characteristic diffraction peaks of magnetite (Fe₃O₄) embedded in amorphous carbon derived from lignin (JCPDS 1-1111), which supports the presence of magnetic iron species (Figure 1n).⁴⁷ Finally, the thermal stability of L-MAC was evaluated by TGA (Figure 10), where a single weight-loss event assigned to carbon oxidation, with a decomposition temperature maximum of around 600 °C, was noted, suggesting high stability. A small increase in weight was also noted at 275 °C, likely resulting from the oxidation of available iron species. 48 Furthermore, a residual mass of 50% was recorded for L-MAC, attributed to the iron oxides contained in the sample.^{48,49}

3.2. Sorption Kinetics and Effect of Contact Time. In order to glean an understanding of the kinetics/mechanism of adsorption, it is essential to establish the sorption rate as a

function of the sorbate—sorbent time of interaction before reaching the sorption equilibrium. S0,51 Batch experimental data were modeled with the kinetic model equations (Weber—Morris intraparticle diffusion, eq 9; pseudo-first-order (PFO), eq 10; pseudo-second-order (PSO), eq 11) (Figure 2). The initial sorption rate was estimated using eq 12, and the sum of squared errors (SSE) provided additional evidence for the best-fit model (eq 13).

$$q_t = K_{id}t^{0.5} + C (9)$$

$$q_t = q_e (1 - e^{-K_1 t}) (10)$$

$$q_t = \frac{q_e^{2} K_2 t}{q_e K_2 t + 1} \tag{11}$$

$$h = K_2 q_e^2 \tag{12}$$

$$\sum_{i=1}^{n} (q_{e,cal} - q_{e,exp})_{i}^{2}$$
(13)

Table 1. Competitive Sorption Kinetic Parameters for Pharmaceutical Mixtures by L-MAC Sorbent

adsorption model	parameters	atenolol	carbamazepine	diclofenac	sulfamethoxazol
	Ki	netics			
first order	experimental q_e (mg/g)	39.27	43.53	45.53	11.30
	predicted q_e (mg/g)	38.93	41.79	44.11	23.95
	K_1 (1/min)	0.64	0.26	0.32	0.56
	SSE	28.02	87.81	73.25	61.30
second order	experimental q_e (mg/g)	39.27	43.53	45.53	24.35
	predicted q_e (mg/g)	39.19	43.25	45.41	24.05
	$K_2 \text{ (mg/g·min)}$	0.09	0.01	0.01	0.15
	h (mg/g·min)	138.23	18.70	20.62	86.76
	SSE	26.02	31.75	31.29	61.20
Weber-Morris intraparticle diffusion	$K_{\rm id} \ ({\rm mg/g \cdot min^{1/2}})$	0.06	0.34	0.34	0.01
	C	38.05	36.50	39.25	23.95
	SSE	26.93	82.18	40.74	62.75
	Iso	therm			
Freundlich	$K_{ m f}$	8.13	1.80	5.63	2.89
	N	0.10	1.00	0.43	0.45
	SSE	1.02	0.32	0.28	0.008
Langmuir	$q_{ m max}~({ m mg/g})$	11.66	23.64	27.97	11.30
	$K_{\rm L}$ (L/mg)	1.12	0.008	0.35	0.17
	SSE	1.00	0.31	0.18	0.007
Linear	$K_{ m d}$	0.54	1.52	1.80	0.64
	SSE	2.19	0.32	1.69	0.80

where q_t and q_e are contaminants sorbed per time (t) and mass of L-MAC (mg/g) at equilibrium, respectively, K_1 (1/min) and K_2 $(g/mg\cdot min)$ are rate constants for PFO and PSO, K_{id} $(mg/g\cdot min^{1/2})$ and C (mg/g) are the rate constant for intraparticle diffusion and constant connected to the thickness of the boundary layer, respectively, and h $(mg/g\cdot min)$ is the initial rate of sorption. Table 1 presents the data obtained from the models.

Table 1 reveals that the adsorption of the pharmaceutical mixture is best fitted by the PSO kinetic model, considering a relatively lower SSE. Therefore, the PSO model suggests that L-MAC interactions with the mixture of competing contaminants involved a fair degree of chemisorption. As shown by the correlation and error coefficients in Table 1, the Weber–Morris diffusion model, which explains the role of external and intraparticle diffusion within the pores of porous materials, adequately described the interactions of ATN and SMZ with L-MAC. This is expected because mass-transfer processes vary for different types of compounds due to molecular differences and diffusion effects. ^{53,54}

Parts a and b of Figure 2 display multiple linearities depicting that other processes and/or mechanisms are involved in the sorbent-sorbate interaction. The intraparticle diffusion model predicts that the overall sorption process starts with a fast reaction, followed by the rate-determining step (slowest step). Thus, in complex and multipollutant adsorption systems, mechanisms beyond film diffusion occur throughout the competitive sorption process. The boundary layer constant (*C*) is greater than zero for adsorption of the pollutant mixture, and it is known that the larger the value of C, the more prominent the impact of interfacial boundary thickness.⁵⁵ The PSO kinetic model suggests that strong interactions, such as electrostatic and covalent bonding, between the various pollutant molecules and the L-MAC's surface may occur, along with diffusional transport into the available pores of the sorbent. 50,56,57

Due to the availability of binding sites and the intermolecular driving force between multiple pollutants, there was fast adsorption, as revealed by the steepness of the curve during the first hour of the sorption process followed by rapid equilibrium and site saturation. The overall adsorption trend follows the order ATN < SMZ < CBZ < DCF (Figure 2), and the models predicted that ATN and SMZ reached equilibrium within the first hour, while it took slightly longer (4 h) before equilibrium was attained for CBZ and DCF, adsorbing >80% of the highest concentration (80 mg/L) of pollutants. The values of the initial rate constant (h) and K_2 also support the fact that a faster sorption rate took place for ATN and SMZ (Table 1), which may be due to unbonded electrons and the molecular configuration of the pollutants.

3.3. Sorption Isotherm. The interactions between contaminants and sorbents as equilibrium is reached are explained by adsorption isotherm models. Of all of the process variables, the sorbate concentration has the biggest impact on the sorption capacity of adsorbents.⁵⁸ Because of this, the amount or concentration of pollutant(s) in the solution is what essentially drives mass transport between the contaminated aqueous phase and the solid phase composed of adsorbents. The competitive adsorption isotherms of the four pharmaceutical compounds were studied using the L-MAC sorbent in Figure S5. The experimental data obtained from batch experiments were fitted with Freundlich, Langmuir, and linear/partition models, and the values are presented in Table 1. The Langmuir model is commonly used to describe the monolayer sorption mechanisms of contaminants on homogeneous surfaces, facilitated by available sorption sites (eq 14), while the Freundlich model (eq 15) is based on the formation of multiple layers of sorbates as the core driving mechanism on a heterogenous surface.⁵⁹ The partitioning/ distribution of the sorbate between the solid-solution interphases is described by the linear model (eq 16). The best-fitted model was determined with the SSE for nonlinear regression.60,61

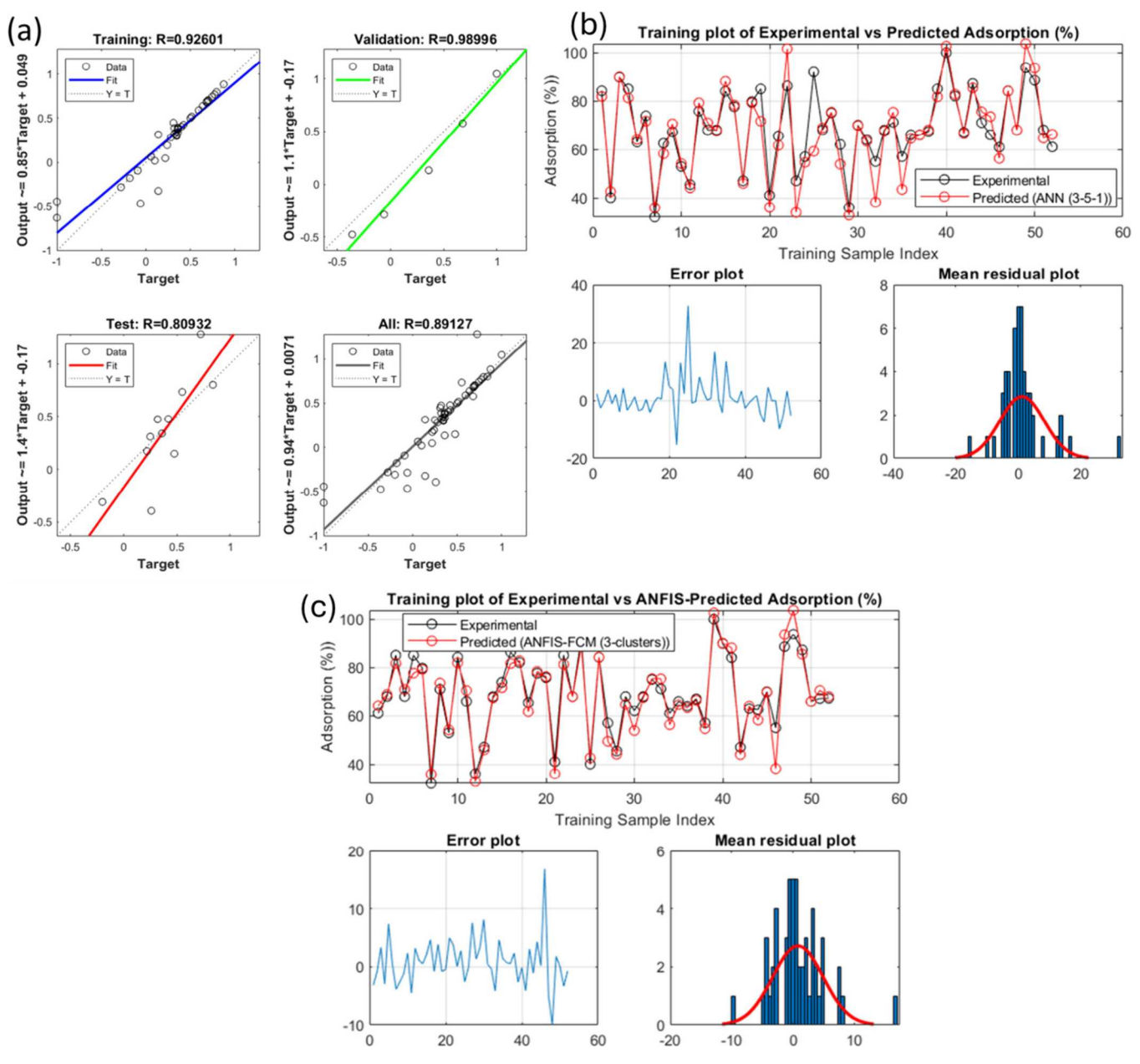


Figure 3. (a) Regression performance of the ANN (3-5-1) training. (b) Comparison plot of the actual and predicted adsorption with the 3-5-1 ANN model at the training phase. (c) Comparison plot of the actual and predicted adsorption with the ANFIS-FCM2 (3 clusters) model at the training phase.

$$q_{\rm e} = \frac{q_{\rm max} K_{\rm L} C_{\rm e}}{1 + K_{\rm L} C_{\rm e}} \tag{14}$$

$$q_{\rm e} = K_{\rm f} C_{\rm e}^N \tag{15}$$

$$q_{e} = K_{d}C_{e} \tag{16}$$

where $C_{\rm e}$ is the contaminant unadsorbed (mg/L) and $q_{\rm e}$ is the contaminant adsorbed (mg/g). $K_{\rm f}$ is the adsorption-capacity-related parameter, $K_{\rm d}$ is the partitioning coefficients, $K_{\rm L}$ is the Langmuir constant, N is the heterogeneity indicator, and $q_{\rm max}$ is the maximum adsorption capacity.

In general, the adsorption trend followed the order of DCF > CBZ > ATN > SMZ, considering the adsorption capacities $(q_{\text{max}} \text{ and } K_{\text{d}})$ and removal efficiencies (Table 1 and Figure S5). This finding is in agreement with the results obtained

from kinetic studies as well (Figure 2). The Langmuir isotherm model had the lowest SSE values in comparison to the Freundlich and Linear models, for the modeling of L-MAC's interaction with the pharmaceuticals (Table 1), suggesting that the overwhelming mechanism of interaction between the L-MAC and pollutant mixture is the monolayer sorption pathway and is largely controlled by available sites on the surface of the sorbents. These deductions are reasonable because of the complex nature of the aqueous matrix that promotes a competitive sorption environment; hence, there are barely enough sites for one pollutant to dominate the first layer, let alone form multiple layers. Thus, each pollutant within the mixture may be limited to a single layer sorbed onto the surface of the adsorbents. The sorption maxima of L-MAC as predicted by the Langmuir model were 11.30, 11.66, 23.64,

and 27.97 mg/g for SMZ, ATN, CBZ, and DCF, respectively (Table 1).

Interestingly, we observed that sorption hysteresis took place during sorbate—sorbent interactions for the four pharmaceutical compounds (Figure S5), providing evidence of sorption irreversibility in aqueous media due to high binding strength and/or mechanical entrapment of the sorbed pollutants within the pore structure of L-MAC. However, we observed >99% adsorption efficiency when environmentally relevant and trace concentrations of not more than 10 ppm of each pollutant are present in the pharmaceutical mixtures. Pharmaceuticals are often detected in trace amounts in aquatic systems (parts per billion and very low parts per million in most cases), suggesting the suitability of the materials for real-world applications.^{7,62} Additionally, the magnetic properties of L-MAC offer the advantage of easy recovery, contributing to an improved process sustainability.

3.4. Effect of the Solution pH. The adsorption process depends on the pH because it can change the sorbate molecule's charge, as well as the materials' net surface charge, which, in turn, affects the sorbent-sorbate interactions. 60,63 Because pH variation is one of the characteristics of aquatic systems and several physicochemical and biological processes are influenced by the pH, research into the role of pH in the competitive adsorption of pharmaceutical mixtures is imperative. 64 Consequently, the point of zero charge (pH_{pzc}) for L-MAC was determined to assess how the material's surface charge is affected by varying the solution pH conditions. L-MAC has a pH_{pzc} of 8.5, which suggests that the composite material is negatively charged at pH > 8.5 and positively charged at pH < 8.5. The effect of pH on the sorption of the pharmaceutical mixture was evaluated for solutions with pH ranges between 2 and 12 (Figure S6). The results obtained suggest that basic media negatively impact the performance of L-MAC for the competitive adsorption of pharmaceuticals, which could be attributed to repulsive tendencies of the negatively charged L-MAC surface and negatively charged molecules/anionic forms of the pollutants in basic conditions.

Furthermore, it is fair to infer that neutral pH favors the sorption of DCF and SMZ with pK_a values <7; hence, pH regulation may not be considered a strict requirement for optimal performance. While electrostatic interactions might be important in some adsorption processes, not all adsorption responds significantly to protonation and hydroxylation. On the other hand, acidification/protonation favors ATN and CBZ (with p K_a values >7), which may be associated with the enhancements of hydrogen bonding between the adsorbents and sorbates at pH < 7.66 This is in line with earlier studies on the adsorption of organic contaminants using pine needle biochar,⁶⁷ grape-stalk-activated carbon,⁶⁸ and coconut-activated carbon. ⁶⁹ The zigzag-like sorption trend of SMZ may be attributed to hydrochemistry due to its dual pK_a values of 1.5 and 5.7. Other mechanisms that may play key roles during the adsorption of pharmaceuticals include hydrogen bonding and π - π interactions due to the aromaticity of the compounds and the graphitic nature of L-MAC, hydrophobic interactions, and van der Waals attractions, among others. These processes are facilitated by the attraction between the π orbitals of the carbon basal planes or the π band of the graphitic layers and the electronic density in the aromatic rings of the pharmaceuticals investigated in this study.⁷⁰

4. PERFORMANCE METRICS OF THE MACHINE-LEARNING MODEL

Continuous testing and assessment were conducted to find the best network design and training methods for adsorption prediction. Furthermore, to understand how operational parameters such as the initial concentration, contact time, and pH affect the percentage adsorption, ANN models were developed with different topologies and training procedures. Table S4 displays the performance metric values for training and testing. The table shows ANN model performance metrics, including hidden layer neurons, for different topologies during training and testing. The performance model at the training phase is better than that at the testing phase. The best model at the testing was 3-5-1 with RMSE, MAD, MAPE, and R values of 12.906, 7.826, 12.567, and 0.863, while at the training phase, values of 9.568, 5.746, 11.085, and 0.8913 were obtained. We note that the training phase results indicate a better generalization ability in comparison to the testing phase. The notable performance based on RMSE, MAD, and MAPE during the training phase suggests that the model is not overfitting the training data and has learned the underlying patterns effectively. Implicit regularization mechanisms, and early stopping criteria used in this model, might have helped to improve generalization, leading to a better performance on the training set.⁷¹

Figure 3 illustrates the training performance of the best ANN model, showcasing regression plots for the training, validation, and test phases. It also presents the overall training regression value (R = 0.8913), which reflects the combined performance metrics from all phases. An overall R value of 0.8913 indicates a strong correlation between predicted and actual values across all datasets. This suggests that the model maintains good predictive accuracy and performs well across the training, validation, and test sets, demonstrating robustness and generalizability. The overall R value serves as a comprehensive measure of the model's performance, highlighting both its strengths (high validation R value) and areas for improvement (slightly lower test R value), making it a positive indicator of the model's consistency and predictive accuracy. The training dataset was initially employed to evaluate the model's efficacy in predicting its training dataset. The comparison plot of the predicted adsorption and the experimentally measured values for the training period is shown in Figure 3b, which demonstrates that the model exhibited a rather accurate prediction performance when trained with the datasets for pharmaceutical mixtures. The significant overlap between the two curves indicates a strong agreement between the predicted and experimental data, which suggests that the ANN model is a powerful tool for predicting the sorption of pharmaceutical mixtures (ATN, CBZ, DCF, and SMZ) onto L-MAC. The experiment was conducted using a testing dataset including 30% of the total data. A comparison plot was created to evaluate the predicted adsorption with the experimentally observed values (Figures S7 and S8). A strong correlation was detected between the predicted values by ANN and the experimentally obtained values for the adsorption of pharmaceutical mixtures (ATN, CBZ, DCF, and SMZ) onto L-MAC, with very little variation. A minimal number of inconsistencies in predicting the adsorption were discovered, which may be attributed to the limited amount of data available for the model. Having a substantial dataset for the

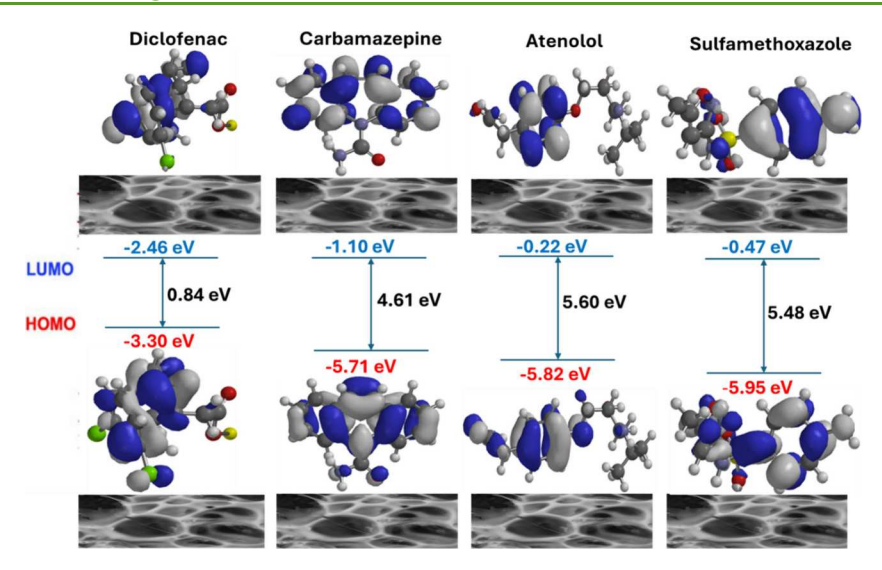


Figure 4. HOMO-LUMO orbitals and calculated descriptors for pharmaceutical mixtures.

predictive model would be expected to enhance its performance.

The ANN and ANFIS models developed in this study are beneficial in predicting and optimizing pharmaceutical mixture adsorption rates onto L-MAC. The models' excellent illustration of the relationship between the initial concentration, contact time, and pH with adsorption rates improves the real-world adsorption performance. This enables optimal adsorption efficiency by fine-tuning the operational settings. The initial concentration of pharmaceutical mixtures is a critical factor influencing the adsorption rate. Moreover, the models exhibit how the activated carbon adsorption capacity varies with the concentration. Another important factor is contact time, which defines how long pharmaceutical mixtures interact with activated carbon. The ANN and ANFIS models demonstrate that extended contact periods increase the adsorption rates until equilibrium, revealing that pharmaceuticals adsorb differently at varying pH levels due to their ionization states and activated carbon surface charge, helping to establish the optimal pH for removal.

Additionally, given the multidimensional nature of the approach used in this study, its potential transition from laboratory scale to field applications will require the expertise of computational scientists, materials chemists, and water treatment professionals, along with associated personnel costs. However, combining AI, molecular simulations, and experimental studies is crucial for the development of novel and more effective adsorbent materials. AI can rapidly analyze large datasets and predict optimal material properties, while molecular simulations provide detailed insights into adsorption mechanisms at the atomic level. Experimental studies validate these predictions and simulations, ensuring practical applicability and guiding further improvements in material designs.

5. MOLECULAR AND DFT STUDIES

In this work, the level of reactivity/binding strength of the studied pharmaceutical mixtures (ATN, CBZ, DCF, and SMZ) was examined via the HOMO energy, LUMO energy, and energy gaps (Figure 4 and Table S5). The calculated energy gaps for the studied pharmaceutical mixtures, as shown in Figure 4, were 0.84, 4.61, 5.60, and 5.48 eV for DCF, CBZ, ATN, and SMZ, respectively. According to Oyebamiji et al.,⁷²

the lower the energy gap, the better the reactivity of the studied compound; thus, DCF with an energy gap of 0.84 eV proved to have a potentially higher tendency to be adsorbed than the other studied compounds, and this indeed agrees with the experimental result in this study. Also, the region with the highest electron density in the HOMO is generally considered to be where the most energetic electrons in a molecule are located. Therefore, the calculated HOMO energy values revealed the propensity of the studied molecules to give electrons to suitable receptors that are deficient in electrons. Moreover, the calculated LUMO energy provides information on the site(s) of the studied compounds that have the highest affinity to accept electrons or facilitate pairing with a suitable sorbent ⁷³ (Table S8).

The calculated HOMO values were -3.30 eV for DCF, -5.71 eV for CBZ, -5.82 eV for ATN, and -5.95 eV for SMZ, resulting in the calculated HOMO energy order of DCF > CBZ > ATN > SMZ. As presented in Figure 4, it was confirmed that DCF has the highest HOMO energy value, and this indicates that it has the highest tendency to donate electrons or facilitate covalent bonding with the carbon- and oxygen-rich biomass-derived sorbent, thereby signifying the order of the chemisorptive adsorption potential of each pharmaceutical compound within the mixture. This agrees with the experimental result obtained as well as the order presented in the experimental section in terms of the maximum adsorption capacity (q_{max}) and adsorption efficiency. Furthermore, the compound with the lowest LUMO energy value is expected to have the highest strength to receive electrons, and the high calculated binding affinity value confirms the high efficiency of DCF (Table S5); therefore, DCF with -2.46 eV and -3.7 kcal/mol is expected to be adsorbed, and this prominently agrees with the results presented in the experimental section of this work (Figures S10-S13). Based on computational, machine learning/AI, and experimental findings, functionalized L-MAC are suitable remediation tools for mixtures of emerging organic pollutants in aqua systems.

6. CONCLUSION

This study synthesized L-MAC for competitive adsorptionbased decontamination of pharmaceutical mixtures. PSO kinetics and Langmuir isotherm modeling indicated sitelimiting monolayer adsorption with chemisorption as the primary mechanism supported by $\pi - \pi$ interactions and hydrogen bonding. DFT corroborated these findings, revealing the reactivity and binding capacity of pharmaceuticals in the order DCF > CBZ > ATN > SMZ, based on HOMO, LUMO, and energy gaps. Machine-learning models (ANN 3-5-1 and ANFIS-FCM) demonstrated superior predictive performances with lower errors and higher accuracy, as shown by RMSE, MAD, and MAPE metrics during training and testing. Minor inconsistencies, particularly in the ANN model, were attributed to limited datasets, suggesting that expanding the dataset would enhance predictive accuracy. This study bridges knowledge gaps by integrating comparative isothermal and kinetic modeling with advanced AI and computational techniques. These insights contribute to developing sustainable materials for water treatment and advancing the field of wastewater treatment and environmental remediation.

ASSOCIATED CONTENT

Supporting Information

The Supporting Information is available free of charge at https://pubs.acs.org/doi/10.1021/acssusresmgt.4c00451.

Schematic representation of the facile synthesis of the L-MAC adsorbent, along with a detailed description of the machine-learning models and equations used in this study, including supplemental adsorption results, such as isotherm modeling, sorption/desorption hysteresis, and pH experiments, as well as the performance metrics of the machine-learning models, with tables and figures included to support the findings, and images from the DFT and molecular studies, illustrating the HOMO–LUMO energy gaps (PDF)

AUTHOR INFORMATION

Corresponding Authors

Adedapo O. Adeola — Department of Chemistry and Biochemistry, The Centre for NanoScience Research, Quebec Centre for Advanced Materials, Concordia University, Montreal, Quebec H4B 1R6, Canada; Email: adedapo.adeola@concordia.ca

Rafik Naccache — Department of Chemistry and Biochemistry, The Centre for NanoScience Research, Quebec Centre for Advanced Materials, Concordia University, Montreal, Quebec H4B 1R6, Canada; orcid.org/0000-0002-3140-4476; Email: rafik.naccache@concordia.ca

Authors

Gianluca Fuoco – Department of Chemistry and Biochemistry, The Centre for NanoScience Research, Quebec Centre for Advanced Materials, Concordia University, Montreal, Quebec H4B 1R6, Canada

Kayode A. Adegoke — Department of Industrial Chemistry, First Technical University, Ibadan 200261, Nigeria; orcid.org/0000-0002-7502-0132

Oluwatobi Adeleke – Department of Mechanical Engineering Science, University of Johannesburg, Johannesburg 2006, South Africa

Abel K. Oyebamiji – Department of Industrial Chemistry, University of Ilesa, Ilesa, Osun State 5089, Nigeria Luis Paramo – Department of Chemistry and Biochemistry, The Centre for NanoScience Research, Quebec Centre for Advanced Materials, Concordia University, Montreal, Quebec H4B 1R6, Canada

Complete contact information is available at: https://pubs.acs.org/10.1021/acssusresmgt.4c00451

Author Contributions

A.O.A.: conceptualization, experimental investigation, methodology, formal analysis, data curation, writing—review and editing, and writing—original draft. G.F. and L.P.: experimental investigation, data curation, and methodology. K.A.A., O.A., and A.K.O.: machine learning/AI, computational investigation, data curation, and writing—original draft. R.N.: writing—review and editing, formal analysis, supervision, project administration, and funding acquisition.

Notes

The authors declare no competing financial interest.

■ ACKNOWLEDGMENTS

R.N. is grateful for the funding provided by the Natural Sciences and Engineering Research Council (NSERC) through the Discovery Grant Program (Grant RGPIN-2016-06629) and for funding through the Research Chair Program by the Concordia University (Montreal, Canada). R.N. also acknowledges funding support from The Quebec Centre for Advanced Materials. G.F. is grateful for funding provided by the NSERC through the Canada Graduate Scholarships-Master's (CGSM) program and the Fonds de Recherche du Quebec-Nature and Technologies (FRQNT). L.P. thanks the National Council of Humanities, Science, and Technology in Mexico (CON-AHCYT) for the support granted through the postgraduate scholarships abroad program.

REFERENCES

- (1) Adeola, A.O.; Paramo, L.; Fuoco, G.; Naccache, R. Emerging hazardous chemicals and biological pollutants in Canadian aquatic systems and remediation approaches: A comprehensive status report. *Science of The Total Environment* **2024**, 954, No. 176267.
- (2) Hernández-Tenorio, R.; González-Juárez, E.; Guzmán-Mar, J.L.; Hinojosa-Reyes, L.; Hernández-Ramírez, A. Review of occurrence of pharmaceuticals worldwide for estimating concentration ranges in aquatic environments at the end of the last decade. *Journal of Hazardous Materials Advances* **2022**, *8*, No. 100172.
- (3) Al Qarni, H.; Collier, P.; O'Keeffe, J.; Akunna, J. Investigating the removal of some pharmaceutical compounds in hospital wastewater treatment plants operating in Saudi Arabia. *Environmental Science and Pollution Research* **2016**, 23, 13003–13014.
- (4) Bahlmann, A.; Brack, W.; Schneider, R.J.; Krauss, M. Carbamazepine and its metabolites in wastewater: Analytical pitfalls and occurrence in Germany and Portugal. *Water Research* **2014**, *57*, 104–114.
- (5) Ebele, A.J.; Abou-Elwafa Abdallah, M.; Harrad, S. Pharmaceuticals and personal care products (PPCPs) in the freshwater aquatic environment. *Emerging Contaminants* **2017**, *3*, 1–16.
- (6) Mestre, A.S.; Carvalho, A.P. Photocatalytic Degradation of Pharmaceuticals Carbamazepine, Diclofenac, and Sulfamethoxazole by Semiconductor and Carbon Materials: A Review. *Molecules* **2019**, 24, 3702.
- (7) Adeola, A.O.; Ore, O.T.; Fapohunda, O.; Adewole, A.H.; Akerele, D.D.; Akingboye, A.S.; Oloye, F.F. Psychotropic Drugs of Emerging Concerns in Aquatic Systems: Ecotoxicology and Remediation Approaches. *Chemistry Africa* **2022**, *5*, 481–508.
- (8) Marques, S. C. R.; Mestre, A.S.; Machuqueiro, M.; Gotvajn, A.Ž.; Marinšek, M.; Carvalho, A.P. Apple tree branches derived activated carbons for the removal of β -blocker atenolol. *Chemical Engineering Journal* **2018**, 345, 669–678.

- (9) Haro, N.K.; Del Vecchio, P.; Marcilio, N.R.; Féris, L.A. Removal of atenolol by adsorption Study of kinetics and equilibrium. *Journal of Cleaner Production* **2017**, *154*, 214–219.
- (10) Yi, X.; Tran, N.H.; Yin, T.; He, Y.; Gin, K.Y.-H. Removal of selected PPCPs, EDCs, and antibiotic resistance genes in landfill leachate by a full-scale constructed wetlands system. *Water Research* **2017**, 121, 46–60.
- (11) Kråkström, M.; Saeid, S.; Tolvanen, P.; Kumar, N.; Salmi, T.; Kronberg, L.; Eklund, P. Ozonation of carbamazepine and its main transformation products: product determination and reaction mechanisms. *Environ. Sci. Pollut Res. Int.* **2020**, *27*, 23258–23269.
- (12) Pan, D.; Zhang, C.; Wang, C.-S.; Zhang, P.; Jiao, X.-Y.; Ma, Q.-R.; Wang, L.-T.; Li, D.-J.; Li, L.-P. Unravelling hidden threats of water disinfection: Toxicity evaluation and toxic products identification during diclofenac degradation. *Environmental Pollution* **2024**, 345, No. 123424.
- (13) Joachim, S.; Beaudouin, R.; Daniele, G.; Geffard, A.; Bado-Nilles, A.; Tebby, C.; Palluel, O.; Dedourge-Geffard, O.; Fieu, M.; Bonnard, M.; Palos-Ladeiro, M.; Turiès, C.; Vulliet, E.; David, V.; Baudoin, P.; James, A.; Andres, S.; Porcher, J.M. Effects of diclofenac on sentinel species and aquatic communities in semi-natural conditions. *Ecotoxicology and Environmental Safety* **2021**, 211, No. 111812.
- (14) Ovung, A.; Bhattacharyya, J. Sulfonamide drugs: structure, antibacterial property, toxicity, and biophysical interactions. *Biophysical Reviews* **2021**, *13*, 259–272.
- (15) Prasannamedha, G.; Kumar, P.S. A review on contamination and removal of sulfamethoxazole from aqueous solution using cleaner techniques: Present and future perspective. *Journal of Cleaner Production* **2020**, 250, No. 119553.
- (16) Shamsudin, M.S.; Azha, S.F.; Ismail, S. A review of diclofenac occurrences, toxicology, and potential adsorption of clay-based materials with surfactant modifier. *Journal of Environmental Chemical Engineering* **2022**, *10*, No. 107541.
- (17) Del, A.; Das, S.; Debnath, A. Fabrication and characterization of organometallic nanocomposite for efficient abatement of dye laden wastewater: CCD optimization, adsorption mechanism, co-existing ions, and cost analysis. *Chemical Physics Letters* **2023**, 830, No. 140820.
- (18) Das, S.; Pal, A.; Debnath, A. Polyaniline-Coated Magnesium Ferrite Nanocomposite: Synthesis, Characterization, Fabrication Cost Analysis and Dye Sorption Behavior with Scale-Up Design. *ChemistrySelect* **2023**, 8, No. e202300928.
- (19) Adeola, A. O., Forbes, P. B. C. Advanced Nanomaterials for Removal of Emerging Organic Pollutants from Water. In *Novel Materials and Water Purification: Towards a Sustainable Future*; Kyriakopoulos, G. L., Zamparas, M. G., Eds.; Royal Society of Chemistry, 2024.
- (20) Das, P.; Debnath, A. Fabrication of MgFe2O4/polyaniline nanocomposite for amputation of methyl red dye from water: Isotherm modeling, kinetic and cost analysis. *J. Dispersion Sci. Technol.* **2023**, *44*, 2587–2598.
- (21) Gkika, D.A.; Liakos, E.V.; Vordos, N.; Kontogoulidou, C.; Magafas, L.; Bikiaris, D.N.; Bandekas, D.V.; Mitropoulos, A.C.; Kyzas, G.Z. Cost Estimation of Polymeric Adsorbents. *Polymers* **2019**, *11*, 925.
- (22) Su, X.; Wang, R.; Li, X.; Araby, S.; Kuan, H.-C.; Naeem, M.; Ma, J. A comparative study of polymer nanocomposites containing multi-walled carbon nanotubes and graphene nanoplatelets. *Nano Materials Science* **2022**, *4*, 185–204.
- (23) Na, P. T. L.; Tuyen, N. D. K.; Dang, B.-T. Sorption of four antibiotics onto pristine biochar derived from macadamia nutshell. *Bioresource Technology* **2024**, 394, No. 130281.
- (24) Das, S.; Rudra Paul, S.; Debnath, A. Fabrication of biochar from jarul (Lagerstroemia speciosa) seed hull for ultrasound aided sequestration of ofloxacin from water: Phytotoxic assessments and cost analysis. *Journal of Molecular Liquids* **2023**, 387, No. 122610.
- (25) Mohamad Nor, N.; Lau, L.C.; Lee, K.T.; Mohamed, A.R. Synthesis of activated carbon from lignocellulosic biomass and its

- applications in air pollution control—a review. Journal of Environmental Chemical Engineering 2013, 1, 658-666.
- (26) Yahya, M.A.; Al-Qodah, Z.; Ngah, C. W. Z. Agricultural biowaste materials as potential sustainable precursors used for activated carbon production: A review. *Renewable and Sustainable Energy Reviews* **2015**, *46*, 218–235.
- (27) Shaheen, J.; Fseha, Y.H.; Sizirici, B. Performance, life cycle assessment, and economic comparison between date palm waste biochar and activated carbon derived from woody biomass. *Heliyon* **2022**, *8*, No. e12388.
- (28) Adeola, A.O.; Cui, M.; Naccache, R. Rhodamine B sequestration using acid-precipitated and microwave-treated softwood lignin: Comparative isotherm, kinetics and thermodynamic studies. *Environmental Technology & Innovation* **2023**, 32, No. 103419.
- (29) Duarte, M.P.; Adeola, A.O.; Fuoco, G.; Jargaille, T.J.; Naccache, R. Efficient decaffeination with recyclable magnetic microporous carbon from renewable sources: Kinetics and isotherm analysis. *Environmental Research* **2024**, 258, No. 119446.
- (30) Semire, B.; Oyebamiji, A.; Odunola, O.A. Design of (2Z)-2-cyano-2-[2-[(E)-2-[5-[(E)-2-(4-dimethylaminophenyl)vinyl]]-2-thienyl]vinyl]pyran-4-ylidene]acetic acid derivatives as D- π -A dye sensitizers in molecular photovoltaics: a density functional theory approach. Research on Chemical Intermediates **2016**, 42, 4605–4619.
- (31) Gui, X.; Chang, T.-R.; Kong, T.; Pan, M.T.; Cava, R.J.; Xie, W. Monoclinic 122-Type BaIr2Ge2 with a Channel Framework: A Structural Connection between Clathrate and Layered Compounds. *Materials* **2017**, *10*, 818.
- (32) Lopera-Valle, A.; Elias, A. Amine Responsive Poly(lactic acid) (PLA) and Succinic Anhydride (SAh) Graft-Polymer: Synthesis and Characterization. *Polymers* **2019**, *11*, 1466.
- (33) Kyesmen, P.I.; Simfukwe, J.; Jubu, P.R.; Adeola, A.O.; Diale, M. The Structural Properties and Photoelectrocatalytic Response of Mn-Doped Hematite Photoanodes Prepared via a Modified Electrodeposition Approach. *ChemElectroChem* **2024**, *11*, No. e202400348.
- (34) Hamilton, A.; Pains Duarte, M.; Naccache, R. Corn Stover Lignin as a Solid Acid Catalyst for the Esterification of Oleic Acid. *Part. Part. Syst. Charact.* **2024**, No. 2400147.
- (35) Khan, A.; Hayat, S.; Zhong, Y.; Arif, A.; Zada, L.; Fang, M. Computational and topological properties of neural networks by means of graph-theoretic parameters. *Alexandria Engineering Journal* **2023**, *66*, 957–977.
- (36) Tan, X.; Wang, Y.; Wu, L.; Yu, Y.; Yu, Q.; Sun, G. An ANFIS-Based indirect control strategy for solar heating system: Exploring PMV approach. *Energy and Buildings* **2024**, *309*, No. 114056.
- (37) Karaboga, D.; Kaya, E. Adaptive network based fuzzy inference system (ANFIS) training approaches: a comprehensive survey. *Artificial Intelligence Review* **2019**, 52, 2263–2293.
- (38) Waziri, I.; Kelani, M.T.; Oyedeji-Amusa, M.O.; Oyebamiji, A.K.; Coetzee, L.-C. C.; Muller, A.J. Comparative investigation of derivatives of (E)-N-((E)-3-phenylallylidene)aniline: Synthesis, structural characterization, biological evaluation, density functional theory analysis, and in silico molecular docking. *Heliyon* **2024**, *10*, No. e26632.
- (39) Chen, X.; Wang, X.; Fang, D. A review on C1s XPS-spectra for some kinds of carbon materials. *Fullerenes, Nanotubes and Carbon Nanostructures* **2020**, 28, 1048–1058.
- (40) Jain, A.; Ghosh, M.; Krajewski, M.; Kurungot, S.; Michalska, M. Biomass-derived activated carbon material from native European deciduous trees as an inexpensive and sustainable energy material for supercapacitor application. *Journal of Energy Storage* **2021**, 34, No. 102178.
- (41) Duarte, M.P.; Silva, R. C. F.; Medeiros, T.P.V.d.; Ardisson, J.D.; Cotta, A. A. C.; Naccache, R.; Teixeira, A.P.d.C. Carbon nanotubes derived from waste cooking oil for the removal of emerging contaminants. *New Journal of Chemistry* **2022**, *46*, 11315–11328.
- (42) Pereira, D.; Gil, M.V.; Esteves, V.I.; Silva, N. J. O.; Otero, M.; Calisto, V. Ex-situ magnetic activated carbon for the adsorption of three pharmaceuticals with distinct physicochemical properties from

- real wastewater. Journal of Hazardous Materials 2023, 443, No. 130258.
- (43) Guo, J.; Wang, R.; Tjiu, W.W.; Pan, J.; Liu, T. Synthesis of Fe nanoparticles@graphene composites for environmental applications. *Journal of Hazardous Materials* **2012**, 225-226, 63–73.
- (44) Thommes, M.; Kaneko, K.; Neimark, A.V.; Olivier, J.P.; Rodriguez-Reinoso, F.; Rouquerol, J.; Sing, K. S. W. Physisorption of gases, with special reference to the evaluation of surface area and pore size distribution (IUPAC Technical Report). *Pure and Applied Chemistry* **2015**, *87*, 1051–1069.
- (45) Khuong, D.A.; Trinh, K.T.; Nakaoka, Y.; Tsubota, T.; Tashima, D.; Nguyen, H.N.; Tanaka, D. The investigation of activated carbon by K2CO3 activation: Micropores- and macropores-dominated structure. *Chemosphere* **2022**, 299, No. 134365.
- (46) Silva, R. C. F.; Ardisson, J.D.; Cotta, A. A. C.; Araujo, M.H.; Teixeira, A.P.d.C. Use of iron mining tailings from dams for carbon nanotubes synthesis in fluidized bed for 17α-ethinylestradiol removal. *Environmental Pollution* **2020**, 260, No. 114099.
- (47) Rocha, L.S.; Pereira, D.; Sousa, E.; Otero, M.; Esteves, V.I.; Calisto, V. Recent advances on the development and application of magnetic activated carbon and char for the removal of pharmaceutical compounds from waters: A review. *Science of The Total Environment* **2020**, 718, No. 137272.
- (48) Chen, X.H.; Chen, C.S.; Chen, Q.; Cheng, F.Q.; Zhang, G.; Chen, Z.Z. Non-destructive purification of multi-walled carbon nanotubes produced by catalyzed CVD. *Materials Letters* **2002**, *57*, 734–738.
- (49) Kumar, A.; Patra, C.; Kumar, S.; Narayanasamy, S. Effect of magnetization on the adsorptive removal of an emerging contaminant ciprofloxacin by magnetic acid activated carbon. *Environ. Res.* **2022**, 206, No. 112604.
- (50) Adeola, A.O.; de Lange, J.; Forbes, P. B. C. Adsorption of antiretroviral drugs, efavirenz and nevirapine from aqueous solution by graphene wool: Kinetic, equilibrium, thermodynamic and computational studies. *Applied Surface Science Advances* **2021**, *6*, No. 100157.
- (51) Akpomie, K.G.; Conradie, J.; Adegoke, K.A.; Oyedotun, K.O.; Ighalo, J.O.; Amaku, J.F.; Olisah, C.; Adeola, A.O.; Iwuozor, K.O. Adsorption mechanism and modeling of radionuclides and heavy metals onto ZnO nanoparticles: a review. *Appl. Water Sci.* **2023**, *13*, 20.
- (52) Sambo, G.s.N.; Adeola, A.O.; Muhammad, S.A. Oil palm wastederived adsorbents for the sequestration of selected polycyclic aromatic hydrocarbon in contaminated aqueous medium. *Appl. Water Sci.* **2024**, *14*, 113.
- (53) Gil, A.; Taoufik, N.; García, A.M.; Korili, S.A. Comparative removal of emerging contaminants from aqueous solution by adsorption on an activated carbon. *Environmental Technology* **2019**, 40, 3017–3030.
- (54) Rosli, M.A.; Daud, Z.; Ridzuan, M.B.; Aziz, N. A. A.; Awang, H.B.; Adeleke, A. O.; Hossain, K.; Ismail, N. Equilibrium isotherm and kinetic study of the adsorption of organic pollutants of leachate by using micro peat-activated carbon composite media. *Desalination Water Treatment* **2019**, *160*, 185–192.
- (55) Sahoo, T. R.; Prelot, B. Adsorption processes for the removal of contaminants from wastewater: the perspective role of nanomaterials and nanotechnology. In *Nanomaterials for the Detection and Removal of Wastewater Pollutants*; Bonelli, B., Freyria, F. S., Rossetti, I., Sethi, R., Eds. Elsevier, 2020; Chapter 7, pp 161–222.
- (56) Anthony, E.T.; Ojemaye, M.O.; Okoh, A.I.; Okoh, O.O. Synthesis of CeO2 as promising adsorbent for the management of free-DNA harboring antibiotic resistance genes from tap-water. *Chemical Engineering Journal* **2020**, 401, No. 125562.
- (57) Iwuozor, K.O.; Akpomie, K.G.; Conradie, J.; Adegoke, K.A.; Oyedotun, K.O.; Ighalo, J.O.; Amaku, J.F.; Olisah, C.; Adeola, A.O. Aqueous phase adsorption of aromatic organoarsenic compounds: A review. *Journal of Water Process Engineering* **2022**, *49*, No. 103059.
- (58) Perveen, S.; Nadeem, R.; Nosheen, F.; Asjad, M.I.; Awrejcewicz, J.; Anwar, T. Biochar-Mediated Zirconium Ferrite

- Nanocomposites for Tartrazine Dye Removal from Textile Wastewater. Nanomaterials (Basel) 2022, 12, 2828.
- (59) Inyinbor, A.A.; Adekola, F.A.; Olatunji, G.A. Liquid phase adsorptions of Rhodamine B dye onto raw and chitosan supported mesoporous adsorbents: isotherms and kinetics studies. *Applied Water Science* **2017**, *7*, 2297–2307.
- (60) Kubheka, G.; Adeola, A.O.; Forbes, P. B. C. Hexadecylamine functionalised graphene quantum dots as suitable nano-adsorbents for phenanthrene removal from aqueous solution. *RSC Adv.* **2022**, *12*, 23922–23936.
- (61) Adeola, A.O.; Forbes, P. B. C. Optimization of the sorption of selected polycyclic aromatic hydrocarbons by regenerable graphene wool. *Water Science and Technology* **2019**, *80*, 1931–1943.
- (62) Mojiri, A.; Zhou, J.L.; Ratnaweera, H.; Rezania, S.; Nazari V, M. Pharmaceuticals and personal care products in aquatic environments and their removal by algae-based systems. *Chemosphere* **2022**, 288, No. 132580.
- (63) Wei, F.; Zhu, Y.; He, T.; Zhu, S.; Wang, T.; Yao, C.; Yu, C.; Huang, P.; Li, Y.; Zhao, Q.; Song, W. Insights into the pH-Dependent Adsorption Behavior of Ionic Dyes on Phosphoric Acid-Activated Biochar. ACS Omega 2022, 7, 46288–46302.
- (64) Bhateria, R.; Jain, D. Water quality assessment of lake water: a review. Sustainable Water Resources Management 2016, 2, 161–173.
- (65) da Silva Vasconcelos de Almeida, A.; Vieira, W.T.; Bispo, M.D.; de Melo, S.F.; da Silva, T.L.; Balliano, T.L.; Vieira, M. G. A.; Soletti, J.I. Caffeine removal using activated biochar from açai seed (Euterpe oleracea Mart): Experimental study and description of adsorbate properties using Density Functional Theory (DFT). *Journal of Environmental Chemical Engineering* **2021**, *9*, No. 104891.
- (66) Sotelo, J.L.; Rodríguez, A.R.; Mateos, M.M.; Hernández, S.D.; Torrellas, S.A.; Rodríguez, J.G. Adsorption of pharmaceutical compounds and an endocrine disruptor from aqueous solutions by carbon materials. *Journal of Environmental Science and Health, Part B* **2012**, 47, 640–652.
- (67) Anastopoulos, I.; Katsouromalli, A.; Pashalidis, I. Oxidized biochar obtained from pine needles as a novel adsorbent to remove caffeine from aqueous solutions. *Journal of Molecular Liquids* **2020**, 304, No. 112661.
- (68) Portinho, R.; Zanella, O.; Féris, L.A. Grape stalk application for caffeine removal through adsorption. *J. Environ. Manage* **2017**, 202, 178–187
- (69) Couto, O.M., Jr; Matos, I.; da Fonseca, I.M.; Arroyo, P.A.; da Silva, E.A.; de Barros, M. A. S. D. Effect of solution pH and influence of water hardness on caffeine adsorption onto activated carbons. *Canadian Journal of Chemical Engineering* **2015**, 93, 68–77.
- (70) Villacañas, F.; Pereira, M. F. R.; Órfão, J. J. M.; Figueiredo, J.L. Adsorption of simple aromatic compounds on activated carbons. *J. Colloid Interface Sci.* **2006**, 293, 128–136.
- (71) Adegoke, K.A.; Adeleke, O.; Adesina, M.O.; Adegoke, R.O.; Bello, O.S. Clean technology for sequestering Rhodamine B dye on modified mango pod using artificial intelligence techniques. *Current Research in Green and Sustainable Chemistry* **2022**, 5, No. 100275.
- (72) Oyebamiji, A. K.; Adeleke, B. B. Quantum chemical studies on inhibition activities of 2,3-dihydroxypropyl-sulfanyl derivative on carbon steel in acidic media. *Int. J. Corrosion Scale Inhibition* **2018**.
- (73) Koopmans, T. Ordering of wave functions and eigenenergies to the individual electrons of an atom. *Physica* **1934**, *I* (1933), 104–113.